Expanding Polymer Chemical Space Utilizing Fischer Carbenes, Brown Allylations, and Electrochemistry

A Dissertation Presented for the

Doctor of Philosophy

Degree

The University of Tennessee, Knoxville

Breana Jade Kyker

December 2022

Copyright © 2022 by Breana J. Kyker
All rights reserved.

DEDICATION

This work is dedicated to my family and friends who have been a support system and an inspiration throughout this journey.

ACKNOWLEDGEMENTS

I would like to thank everyone who has played a role in my academic accomplishments. First, I would like to thank J.T. Hicks and Tim Michaels for teaching me the importance of perseverance, a strong work ethic, and the impact of having a creative outlet. A special thank you goes to Amber McWilliams and Dr. Bryan Wakefield for all they have taught me – whether it be in the classroom, the research lab, or professionally – they have played a large role in shaping my love of chemistry. Additionally, I owe a deep sense of gratitude to my advisor, Dr. Johnathan Brantley, for expecting only the best from me and pushing me to work harder through the difficult times. I would also like to thank Dr. Michael Best, Dr. Brian Long, Dr. Steven Neal, and Dr. Xian Carroll for all the support and guidance they have provided throughout my time at UTK. Finally, thanks to Dr. Alicia Doerr, for being the best friend I could ask for and always being there when I needed her.

ABSTRACT

Polymers have become ubiquitous in our everyday lives, and their various properties (which arise from the functional motifs found within the material) have helped them find a number of applications. Tuning material properties can be achieved either through polymerizing unique monomers with distinct chemical (or structural) elements, or post-polymerization modifications (which require the development of new synthetic methodologies). The research reported herein aims to address both of these grand challenges in materials science. We explore how the incorporation of metal and metalloid fragments affects polymer synthesis and bulk material properties, as well as how these synthetic handles can be subsequently engaged through further chemical transformation. Beyond this, we have developed a new electrochemical methodology that enables both functionalization and degradation of various polymeric substrates. These studies have allowed for the exploration of new chemical space in polymer science, as well as presented new platforms by which structure-property relationships can be interrogated.

TABLE OF CONTENTS

CHAPTER 1: INTRODUCTION 1
Overview – Synthesis and Modification of Soft Materials 2
Synthesis and Applications of Metallopolymers 2
Metallopolymer Self-Assembly 5
Optical Materials 8
Energy Storage and Conversion 8
Stimuli-Responsive Materials 10
Self-healing Materials 12
Biological Applications 14
Metallopolymers in Catalysis 14
Fischer Carbenes 16
Post-Synthetic Modifications 20
Post Polymerization Modifications Utilizing Pericyclic Reactions 21
Post Polymerization Modifications Utilizing C-H Activation 23
Post-Polymerization Modification: Boron-Containing Materials 23
Electrochemical Post-Polymerization Modification 27
Research Objectives 30
References 32
CHAPTER 2: SYNTHESIS AND REACTIVITY OF METALLOCARBENE-CONTAINING POLYMERS 56
Abstract 57
Introduction 57
Materials and Methods 60
General Considerations 60
Synthetic Considerations 60
Results and Discussion 67
Polymerization Studies and Material Characterization 67
Block Copolymer Synthesis and Post Polymerization Modifications 72
CO Release Experiments 74

Summary 82
Appendix 83
UV-vis absorbance data for CO release studies 83
Thermomechanical Data 83
References 97
CHAPTER 3: ELUCIDATING THE ORIGIN OF DIVERGENT ROMP ACTIVITY IN METALLOCARBENE MONOMERS 106
Abstract 107
Introduction 107
Results and Discussion 110
Materials and Methods 122
General Considerations 122
Synthetic Considerations 124
Synthesis of 3.1 124
Synthesis of 3.2 126
Synthesis of 3.4 126
Synthesis of 3.5 127
Polymerization Studies and Material Characterization 127
General Polymerization Kinetics Collection and Analysis Procedures 127
Chain Extension Experiments with Carbenes from Carbene Initiated Chain Ends 127
CO Detection Control – Addition of Pyridine to 3.1_{Cr} 128
Summary 128
Appendix 129
References 134
CHAPTER 4: POLYMER SCAFFOLD EDITING VIA BROWN ALLYLATIONS 143
Abstract 144
Introduction 144
Materials and Methods 151
General Considerations 151
Synthetic Considerations 151

Polymerization Optimization and Considerations 152
Brown allylation Methodology and Substrate Scope 152
Substrate Scope and Characterization 152
Summary 157
Appendix 159
References 165
CHAPTER 5: ELECTROEDITING OF SOFT POLYMER BACKBONES 170
Abstract 171
Introduction 171
Results and Discussion 174
Materials and Methods 192
General Considerations 192
Synthetic Procedures 195
High M_n cis-polynorbornene 195
Low M_n polynorbornene 196
Polystyrene 196
Poly(cyclooctene) 199
Experiments Related to Homogeneous Electrochemical Degradations of 5.1 199
Degradation of 1 in the Absence of Electrolysis 199
Degradation of 1 using a Referenced Potential (2.18 V) 201
Analysis of 5.1 using Cyclic Voltammetry 201
Electrode Screen for Electrochemical Degradation of 5.1 201
Impact of Cell Potential on the Degradation of 5.1 204
Kinetic Analysis of the Electrochemical Degradation of 5.1 204
Electrolysis of a Low M_n sample of 5.1 207
Experiments to Probe the Scope of Electrochemical Polymer Degradation 207
Electrochemical Degradation of cis-1,4-Polybutadiene 207
Electrochemical Degradation of cis-1,4-Polyisoprene 209
Electrochemical Degradation of Poly(cyclooctene) 209

Experimental Procedure for Selective Electrochemical Degradation of 5.1 in the Presence of Polystyrene 209
Experiments to Confirm Radical Cation Formation 210
Electrochemical Degradation of 5.1 in the Presence of 9,10-Dihydroanthracene (DHA) 210
Control Experiment: Electrolysis of DHA in the Absence of Polymer 210
Photoredox-Mediated Degradation of 5.1 213
Experiments Related to Electrochemical Degradations of Heterogenous Samples of 5.1 213
Heterogenous Electrochemical Degradation of 5.1 213
Confirmation of Heterogenous Conditions by NMR Spectroscopy 213
Experiments Related to Electrochemical Polymer Azidation 214
Electrochemical Azidation of 5.1 214
Control Experiment: Azidation of 5.1 without Applied Potential 214
Control Experiment: Azidation of 5.1 without $MnBr_2$ 216
Electrochemical Azidation of 5.1 at Low (2.5 V) and High (3.2 V) Potentials 216
Electrochemical Azidation of 5.1 with Different Electrode Combinations 217
Electrochemical Azidation of cis-1,4-Polybutadiene 217
Electrochemical Azidation of cis-1,4-Polyisoprene 219
Electrochemical Azidation of Poly(cyclooctene) 219
Experiments to Estimate Degree of Azidation of 5.1 220
NMR Analysis of Low M_n Azidated Material 220
Cu-Mediated Cycloaddition for UV-vis Determination of Azide Content 220
Determination of % pyrene content in 5.3 222
Summary 222
Appendix 223
Determination of Faradaic Efficiency 223
References 257
CHAPTER 6: SUMMARY AND OUTLOOK 267
Functional Materials 268

Polymerization of Fischer Carbenes 268
Post-polymerization Modifications 270
Brown Allylation Chemistry 270
Electrochemistry 270
VITA 272

LIST OF TABLES

Table 2.1. Selected Molecular Weight Data for 2.P1 65
Table 2.2. Initial Catalyst Screen for Polymerization of 1 68
Table 2.3. Optimization of Polymerizaation of 2.1 Using Catalyst 2.4 71
Table 2.4. Catalyst Screening for Polymerization of 2.1 71
Table 4.1. SEC data for catalyst screening for the polymerization of 4.1..... 148
Table 5.1. Electrode screen for electrochemical azidation of 5.1..... 188
Table 5.2. Electrode screen for the electrochemical degradation of 5.1. 203
Table 5.3. Kinetic study for the electrochemical degradation of 5.1..... 206
Table 5.4. Kinetic data for electrochemical degradation of 5.1 in the presence of DHA. ... 212

LIST OF FIGURES

Figure 1.1. Representative Metallopolymer Architectures....4
Figure 1.2. Poly(vinyl ferrocene) and representative CV....4
Figure 1.3. Schematic Representation of Metallopolymer Applications. Adapted from *Prog. Polym. Sci.* 2021, 119, 101428....6
Figure 1.4. Block Copolymer 1.3....7
Figure 1.5. White-Light Emitting Polymers 1.4, 1.5, and 1.6....9
Figure 1.6. Polymers 1.7 for electrochemistry and 1.8 for semi-conductors....11
Figure 1.7. Metallopolymers 1.9 and 1.10 exhibiting Stimuli-Responsive behavior....11
Figure 1.8. Metallopolymers utilized for biological applications....15
Figure 1.9. Previous reports of Fischer-carbene containing polymers....19
Figure 2.1. UV-vis Profiles for 2.5 (violet), 2.5•(CO) (red), and 2.5•$(CO)_2$ (green)....63
Figure 2.2. SEC Data for 2.P1 with THF as Eluent....65
Figure 2.3. Representative IR Spectrum for 2.P1....66
Figure 2.4. ^{1}H NMR Spectra from Analysis of 2.2a Poisoning. 2.2a (red), 2.2a 5 Minutes after 1 Equivalent of 2.1 Added (green), 2.2a 4 Hours after Addition of 2.1 (teal), and 2.2a after Exposure to $CO_{(g)}$ (purple)....70
Figure 2.5. Representative TGA Thermogram of 2.P1 (Ramp Rate of 10 °C/min in N_2)....73
Figure 2.6. Representative DMA Stress Strain Plot for 2.P1 (0.1% strain/min)....73
Figure 2.7. IR Spectrum for 2.P1 Following Demetallation. Blue Box Indicates Region Where Initial CO Stretches Appeared....75
Figure 2.8. SEC Traces of 2.P1 before (violet) and after (red) Irradiation....75
Figure 2.9. Determination of CO Release from 2.P1. (A) Calibration curve for CO release measurement via IR spectroscopy. Inset shows the CO stretching frequencies of a 2.P1 sample before (black) and after (red) irradiation. (B) UV−vis spectra for CO sensor 2.5 (violet) showing binding of CO released from 2.P1 (red)....77
Figure 2.10. Deconvoluted UV-vis Spectrum of 2.5 after Transfer of Headspace from 2.P1 Solution Irradiated under Aerobic Conditions. Spectrum is Consistent with an 81:19 Mixture of 2.5•(CO) and 2.5•$(CO)_2$....78

Figure 2.11. Deconvoluted UV-vis Spectrum of 2.5 after Transfer of Headspace from 2.P1 Solution Irradiated under Anaerobic Conditions. Spectrum is Consistent with 71:29 Mixture of 2.5•(CO) and 2.5 78
Figure 2.12. Deconvoluted UV-vis Spectrum of 2.5 after Transfer of Headspace from 2.P1 Solution Kept in the Dark under Aerobic Conditions. Spectrum is Consistent with 85:15 mixture of 2.5•(CO) and 2.5 79
Figure 2.13. UV-vis Spectrum of 2.5 after Transfer of Headspace from 2.P1 Solution Kept in the Dark under Anaerobic Conditions. Overlay of 2.5 before (purple) and after (red) Transfer of Headspace Shows No Change 80
Figure 2.14. IR Spectrum for 2.5 84
Figure 2.15. IR Spectrum for 2.5•(CO) 84
Figure 2.16. IR Spectrum for 2.5•$(CO)_2$ 85
Figure 2.17. Calibration Curve for Determining Molar Absorptivity of 2.5•(CO) 85
Figure 2.18. Apparatus for Irradiation of 2.P1 and Transfer of CO from Headspace to a Solution of 2.5 86
Figure 2.19. Emission Spectrum of 33 W Compact Fluorescent Lamp 86
Figure 2.20. UV-vis Overlay of 2.1 & 2.P1, λ_{max} = 246 nm. Inset: UV-vis profile from SEC of 2.P1 with $CHCl_3$ as Eluent (M_n = 341,000 Da; 23.17 mL retention volume) 87
Figure 2.21. ^{1}H NMR Spectrum for 2.1. Peaks for Major Diastereomer are Picked and Integrated. Minor Diastereomers are Labelled with *. 88
Figure 2.22. ^{13}C NMR Spectrum for 2.1. Peaks for Major Diastereomer are Picked and Integrated. Minor Diastereomers are Labelled with *. 89
Figure 2.23. ^{1}H NMR Spectrum for 2.5. 90
Figure 2.24. ^{13}C NMR Spectrum for 2.5. 90
Figure 2.25. ^{1}H NMR Spectrum for 2.5•(CO). 91
Figure 2.26. ^{13}C NMR Spectrum for 2.5•(CO). 91
Figure 2.27. ^{1}H NMR Spectrum for 2.5•$(CO)_2$. * Denotes Acetic Acid. 92
Figure 2.28. ^{13}C NMR Spectrum for 2.5•$(CO)_2$. * Denotes Acetic Acid. 92
Figure 2.29. ^{1}H NMR Spectrum for Polymerization of 2.1 with 2.2a initially (teal) and after two weeks (red). 93

Figure 2.30. ^{1}H NMR Spectrum for 2.P1. 94
Figure 2.31. ^{13}C NMR Spectrum for 2.P1. 94
Figure 2.32. ^{1}H NMR Spectrum for Block Copolymer Consisting of a Tungsten Block and Norbornene Block. 95
Figure 2.33. ^{1}H NMR Spectrum for Demetallation of 2.P1 (red) with Starting Polymer (blue). 96
Figure 3.1. UV-vis overlay of 2.5 before addition of 3-bromopyridine to 3.1_W (purple) and after addition of 3-bromopyridine to 3.1_W (red). 111
Figure 3.2. ^{1}H NMR spectra for stoichiometric experiment between 3.1_W and G3. 1) G3 only, 2) G3 plus 3.1_W, t_0, 3) G3 plus 3.1_W, t_{60} 111
Figure 3.2. SEC data for $3.P1_{Cr}$ from triple detection 113
Figure 3.4. ^{1}H NMR spectra for Iterative stoichiometric addition of 3.1_W to G3. 1) G3 only, 2) G3 plus 1 equivalent 3.1_W, 3) G3 plus 2 equivalents 3.1_W, 4) G3 plus 3 equivalents 3.1_W, 5) G3 plus 4 equivalents 3.1_W. 114
Figure 3.5. ^{1}H NMR spectra for stoichiometric experiment between G3 and 3.1_{Cr}. 1) G3 only, 2) G3 plus 3.1_{Cr}, t_0, 3) G3 plus 3.1_{Cr}, t_{60}. 115
Figure 3.6. SEC data for A) initiation with 3.1_W followed by chain extension with 3.1_W and B) initiation with 3.1_{Cr} followed by chain extension with 3.1_{Cr}. 117
Figure 3.7. Chain extension with norbornene from ruthenium initiated 3.1_W. A) SEC data for chain-extended material exhibiting UV-signal, B) UV-vis absorbance profile of 3.1_W overlay with chain-extended material. 117
Figure 3.8. Representative ^{1}H NMR kinetics data for polymerization of 3.1_{Cr} (collected at -5 ºC). Highlighted area indicates vinyl resonances of 3.1_{Cr}; selected spectra are at 90-second intervals between 4:30 minutes and 12 minutes. 118
Figure 3.9. Eyring plot for 3.1_{Cr}. Each data point is measured in triplicate. 119
Figure 3.10. Initiation and Propagation Energies for G3 with 3.1. Blue represents 3.1_W, while black represents 3.1_{Cr}. 121
Figure 3.11. SEC data from triple detection for initial polymerization of 3.5 123
Figure 3.12. Representative ^{1}H NMR spectrum for 3.1_{Cr}. * denotes grease 129
Figure 3.13. Representative ^{1}H NMR spectrum for 3.2 *exo* 129

Figure 3.14. Representative ^{1}H NMR spectrum for 3.2 *endo.* * denotes ethyl acetate..... 130
Figure 3.15. ^{1}H NMR spectra for 3.4_{W}. * denotes DCM, ▲ denotes water, and ■ denotes grease 130
Figure 3.16. ^{1}H NMR spectrum for 3.5_{W}. * denotes grease 131
Figure 3.17. ^{1}H NMR spectra for the addition of pyridine to 3.1_{W}. 1) 3.1_{W} only, 2) 3-bromopyridine only, 3) 3.1_{W} plus 3-bromopyridine, t_0, 4) 3.1_{W} plus 3-bromopyridine, t_{60} 132
Figure 3.18. ^{1}H NMR spectra for control experiment between G3 and norbornene. 1) G3 only, 2) G3 plus norbornene, t0, 3) G3 plus norbornene, t60. 133
Figure 4.1. Catalyst screening for the polymerization of 4.1 148
Figure 4.2. SEC data for Brown allylation with benzaldehyde. Red indicates 4.P1, and purple indicates 4.P2. 153
Figure 4.3. SEC data for Brown allylation with anisaldehyde. Red indicates 4.P1, and purple indicates 4.P8. 155
Figure 4.4. SEC data for brown allylation with p-trifluoromethylbenzaldehyde. Red indicates 4.P1 and purple indicates 4.P9. 155
Figure 4.5. SEC data for Brown allylation with o-nitrobenzaldehyde. Red indicates 4.P1, and purple indicates 4.P10. 156
Figure 4.6. SEC data for Brown allylation with p-nitrobenzaldehyde. Red indicates 4.P1, and purple indicates 4.P11 156
Figure 4.7. SEC data for Brown allylation with p-bromobenzaldehyde. Red indicates 4.P1, and purple indicates 4.P13 158
Figure 4.8. ^{1}H NMR spectrum for 4.1. * denotes water 159
Figure 4.9. ^{1}H NMR spectrum for 4.P1 in $CDCl_3$ 159
Figure 4.10. ^{1}H NMR spectrum for 4.P2 in $CDCl_3$. ▲ denotes methanol. * denotes water. 160
Figure 4.11. ^{13}C NMR spectrum for 4.P2 in $CDCl_3$. 160
Figure 4.12. ^{1}H NMR spectrum for 4.P4 in $CDCl_3$. ▲ denotes BHT. 161
Figure 4.13. ^{1}H NMR spectrum for 4.P7 in $CDCl_3$. ▲ denotes BHT. * denotes methanol.. 161

Figure 4.14. ^{1}H NMR spectrum for 4.P9 in $CDCl_3$. ▲ denotes BHT. ■ denotes methanol. * denotes water. 162
Figure 4.15. ^{13}C NMR spectrum for 4.P9 in $CDCl_3$. 162
Figure 4.16. ^{1}H NMR spectrum for 4.P10 in $CDCl_3$. ▲ denotes BHT. * denotes water. 163
Figure 4.17. ^{13}C NMR spectrum for 4.P10 in $CDCl_3$. 163
Figure 4.18. ^{1}H NMR spectrum for 4.P13 in $CDCl_3$. @ denotes residual xxxx. ▲ denotes BHT. ■ denotes methanol. * denotes water. 164
Figure 4.19. ^{13}C NMR spectrum for 4.P13 in $CDCl_3$. 164
Figure 5.1. SEC data from conventional calibration for electrochemical degradation of 5.1. Solid trace represents polymer before electrolysis. Dotted traces represent polymer after electrolysis at 2.5 V (red) and 3.2 V (blue). 176
Figure 5.2. Electrochemical degradation study using 5.1. (A) Molecular weight evolution as a function of electrolysis time (as determined by SEC). (B) Representative kinetic plot for the electrochemical degradation of 5.1. 176
Figure 5.3. Mark-Houwink plot from triple detection for material following electrochemical degradation of 5.1. The black line represents 5.1 prior to electrolysis and the red line represents the polymer following 60 min of electrolysis. 177
Figure 5.4. M_n (determined by triple detection SEC) as a function of electrolysis time during the electrochemical degradation of 5.1. 177
Figure 5.5. Overlayed kinetic plot using data from the electrochemical degradation of 5.1 in the presence of DHA (red) and absence of DHA (blue). 178
Figure 5.6. SEC data from triple detection for photoredox-mediated degradation of 5.1. Solid trace represents polymer pre-irradiation and dotted trace represents polymer post-irradiation. 180
Figure 5.7. SEC data from conventional calibration for the electrochemical degradation of *cis*-1,4-polyisoprene at 2.5 V. Solid trace represents polymer before electrolysis and dotted trace represents polymer after electrolysis. 181
Figure 5.8. SEC data from conventional calibration for the electrochemical degradation of *cis*-1,4-polybutadiene at 2.5 V. Solid trace represents polymer before electrolysis and dotted trace represents polymer after electrolysis. 181

Figure 5.9. SEC data from triple detection for the electrochemical degradation of poly(cyclooctene) at 3.2 V. Solid trace represents polymer before electrolysis and dotted trace represents polymer after electrolysis..... 182
Figure 5.10. Chemoselective degradations of polymer mixtures. SEC analysis of a polymer mixture (polynorbornene and polystyrene; black) showing selective degradation of polynorbornene following electrolysis (red)..... 183
Figure 5.11. UV visualization (294 nm) of SEC data for selective electrochemical degradation of 5.1. UV visualization of the SEC data for a mixed polymer sample prior to electrolysis (black) 183
Figure 5.12. Heterogeneous degradation of 5.1. SEC analysis following heterogenous polymer electroactivation showed a clear reduction in molecular weight with increasing electrolysis time. Inset picture shows a representative experiment with the insoluble polymer highlighted by a red arrow. 185
Figure 5.13. ^{1}H NMR spectra for heterogeneous degradation of 5.1. Black: 5.1 in $CDCl_3$. Grey: Electrolyte in CD_3CN. Blue: Aliquot of reaction mixture prior to electrolysis in CD_3CN. Red: Aliquot of reaction mixture post-electrolysis in CD_3CN. Purple highlights represent characteristic chemical shifts of 5.1. 186
Figure 5.14. Overlayed IR spectra for azidation of 5.1 under various conditions. Spectra for unfunctionalized 5.1 (black), background functionalization in the absence of an applied potential (red), and background functionalization in the absence of $MnBr_2$ (blue, dashed) are shown. The IR spectrum from the material prepared under our standard conditions (red, dashed) has been included for comparison..... 187
Figure 5.15. IR spectra from the electrode screen for preparing 5.2. Legend shows electrode combinations in anode/cathode format. 188
Figure 5.16. IR spectra for the electrochemical azidation of 1,4-polybutadiene. Black line represents polymer before electrolysis. Red line represents solid polymer isolated following electrolysis..... 189
Figure 5.17. SEC data from triple detection for 1,4-polybutadiene before (black trace) and after azidation (dotted red trace)..... 189

Figure 5.18. IR spectra for the electrochemical azidation of *cis*-1,4-polyisoprene. Black line represents polymer before electrolysis. Red line represents solid polymer isolated after electrolysis. 190
Figure 5.19. SEC data from triple detection for *cis*-1,4-polyisoprene before (black trace) and after azidation (dotted red trace). 190
Figure 5.20. IR spectra for the electrochemical azidation of poly(cyclooctene). Black line represents polymer before electrolysis. Red line represents solid polymer isolated after electrolysis. 191
Figure 5.21. SEC data from triple detection for poly(cyclooctene) before (black trace) and after azidation (dotted red trace). 191
Figure 5.22. Cartoon representation of azidation of a low M_n sample of 5.1 and subsequent Cu-mediated azide/alkyne coupling. A) IR spectra for 5.1 (blue), 5.2 (red), and 5.3 (green). B) UV-vis absorbance spectra of 5.2 (red) and 5.3 (green). The absorbance spectrum of 1-ethynyl pyrene is provided for reference (purple). 193
Figure 5.23. SEC data from conventional calibration depicting RI and UV signals (at 350 nm) for 5.2 (A) and 5.3 (B) to confirm presence of pyrene moiety. 193
Figure 5.24. UV-vis calibration curve for ethynyl pyrene. Black square represents 9.29 μM with respect to pyrene coupled repeat units in 5.3. 194
Figure 5.25. Proposed mechanism for electrochemical editing of olefin-containing polymers. 194
Figure 5.26. SEC data from triple detection for high M_n *cis*-polynorbornenes used in this study. 197
Figure 5.27. SEC data from conventional calibration for high M_n *cis*-polynorbornenes used in this study. 197
Figure 5.28. SEC data from triple detection for low M_n polynorbornenes used in this study. 198
Figure 5.29. SEC data from conventional calibration for low M_n polynorbornenes used in this study. 198

Figure 5.30. SEC data from triple detection for degradation of 5.1 in the absence of electrolysis. Solid trace represents the initial polymer, and the dotted trace represents polymer isolated after the experiment. 200
Figure 5.31. SEC data from triple detection for referenced degradation of 5.1 (2.18 V). Solid trace represents polymer before electrolysis and dotted trace represents polymer after electrolysis. 202
Figure 5.32. Cyclic voltammogram of 5.1 using ferrocene as an internal standard. Oxidation peak associated with ferrocene represented by *. 202
Figure 5.33. SEC data from triple detection for electrochemical degradation of 5.1 electrode screen. Legend shows electrode combinations used for the screen in the format of anode/cathode. 205
Figure 5.34. M_z (determined by triple detection SEC) as function of electrolysis time during the electrochemical degradation of 5.1. 205
Figure 5.35. SEC data from conventional calibration before (purple) and after (red) electrolysis of low M_n 5.1. 208
Figure 5.36. SEC data from triple detection showing the evolution of molecular weight as a function of electrolysis time for the electrochemical degradation of 5.1 in the presence of DHA. 211
Figure 5.37. M_n (determined by triple detection SEC) as a function of electrolysis time for the electrochemical degradation of 5.1 in the presence of DHA. 211
Figure 5.38. M_z (determined by triple detection SEC) as a function of electrolysis time for the electrochemical degradation of 5.1 in the presence of DHA. 212
Figure 5.39. SEC data from conventional calibration for a low M_n sample of 5.1 before (black) and after (red) electrochemical azidation. 215
Figure 5.40. SEC data from triple detection for a high M_n sample of 5.1 before (black) and after (red) electrochemical azidation 215
Figure 5.41. IR spectra for the electrochemical azidation of 5.1 at different potentials. Spectra for unfunctionalized 5.1 (black), material following azidation at 2.5 V (blue), and material following azidation at 3.2 V (red) are shown. 218

Figure 5.42. ^{1}H NMR spectrum for cis-1,4-polybutadiene in $CDCl_3$. Spectrum taken following filtration and reprecipitation. * denotes water 226
Figure 5.43. ^{13}C NMR spectrum for *cis*-1,4-polybutadiene in $CDCl_3$. Spectrum taken following filtration and reprecipitation 227
Figure 5.44. ^{1}H NMR spectrum for *cis*-1,4-polyisoprene in $CDCl_3$ 228
Figure 5.45. ^{13}C NMR spectrum for *cis*-1,4-polyisoprene in $CDCl_3$ 229
Figure 5.46. ^{1}H NMR spectrum of high-*cis* polynorbornene in $CDCl_3$. * denotes water. 230
Figure 5.47. ^{13}C NMR spectrum of high-*cis* polynorbornene in $CDCl_3$. 231
Figure 5.48. ^{1}H NMR spectrum for low M_n polynorbornene in $CDCl_3$. * denotes water. 232
Figure 5.49. ^{13}C NMR spectrum for low M_n polynorbornene in $CDCl_3$. 232
Figure 5.50. ^{1}H NMR spectrum for polystyrene in $CDCl_3$. ▲ denotes tetrahydrofuran and ◆ denotes grease 233
Figure 5.51. ^{1}H NMR spectrum for poly(cyclooctene) in $CDCl_3$. * denotes water 234
Figure 5.52. ^{13}C NMR spectrum for poly(cyclooctene) in $CDCl_3$. 235
Figure 5.53. ^{1}H NMR overlay for 5.1 in $CDCl_3$ following electrolysis. Red shows material before electrolysis, and blue shows material after electrolysis. Inset contains enhanced baseline to show new aldehydic resonance in post-electrolysis material. * denotes water, and ▲ denotes THF. 236
Figure 5.54. ^{13}C NMR spectrum for 5.1 in $CDCl_3$ following electrolysis. 237
Figure 5.55. ^{1}H NMR overlay for a low M_n sample of 5.1 before (red) and after (blue) electrolysis. ▲ denotes THF and * denotes methanol 238
Figure 5.56. ^{1}H NMR overlay for *cis*-1,4-polybutadiene in $CDCl_3$ following electrolysis. Red shows material before electrolysis, and blue shows material after electrolysis. Insets contain enhanced baselines to show new aldehydic (A) and vinyl (B) resonances in post-electrolysis material. * denotes water 239
Figure 5.57. ^{13}C NMR spectrum for *cis*-1,4-polybutadiene in $CDCl_3$ following electrolysis. 240
Figure 5.58. ^{1}H NMR overlay for *cis*-1,4-polyisoprene in $CDCl_3$ following electrolysis. Red shows material before electrolysis, and blue shows material after electrolysis. Inset contains enhanced baseline to show new aldehydic resonances in post-electrolysis material. * denotes water. 241

Figure 5.59. ^{13}C NMR spectrum for *cis*-1,4-polyisoprene in $CDCl_3$ following electrolysis. .. 242
Figure 5.60. ^{1}H NMR spectrum for poly(cyclooctene) in $CDCl_3$ following electrolysis. * denotes water. 243
Figure 5.61. ^{13}C NMR spectrum for poly(cyclooctene) in $CDCl_3$ following electrolysis. 243
Figure 5.62. ^{1}H NMR spectra for electrolysis of DHA control. 1) DHA prior to electrolysis. 2) DHA following silica plug after electrolysis. 244
Figure 5.63. ^{1}H NMR spectrum for 5.1 in $CDCl_3$ following photochemical degradation. * denotes water 245
Figure 5.64. ^{1}H NMR spectrum for 5.2 in $CDCl_3$. * denotes water and ▲ denotes grease.246
Figure 5.65. ^{13}C NMR spectrum for 5.2 in $CDCl_3$..... 247
Figure 5.66. ^{1}H NMR spectrum for electrochemically azidated 1,4-polybutadiene in $CDCl_3$ following electrolysis. ❖ denotes MeOH. Inset contains enhanced baseline to show new signals consistent with azidation. 248
Figure 5.67. ^{13}C NMR spectrum for electrochemically azidated 1,4-polybutadiene in $CDCl_3$ following electrolysis. 249
Figure 5.68. ^{1}H NMR spectrum for electrochemically azidated *cis*-1,4-polyisoprene in $CDCl_3$ following electrolysis. ❖ denotes MeOH. Inset contains enhanced baseline to show new signals consistent with azidation. 250
Figure 5.69. ^{13}C NMR spectrum for electrochemically azidated *cis*-1,4-polyisoprene in $CDCl_3$ following electrolysis. 250
Figure 5.70. ^{1}H NMR spectrum for electrochemically azidated poly(cyclooctene) in $CDCl_3$ following electrolysis. ❖ denotes MeOH. 251
Figure 5.71. ^{13}C NMR spectrum for electrochemically azidated poly(cyclooctene) in $CDCl_3$ following electrolysis. 252
Figure 5.72. ^{1}H NMR spectra for determination of degree of azidation. Top spectrum represents 5.1 and bottom spectrum represents 5.2. Purple and blue boxes highlight the cyclopentyl methylene and azidated methine resonances, respectively. 253
Figure 5.73. ^{1}H NMR spectrum for 5.3 in $CDCl_3$. ▲ denotes acetone, * denotes water, and ❦ denotes grease. 254
Figure 5.74. ^{13}C NMR spectrum for 5.3 in $CDCl_3$. 254

Figure 5.75. ^{1}H NMR spectra of 5.2 (top) and 5.3 (bottom). Shaded regions show signals for coupled pyrene (red), azide methine (blue), and unfunctionalized methylene (purple). 255
Figure 5.76. MALDI-TOF spectrum following electrolysis of a low M_n 5.1. Inset shows expansion of region from 4000-7000 m/z. 256

LIST OF SCHEMES

Scheme 1.1. Redox controlled self-assembly of 1.2 6
Scheme 1.2. Self-healing metallopolymers 1.11, 1.12, and 1.13 13
Scheme 1.3. Synthetic Routes for Accessing Fischer Carbenes. 17
Scheme 1.4. Pericyclic rearrangements in polymers 22
Scheme 1.5. Polyolefin upcycling through C-H activation 24
Scheme 1.6. Examples of Suzuki cross-coupling in polymer architectures 26
Scheme 1.7. eATRP 29
Scheme 1.8. Electrochemical modifications of polymers 31
Scheme 2.1. Synthetic Strategies to Access Metallocarbene-Containing Polymers 59
Scheme 2.2. Synthesis of 2.1 61
Scheme 2.3. Synthetic Utility of Metallocarbene Polymers 66
Scheme 3.1. Examples of Factors Affecting Polymerization Rate with Ruthenium Catalysts 109
Scheme 3.2. Synthesis of 3.5 123
Scheme 3.3. Synthesis of 3.1 125
Scheme 4.1. Synthetic manipulations of boron-containing polymers 147
Scheme 4.2. Synthesis of 4.1 148
Scheme 4.3. Substrate Scope for Post-Polymerization Brown Allylation 150
Scheme 5.1. Selected Examples of Modern Polymer Upcycling and Degradation Strategies 173
Scheme 5.2. Photoredox-mediated degradation of 5.1 180
Scheme 5.3. Azidation of 1 Under Optimized Conditions 221
Scheme 5.4. Cu-Mediated Cycloaddition Between 2 and Ethynyl Pyrene 221

CHAPTER 1: INTRODUCTION

Overview – Synthesis and Modification of Soft Materials

Functional materials – materials that can exhibit a wide array of properties and functions depending on their inherently modifiable structures - are becoming increasingly popular among the materials science community. These materials can be leveraged for a wide range of applications, such as 3D printing,[1,2] energy harvesting and storage,[3,4] artificial muscles,[5,6] robotics,[7,8] biomedical devices,[9,10] sensors,[11,12] among others.[13–17] Furthermore, functional materials can be leveraged for structure-property studies.[18] Despite their wide utility, the synthesis of these materials remains a challenge for materials scientists. Overcoming this obstacle can be realized through research directed at exploring new chemical space with respect to polymers. Being able to control the structures of polymers allows us to control the physical properties of the materials, and therefore, the applications. Additionally, this ability allows us to explore new polymer chemical space. Studying the methodologies and mechanisms behind how new chemistries are paired with polymers is of great importance for expanding these approaches to functional materials. Primarily, the routes to obtain functional materials include polymerization of unique monomers and post-polymerization modification. Each of these methods will be described in detail below, and in-depth studies have been included in the following chapters. Specifically, we have focused on using metal carbenes as monomers for polymerization and developing new methods for the modification of polymers. A brief discussion of how each of these functional handles can be used is discussed below.

Synthesis and Applications of Metallopolymers

Since Staudinger's initial report of polymerization,[19] many distinct polymers have been investigated. Synthetic polymer chemists have identified a range of methods (anionic, cationic, radical, and metathesis polymerization) that take advantage of intrinsically polymerizable functional groups. The advent of these new polymerization techniques has allowed for a diverse array of compounds to be labelled as "monomers." However, accessing functional materials is complicated by the reactivity of the new functional subunits; often, this reactivity is eliminated or hindered in the polymerization process. Various organic compounds are among the most common functional groups for polymerization, including olefins, esters, amides, and others. These functional groups allow for tunability within the material. For

example, many water purification plants take advantage of lower critical solution temperature (LCST) behavior, utilizing poly-N-isopropylacrylamide (pNIPAm) as a flocculant for the removal of solid wastes from water. Changing the molecular weight of the polymer, the substituents on the N group, or the % acrylamide within the polymer allows for tuning of the materials properties.

Beyond these organic moieties lie transition metals, which have provided rich synthetic utility in both organic and inorganic methodology. Incorporation of metal moieties into polymeric compounds can impart further properties with respect to electronics,[20] optics,[21–23] and conductivity and thermal stability[23] by taking advantage of the inherent reactivity of the metal. While reports of utilization of transition metals as monomers have only recently emerged, metal fragments have been incorporated into a variety of polymeric architectures (linear,[24] branched,[25] and dendrimers;[26] Figure 1.1). Beyond embedding metal species into polymers, these materials hold promise for applications in electronic,[27–29] stimuli-responsive,[30–32] and optical materials[33–35] (among others[36]).

The first metallopolymer, poly(vinyl ferrocene) (**1.1**; Figure 1.2), was reported by Arimoto in 1955.[37] This polymer was reported to have stimuli-responsive behavior, possessing the same redox properties as the monomer. Though this was a novel advance in polymer chemistry, the synthesis of this material was conducted via an uncontrolled, anionic mechanism. Over the next few decades, further attempts at incorporation of metal species into polymers proved difficult (due to the poor solubility of the final materials and metal leeching).[38] In the 1990's, new synthetic methodologies, such as reversible-addition fragmentation chain-transfer (RAFT),[39] atom transfer radical polymerization (ATRP),[40,41] and ring opening metathesis polymerization (ROMP)[42–44] were developed, enabling facile incorporation of metal subunits into polymers through their functional group compatibility. Since these developments, many advances have been made with respect to metallopolymers, and they have found applications in electronics,[20,23] optics,[45,46] catalysis,[47] and medicine,[48] among others.[49–51] Indeed, an excellent and comprehensive review by Newkome and Schubert describes the numerous efforts reported regarding metallopolymer applications.[49] Despite these advances, there is still vast unexplored chemical space concerning metallopolymers, which can be addressed by using metal moieties with synthetic versatility

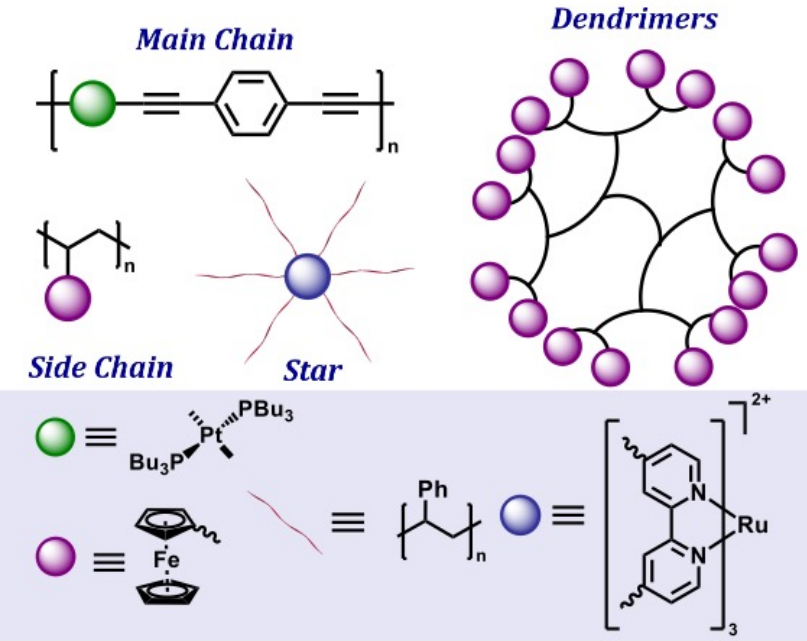


Figure 1.1. Representative Metallopolymer Architectures

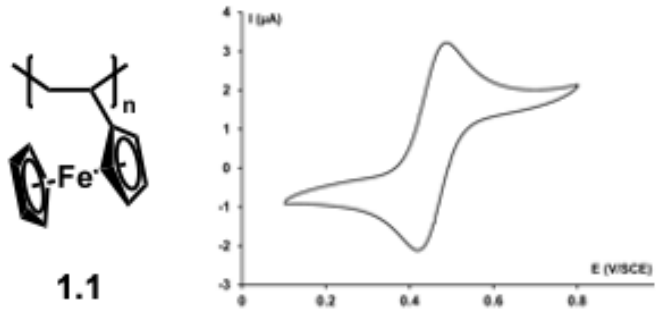


Figure 1.2. Poly(vinyl ferrocene) and representative CV

and unique material properties, allowing the field of metallopolymers to remain an area of growing interest. A brief survey of relevant literature follows, including important advances in metallopolymers as well as rationale for utilization of Fischer carbenes as monomers (described in Chapters 2 and 3).

As stated, metallopolymers have found a broad range of applications due to their ability to combine the inherent properties of polymers and metals. Figure 1.3 illustrates some of the most common applications of metallopolymers, exemplifying their importance to the materials community.

Metallopolymer Self-Assembly

Taking cues from biology's micelles, self-assembly has been an important area of study in polymeric materials. There are many different morphological conformations that can be adopted by polymers, allowing for the utilization of these materials across a broad range of applications such as drug delivery and conductive materials. Polymers often adopt various morphological conformations due to their inherent makeup. For example, block copolymers made from hydrophilic and hydrophobic blocks easily form micelles in solution. Further, self-assembly can be triggered by various stimuli (e.g., light,[52,53] sonication,[54,55] heat[56,57]) during polymer synthesis through polymerization-induced self-assembly. While these mechanisms for self-assembly are well-studied, the utilization of metallopolymers for self-assembling purposes can overcome many of the limitations with respect to self-assembly (e.g., particle size, thermal stability) due to the metal's ability to act as both a structural component and a tunable element.[58] Manners has accomplished significant work in the field of self-assembling metallopolymers by utilizing a variety of metal-containing compounds as monomers and exploring their applications. For example, polystyrene-*block*-polyferrocenylsilane copolymers (**1.2**; Scheme 1.1) exhibit redox-controlled reversible self-assembly in nonpolar solutions to provide micelles with the ferrocenylsilane block in the core.[59] Because pNIPAm is often used for water purification purposes due to its LCST behavior, further modification of this material to impart self-assembly behavior is desirable. Yoshida synthesized pNIPAm-*block*-Ru(bpy)$_3$ (**1.3**; Figure 1.4)to determine the effects of incorporation of the ruthenium species within the polymer.[60] This material was found to exhibit self-flocculating tendencies and retain the LCST behavior found in pNIPAm homopolymers, however at different thresholds. The material was

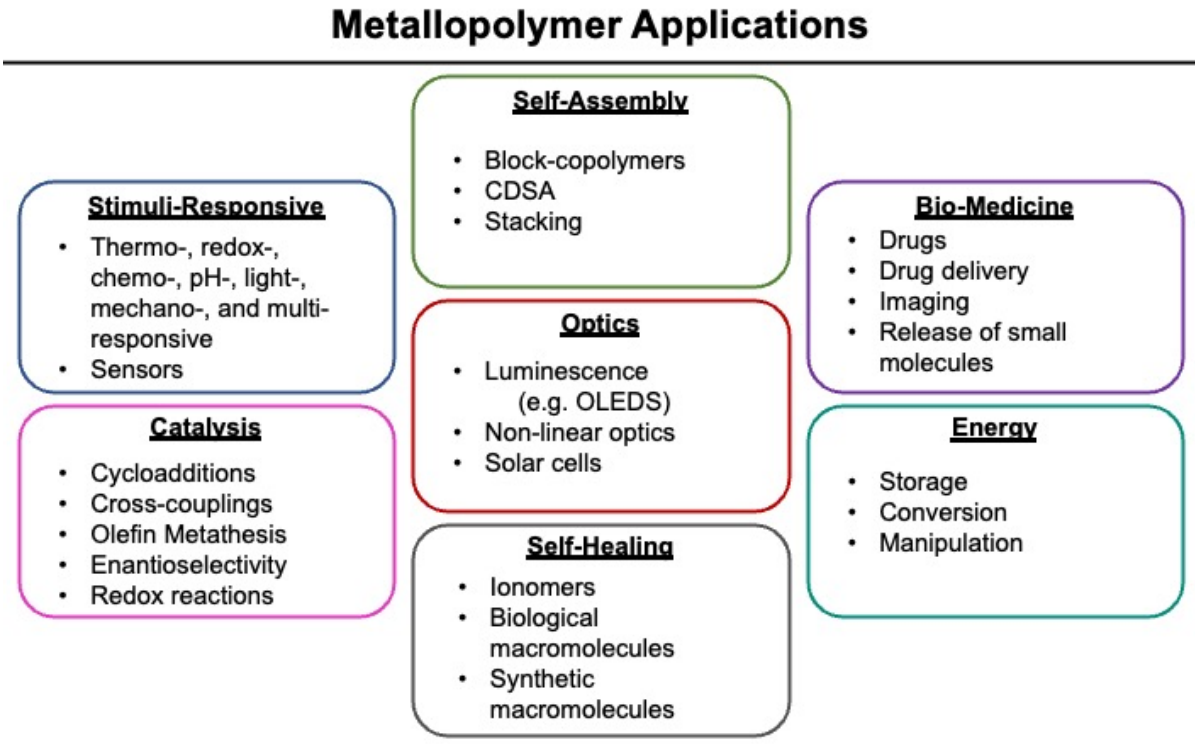
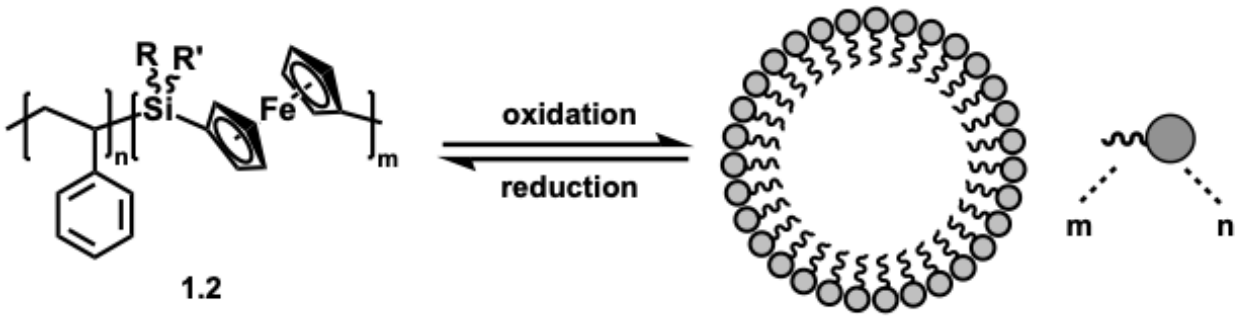
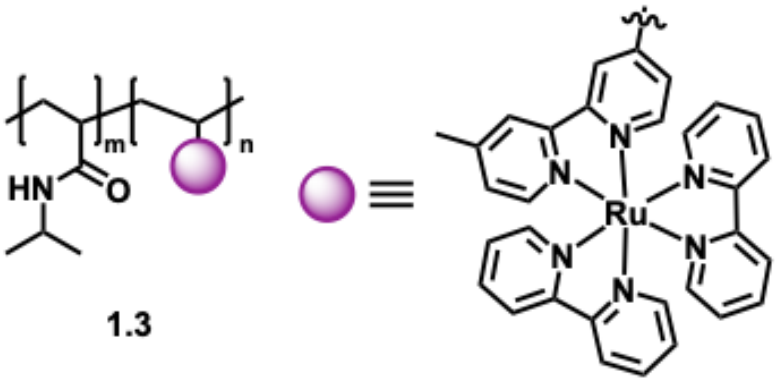


Figure 1.3. Schematic Representation of Metallopolymer Applications. Adapted from *Prog. Polym. Sci.* 2021, 119, 101428

Scheme 1.1. Redox controlled self-assembly of **1.2**



1.2



1.3

Figure 1.4. Block Copolymer 1.3

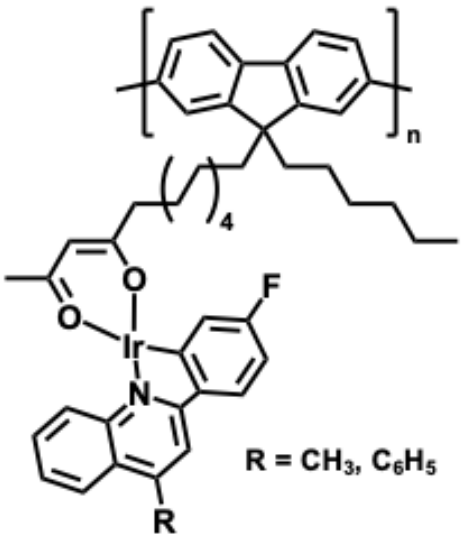
also found to respond to redox stimuli, corresponding to swelling and deswelling of the gel with the Ru^{II}/Ru^{III} cycle, and the development of these materials holds promise for optical, rheological, and biomedical applications.

Optical Materials

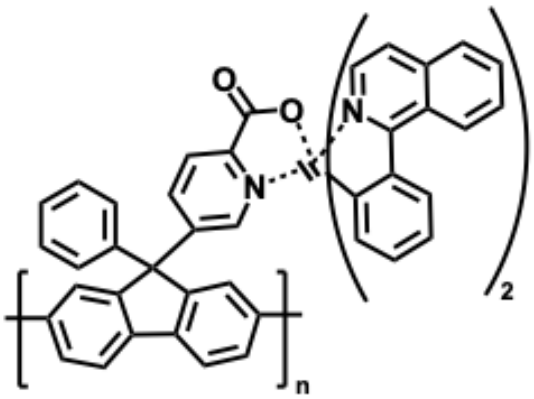
Metallopolymers have found use in optical materials, allowing for the synthesis of many light emitting devices. The ability to emit white light from a single material has proven to be a challenge; however, the Wang group has reported the combination of a blue-fluorescent polyfluorene with orange-fluorescent iridium complexes in the side chains (**1.4**; Figure 1.5)to arrive at the desired emission of white light.[61] The synthesis of these materials was achieved by doping small amounts of the iridium complex into the polymer as a chelate after the polymer was synthesized, and the efficiency of photoluminescence in these polymers was directly related to the amount of iridium contained in the polymer network, with very low (< 3 mol%) loadings of iridium providing the best emission properties. Along with this, Zhang and Cao have reported utilization of a combination of green- and red- emitting polyfluorenes (**1.5**; Figure 1.5) to achieve the emission of white light from metallopolymers.[62] The materials were synthesized via iterative Suzuki couplings to combine the green-emitting fluorene backbone with a red-emitting iridium complex. The electroluminescence of these materials was studied, and pure white light emissions could be achieved when loadings of the fluorene unit were about 99.9 mol %. However, these materials exhibited lower electroluminescent efficiency as compared to polymers with the fluorophore in the backbone and the phosphor in the side chain. Finally, Shu and coworkers reported the synthesis of white light emitting metallopolymers utilizing a balance of red-, green-, and blue-light emitting fluorene components with an iridium complex (**1.6**; Figure 1.5).[63] These materials exhibited moderate electroluminescent efficiency for the emission of white light when compared to non-conjugated platinum-containing polymers that are often used in polymer light emitting devices.

Energy Storage and Conversion

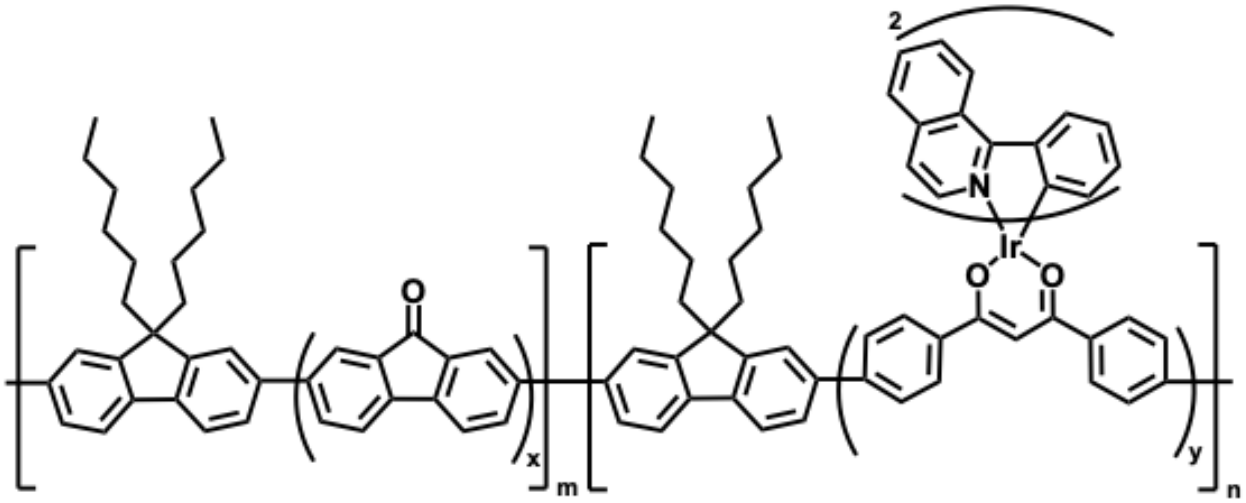
Further, metallopolymers have been used in devices for both energy conversion and energy storage. To this end, there has been significant work utilizing ferrocene moieties in



1.4



1.5



1.6

Figure 1.5. White-Light Emitting Polymers 1.4, 1.5, and 1.6

polymers to take advantage of its inherent redox properties. Schubert and coworkers have shown that poly(fluorenylethynylene) copolymers including pendant ferrocene moieties (**1.7**; Figure 1.6) can be used as cathodic materials in electrochemistry.[64] Importantly, Sonogashira cross-coupling allowed for the synthesis of polymers ranging in number of active redox centers. These materials showed excellent charge transport properties, and they could be used in redox transformations for over 100 cycles while retaining high levels of electrical discharge capacity. Another approach by Choi has utilized a polymer backbone that is commonly used in organic thin film transistors – PFT2 (comprised of phenylene, fluorene, and thiophene monomer units) – which was modified by addition of a phenyl bromide functionalized ferrocene to incorporate the ferrocene into the polymer backbone during synthesis (**1.8**; Figure 1.6).[65] They were able to achieve the desired polymer in good yield (89%), and CV analysis of the material revealed two reversible redox events (attributed to ferrocene and the conjugated polymer backbone). This material tolerated on/off switching for over 100 cycles and exemplified semi-conducting behavior. These reports exemplify the numerous applications and advantages held by metallopolymers for energy.

Stimuli-Responsive Materials

In addition to optical- and electrochemical- stimuli, metallopolymers have been studied as stimuli-responsive materials for sensor and device design. Recent reports have allowed the incorporation of metals into polymers that react to a variety of stimuli, including temperature, pH, light, and others. For example, Lawrence has reported a vinyl ferrocene-block-vinyl anthracene copolymer (**1.9**; Figure 1.7)which can be utilized as a pH sensor.[66] The material showed good stability across a range of temperatures, and the non-pH-responsive ferrocenyl moiety could be utilized as a non-drifting reference electrode for comparison with the pH-responsive anthracene unit contained within the polymer. Another important example was reported by Demas, who showed that a ruthenium-based star polymer (**1.10**; Figure 1.7)could be used for oxygen sensing.[67] The star architecture was selected because Demas speculated it would provide higher degrees of homogeneity when compared to linear polymers. This material was deposited onto glass in the film state and its luminescence properties were measured via Stern-Vulmer quenching to measure its applicability as an oxygen sensor. Though an improvement from previous systems,[68,69] the ruthenium star polymer still could

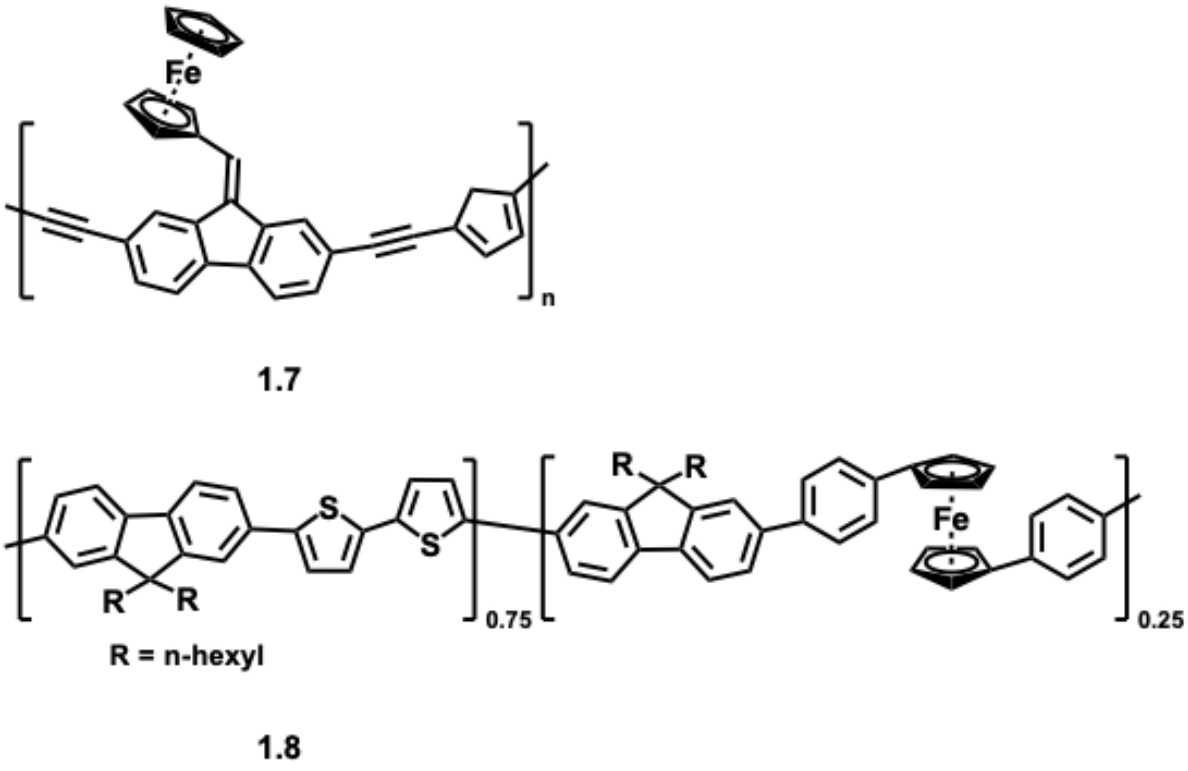


Figure 1.6. Polymers 1.7 for electrochemistry and 1.8 for semi-conductors

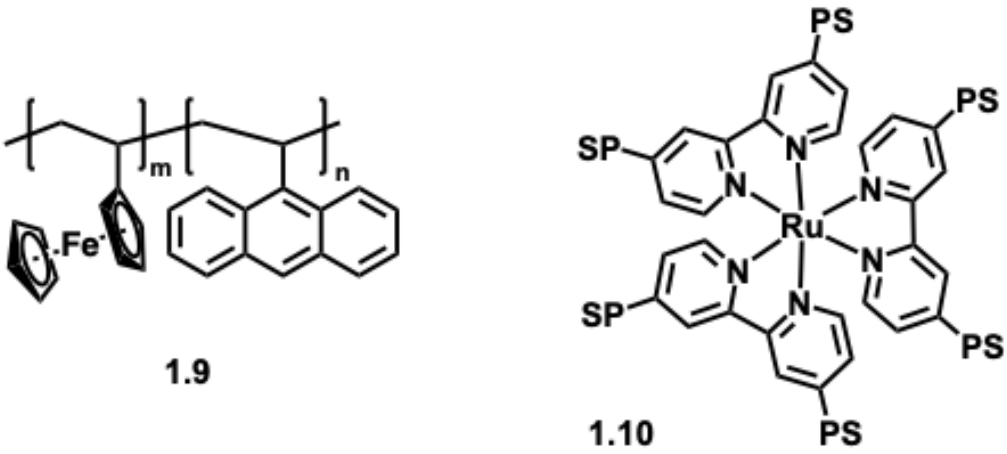


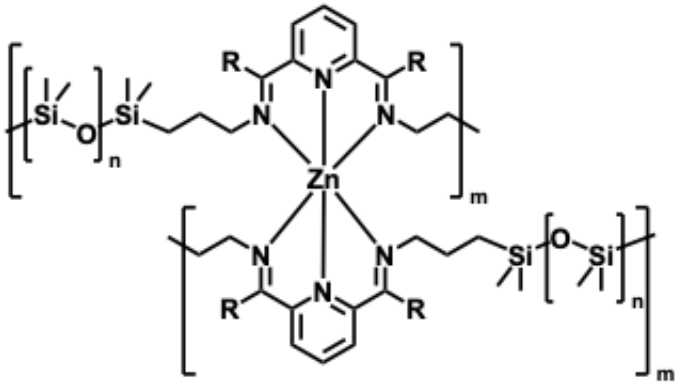
Figure 1.7. Metallopolymers 1.9 and 1.10 exhibiting Stimuli-Responsive behavior

not achieve homogeneity within the system, leading to complex analysis of data received. These examples suggest that metallopolymers hold promise as sensors.

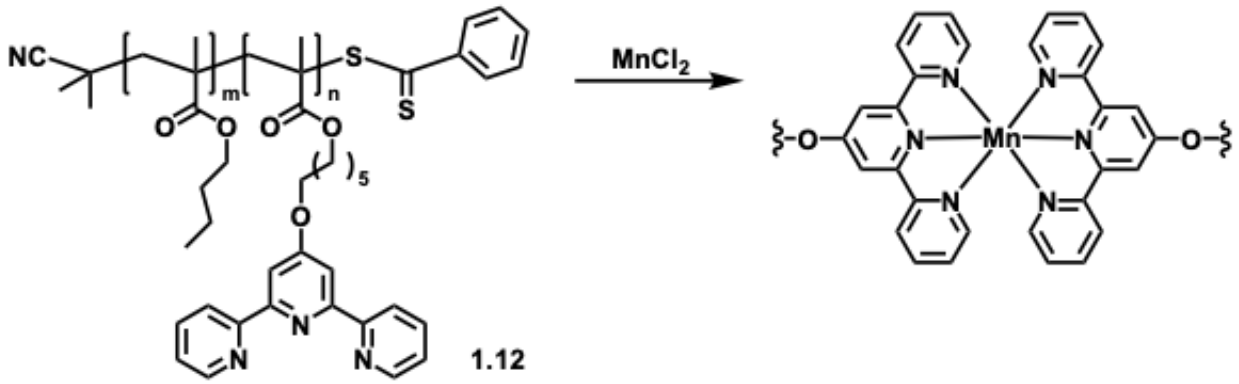
Self-healing Materials

Self-healing materials are utilized for a variety of applications. Various functional groups and strategies can be used to induce self-healing behavior in polymeric materials. Various functional groups are utilized in self-healing materials due to their reactivity; these functional groups are often copolymerized with reactive components as a means for chemically induced cross-linking. For example, thiols are often appended as polymer side chains, as redox manipulations can toggle the material between the free thiol and the dithiol linkage.[70] In addition, cyclic side chains such as furan and maleimide can be utilized for Diels-Alder to make these connections.[71] Further, photochemical manipulations are often used for self-healing to induce cross-linking in polymeric materials.[72] Self-healing properties have been studied extensively with a variety of organic polymers, however, the incorporation of metal containing fragments into these polymers has allowed for the expansion of the field due to the availability of new bonding motifs and interactions at the molecular level.[73,74] Utilization of zinc coordination complexes within poly(dimethylsiloxane) samples has allowed for self-healing behavior to be observed (**1.11**; Scheme 1.2), as after elastically breaking the sample, new cross-links were able to form between the zinc coordination sites, and the material regained its elastic properties.[75] Furthermore, the self-healing properties of manganese containing metallopolymers (**1.12**; Scheme 1.2)have been studied by Schubert after damaging with a scalpel or laser.[76] The self-healing capabilities of the manganese terpyridine polymer were greater than 75% in both cases, however, damage caused by the laser took longer to heal as the material was completely sublimated away at the damage site. Palladium hydrogels are often utilized as self-healing materials. For example, Yan has reported a carbon monoxide (CO)-responsive palladium hydrogel (**1.13**; Scheme 1.2) that exhibits reversible cross-linking when exposed to CO.[77] The utilization of metals in self-healing materials has helped expand the scope of these polymers, as well as improve their healing times and strength.

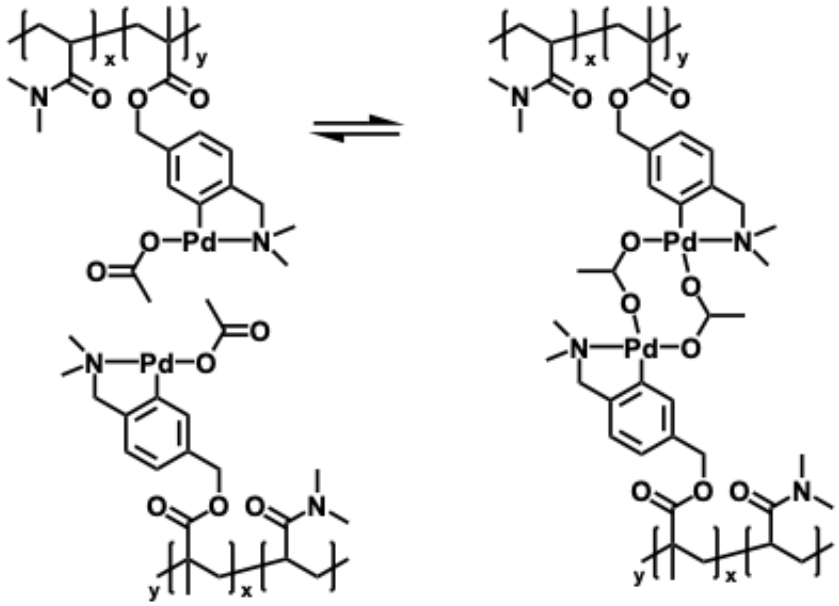
Scheme 1.2. Self-healing metallopolymers 1.11, 1.12, and 1.13



1.11



1.12



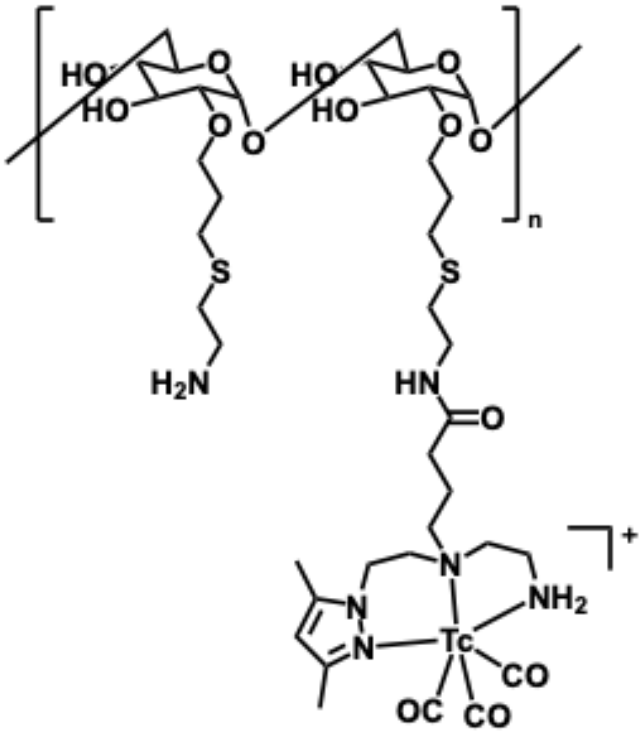
1.13

Biological Applications

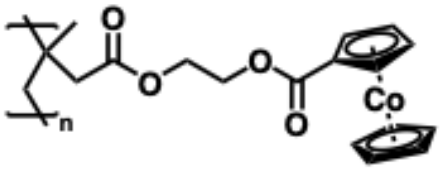
Metallopolymers have been utilized in biological applications in a variety of ways; as biomedical devices and as drug delivery systems. For example, technetium and rhenium tricarbonyl fragments have been added to dextran samples (**1.14**; Figure 1.8) for the targeting of lymph nodes at the site of cancerous tumors with high efficacy and *in vitro* stability in animal models.[78] Beyond this, metallopolymers have been utilized for their antibacterial properties. Tang has reported the utilization of cobaltocenium containing polymers (**1.15**; Figure 1.8) as effective leads in anti-MRSA technology.[48] When coupling the cobaltocenium polymers with antibiotics, the bioconjugated materials significantly outperformed either the antibiotics or the metallopolymers alone in terms of efficacy against MRSA. These examples articulate the importance of studies involving the incorporation of metallopolymers into biomedical research, as the addition of metals could increase the efficacy of many drugs.

Metallopolymers in Catalysis

At the molecular level, metallopolymers have also found use in catalysis for synthetic transformations. These transformations have involved cycloadditions, cross-couplings reactions, hydrogen evolution, and enzymology, among others. Ward has reported the enantioselective hydrogenation of acetamidoacrylic acid to acetamidoalanine with a rhodium tagged biotin catalyst with > 92% ee.[79] Further, Roelfes and coworkers developed a copper tagged bovine pancreatic protein to carry out enantioselective Michael additions and diels-alder reactions.[80] The copper tagged bovine protein allowed for the transformation of a variety of substrates to the desired compounds in good yield and moderate %ee (up to 85%) with low catalyst loadings (10% bovine peptide). The development of artificial metalloenzymes for synthetic transformations holds promise for greener routes in organometallic catalysis.[81] Work by Arnold has investigated changes to cytochrome P450 for C-H activation to form new C-N bonds.[82–84] Hartwig has reported the utilization of cytochrome P450 for C-H activation via carbene insertion.[85] Finally, Hyster has reported the reduction of carbonyls via a Ru-based reductase enzyme.[86] Furthermore, the intrinsic reactivity of metals suggests that polymer supported catalysts can increase recyclability and recovery of catalysts in metal-mediated transformations. Specifically, immobilization of a palladium complex within a polystyrene



1.14



1.15

Figure 1.8. Metallopolymers utilized for biological applications

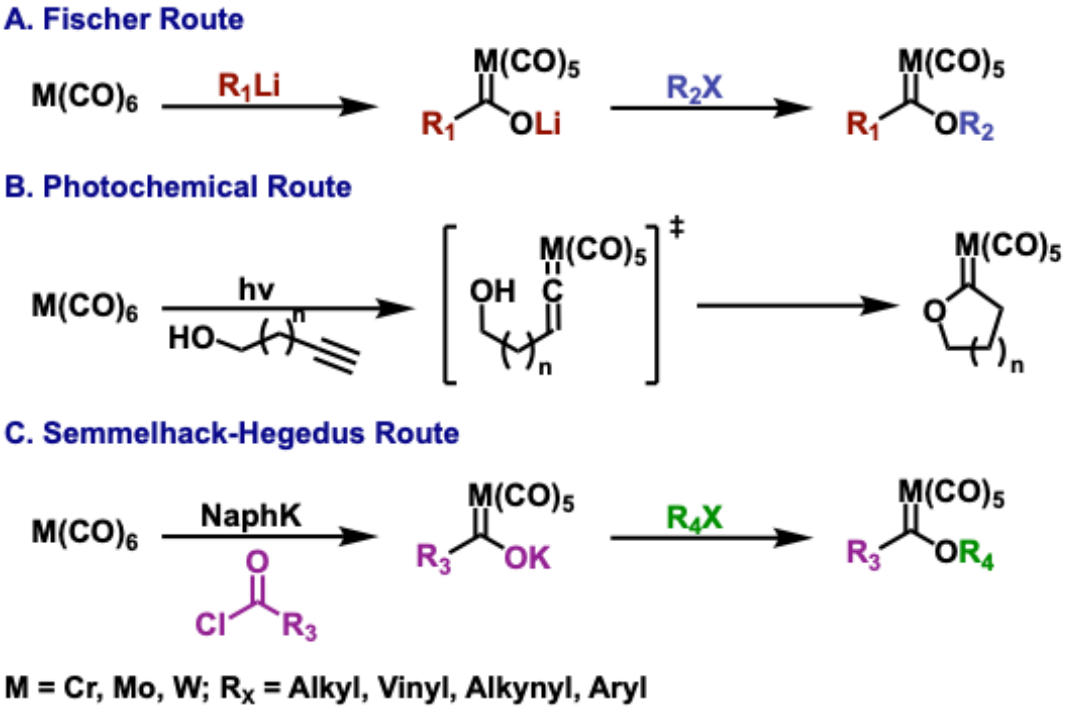
support has allowed for recyclable utilization of catalysts for Sonogashira and Suzuki-Miyaura cross-coupling chemistry, allowing for decreased catalyst loading and retention of catalytic activity.[87] These reports instill hope that utilization of metals in polymeric architectures will allow for the application of new chemistry in polymeric architectures.

Fischer Carbenes

While each of these examples of the applications of metallopolymers show that there are numerous ways these materials can be utilized, leveraging the inherent reactivity of these transition metals has not been the focus, which is surprising due to the impact of transition metal chemistry on synthetic transformations. Carbenes are often reactive intermediates that allow a variety of synthetic transformations to occur (e.g., cyclopropanations[88] and metathesis[89]), but persistent carbenes have been incorporated into polymeric architectures.[90,91] Fischer carbenes, specifically, have been largely overlooked for use in polymeric materials, despite their stability and synthetic utility (e.g. cycloadditions,[92–94] acid-base reactions,[95,96] benzannulations,[97–99] etc.). Incorporation of metallocarbenes into polymers would allow for utilization of these reactive handles for post-synthetic modification as well as use of these fragments for direct tailoring of the materials properties. The range of synthetic applications that Fischer carbenes hold could ultimately be used for post-synthetic modification of bulk materials. Therefore, access to well-defined metallocarbene-containing polymers could yield new platforms for the development of functional materials.

Fischer reported the first tungsten metallocarbene in 1964,[100] but other carbenes containing chromium,[101] molybdenum,[102] rhodium,[103] nickel,[104] and iron[104] were subsequently reported. These complexes typically tolerate ambient atmosphere and retain their synthetic utility for use in many reactions such as cycloadditions and metathesis. In addition to their synthetic utility and ease of handling, Fischer carbenes are isolobal with esters – leading to similar reactivity between the two functionalities. Fischer carbenes can be accessed through a variety of methods: the Fischer route, a photochemical route, and the Semmelhack-Hegedus route (Scheme 1.3). The Fischer route employs alkylation of the metal carbonyl with an alkyllithium reagent, followed by the addition of a secondary alkylation reagent, typically Meerwein salts, to achieve alkylation of the heteroatom (Scheme 1.3A). Fischer carbenes can be access photochemically by causing photolytic cleavage of CO from

Scheme 1.3. Synthetic Routes for Accessing Fischer Carbenes.



M = Cr, Mo, W; R_X = Alkyl, Vinyl, Alkynyl, Aryl

the metal center in the presence of an alkynol. The activated complex undergoes a rearrangement to provide cyclic carbenes (Scheme 1.3B). Finally, the Semmelhack-Hegedus route allows for the utilization of acid chlorides and amides as alkylating agents after a sodium naphthalenide reduction of the metal carbonyl (Scheme 1.3C).

Development of Fischer carbene containing polymers is an area that holds promise for discovery of new chemical space within materials science. The incorporation of these subunits into polymeric architectures would lead to useful additions to the class of functional materials, as these carbenes can serve as reactive groups or as persistent species. Fischer carbenes have been added to polymers in a post-synthetic manner,[105] however, the appendage of these carbenes was limited to chain ends, providing very little incorporation of metal into the overall material. Beyond this, there are only two examples of these metal species being utilized for polymerization. Macomber and colleagues first reported the autopolymerization of a tungsten vinyl carbene (**1.16**; Figure 1.9);[106] unfortunately, the isolated polymer was an intractable glass, only to be characterized after oxidative demetallation with DMSO to afford the corresponding acrylate. In addition, Masuda later reported the synthesis of oligomeric species via the polycondensation of α,ω-bis-carbenes (**1.17**; Figure 1.9).[107] These materials could only be achieved with limited range of degree of polymerization (DP; < 25 repeats) and high dispersity (Đ ~ 2.5). Beyond these limitations, the polymers were found to rapidly decompose at elevated temperatures (90 °C). Given the absence of further reports of Fischer carbene containing polymers in the literature, these examples (despite their flaws) instill hope that Fischer carbene metallopolymers will find applications in materials science because their synthetic utility could yield materials with wider applicability. For example, post-polymerization modifications generally require lengthy reaction times or have difficulty achieving good yield,[108] but with the unique reactivity of carbenes, the difficulty of the task may be obviated. As stated, polymers containing Fischer carbenes are known to undergo oxidative demetallation with DMSO, to full conversion with high yield.[106] Considering this example and the wealth of opportunities for post-polymerization modifications imparted by the synthetic utility of Fischer carbenes, these materials could provide an array of functional materials with varying reactivity. The expansion of the metallopolymer field to include Fischer carbene-

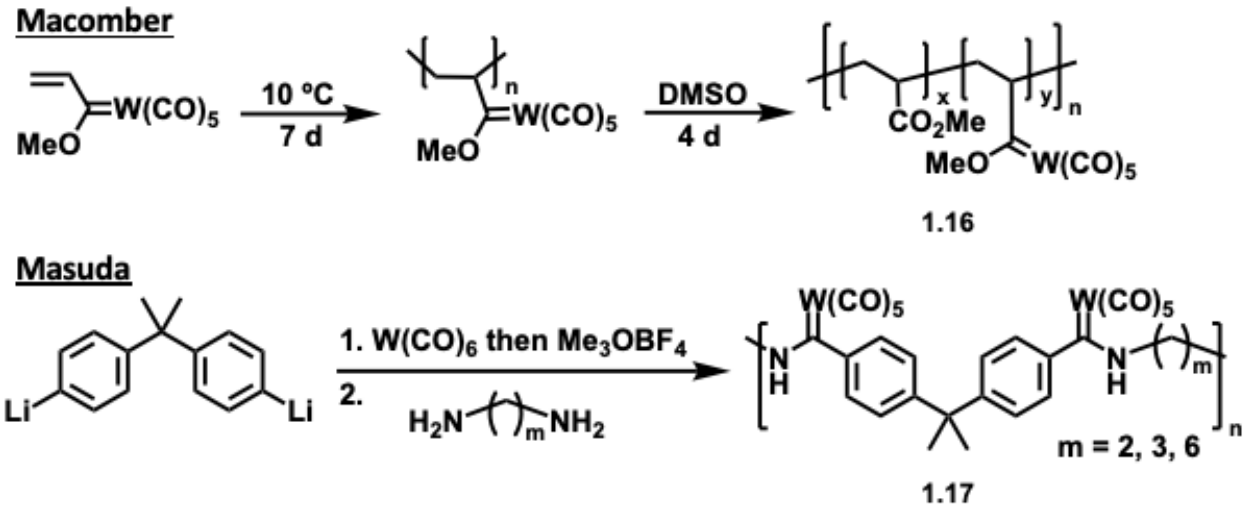


Figure 1.9. Previous reports of Fischer-carbene containing polymers

containing metallopolymers, in a broader sense, would add useful knowledge and applications to our chemical repertoire (e.g. stimuli-responsive behavior and post-processible materials).

In sum, Fischer carbenes are metal complexes that have their own rich synthetic utility. Additionally, these compounds are relatively easy to make, bench stable, and easy to purify. The reactivity that Fischer carbenes possess arises from the isolobal analogy between these metal carbenes and esters. Thus, we envision that Fischer carbenes can be incorporated into polymers via common ester polymerization techniques. ROMP of Fischer carbene containing monomers has been reported and is detailed in Chapter 2. Further investigation into the mechanistic differences between ROMP of chromium and tungsten carbenes was conducted and is reported in Chapter 3.

Post-Synthetic Modifications

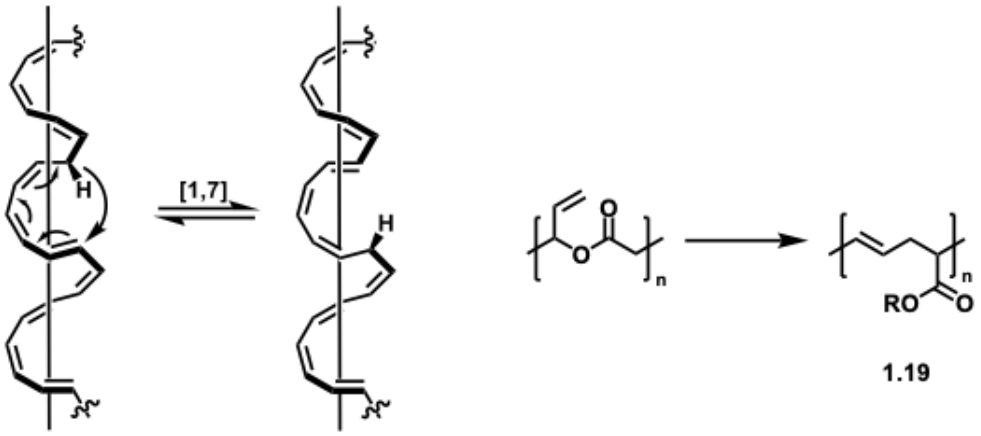
While polymerization of unique monomers can provide new functional materials, the direct modification of existing polymer scaffolds is a powerfully simple method for tuning material properties. Post-synthetic modifications of polymers involve harnessing a polymer's reactivity to perform synthetic manipulations, and these studies have investigated the effects of functionalization after polymerization, which has led to generation of new materials with respect to both repeating unit and overall architecture. There have been many examples of post polymerization modifications that modify polymer side chains, including diels-alder reactions[109] and thiol additions,[110] among others.[111,112] These examples further exemplify the principle that structure dictates function, providing insight into how incorporation of new functionalities into polymer backbones affects the overall materials properties. Many examples involving the functionalization of polymer end groups utilize or etherifications to append long chains to the ends of polymers. Other examples have shown that polymer end groups can be utilized to grow brush polymers via controlled radical polymerizations. There are also examples of appending a PEG chain to the terminal ends of a polymer to induce water solubility or self-assembly in desirable solvents. These transformations all have some manner of affecting overall material properties. The methodologies used in post-polymerization modifications must be applied in much the same way that organic chemists undergo reaction optimization. In a sense, these post-polymerization modifications are simply organic chemistry

on macromolecules. Knowing this, there are other factors to consider beyond optimizing yield and conversion. Oftentimes, post-polymerization modifications can lead to intractable materials, or materials that have vastly different solubilities or behaviors than their starting counterparts. These additional considerations must be handled carefully to allow for full characterization of materials as well as looking forward to the application and processibility of the materials in the future. In addition to their applied utility, synthesis of functional materials is an important topic because it can eliminate the need for synthesis and optimization of a unique polymer for every new application – which is achieved through a diversity-oriented synthesis approach, where a reactive handle is installed at outset, and a variety of other functionalities can be appended to the polymer to achieve the desired material properties. A brief survey of relevant literature follows to highlight precedent and opportunities for growth.

Post Polymerization Modifications Utilizing Pericyclic Reactions

Pericyclic reactions are powerful transformations that have been utilized for the synthesis of a variety of small molecule targets due to their ability to generate both structural and stereochemical complexity. The application of this class of reactions to polymers has been accomplished through Diels-Alder reactions with various substrates. A subset of pericyclic reactions – sigmatropic rearrangements – has been underutilized until recently. Roald Hoffmann postulated that the use of sigmatropic rearrangements in polymers would amount to a wide range of synthetic and materials applications and reported the computational work to support his hypothesis (**1.18**; Scheme 1.4).[113–117] Despite this, few of examples of sigmatropic rearrangements on polymers have been reported. Zhukhovitskiy has reported utilization of an Ireland-Claisen rearrangement in polymer architectures to provide new vinyl polymers with pendent esters (**1.19**; Scheme 1.4) from polyester containing materials.[118] The process utilizes mild conditions to induce a sigmatropic rearrangement within the polymer backbone as a form of skeletal editing. Furthermore, the T_g of the resultant materials changed drastically when compared to the starting polymers. Swager has reported synthesis of graphenic materials through a Johnson-Claisen rearrangement (**1.20**; Scheme 1.4).[119] Graphene oxide was functionalized via an etherification, followed by the rearrangement. While graphene oxide is considered an insulator, the functionalized material exhibited conductive

Scheme 1.4. Pericyclic rearrangements in polymers

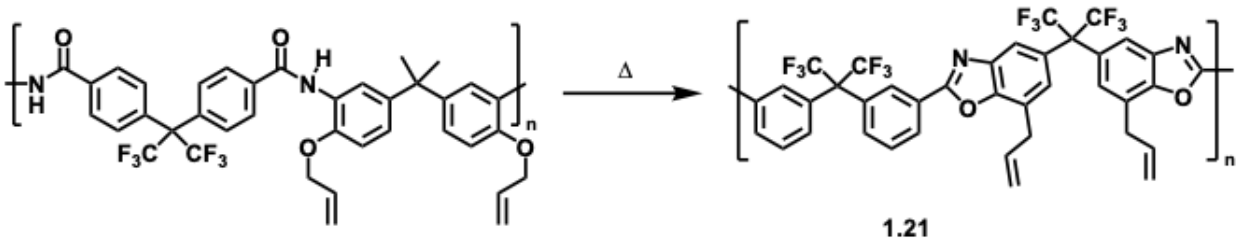


1.18

1.19



1.20



1.21

behavior. In addition, the post-claisen materials could be harnessed for further functionalization under various conditions. Further, the thermal Claisen rearrangement of functionalized polyamides has been reported by Abetz (**1.21**; Scheme 1.4).[120] These materials exhibited reactivity that could be harnessed for further modification as well. Abetz has also reported the thermal rearrangement of ortho-allyloxypolyimides.[121] In this case, the thermal rearrangement could be utilized to promote cross-linking of materials, leading to an increase in the thermal stability of the materials. Though these examples are excellent, the scope of these reactions is limited to Claisen and Claisen-type rearrangements. Harnessing the power of these rearrangements could lead to significant advances in the field of polymer modification.

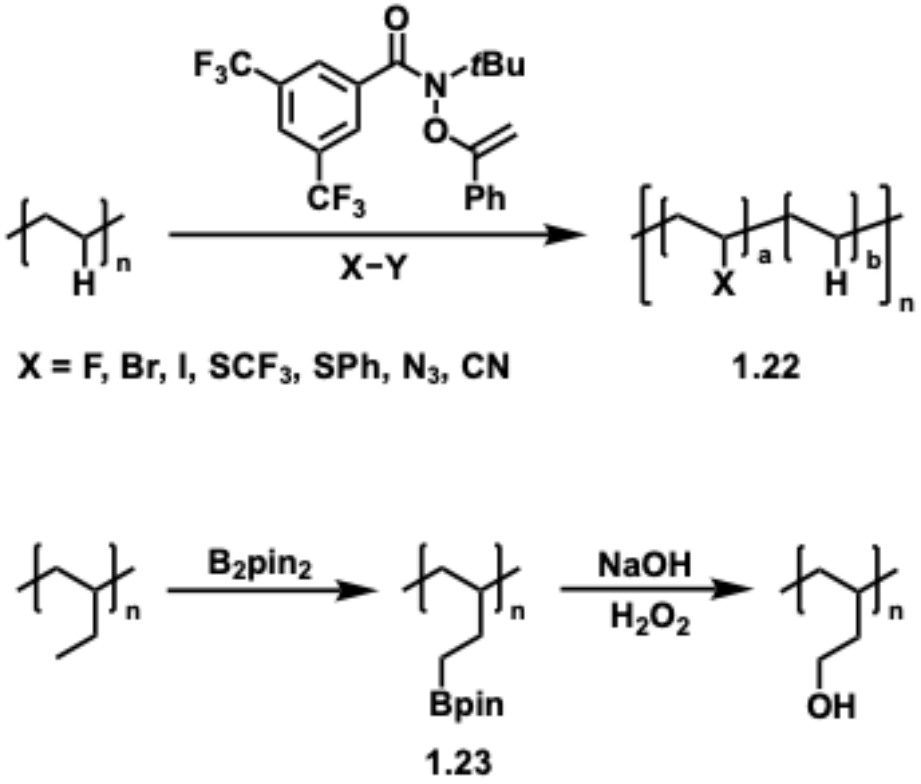
Post Polymerization Modifications Utilizing C-H Activation

Post-polymerization modification has been utilized for many purposes, and these transformations can greatly impact the properties of a polymer, even with low amounts of functionalization, as shown by Leibfarth[122] and Hillmyer.[123] Recently, Leibfarth has exemplified diversification of C-H bonds through radical chain transfer with a hydroxamate catalyst (**1.22**; Scheme 1.5).[124] Further, these reactions conditions could even be applied to consumer plastics. Hillmyer and Hartwig have shown the Rh-catalyzed C-H activation of polypropylenes to provide boronic ester functionalized materials that could be utilized for further modification to provide alcohol functionalized polypropylene (**1.23**; Scheme 1.5). [123] This methodology is applicable towards both tactic and atactic materials and the newly appended alcohol groups could be utilized to for appending further functionality to the side chains. These examples show that minor changes in polymer architectures can lead to massive changes in the materials properties, and therefore, applications. There are many types of organic transformations that have been studied as means of post-polymerization modification, among which are methods that append new functionalities to polymer side chains, functionalize the polymer's end group, and edit the polymer's backbone.

Post-Polymerization Modification: Boron-Containing Materials

Beyond organic monomers and metal moieties are main group elements. Metalloids have been incorporated into polymers to impart unique chemical and physical properties in

Scheme 1.5. Polyolefin upcycling through C-H activation



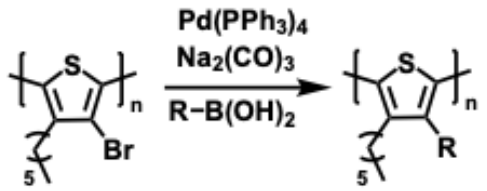
the same manner as their organic and metallic counterparts. Boron,[125–127] silicon,[128,129] germanium,[130,131] arsenic,[132,133] antimony,[134] and tellurium[135,136] have all been incorporated into polymer networks with a host of unique applications. Of these, borylated polymers are particularly attractive candidates for functional materials (due to the rich synthetic utility of boron). Boron-containing functionalities have been used in many synthetic transformations, such as hydroboration,[137–140] as well as many multicomponent reactions such as Petasis[141,142] and Zweifel[143] chemistry, and even more to include Matteson homologations[144–146] and Suzuki cross coupling chemistry.[147–149] Each of these reactions has had a profound impact on the synthetic community, yet the application of these transformations to polymer architectures has been limited.

There has been significant work in the field of boron containing polymers with far reaching impacts in a variety of applications,[127] including biomedical research,[13] stimuli-responsive materials,[126] and storage.[125] Beyond this, utilizing the unique chemical properties that are inherently possessed by boron containing materials has proven useful as of late in synthetic transformations in polymer chemistry. The extension of these powerful transformations into polymer synthesis could have a great impact on the various functionalities available to polymer chemists for the investigation of how various functionalities impact polymer properties.

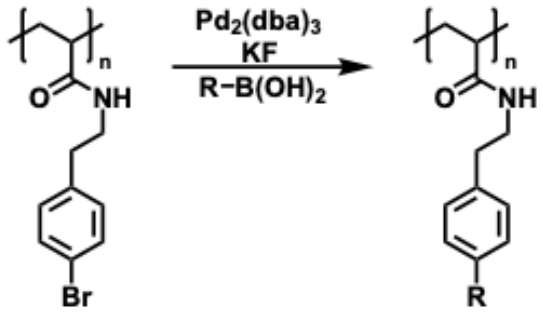
Several reports have utilized bromide-functionalized polymers to promote Suzuki-Miyaura cross-coupling with small molecule boronates. Holdcroft showed the functionalization of polythiophenes (**1.24**; Scheme 1.6) with high degrees of functionalization (99%) and 11 different substrates.[150] Later, Magenau reported cross-coupling with polyacrylamides (**1.25**; Scheme 1.6) with 11 substrates, achieving up to 90% functionalization.[151] Finally, Sumerlin reported the functionalization of styrenyl bromides (**1.26**; Scheme 1.6) with 4 boronic ester substrates with high degrees of functionalization (95%).[152]

Recently, Jacobs and Brantley reported the polymerization of allenyl boronate systems.[153] In this report, an allenyl boronic ester was polymerized with a Ni catalyst (ref for endo) to high yield and conversion (**1.27**; Scheme 1.6). These materials exhibited living character, allowing for construction of complex architectures (block copolymers). Furthermore, these polymers were amenable to post-polymerization modification via Suzuki-

Scheme 1.6. Examples of Suzuki cross-coupling in polymer architectures



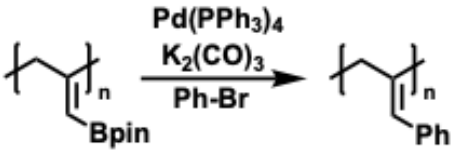
1.24



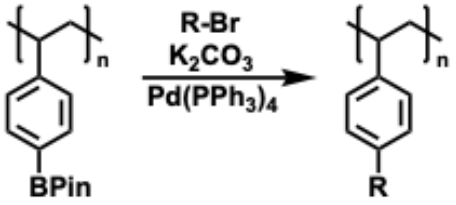
1.25



1.26



1.27



1.28

Miyaura coupling. Thermal and mechanical properties could also be modulated via incorporation of other monomers, making these materials excellent candidates for functional materials. The utility of these materials has exemplified the importance of synthesizing polymers with C—B motifs incorporated within.

Afterwards, Jacobs and Brantley reported the diversification of polymeric materials through Suzuki-Miyaura coupling on phenyl boronic ester containing polymers.[154] The borylated polystyrenes could be prepared in good yield and conversion (**1.28**; Scheme 1.6). The Suzuki-Miyaura coupling is reported with a substrate scope including 12 different targets, showing that a wide range of aromatic, heteroaromatic, and vinylic substrates could be utilized, while observing high conversions and mass recoveries in most cases. Furthermore, the coupled products could be used for a second round of synthetic transformations. These borylated polystyrenes have provided access to functional materials through the diversification of polymer scaffolds, allowing for the alleviate of the need to polymerize unique monomers each time a new polymer is needed, as well as expand the methodology toolbox for synthetic polymer chemists in achieving high degrees of post-polymerization modification in a robust manner.

One particular transformation that utilizes boron-containing functionalities is the Brown Allylation.[155] Brown first reported this rearrangement reaction in 1982,[156] and further investigations have shown how asymmetric variants can be utilized.[157,158] One of the most important features within the mechanism for the allylation is that there is a chair-like transition state between the aldehydes and the allylic boronates. These reactions can also form homoallylic amines through the utilization of imines. Since Brown's seminal report, this transformation has been employed in a variety of syntheses including antibiotics. Despite the simplicity of this powerful transformation, it has yet to be applied to polymeric architectures. Therefore, we envision the use of allylic boronate esters to promote rearrangements in polymer scaffolds. The progress in these endeavors is detailed in Chapter 4.

Electrochemical Post-Polymerization Modification

Another way to modify polymers after they have been synthesized is through the development of methodologies for the functionalization of polymers. Polymer functionalization is currently accomplished through enzymolysis,[159,160] ozonolysis,[161,162] and

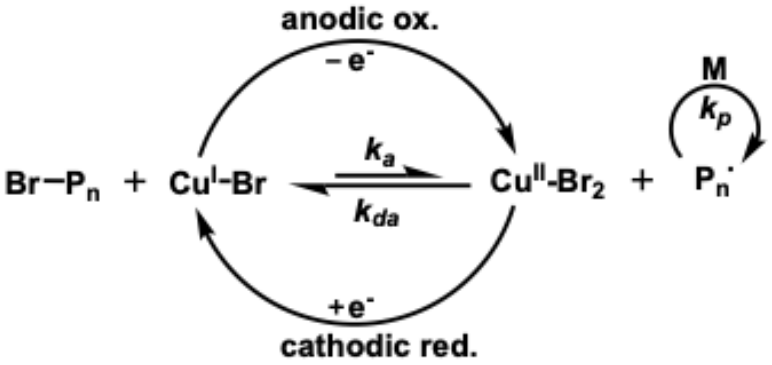
photochemistry,[163,164] among various other chemical and physical methods.[165,166] Each of these examples has their pros and cons, due to the amount of time necessary for the transformation, the use of harsh chemicals or temperatures, or the lack of widely available resources.

Electrochemistry is a powerful tool for chemists and has been utilized for many applications and transformations. Pioneering groups such as Song Lin and Phil Baran have laid the groundwork for applying electrochemistry to organic synthesis. These synthetic transformations have allowed organic chemists to access a variety of functionalizations. While these discoveries have helped expand the chemical space available to synthetic organic chemists, these methodologies have yet to be applied to synthetic polymer chemistry – an area where functionalization and modification of material structure allows for significant changes in material function and application.

Electrochemical organic synthesis has been a blossoming area of research in the 21st century.[167–169] The various potentials and electrode materials available have made the synthesis of new organic compounds feasible, including many functional groups and chemical architectures. In terms of oxidations, amines,[170,171] amides,[172,173] alcohols,[174,175] carbonyls,[176–178] and various acids[179,180] can be anodically oxidized with good conversion and recovery. On the other hand, reductions have also been quite popular. Reduction of aldehydes and ketones,[181] esters and amides,[182,183] and alkenes[184,185] have all been reported with high fidelity and facile workup. Furthermore, the sequential pairing of anodic oxidation and cathodic reduction has allowed for the synthesis of new compounds (e.g., nitriles, ethers) in a one-pot approach. Even still, there has been a great body of work showing that electrochemical transformations give rise to facile umpolung chemistry.[186–188] Given the broad synthetic utility available to organic chemists via electrochemistry, the scarcity of electrosynthetic transformations that have been applied to polymer chemistry is quite surprising.

Matyjaszewski has reported eATRP (Scheme 1.7),[189,190] in which the active copper species that aids in polymerization is toggled between its charge states via electrochemical charge. The utilization of eATRP has allowed for polymerization of monomers that are sensitive to heat or light. Aside from this report, electrochemical methodology on polymers is limited.

Scheme 1.7. eATRP



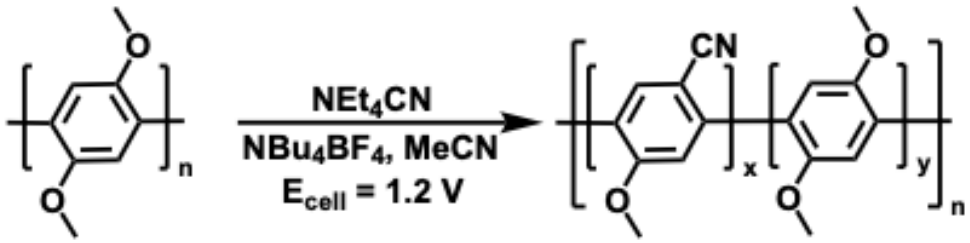
The utilization of electrochemistry for synthetic polymer chemistry has been largely limited to conducting materials, rather than synthetic transformations of polymers. Currently, examples that do include the synthetic transformations of polymers includes cyanations (**1.29**; Scheme 1.8) and chlorinations (**1.30**; Scheme 1.8) in the film state.[191–194] These examples allowed for functionalization in modest yields (17% and 72%, respectively) and were able to be conducted heterogeneously. In addition, Duan reported tandem hydrolysis-electrolysis of PET (**1.31**; Scheme 1.8) to provide H_2 fuel.[195] We discovered that electrochemical editing of soft polymers can enable both functionalization and polymer degradation (Chapter 5).

Research Objectives

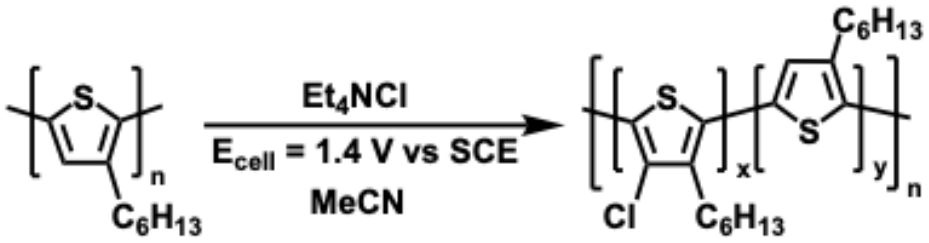
Here, we explore new chemical space with respect to polymeric materials. The impact of this work will allow synthetic polymer chemists to explore new reactivity and methodologies, as well as provide new materials with potential applications impacting a wide range of occupations. The overall objective of this research is to determine how incorporation of unique synthetic building blocks into polymer architectures affects material properties. Specifically, Fischer carbenes will be used for the polymerization of unique monomers, Brown allylation chemistry will be studied as a post-synthetic modification on boron-containing polymers, and electrochemistry will be studied as a new methodology for the manipulation of polymer backbone modifications.

In Chapter 2, a summary of the initial work towards the ring opening metathesis polymerization of Fischer carbenes is described. We want to understand the effects of incorporation of Fischer carbenes on material properties, as well as harness their reactivity for modification of polymeric materials. In Chapter 3, divergent reactivity between chromium and tungsten carbenes in ROMP is investigated. A deeper mechanistic understanding of the difference between these carbenes is in progress. Chapter 4 details the investigation of post polymerization modifications utilizing Brown allylations. The design, synthesis, and utilization of a model polymer scaffold has been investigated. The effects of electronics and sterics with respect to substrate scope is also analyzed. In Chapter 5, the development of an electrochemical method for polymer degradation and functionalization is described. The impact of electrochemical polymer modification has been determined.

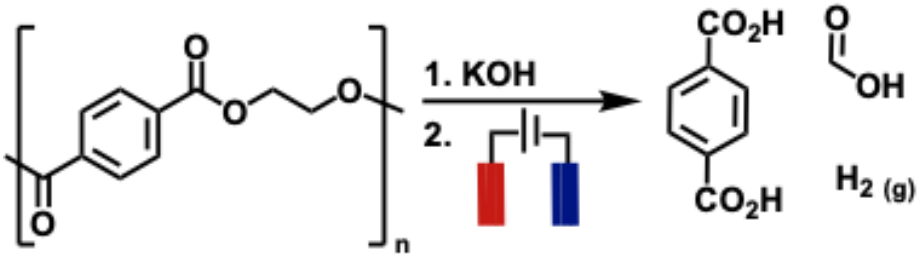
Scheme 1.8. Electrochemical modifications of polymers



1.29



1.30



1.31

References

(1) Wallin, T. J.; Pikul, J.; Shepherd, R. F. 3D Printing of Soft Robotic Systems. *Nature Reviews Materials* **2018**, *3* (6), 84–100. https://doi.org/10.1038/s41578-018-0002-2.

(2) Kim, Y.; Yuk, H.; Zhao, R.; Chester, S. A.; Zhao, X. Printing Ferromagnetic Domains for Untethered Fast-Transforming Soft Materials. *Nature* **2018**, *558* (7709), 274–279. https://doi.org/10.1038/s41586-018-0185-0.

(3) Wang, Z.; Li, H.; Tang, Z.; Liu, Z.; Ruan, Z.; Ma, L.; Yang, Q.; Wang, D.; Zhi, C. Hydrogel Electrolytes for Flexible Aqueous Energy Storage Devices. *Advanced Functional Materials* **2018**, *28* (48), 1804560. https://doi.org/10.1002/ADFM.201804560.

(4) Zeng, W.; Tao, X. M.; Chen, S.; Shang, S.; Chan, H. L. W.; Choy, S. H. Highly Durable All-Fiber Nanogenerator for Mechanical Energy Harvesting. *Energy & Environmental Science* **2013**, *6* (9), 2631–2638. https://doi.org/10.1039/C3EE41063C.

(5) Acome, E.; Mitchell, S. K.; Morrissey, T. G.; Emmett, M. B.; Benjamin, C.; King, M.; Radakovitz, M.; Keplinger, C. Hydraulically Amplified Self-Healing Electrostatic Actuators with Muscle-like Performance. *Science (1979)* **2018**, *359* (6371), 61–65. https://doi.org/10.1126/SCIENCE.AAO6139/SUPPL_FILE/AAO6139S8.MP4.

(6) Qiu, Y.; Zhang, E.; Plamthottam, R.; Pei, Q. Dielectric Elastomer Artificial Muscle: Materials Innovations and Device Explorations. *Accounts of Chemical Research* **2019**, *52*, 316–325. https://doi.org/10.1021/ACS.ACCOUNTS.8B00516/ASSET/IMAGES/LARGE/AR-2018-005169_0013.JPEG.

(7) Li, J.; Geng, L.; Wang, G.; Chu, H.; Wei, H. Self-Healable Gels for Use in Wearable Devices. *Chemistry of Materials* **2017**, *29* (21), 8932–8952. https://doi.org/10.1021/ACS.CHEMMATER.7B02895/ASSET/IMAGES/LARGE/CM-2017-02895R_0017.JPEG.

(8) Wang, C.; Sim, K.; Chen, J.; Kim, H.; Rao, Z.; Li, Y.; Chen, W.; Song, J.; Verduzco, R.; Yu, C. Soft Ultrathin Electronics Innervated Adaptive Fully Soft Robots. *Advanced Materials* **2018**, *30* (13), 1706695. https://doi.org/10.1002/ADMA.201706695.

(9) Cooke, M. E.; Jones, S. W.; ter Horst, B.; Moiemen, N.; Snow, M.; Chouhan, G.; Hill, L. J.; Esmaeli, M.; Moakes, R. J. A.; Holton, J.; Nandra, R.; Williams, R. L.; Smith, A. M.; Grover, L. M. Structuring of Hydrogels across Multiple Length Scales for Biomedical Applications. *Advanced Materials* **2018**, *30* (14), 1705013. https://doi.org/10.1002/ADMA.201705013.

(10) Chan, B. Q. Y.; Low, Z. W. K.; Heng, S. J. W.; Chan, S. Y.; Owh, C.; Loh, X. J. Recent Advances in Shape Memory Soft Materials for Biomedical Applications. *ACS Applied Materials and Interfaces* **2016**, *8* (16), 10070–10087. https://doi.org/10.1021/ACSAMI.6B01295/ASSET/IMAGES/LARGE/AM-2016-01295N_0018.JPEG.

(11) Hsu, P. C.; Kong, D.; Wang, S.; Wang, H.; Welch, A. J.; Wu, H.; Cui, Y. Electrolessly Deposited Electrospun Metal Nanowire Transparent Electrodes. *J Am Chem Soc* **2014**, *136* (30), 10593–10596. https://doi.org/10.1021/JA505741E/SUPPL_FILE/JA505741E_SI_001.PDF.

(12) Yin, M. jie; Gu, B.; An, Q. F.; Yang, C.; Guan, Y. L.; Yong, K. T. Recent Development of Fiber-Optic Chemical Sensors and Biosensors: Mechanisms, Materials, Micro/Nano-Fabrications and Applications. *Coordination Chemistry Reviews* **2018**, *376*, 348–392. https://doi.org/10.1016/J.CCR.2018.08.001.

(13) Cambre, J. N.; Sumerlin, B. S. Biomedical Applications of Boronic Acid Polymers. *Polymer (Guildf)* **2011**, *52* (21), 4631–4643. https://doi.org/10.1016/J.POLYMER.2011.07.057.

(14) Stuart, M. A. C.; Huck, W. T. S.; Genzer, J.; Müller, M.; Ober, C.; Stamm, M.; Sukhorukov, G. B.; Szleifer, I.; Tsukruk, V. v.; Urban, M.; Winnik, F.; Zauscher, S.; Luzinov, I.; Minko, S. Emerging Applications of Stimuli-Responsive Polymer Materials. *Nature Materials* **2010**, *9* (2), 101–113. https://doi.org/10.1038/nmat2614.

(15) Marder, S. R.; Perry, J. W. Molecular Materials for Second-Order Nonlinear Optical Applications. *Advanced Materials* **1993**, *5* (11), 804–815. https://doi.org/10.1002/adma.19930051104.

(16) Li, J.; Wong, W. Y.; Tao, X. M. Recent Advances in Soft Functional Materials: Preparation, Functions and Applications. *Nanoscale* **2020**, *12* (3), 1281–1306. https://doi.org/10.1039/C9NR07035D.

(17) Fréchet, J. M. J. Functional Polymers and Dendrimers: Reactivity, Molecular Architecture, and Interfacial Energy. *Science* **1994**, *263* (5154), 1710–1715.

(18) Carraher, C. E.; Seymour, R. B. *Structure—Property Relationships in Polymers*; Springer Science & Business Media, 2012.

(19) Staudinger, H. Über Polymerisation. *Berichte der deutschen chemischen Gesellschaft (A and B Series)* **1920**, *53* (6), 1073–1085. https://doi.org/10.1002/CBER.19200530627.

(20) Manners, I. Polyferrocenylsilanes: Metallopolymers for Electronic and Photonic Applications. *Journal of Optics A: Pure and Applied Optics* **2002**, *4* (6), S221. https://doi.org/10.1088/1464-4258/4/6/356.

(21) Paquet, C.; Cyr, P. W.; Kumacheva, E.; Manners, I. Polyferrocenes: Metallopolymers with Tunable and High Refractive Indices. *Chemical Communications* **2004**, *0* (2), 234–235. https://doi.org/10.1039/B311934C.

(22) Ho, C. L.; Wong, W. Y. Metal-Containing Polymers: Facile Tuning of Photophysical Traits and Emerging Applications in Organic Electronics and Photonics. *Coordination Chemistry Reviews* **2011**, *255* (21–22), 2469–2502. https://doi.org/10.1016/J.CCR.2011.01.052.

(23) Sun, Z.; Li, J.; Wong, W.-Y.; Sun, Z.; Wong, Y. W.; Li, J. W.; Wong, Y. Emerging Organic Thermoelectric Applications from Conducting Metallopolymers. *Macromolecular Chemistry and Physics* **2020**, *221* (12), 2000115. https://doi.org/10.1002/MACP.202000115.

(24) Chawdhury, N.; Köhler, A.; Friend, R. H.; Younus, M.; Long, N. J.; Raithby, P. R.; Lewis, J. Synthesis and Electronic Structure of Platinum-Containing Poly-Ynes with Aromatic and Heteroaromatic Rings. *Macromolecules* **1998**, *31* (3), 722–727. https://doi.org/10.1021/MA971267U.

(25) Tse, C. W.; Man, K. Y. K.; Cheng, K. W.; Mak, C. S. K.; Chan, W. K.; Yip, C. T.; Liu, Z. T.; Djurišić, A. B. Layer-by-Layer Deposition of Rhenium-Containing Hyperbranched

Polymers and Fabrication of Photovoltaic Cells. *Chemistry European Journal* **2007**, *13* (1), 328–335. https://doi.org/10.1002/chem.200600838.

(26) Roberts, R. L.; Schwich, T.; Corkery, T. C.; Cifuentes, M. P.; Green, K. A.; Farmer, J. D.; Low, P. J.; Marder, T. B.; Samoc, M.; Humphrey, M. G. Organometallic Complexes for Nonlinear Optics. 45. Dispersion of the Third-Order Nonlinear Optical Properties of Triphenylamine-Cored Alkynylruthenium Dendrimers. *Advanced Materials* **2009**, *21* (22), 2318–2322. https://doi.org/10.1002/adma.200803669.

(27) Resendes, R.; Berenbaum, A.; Stojevic, G.; Jäkle, F.; Bartole, A.; Zamanian, F.; Dubois, G.; Hersom, C.; Balmain, K.; Manners, I. Application of Ring-Opened Poly(Ferrocene)s as Protective Charge Dissipation Coatings for Dielectrics. *Advanced Materials* **2000**, *12* (5), 327–330. https://doi.org/10.1002/(SICI)1521-4095(200003)12:5<327::AID-ADMA327>3.0.CO;2-L.

(28) Liu, S.; Zhang, K.; Lu, J.; Zhang, J.; Yip, H.-L.; Huang, F.; Cao, Y. High-Efficiency Polymer Solar Cells via the Incorporation of an Amino-Functionalized Conjugated Metallopolymer as a Cathode Interlayer. *J. Am. Chem. Soc.* **2013**, *135*, 15326–15329. https://doi.org/10.1021/ja408363c.

(29) Zhang, H.-T.; Subramanian, P.; Fussa-Rydel, O.; Bebel, J. C.; Hupp, J. T. Electrochromic Devices Based on Thin Metallopolymeric Films. *Solar Energy Materials and Solar Cells* **1992**, *25* (3–4), 315–325. https://doi.org/10.1016/0927-0248(92)90076-2.

(30) Péter, M.; Hempenius, M. A.; Kooij, E. S.; Jenkins, T. A.; Roser, S. J.; Knoll, W.; Vancso, G. J. Electrochemically Induced Morphology and Volume Changes in Surface-Grafted Poly(Ferrocenyldimethylsilane) Monolayers. *Langmuir* **2004**, *20* (3), 891–894. https://doi.org/10.1021/LA035656V.

(31) Gu, H.; Mu, S.; Qiu, G.; Liu, X.; Zhang, L.; Yuan, Y.; Astruc, D. Redox-Stimuli-Responsive Drug Delivery Systems with Supramolecular Ferrocenyl-Containing Polymers for Controlled Release. *Coordination Chemistry Reviews* **2018**, *364*, 51–85. https://doi.org/10.1016/J.CCR.2018.03.013.

(32) Zhang, K. Y.; Liu, S.; Zhao, Q.; Huang, W. Stimuli–Responsive Metallopolymers. *Coordination Chemistry Reviews* **2016**, *319*, 180–195. https://doi.org/10.1016/J.CCR.2016.03.016.

(33) Lacroix, P. G.; Lin, W.; Wong, G. K. Poly(Vinylpyridine) and Related Polymers as Guests for Organotransition-Metal-Based NLO Chromophores. *Chemical Materials* **1995**, *7*, 1293.

(34) Arsenault, A. C.; Míguez, H.; Kitaev, V.; Ozin, G. A.; Manners, I. A Polychromic, Fast Response Metallopolymer Gel Photonic Crystal with Solvent and Redox Tunability: A Step Towards Photonic Ink (P-Ink). *Advanced Materials* **2003**, *15* (6), 503–507. https://doi.org/10.1002/adma.200390116.

(35) Calvert, J. M.; Meyer, T. J. Poly(Pyridyl)Ruthenium(II) Complexes of Poly(4-Vinylpyridine). Synthesis, Characterization, and Investigation of Optical and Electrochemical Properties. *Inorganic Chemistry* **1981**, *20* (1), 27–33. https://doi.org/10.1021/ic50215a008.

(36) Vandermeulen, G. W. M.; Kim, T. K.; Wang, Z.; Manners, I. Metallopolymer−Peptide Conjugates: Synthesis and Self-Assembly of Polyferrocenylsilane Graft and Block Copolymers Containing a β-Sheet Forming Gly-Ala-Gly-Ala Tetrapeptide Segment. *Biomacromolecules* **2006**, *7* (4), 1005–1010. https://doi.org/10.1021/BM050732P.

(37) Arimoto, F. S.; Haven, A. C. Derivatives of Dicyclopentadienyliron. *J Am Chem Soc* **1955**, *77* (23), 6295–6297. https://doi.org/10.1021/ja01628a068.

(38) Natanson, E. M.; Bryk, M. T. Metallopolymers. *Russian Chemical Reviews* **1972**, *41* (8), 671–686.

(39) Chiefari, J.; Chong, Y. K.; Ercole, F.; Krstina, J.; Jeffery, J.; Le, T. P. T.; Mayadunne, R. T. A.; Meijs, G. F.; Moad, C. L.; Moad, G.; Rizzardo, E.; Thang, S. H. Living Free-Radical Polymerization by Reversible Addition - Fragmentation Chain Transfer: The RAFT Process. *Macromolecules* **1998**, *31* (16), 5559–5562. https://doi.org/10.1021/MA9804951/ASSET/IMAGES/LARGE/MA9804951F00003.JPEG.

(40) Wang, J. S.; Matyjaszewski, K. Controlled/"Living" Radical Polymerization. Atom Transfer Radical Polymerization in the Presence of Transition-Metal Complexes. *J Am Chem Soc* **1995**, *117* (20), 5614–5615. https://doi.org/10.1021/JA00125A035/ASSET/JA00125A035.FP.PNG_V03.

(41) Kato, M.; Kamigaito, M.; Sawamoto, M.; Higashimura, T. Polymerization of Methyl Methacrylate with the Carbon Tetrachloride/Dichlorotris-(Triphenylphosphine)Ruthenium(II)/ Methylaluminum Bis(2,6-Di-Tert-Butylphenoxide) Initiating System: Possibility of Living Radical Polymerization. *Macromolecules* **1995**, *28* (5), 1721–1723. https://doi.org/10.1021/MA00109A056/ASSET/MA00109A056.FP.PNG_V03.

(42) Nguyen, S. B. T.; Johnson, L. K.; Grubbs, R. H.; Ziller, J. W. Ring-Opening Metathesis Polymerization (ROMP) of Norbornene by a Group VIII Carbene Complex in Protic Media. *J Am Chem Soc* **1992**, *114* (10), 3974–3975. https://doi.org/10.1021/JA00036A053/SUPPL_FILE/JA00036A053_SI_001.PDF.

(43) Schwab, P.; France, M. B.; Ziller, J. W.; Grubbs, R. H. A Series of Well-Defined Metathesis Catalysts–Synthesis of [RuCl2(□CHR′)(PR3)2] and Its Reactions. *Angewandte Chemie International Edition in English* **1995**, *34* (18), 2039–2041. https://doi.org/10.1002/ANIE.199520391.

(44) Schrock, R. R. High-Oxidation-State Molybdenum and Tungsten Alkylidyne Complexes. *Accounts of Chemical Research* **1986**, *19* (11), 342–348. https://doi.org/10.1021/AR00131A003/ASSET/AR00131A003.FP.PNG_V03.

(45) de Bettencourt-Dias, A.; Rossini, J. S. K. Ligand Design for Luminescent Lanthanide-Containing Metallopolymers. *Inorganic Chemistry* **2016**, *55*, 9954–9963. https://doi.org/10.1021/acs.inorgchem.6b00946.

(46) Paquet, C.; Cyr, P. W.; Kumacheva, E.; Manners, I. Polyferrocenes: Metallopolymers with Tunable and High Refractive Indices. *Chemical Communications* **2004**, *0* (2), 234. https://doi.org/10.1039/b311934c.

(47) Qu, R.; Suo, H.; Gu, Y.; Weng, Y.; Qin, Y. Sidechain Metallopolymers with Precisely Controlled Structures: Synthesis and Application in Catalysis. *Polymers (Basel)* **2022**, *14* (6), 1128. https://doi.org/10.3390/POLYM14061128.

(48) Zhang, J.; Chen, Y. P.; Miller, K. P.; Ganewatta, M. S.; Bam, M.; Yan, Y.; Nagarkatti, M.; Decho, A. W.; Tang, C. Antimicrobial Metallopolymers and Their Bioconjugates with Conventional Antibiotics against Multidrug-Resistant Bacteria. *J. Am. Chem. Soc.* **2014**, *136*, 4873–4876. https://doi.org/10.1021/ja5011338.

(49) Götz, S.; Zechel, S.; Hager, M. D.; Newkome, G. R.; Schubert, U. S. Versatile Applications of Metallopolymers. *Progress in Polymer Science* **2021**, *119*, 101428. https://doi.org/10.1016/J.PROGPOLYMSCI.2021.101428.

(50) Wang, Y.; Astruc, D.; Abd-El-Aziz, A. S. Metallopolymers for Advanced Sustainable Applications. *Chemical Society Reviews* **2019**, *48* (2), 558–636. https://doi.org/10.1039/C7CS00656J.

(51) Whittell, G. R.; Hager, M. D.; Schubert, U. S.; Manners, I. Functional Soft Materials from Metallopolymers and Metallosupramolecular Polymers. *Nature Materials* **2011**, *10* (3), 176–188. https://doi.org/10.1038/nmat2966.

(52) Paz-Simon, H. de; Chemtob, A.; Crest, F.; Croutxé-Barghorn, C.; Michelin, L.; Vidal, L.; Rigolet, S.; Lebeau, B. Thick Mesostructured Films via Light Induced Self-Assembly. *RSC Advances* **2012**, *2* (31), 11944–11952. https://doi.org/10.1039/C2RA21676K.

(53) Stenhammar, J.; Wittkowski, R.; Marenduzzo, D.; Cates, M. E. Light-Induced Self-Assembly of Active Rectification Devices. *Science Advances* **2016**, *2* (4). https://doi.org/10.1126/SCIADV.1501850/SUPPL_FILE/1501850_SM.PDF.

(54) Deng, C.; Fang, R.; Guan, Y.; Jiang, J.; Lin, C.; Wang, L. Sonication-Induced Self-Assembly of Flexible Tris(Ureidobenzyl)Amine : From Dimeric Aggregates to Supramolecular Gels. *Chemical Communications* **2012**, *48* (64), 7973–7975. https://doi.org/10.1039/C2CC33408A.

(55) Riaz, S.; Feng, W.; Khan, A. F.; Nawaz, M. H. Sonication-Induced Self-Assembly of Polymeric Porphyrin–Fullerene: Formation of Nanorings. *Journal of Applied Polymer Science* **2016**, *133* (24). https://doi.org/10.1002/APP.43537.

(56) Seguini, G.; Giammaria, T. J.; Lupi, F. F.; Sparnacci, K.; Antonioli, D.; Gianotti, V.; Vita, F.; Placentino, I. F.; Hilhorst, J.; Ferrero, C.; Francescangeli, O.; Laus, M.; Perego, M. Thermally Induced Self-Assembly of Cylindrical Nanodomains in Low Molecular Weight PS-b-PMMA Thin Films. *Nanotechnology* **2014**, *25* (4), 045301. https://doi.org/10.1088/0957-4484/25/4/045301.

(57) Ou, C. W.; Su, C. H.; Jeng, U. S.; Hsu, S. H. Characterization of Biodegradable Polyurethane Nanoparticles and Thermally Induced Self-Assembly in Water Dispersion.

ACS Applied Materials and Interfaces **2014**, *6* (8), 5685–5694. https://doi.org/10.1021/AM500213T/SUPPL_FILE/AM500213T_SI_001.PDF.

(58) Covalent organic frameworks, metal organic frameworks, and metal organic nanotubes are all common architectures in polymer science with their own host of applications. However, these materials are outside the scope of this dissertation.

(59) Rider, D. A.; Winnik, M. A.; Manners, I. Redox-Controlled Micellization of Organometallic Block Copolymers. *Chemical Communications* **2007**, *0* (43), 4483. https://doi.org/10.1039/b704200k.

(60) Suzuki, D.; Sakai, T.; Yoshida, R. Self-Flocculating/Self-Dispersing Oscillation of Microgels. *Angewandte Chemie International Edition* **2008**, *47* (5), 917–920. https://doi.org/10.1002/ANIE.200703953.

(61) Mei, C.; Ding, J.; Yao, B.; Cheng, Y.; Xie, Z.; Geng, Y.; Wang, L. Synthesis and Characterization of White-Light-Emitting Polyfluorenes Containing Orange Phosphorescent Moieties in the Side Chain. *Journal of Polymer Science Part A: Polymer Chemistry* **2007**, *45* (9), 1746–1757. https://doi.org/10.1002/POLA.21942.

(62) Zhang, K.; Chen, Z.; Yang, C.; Tao, Y.; Zou, Y.; Qin, J.; Cao, Y. Stable White Electroluminescence from Single Fluorene -Based Copolymers : Using Fluorenone as the Green Fluorophore and an Iridium Complex as the Red Phosphor on the Main Chain. *Journal of Materials Chemistry* **2008**, *18* (3), 291–298. https://doi.org/10.1039/B714317F.

(63) Wu, F. I.; Yang, X. H.; Neher, D.; Dodda, R.; Tseng, Y. H.; Shu, C. F. Efficient White-Electrophosphorescent Devices Based on a Single Polyfluorene Copolymer. *Advanced Functional Materials* **2007**, *17* (7), 1085–1092. https://doi.org/10.1002/ADFM.200600697.

(64) Xiang, J.; Burges, R.; Häupler, B.; Wild, A.; Schubert, U. S.; Ho, C. L.; Wong, W. Y. Synthesis, Characterization and Charge–Discharge Studies of Ferrocene-Containing Poly(Fluorenylethynylene) Derivatives as Organic Cathode Materials. *Polymer (Guildf)* **2015**, *68*, 328–334. https://doi.org/10.1016/J.POLYMER.2015.01.054.

(65) Choi, T.-L.; Lee, K.-H.; Joo, W.-J.; Lee, S.; Lee, T.-W.; Chae, M. Y. Synthesis and Nonvolatile Memory Behavior of Redox-Active Conjugated Polymer-Containing

Ferrocene. *J Am Chem Soc* **2007**, *129*, 9842–9843. https://doi.org/10.1021/ja0717459.

(66) Robinson, K. L.; Lawrence, N. S. Redox-Sensitive Copolymer: A Single-Component PH Sensor. *Analytical Chemistry* **2006**, *78* (7), 2450–2455. https://doi.org/10.1021/AC051787K/ASSET/IMAGES/LARGE/AC051787KF00006.JPEG.

(67) Payne, S. J.; Fiore, G. L.; Fraser, C. L.; Demas, J. N. Luminescence Oxygen Sensor Based on a Ruthenium(II) Star Polymer Complex. *Analytical Chemistry* **2010**, *82* (3), 917–921. https://doi.org/10.1021/AC9020837/ASSET/IMAGES/LARGE/AC-2009-020837_0002.JPEG.

(68) Fraser, C. L.; Smith, A. P. Metal Complexes with Polymeric Ligands: Chelation and Metalloinitiation Approaches to Metal Tris(Bipyridine)-Containing Materials. *J Polym Sci A: Polym Chem* **2000**, *38*, 4704–4716. https://doi.org/10.1002/1099-0518.

(69) Wang, Z.; Mcwilliams, A. R.; Evans, C. E. B.; Lu, X.; Chung, S.; Winnik, M. A.; Manners, I. Covalent Attachment of Ru II Phenanthroline Complexes to Polythionylphosphazenes: The Development and Evaluation of Single-Component Polymeric Oxygen Sensors. *Advanced Functional Materials* **2002**, *12*, 415–419. https://doi.org/10.1002/1616-3028.

(70) Chujo, Y.; Sada, K.; Naka, A.; Nomura, R.; Saegusa, T. Synthesis and Redox Gelation of Disulfide-Modified Polyoxazoline. *Macromolecules* **1993**, *26* (5), 883–887. https://doi.org/10.1021/MA00057A001/ASSET/MA00057A001.FP.PNG_V03.

(71) Chujo, Y.; Sada, K.; Saegusa, T. Reversible Gelation of Polyoxazoline by Means of Diels-Alder Reaction. *Macromolecules* **1990**, *23* (10), 2636–2641. https://doi.org/10.1021/MA00212A007/ASSET/MA00212A007.FP.PNG_V03.

(72) Ji, S.; Cao, W.; Yu, Y.; Xu, H. Visible-Light-Induced Self-Healing Diselenide-Containing Polyurethane Elastomer. *Advanced Materials* **2015**, *27* (47), 7740–7745. https://doi.org/10.1002/ADMA.201503661.

(73) Sandmann, B.; Bode, S.; Hager, M. D.; Schubert, U. S. Metallopolymers as an Emerging Class of Self-Healing Materials. In *Hierarchical Macromolecular Structures: 60 Years*

After the Staudinger Nobel Prize II; Springer New York LLC, 2013; Vol. 262, p 257. https://doi.org/10.1007/12_2013_242/FIGURES/9.

(74) Li, H.; Yang, P.; Pageni, P.; Tang, C. Recent Advances in Metal-Containing Polymer Hydrogels. *Macromolecular Rapid Communications* **2017**, *38* (14), 1700109. https://doi.org/10.1002/MARC.201700109.

(75) Wang, D. P.; Lai, J. C.; Lai, H. Y.; Mo, S. R.; Zeng, K. Y.; Li, C. H.; Zuo, J. L. Distinct Mechanical and Self-Healing Properties in Two Polydimethylsiloxane Coordination Polymers with Fine-Tuned Bond Strength. *Inorganic Chemistry* **2018**, *57* (6), 3232–3242. https://doi.org/10.1021/ACS.INORGCHEM.7B03260/SUPPL_FILE/IC7B03260_SI_003.AVI.

(76) Abend, M.; Kunz, C.; Stumpf, S.; Gräf, S.; Zechel, S.; Müller, F. A.; Hager, M. D.; Schubert, U. S. Femtosecond Laser-Induced Scratch Ablation as an Efficient New Method to Evaluate the Self-Healing Behavior of Supramolecular Polymers. *Journal of Materials Chemistry A* **2019**, *7* (5), 2148–2155. https://doi.org/10.1039/C8TA07063F.

(77) Xu, M.; Hao, X.; Hu, Z.; Yan, Q. Palladium-Bridged Polymers as CO-Biosignal-Responsive Self-Healing Hydrogels. *Polymer Chemistry* **2020**, *11* (4), 779–783. https://doi.org/10.1039/C9PY01660K.

(78) Morais, M.; Subramanian, S.; Pandey, U.; Samuel, G.; Venkatesh, M.; Martins, M.; Pereira, S.; Correia, J. D. G.; Santos, I. Mannosylated Dextran Derivatives Labeled with Fac -[M(CO)3] + (M = 99mTc, Re) for Specific Targeting of Sentinel Lymph Node. *Molecular Pharmaceutics* **2011**, *8* (2), 609–620. https://doi.org/10.1021/MP100425P/SUPPL_FILE/MP100425P_SI_001.PDF.

(79) Collot, J.; Gradinaru, J.; Humbert, N.; Skander, M.; Zocchi, A.; Ward, T. R. Artificial Metalloenzymes for Enantioselective Catalysis Based on Biotin-Avidin. *J Am Chem Soc* **2003**, *125* (30), 9030–9031. https://doi.org/10.1021/JA035545I/SUPPL_FILE/JA035545ISI20030602_112740.PDF.

(80) Coquiere, D.; Bos, J.; Beld, J.; Roelfes, G. Enantioselective Artificial Metalloenzymes Based on a Bovine Pancreatic Polypeptide Scaffold. *Angewandte Chemie International Edition* **2009**, *48* (28), 5159–5162. https://doi.org/10.1002/ANIE.200901134.

(81) Bloomer, B. J.; Clark, D. S.; Hartwig, J. F. Progress, Challenges, and Opportunities with Artificial Metalloenzymes in Biosynthesis. *Biochemistry* **2021**. https://doi.org/10.1021/ACS.BIOCHEM.1C00829/ASSET/IMAGES/MEDIUM/BI1C00829_0009.GIF.

(82) Liu, Z.; Calvó-Tusell, C.; Zhou, A. Z.; Chen, K.; Garcia-Borràs, M.; Arnold, F. H. Dual-Function Enzyme Catalysis for Enantioselective Carbon–Nitrogen Bond Formation. *Nature Chemistry* **2021**, *13* (12), 1166–1172. https://doi.org/10.1038/s41557-021-00794-z.

(83) Athavale, S. v.; Gao, S.; Liu, Z.; Mallojjala, S. C.; Hirschi, J. S.; Arnold, F. H. Biocatalytic, Intermolecular C–H Bond Functionalization for the Synthesis of Enantioenriched Amides. *Angewandte Chemie - International Edition* **2021**, *60* (47), 24864–24869. https://doi.org/10.1002/ANIE.202110873.

(84) Zhang, J.; Huang, X.; Zhang, R. K.; Arnold, F. H. Enantiodivergent α-Amino C-H Fluoroalkylation Catalyzed by Engineered Cytochrome P450s. *J Am Chem Soc* **2019**, *141* (25), 9798–9802. https://doi.org/10.1021/JACS.9B04344/SUPPL_FILE/JA9B04344_SI_003.CIF.

(85) Liu, Z.; Huang, J.; Gu, Y.; Clark, D. S.; Mukhopadhyay, A.; Keasling, J. D.; Hartwig, J. F. Assembly and Evolution of Artificial Metalloenzymes within E. Coli Nissle 1917 for Enantioselective and Site-Selective Functionalization of C—H and C═C Bonds. *J Am Chem Soc* **2022**, *144* (2), 883–890. https://doi.org/10.1021/JACS.1C10975/SUPPL_FILE/JA1C10975_SI_001.PDF.

(86) Sandoval, B. A.; Kurtoic, S. I.; Chung, M. M.; Biegasiewicz, K. F.; Hyster, T. K. Photoenzymatic Catalysis Enables Radical-Mediated Ketone Reduction in Ene-Reductases. *Angewandte Chemie International Edition* **2019**, *58* (26), 8714–8718. https://doi.org/10.1002/ANIE.201902005.

(87) Mikhaylov, V. N.; Sorokoumov, V. N.; Korvinson, K. A.; Novikov, A. S.; Balova, I. A. Synthesis and Simple Immobilization of Palladium(II) Acyclic Diaminocarbene

Complexes on Polystyrene Support as Efficient Catalysts for Sonogashira and Suzuki-Miyaura Cross-Coupling. *Organometallics* **2016**, *35* (11), 1684–1697. https://doi.org/10.1021/ACS.ORGANOMET.6B00144/SUPPL_FILE/OM6B00144_SI_003.XYZ.

(88) Nakamura, M.; Hirai, A.; Nakamura, E. Reaction Pathways of the Simmons-Smith Reaction. *J Am Chem Soc* **2003**, *125* (8), 2341–2350. https://doi.org/10.1021/JA026709I/SUPPL_FILE/JA026709ISI20021231_034328.RTF.

(89) Buchmeiser, M. R. Molybdenum Imido, Tungsten Imido and Tungsten Oxo Alkylidene N-Heterocyclic Carbene Olefin Metathesis Catalysts. *Chemistry – A European Journal* **2018**, *24* (54), 14295–14301. https://doi.org/10.1002/CHEM.201802497.

(90) Powell, A. B.; Bielawski, C. W.; Cowley, A. H. Design, Synthesis, and Study of Main Chain Poly(N-Heterocyclic Carbene) Complexes: Applications in Electrochromic Devices. *J Am Chem Soc* **2010**, *132* (29), 10184–10194. https://doi.org/10.1021/JA104051X/SUPPL_FILE/JA104051X_SI_005.CIF.

(91) Powell, A. B.; Suzuki, Y.; Ueda, M.; Bielawski, C. W.; Cowley, A. H. A Recyclable, Self-Supported Organocatalyst Based on a Poly(N-Heterocyclic Carbene). *J Am Chem Soc* **2011**, *133* (14), 5218–5220. https://doi.org/10.1021/JA200602E/SUPPL_FILE/JA200602E_SI_003.PDF.

(92) Dragisich, V.; Wulff, W. D.; Hoogsteen, K. Imino Carbene Complexes of Tungsten and Chromium as Synthons for Nitrile Ylides in Reactions with Alkynes, Alkenes, Nitriles, and Aldehydes. *Organometallics* **1990**, *9* (11), 2867–2870. https://doi.org/10.1021/OM00161A009/SUPPL_FILE/OM00161A009_SI_001.PDF.

(93) Barluenga, J.; Bernad, P. L.; Concellón, J. M. High-Diastereoselective and Enantioselective Cyclopropanation of r,-Unsaturated Fischer Carbene Complexes: Synthesis of Chiral 1,2-Disubstituted and 1,2,3-Trisubstituted Cyclopropanes. *Journal of Organic Chemistry* **1997**, *62*, 6870–6875.

(94) Barluenga, J.; Bernad, P. L.; Concellon, J. M. Total Diastereoselective Synthesis of Chromium Cyelopropylcarbene Complexes. *Tetrahedron Letters* **1995**, *36* (22), 3937–3940.

(95) Wang, H.; Hsung, R. P.; Wulff, W. D. Preparation of Alkenyl Fischer Carbene Complexes via Aldol Condensation with Enolizable Aldehydes. *Tetrahedron Letters* **1998**, *39* (14), 1849–1852. https://doi.org/10.1016/S0040-4039(98)00130-0.

(96) Barluenga, J.; Aznar, F.; Fernández, M. Formal [4 + 3], [4 + 2], [4 + 1] Cycloadditions and Acid-Base Reaction of 2-Methyl-1,3-Dimorpholino-1,3-Butadiene with Fischer Carbene Complexes. *Chemistry – A European Journal* **1997**, *3* (10), 1629–1637. https://doi.org/10.1002/CHEM.19970031012.

(97) Gleichmann, M. M.; Do, K. H.; Hess, B. A. Intermediates and Transition Structures of the Benzannulation of Heteroatom-Stabilized Chromium Carbene Complexes with Ethyne: A Density Functional Study. *J. Am. Chem. Soc.* **1996**, *118*, 10551–10560.

(98) Hofmann, P.; Hämmerle, M. The Mechanism of the Dötz Reaction: Chromacyclobutenes by Alkyne–Carbene Coupling? *Angewandte Chemie International Edition in English* **1989**, *28* (7), 908–910. https://doi.org/10.1002/ANIE.198909081.

(99) Dotz, K. H.; Tomuschat, P. Annulation Reactions of Chromium Carbene Complexes: Scope, Selectivity, and Recent Developments. *Chem. Soc. Rev* **1999**, *28*, 187–198.

(100) Fischer, E. O.; Maasböl, A. On the Existence of a Tungsten Carbonyl Carbene Complex. *Angewandte Chemie International Edition* **1964**, *3* (8), 580–581. https://doi.org/10.1002/anie.196405801.

(101) Klabunde, U.; Fischer, E. O. Two New Chromium Carbonyl Carbene Complexes. *J Am Chem Soc* **1967**, 7141–7142.

(102) Hegedus, L. S.; Schultze, L. M.; Toro, J.; Yijun, C. Photolytic Reaction of Chromium and Molybdenum Carbene Complexes with Imines. *Tetrahedron* **1985**, *41* (24), 5833–5838. https://doi.org/10.1016/S0040-4020(01)91422-X.

(103) Barluenga, J.; Vicente, R.; López, L.; Rubio, E.; Tomás, M.; Álvarez-Rúa, C. New Fischer Carbene Complexes of Rhodium(I): Preparation and 2-Cyclopentenone Ring Synthesis by Annelation to Alkynes. *J. Am. Chem. Soc.* **2004**, *126* (2), 470–471. https://doi.org/10.1021/JA038817Q.

(104) Fischer, E. O.; Beck, H.-J. Transfer of Methoxyphenylcarbene Ligands from Molybdenum to Iron and Nickel. *Angewandte Chemie International Edition in English* **1970**, *9* (1), 72–73. https://doi.org/10.1002/anie.197000721.

(105) Barluenga, J.; Prado, A. de; Santamaria, J.; Tomas, M. Polymer-Bound Fischer Tungsten Carbene Complexes: Synthesis and Reactivity. *Organometallics* **2005**, *24*, 3614–3617. https://doi.org/10.1021/om0503186.

(106) Macomber, D. W.; Hung, M. H.; Liang, M.; Verma, A. G.; Madhukar, P. New Organometallic Polymers Containing Tungsten Carbene Complexes. *Macromolecules* **1988**, *21* (4), 1187–1189. https://doi.org/10.1021/ma00182a061.

(107) Nomura, R.; Watanabe, K.; Masuda, T. Synthesis of Metal - Carbene Containing Polymers by Polycondensation of a Bifunctional Alkoxycarbene with Diamines. *Macromolecules* **2000**, *33*, 1936–1939. https://doi.org/10.1021/ma990599r.

(108) Günay, K. A.; Theato, P.; Klok, H.-A. Standing on the Shoulders of Hermann Staudinger: Post-Polymerization Modification from Past to Present. *Journal of Polymer Science Part A: Polymer Chemistry* **2013**, *51* (1), 1–28. https://doi.org/10.1002/pola.26333.

(109) Dispinar, T.; Sanyal, R.; Sanyal, A. A Diels-Alder/Retro Diels-Alder Strategy to Synthesize Polymers Bearing Maleimide Side Chains. *Journal of Polymer Science Part A: Polymer Chemistry* **2007**, *45* (20), 4545–4551. https://doi.org/10.1002/POLA.22299.

(110) Justynska, J.; Hordyjewicz, Z.; Schlaad, H. Toward a Toolbox of Functional Block Copolymers via Free-Radical Addition of Mercaptans. *Polymer (Guildf)* **2005**, *46* (26), 12057–12064. https://doi.org/10.1016/J.POLYMER.2005.10.104.

(111) Theato, P.; Klok, H.-A. *Functional Polymers by Post-Polymerization Modification: Concepts, Practical Guidelines, and Applications*, 1st ed.; 2013.

(112) Maiti, B.; Kumar, S.; de Priyadarsi. Controlled RAFT Synthesis of Side-Chain Oleic Acid Containing Polymers and Their Post-Polymerization Functionalization. *RSC Advances* **2014**, *4* (99), 56415–56423. https://doi.org/10.1039/C4RA08872G.

(113) Tantillo, D. J.; Hoffmann, R. Snakes and Ladders. The Sigmatropic Shiftamer Concept. *Accounts of Chemical Research* **2006**, *39* (7), 477–486. https://doi.org/10.1021/AR0680926/ASSET/IMAGES/LARGE/AR0680926H00013.JPEG.

(114) Tantillo, D. J.; Hoffmann, R. Hydrogen Migration Over Organic Tapes: [1,5] Sigmatropic Shiftamers. *European Journal of Organic Chemistry* **2004**, *2004* (2), 273–280. https://doi.org/10.1002/EJOC.200300583.

(115) Tantillo, D. J.; Hoffmann, R. Helicoid Shiftamers for the Transport of π-Clumps and Charges. *Helvetica Chimica Acta* **2003**, *86* (11), 3525–3532. https://doi.org/10.1002/HLCA.200390297.

(116) Tantillo, D. J.; Hoffmann, R. Sigmatropic Shiftamers: Fluxionality in Broken Ladderane Polymers. *Angewandte Chemie* **2002**, *114* (6), 1075–1078. https://doi.org/10.1002/1521-3757.

(117) Tantillo, D. J.; Hoffmann, R. Helicoid Shiftamers. *J Am Chem Soc* **2002**, *124* (24), 6836–6837. https://doi.org/10.1021/JA020425G/SUPPL_FILE/JA020425G_S.PDF.

(118) Ditzler, R. A. J.; Zhukhovitskiy, A. v. Sigmatropic Rearrangements of Polymer Backbones: Vinyl Polymers from Polyesters in One Step. *J Am Chem Soc* **2021**, *143* (48), 20326–20331. https://doi.org/10.1021/JACS.1C09657/ASSET/IMAGES/LARGE/JA1C09657_0004.JPEG.

(119) Sydlik, S. A.; Swager, T. M. Functional Graphenic Materials Via a Johnson–Claisen Rearrangement. *Advanced Functional Materials* **2013**, *23* (15), 1873–1882. https://doi.org/10.1002/ADFM.201201954.

(120) de La Viuda, M. R.; Tena, A.; Neumann, S.; Willruth, S.; Filiz, V.; Abetz, V. Novel Functionalized Polyamides Prone to Undergo Thermal Claisen Rearrangement in the Solid State. *Polymer Chemistry* **2018**, *9* (29), 4007–4016. https://doi.org/10.1039/C8PY00467F.

(121) Meis, D.; Tena, A.; Neumann, S.; Georgopanos, P.; Emmler, T.; Shishatskiy, S.; Rangou, S.; Filiz, V.; Abetz, V. Thermal Rearrangement of Ortho -Allyloxypolyimide Membranes and the Effect of the Degree of Functionalization. *Polymer Chemistry* **2018**, *9* (29), 3987–3999. https://doi.org/10.1039/C8PY00530C.

(122) Williamson, J. B.; Czaplyski, W. L.; Alexanian, E. J.; Leibfarth, F. A. Regioselective C–H Xanthylation as a Platform for Polyolefin Functionalization. *Angewandte Chemie International Edition* **2018**, *57* (21), 6261–6265. https://doi.org/10.1002/ANIE.201803020.

(123) Bae, C.; Hartwig, J. F.; Boaen Harris, N. K.; Long, R. O.; Anderson, K. S.; Hillmyer, M. A. Catalytic Hydroxylation of Polypropylenes. *J Am Chem Soc* **2005**, *127* (2), 767–776.

https://doi.org/10.1021/JA044440S/SUPPL_FILE/JA044440SSI20041019_094410.PDF.

(124) Fazekas, T. J.; Alty, J. W.; Neidhart, E. K.; Miller, A. S.; Leibfarth, F. A.; Alexanian, E. J. Diversification of Aliphatic C-H Bonds in Small Molecules and Polyolefins through Radical Chain Transfer. *Science (1979)* **2022**, *375* (6580), 545–550. https://doi.org/10.1126/SCIENCE.ABH4308/SUPPL_FILE/SCIENCE.ABH4308_SM.PDF.

(125) Chauhan, N. P. S.; Hosmane, N. S.; Mozafari, M. Boron-Based Polymers: Opportunities and Challenges. *Materials Today Chemistry* **2019**, *14*, 100184. https://doi.org/10.1016/J.MTCHEM.2019.08.003.

(126) Mellerup, S. K.; Wang, S.; Zhou, W.-X.; Soren, S.; Mellerup, K.; Mellerup Ab, S. K. Boron-Based Stimuli Responsive Materials. *Chemical Society Reviews* **2019**, *48* (13), 3537–3549. https://doi.org/10.1039/C9CS00153K.

(127) Cheng, F.; Jäkle, F. Boron-Containing Polymers as Versatile Building Blocks for Functional Nanostructured Materials. *Polymer Chemistry* **2011**, *2* (10), 2122–2132. https://doi.org/10.1039/C1PY00123J.

(128) Mark, J. E. Silicon-Containing Polymers. In *Advances in Chemistry*; 1989; Vol. 224, pp 47–68. https://doi.org/10.1021/BA-1990-0224.CH002.

(129) Kawakami, Y.; Kakihana, Y.; Ooi, O.; Oishi, M.; Suzuki, K.; Shinke, S.; Uenishi, K. Control of Stereochemical Structures of Silicon-Containing Polymeric Systems. *Polymer International* **2009**, *58* (3), 279–284. https://doi.org/10.1002/PI.2524.

(130) Carraher, C. E.; Pittman, C. U.; Zeldin, M.; Abd-El-Aziz, A. S. Organogermanium Polymers. In *Macromolecules Containing Metal and Metal-Like Elements*; John Wiley & Sons, Ltd, 2005; Vol. 4, pp 225–261. https://doi.org/10.1002/0471712566.CH9.

(131) Gómez, F. J.; Wagener, K. B. Germanium-Containing Polymers via Acyclic Diene Metathesis. *Journal of Organometallic Chemistry* **1999**, *592* (2), 271–277. https://doi.org/10.1016/S0022-328X(99)00558-6.

(132) Imoto, H.; Naka, K. Recent Progress on Arsenic-Containing Functional Polymers. *Polymer (Guildf)* **2022**, *241*, 124464. https://doi.org/10.1016/J.POLYMER.2021.124464.

(133) Imoto, H. Development of Macromolecules and Supramolecules Based on Silicon and Arsenic Chemistries. *Polymer Journal* **2018**, *50* (9), 837–846. https://doi.org/10.1038/s41428-018-0068-0.

(134) Carraher, C. E. Antimony-Containing Polymers. In *Inorganic and Organometallic Macromolecules*; 2008; pp 405–419.

(135) Wang, L.; Cao, W.; Xu, H. Tellurium-Containing Polymers: Towards Biomaterials and Optoelectronic Materials. *ChemNanoMat* **2016**, *2* (6), 479–488. https://doi.org/10.1002/CNMA.201600076.

(136) Cao, W.; Wang, L.; Xu, H. Selenium/Tellurium Containing Polymer Materials in Nanobiotechnology. *Nano Today* **2015**, *10* (6), 717–736. https://doi.org/10.1016/J.NANTOD.2015.11.004.

(137) Zweifel, G.; Brown, H. C. Hydration of Olefins, Dienes, and Acetylenes via Hydroboration. *Organic Reactions* **2011**, 1–54. https://doi.org/10.1002/0471264180.OR013.01.

(138) Mao, L.; Bose, S. K. Hydroboration of Enynes and Mechanistic Insights. *Advanced Synthesis & Catalysis* **2020**, *362* (20), 4174–4188. https://doi.org/10.1002/ADSC.202000603.

(139) Shegavi, M. L.; Bose, S. K. Recent Advances in the Catalytic Hydroboration of Carbonyl Compounds. *Catalysis Science & Technology* **2019**, *9* (13), 3307–3336. https://doi.org/10.1039/C9CY00807A.

(140) Rezaei Bazkiaei, A.; Findlater, M.; Gorden, A. E. V. Applications of Catalysis in Hydroboration of Imines, Nitriles, and Carbodiimides. *Organic & Biomolecular Chemistry* **2022**, *20* (18), 3675–3702. https://doi.org/10.1039/D2OB00162D.

(141) Candeias, N. R.; Montalbano, F.; Cal, P. M. S. D.; Gois, P. M. P. Boronic Acids and Esters in the Petasis-Borono Mannich Multicomponent Reaction. *Chemical Reviews* **2010**, *110* (10), 6169–6193. https://doi.org/10.1021/CR100108K/ASSET/IMAGES/MEDIUM/CR-2010-00108K_0073.GIF.

(142) Wu, P.; Givskov, M.; Nielsen, T. E. Reactivity and Synthetic Applications of Multicomponent Petasis Reactions. *Chemical Reviews* **2019**, *119* (20), 11245–11290.

https://doi.org/10.1021/ACS.CHEMREV.9B00214/ASSET/IMAGES/MEDIUM/CR9B00214_0046.GIF.

(143) Armstrong, R. J.; Aggarwal, V. K. 50 Years of Zweifel Olefination: A Transition-Metal-Free Coupling. *Synthesis (Stuttg)* **2017**, *49* (15), 3323–3336. https://doi.org/10.1055/S-0036-1589046.

(144) Donald S. Matteson. The Use of Chiral Organoboranes in Organic Synthesis. *Synthesis (Stuttg)* **1986**, *1986*, 973–985.

(145) Collins, B. S. L.; Wilson, C. M.; Myers, E. L.; Aggarwal, V. K. Asymmetric Synthesis of Secondary and Tertiary Boronic Esters. *Angewandte Chemie International Edition* **2017**, *56* (39), 11700–11733. https://doi.org/10.1002/ANIE.201701963.

(146) Yeung, K.; Mykura, R. C.; Aggarwal, V. K. Lithiation–Borylation Methodology in the Total Synthesis of Natural Products. *Nature Synthesis* **2022**, *1* (2), 117–126. https://doi.org/10.1038/s44160-021-00012-1.

(147) Lennox, A. J. J.; Lloyd-Jones, G. C. Selection of Boron Reagents for Suzuki–Miyaura Coupling. *Chemical Society Reviews* **2013**, *43* (1), 412–443. https://doi.org/10.1039/C3CS60197H.

(148) Singh Gujral, S.; Khatri, S.; Riyal, P. Suzuki Cross Coupling Reaction- A Review. *Indo Global Journal of Pharmaceutical Sciences* **2012**, *2* (4), 351–367.

(149) Buchspies, J.; Szostak, M. Recent Advances in Acyl Suzuki Cross-Coupling. *Catalysts* **2019**, *9* (1), 53. https://doi.org/10.3390/CATAL9010053.

(150) Li, Y.; Vamvounis, G.; Yu, J.; Holdcroft, S. A Novel and Versatile Methodology for Functionalization of Conjugated Polymers. Transformation of Poly(3-Bromo-4-Hexylthiophene) via Palladium-Catalyzed Coupling Chemistry. *Macromolecules* **2001**, *34*, 3130–3132. https://doi.org/10.1021/ma010293w.

(151) Howe, D. H.; Mcdaniel, R. M.; Magenau, A. J. D. From Click Chemistry to Cross-Coupling: Designer Polymers from One Efficient Reaction. *Macromolecules* **2017**, *50*, 8010–8018. https://doi.org/10.1021/acs.macromol.7b02041.

(152) Kubo, T.; Scheutz, G. M.; Latty, T. S.; Sumerlin, B. S. Synthesis of Functional and Boronic Acid-Containing Aliphatic Polyesters via Suzuki Coupling. *Chemical Communications* **2019**, *55* (39), 5655–5658. https://doi.org/10.1039/C9CC01975H.

(153) Jacobs, B. P.; Brantley, J. N. Vinyl-Addition Polymerizations of Borylated Allenes. *Macromolecules* **2021**, *54* (18), 8822–8828. https://doi.org/10.1021/ACS.MACROMOL.1C01253/ASSET/IMAGES/LARGE/MA1C01253_0006.JPEG.

(154) Jacobs, B. P.; Brantley, J. N. Exploring Combinatorial Approaches to Polymer Diversification. *Macromolecules* **2020**, *53* (21), 9287–9293. https://doi.org/10.1021/ACS.MACROMOL.0C01538/ASSET/IMAGES/LARGE/MA0C01538_0004.JPEG.

(155) Boiarska, Z.; Braga, T.; Silvani, A.; Passarella, D. Brown Allylation: Application to the Synthesis of Natural Products. *European Journal of Organic Chemistry* **2021**, *2021* (22), 3214–3222. https://doi.org/10.1002/EJOC.202100258.

(156) Brown, H. C.; Desai, M. C.; Jadhav, P. K. Hydroboration. 61. Diisopinocampheylborane of High Optical Purity. Improved Preparation and Asymmetric Hydroboration of Representative Cis-Disubstituted Alkenes. *J. Org. Chem* **1982**, *47*, 5065–5069.

(157) Brown, H. C.; Bhat, K. S.; Ramnarayan, R. S. Chiral Synthesis via Organoboranes. 21. Allyl- and Crotylboration of a-Chiral Aldehydes with Diisopinocampheylboron as the Chiral Auxiliary. *J. Org. Chem.* **1989**, *54* (1), 1570–1576.

(158) Randad, R. S.; Bhat, K. S.; Brown, H. C. B-Allyldiisopinocampheylborane: A Remarkable Reagent for the Diastereoselective Allylboration of a-Substituted Chiral Aldehydes. *J. Org. Chem.* **1987**, *52*, 319–320.

(159) Crawford, D. L.; Pometto, A. L.; Crawford, R. L. Lignin Degradation by Streptomyces Viridosporus: Isolation and Characterization of a New Polymeric Lignin Degradation Intermediate. *Applied and Environmental Microbiology* **1983**, *45* (3), 898–904. https://doi.org/10.1128/AEM.45.3.898-904.1983.

(160) Khan, I.; Ray Dutta, J.; Ganesan, R. Lactobacillus Sps. Lipase Mediated Poly (ε-Caprolactone) Degradation. *International Journal of Biological Macromolecules* **2017**, *95*, 126–131. https://doi.org/10.1016/J.IJBIOMAC.2016.11.040.

(161) Sun, J.; Aly, K. I.; Kuckling, D. Synthesis of Hyperbranched Polymers from Vegetable Oil Based Monomers via Ozonolysis Pathway. *Journal of Polymer Science Part A: Polymer Chemistry* **2017**, *55* (12), 2104–2114. https://doi.org/10.1002/POLA.28600.

(162) Solanky, S. S.; Singh, R. P. Ozonolysis of Natural Rubber: A Critical Review. *Progress in Rubber and Plastics Technology* **2001**, *17* (1), 13–58.

(163) Day, M.; Wiles, D. M. Photochemical Degradation of Poly(Ethylene Terephthalate). II. Effect of Wavelength and Environment on the Decomposition Process. *Journal of Applied Polymer Science* **1972**, *16* (1), 191–202. https://doi.org/10.1002/APP.1972.070160117.

(164) Rabek, Jan. F. Photochemical Aspects of Degradation of Polymers. In *Polymer Photodegradation*; Springer, Dordrecht, 1995; pp 24–66. https://doi.org/10.1007/978-94-011-1274-1_2.

(165) Kulkarni, A.; Dasari, H. Current Status of Methods Used In Degradation of Polymers: A Review. *MATEC Web of Conferences* **2018**, *144*, 02023. https://doi.org/10.1051/MATECCONF/201814402023.

(166) Houchin, M. L.; Topp, E. M. Chemical Degradation of Peptides and Proteins in PLGA: A Review of Reactions and Mechanisms. *Journal of Pharmaceutical Sciences* **2008**, *97* (7), 2395–2404. https://doi.org/10.1002/JPS.21176.

(167) Yan, M.; Kawamata, Y.; Baran, P. S. Synthetic Organic Electrochemical Methods Since 2000: On the Verge of a Renaissance. *Chemical Reviews* **2017**, *117*, 13230–13319.

(168) Horn, E. J.; Rosen, B. R.; Baran, P. S. Synthetic Organic Electrochemistry: An Enabling and Innately Sustainable Method. *ACS Central Science* **2016**, *2*, 302–308. https://doi.org/10.1021/acscentsci.6b00091.

(169) Little, R. D. A Perspective on Organic Electrochemistry. *Journal of Organic Chemistry* **2020**, *85*, 13375–13390.

(170) Siu, T.; Yudin, A. K. Electrochemical Imination of Sulfoxides Using N-Aminophthalimide. *Organic Letters* **2002**, *4* (11), 1839–1842. https://doi.org/10.1021/OL0257530/SUPPL_FILE/OL0257530_S2.CIF.

(171) Gong, M.; Huang, J. M. Electrochemical Oxidative C–H/N–H Coupling between γ-Lactams and Anilines. *Chemistry – A European Journal* **2016**, *22* (40), 14293–14296. https://doi.org/10.1002/CHEM.201602454.

(172) Xu, H. C.; Campbell, J. M.; Moeller, K. D. Cyclization Reactions of Anode-Generated Amidyl Radicals. *Journal of Organic Chemistry* **2014**, *79* (1), 379–391. https://doi.org/10.1021/JO402623R/SUPPL_FILE/JO402623R_SI_001.PDF.

(173) Zhao, H. B.; Hou, Z. W.; Liu, Z. J.; Zhou, Z. F.; Song, J.; Xu, H. C. Amidinyl Radical Formation through Anodic N–H Bond Cleavage and Its Application in Aromatic C–H Bond Functionalization. *Angewandte Chemie International Edition* **2017**, *56* (2), 587–590. https://doi.org/10.1002/ANIE.201610715.

(174) Kashiwagi, Y.; Kurashima, F.; Chiba, S.; Anzai, J. I.; Osa, T.; Bobbitt, J. M. Asymmetric Electrochemical Lactonization of Diols on a Chiral 1-Azaspiro[5.5]Undecane N -Oxyl Radical Mediator-Modified Graphite Felt Electrode. *Chemical Communications* **2003**, *0* (1), 114–115. https://doi.org/10.1039/B209871G.

(175) Schämann, M.; Schäfer, H. J. TEMPO-Mediated Anodic Oxidation of Methyl Glycosides and 1-Methyl and 1-Azido Disaccharides. *European Journal of Organic Chemistry* **2003**, *2003* (2), 351–358. https://doi.org/10.1002/EJOC.200390041.

(176) Green, R. A.; Pletcher, D.; Leach, S. G.; Brown, R. C. D. N-Heterocyclic Carbene-Mediated Oxidative Electrosynthesis of Esters in a Microflow Cell. *Organic Letters* **2015**, *17* (13), 3290–3293. https://doi.org/10.1021/ACS.ORGLETT.5B01459/SUPPL_FILE/OL5B01459_SI_001.PDF.

(177) Kang, L. S.; Luo, M. H.; Lam, C. M.; Hu, L. M.; Little, R. D.; Zeng, C. C. Electrochemical C–H Functionalization and Subsequent C–S and C–N Bond Formation: Paired Electrosynthesis of 3-Amino-2-Thiocyanato-α,β-Unsaturated Carbonyl Derivatives Mediated by Bromide Ions. *Green Chemistry* **2016**, *18* (13), 3767–3774. https://doi.org/10.1039/C6GC00666C.

(178) Qian, P.; Su, J. H.; Wang, Y.; Bi, M.; Zha, Z.; Wang, Z. Electrocatalytic C-H/N-H Coupling of 2′-Aminoacetophenones for the Synthesis of Isatins. *Journal of Organic Chemistry* **2017**, *82* (12), 6434–6440. https://doi.org/10.1021/ACS.JOC.7B00635/SUPPL_FILE/JO7B00635_SI_001.PDF.

(179) Qian, P.; Bi, M.; Su, J.; Zha, Z.; Wang, Z. Electrosynthesis of (E)-Vinyl Sulfones Directly from Cinnamic Acids and Sodium Sulfinates via Decarboxylative Sulfono

Functionalization. *Journal of Organic Chemistry* **2016**, *81* (11), 4876–4882. https://doi.org/10.1021/ACS.JOC.6B00661/ASSET/IMAGES/LARGE/JO-2016-00661R_0005.JPEG.

(180) Luo, Y. C.; Pan, X. J.; Yuan, G. Q. An Efficient Electrochemical Synthesis of Vinyl Sulfones from Sodium Sulfinates and Olefins. *Tetrahedron* **2015**, *71* (14), 2119–2123. https://doi.org/10.1016/J.TET.2015.02.048.

(181) Batanero, B.; Barba, F. Facile Conversion of O-Quinones into 1,3-Dioxoles. *Organic Letters* **2005**, *7* (13), 2567–2569. https://doi.org/10.1021/OL050614E/SUPPL_FILE/OL050614ESI20050512_081528.PDF.

(182) Edinger, C.; Waldvogel, S. R. Electrochemical Deoxygenation of Aromatic Amides and Sulfoxides. *European Journal of Organic Chemistry* **2014**, *2014* (24), 5144–5148. https://doi.org/10.1002/EJOC.201402714.

(183) Ozaki, S.; Yoshinaga, H.; Matsui, E.; Adachi, M. Synthesis of Cyclic Ketones by Electrochemical Reduction of S-(2-Methoxycarbonyl)Phenyl Thiolesters. *Journal of Organic Chemistry* **2001**, *66* (7), 2503–2505. https://doi.org/10.1021/JO001578U/ASSET/IMAGES/LARGE/JO001578UN00001.JPEG.

(184) Sengmany, S.; Léonel, E.; Paugam, J. P.; Nédélec, J. Y. Cyclopropane Formation by Nickel-Catalysed Electroreductive Coupling of Activated Olefins and Unactivated Gem-Dibromo Compounds. *Tetrahedron* **2002**, *58* (2), 271–277. https://doi.org/10.1016/S0040-4020(01)01133-4.

(185) Durandetti, M.; Nédélec, J. Y.; Périchon, J. An Electrochemical Coupling of Organic Halide with Aldehydes, Catalytic in Chromium and Nickel Salts. the Nozaki-Hiyama-Kishi Reaction. *Organic Letters* **2001**, *3* (13), 2073–2074. https://doi.org/10.1021/OL016033G/ASSET/IMAGES/MEDIUM/OL016033GU00004A.GIF.

(186) Fox, D. P.; Little, R. D.; Baizer, M. M. Intramolecular Electroreductive Cyclization. *Journal of Organic Chemistry* **1985**, *50*, 2202–2204.

(187) Anderson, J. D.; Baizer, M. M.; Petrovich, J. P. Electrolytic Reductive Coupling. XIII. Intramolecular Reductive Coupling. Electrohydrocyclization. *Journal of Organic Chemistry* **1966**, *31*, 3890–3897.

(188) Baizer, M. M. Electrolytic Reductive Coupling: I. Acrylonitrile. *J Electrochem Soc* **1964**, *111*, 215–222.

(189) Magenau, A. J. D.; Strandwitz, N. C.; Gennaro, A.; Matyjaszewski, K. Electrochemically Mediated Atom Transfer Radical Polymerization. *Science (1979)* **2011**, *332* (6025), 81–84. https://doi.org/10.1126/SCIENCE.1202357/SUPPL_FILE/MAGENAU_SOM.PDF.

(190) Chmielarz, P.; Fantin, M.; Park, S.; Isse, A. A.; Gennaro, A.; Magenau, A. J. D.; Sobkowiak, A.; Matyjaszewski, K. Electrochemically Mediated Atom Transfer Radical Polymerization (EATRP). *Progress in Polymer Science* **2017**, *69*, 47–78. https://doi.org/10.1016/J.PROGPOLYMSCI.2017.02.005.

(191) Fabre, B.; Simonet, J. Post-Polymerization Electrochemical Functionalization of a Conducting Polymer: Anodic Cyanation of Poly(p-Dimethoxybenzene). *Journal of Electroanalytical Chemistry* **1996**, *416* (1–2), 187–189. https://doi.org/10.1016/S0022-0728(96)01014-5.

(192) Qi, Z.; Rees, N. G.; Pickup, P. G. Electrochemically Induced Substitution of Polythiophenes and Polypyrrole. *Chemistry of Materials* **1996**, *8* (3), 701–707. https://doi.org/10.1021/CM950416P.

(193) Soudan, P.; Lucas, P.; Breau, L.; Bélanger, D. Electrochemical Modification of Poly(3-(4-Fluorophenyl)Thiophene). *Langmuir* **2000**, *16* (9), 4362–4366. https://doi.org/10.1021/LA991676E.

(194) Inagi, S.; Hayashi, S.; Hosaka, K.; Fuchigami, T. Facile Functionalization of a Thiophene - Fluorene Alternating Copolymer via Electrochemical Polymer Reaction. *Macromolecules* **2009**, *42* (12), 3881–3883. https://doi.org/10.1021/MA900561F/SUPPL_FILE/MA900561F_SI_001.PDF.

(195) Zhou, H.; Ren, Y.; Li, Z.; Xu, M.; Wang, Y.; Ge, R.; Kong, X.; Zheng, L.; Duan, H. Electrocatalytic Upcycling of Polyethylene Terephthalate to Commodity Chemicals and

H2 Fuel. *Nature Communications* **2021**, *12* (1), 1–9. https://doi.org/10.1038/s41467-021-25048-x.

CHAPTER 2: SYNTHESIS AND REACTIVITY OF METALLOCARBENE-CONTAINING POLYMERS

A version of this chapter was originally published by Breana J. Wilson and Johnathan N. Brantley: Wilson, B. J.; Brantley, J. N. Synthesis and Reactivity of Metallocarbene-Containing Polymers. *J. Am. Chem. Soc*. **2019**, 141, 32, 12453-12457 DOI: 10.1021/jacs.9b04077

Minor text revisions and figure placement changes have been made. All experimentation and data collection was completed by Breana J. Wilson, as well as writing of the document in conjunction with Dr. Johnathan N. Brantley, the PI for this work.

Abstract

Metallopolymers are an emerging class of materials with potential utility as semiconductors, catalysts, optical device components, and stimuli responsive networks. While polymer frameworks have been decorated with an array of organometallic moieties, the incorporation of metallocarbenes has been largely overlooked. Here, we report ring-opening metathesis polymerization as a strategy for the synthesis of Fischer carbene containing polymers. High degrees of polymerization were observed (> 800 repeats), and the isolated materials exhibited exceptional solubility and thermal stability. The tungsten carbene subunits were readily incorporated into block copolymers and could be modified through subsequent transformations. Moreover, the metallocarbene polymers were found to release carbon monoxide upon exposure to light or oxygen, which is unusual for tungsten carbene complexes These metallocarbene-containing polymers could represent new platforms for the development of functional materials.

Introduction

The design of polymers with bespoke physical or chemical properties has long served as an impetus for innovation in materials science. Embedding tunable structural elements within polymeric architectures is particularly enticing, as these motifs can be engaged through post-synthetic transformations to rapidly access structural (or functional) diversity.[1,2] While purely organic moieties have traditionally been leveraged for creating functional networks, organometallic complexes have emerged as attractive alternatives.[3] Metal complexes have been incorporated into an array of polymer architectures,[4–7] and the resultant

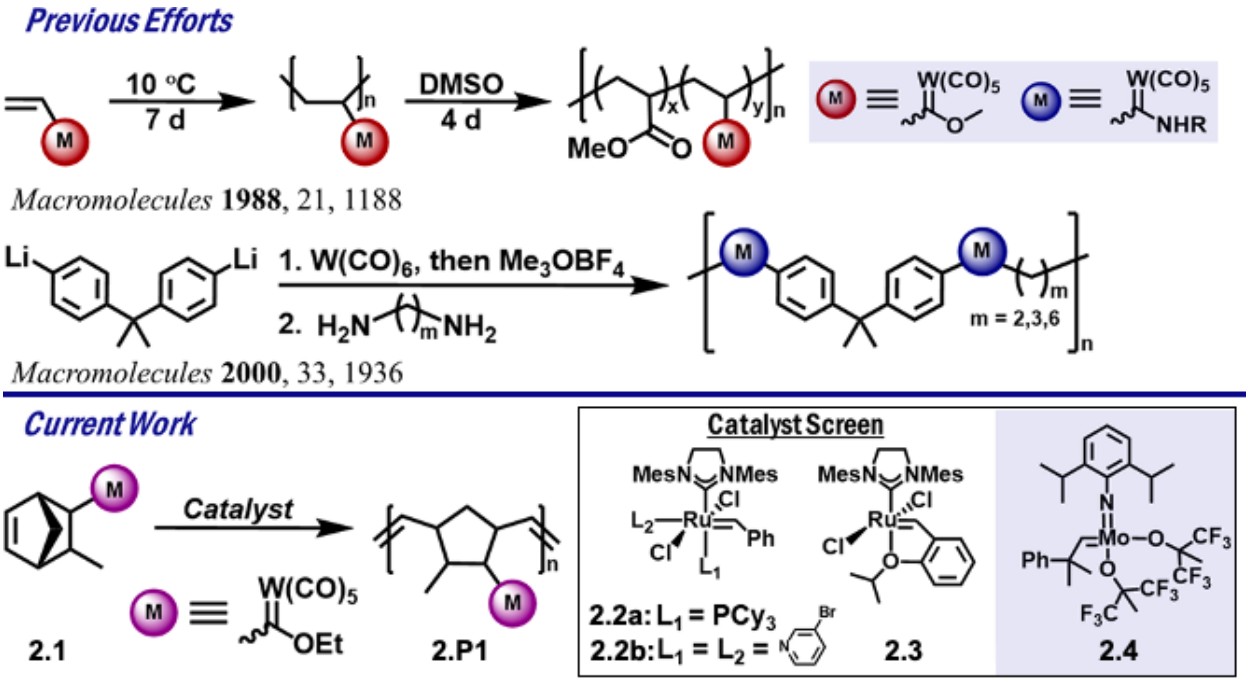
metallopolymers hold promise for use in electronic,[8–10] stimuli responsive,[11–13] optical,[14–16] and other functional materials.[17,18]

Despite these successes, opportunities to advance metallopolymer synthesis and design remain. For example, these materials are often prepared via polymerization of a ligand architecture and subsequent doping with a metal salt. This strategy inherently complicates the synthesis of materials with precisely tailored microstructures (e.g., gradient homo- or heterometallic polymers). Moreover, the incorporation of reactive metallic groups is an enticing strategy for accessing polymers with intrinsic dispositions toward structural tailoring. Salient examples include toggling a metallopolymer's redox state to promote self-assembly,[19–21] or harnessing dynamic ligand binding for self-healing.[22–24] These reports (and others[6,25–27]) illustrate that exploring new chemical space in metallopolymers is imperative for realizing materials with unique functions and properties.

Metallocarbenes, particularly Fischer-type complexes,[28–33] are promising (albeit, underexplored) candidates for reactive components within metallopolymers.[34–37] Given their broad synthetic utility and functional group tolerance,[38] Fischer carbene-containing polymers could exhibit highly tunable structures and properties; unfortunately, the reliable polymerization of a Fischer carbene complex has proven elusive.[39,40] Macomber originally reported the autopolymerization of a tungsten vinyl carbene,[41] but the resulting glass could only be characterized following oxidative demetallation (Scheme 2.1). Nomura later disclosed the synthesis of oligomeric species via the polycondensation of α,ω-bis-carbenes.[42] These materials exhibited low degrees of polymerization (≤ 25 repeats), high dispersity (Đ ~ 2.5), and rapidly decomposed at modest temperatures (90 °C). Although encouraging, these initial discoveries are conspicuous in their relative isolation. Indeed, we are unaware of any subsequent effort to improve upon these results to realize a functional material containing Fischer carbene complexes.

Given the isolobal relationship between Fischer carbenes and esters, we envisioned these complexes could exhibit polymerization tendencies reminiscent of common ester-containing monomers. In light of this, as well as the established compatibility between Fischer carbenes and metathesis catalysts,[43,44] we pursued ring opening metathesis polymerization (ROMP) as a strategy for accessing metallocarbene-containing polymers (Scheme 2.1).

Scheme 2.1. Synthetic Strategies to Access Metallocarbene-Containing Polymers



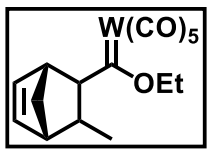
Materials and Methods

General Considerations

Unless otherwise noted, solvents were dried on an MBraun solvent purification system with 3Å molecular sieves and degassed with three freeze-pump-thaw cycles. All other reagents were obtained from commercial sources and used without further purification. Oxygen and water sensitive manipulations were performed in a nitrogen filled MBraun glovebox or using standard Schlenk techniques. All polymerizations were performed in a N_2 filled glovebox. ^{1}H and ^{13}C NMR data were collected on a Varian 500 MHz NMR or a Varian 300 MHz NMR spectrometer. Chemical shifts (δ) are reported in ppm using the residual solvent as reference. IR spectra were collected on a Thermo Scientific Nicolet iS5 spectrometer with an ATR iD7 attachment (germanium crystal) for solid samples and a Transmission iD1 attachment with flow cell for liquid samples. UV-visible absorbance spectra were recorded using an Agilent Cary 100 series UV-Vis spectrophotometer. The CFL emission spectrum was obtained using an Ocean Optics USB4000 detector with a slit of 25 μm and an integration time of 6000 μs. Thermogravimetric analysis (TGA) was performed on a TA Instruments TGA Q500 and Dynamic Mechanical Analysis (DMA) data were collected on a TA Instruments DMA Q800 with a film tension clamp. Size Exclusion Chromatography (SEC) data were collected on an Omnisec Resolve and Omnisec Reveal System using triple detection with detectors in series: UV, light scattering, viscometer, and refractive index and three Viscotek styrene divinylbenzene copolymer columns (in series T3000, T4000, and T5000) at a flow rate of 1 mL/min and thermostatted to 30 °C using either tetrahydrofuran (THF) or chloroform ($CHCl_3$) as the eluent. Molecular weight and dispersity data from triple detection are reported.

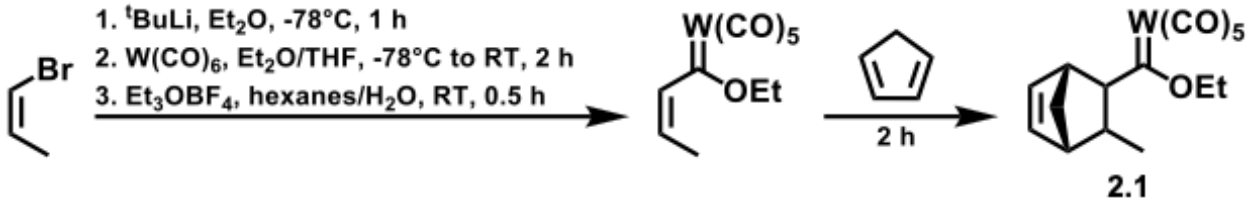
Synthetic Considerations

Synthesis of **2.1**



Tungsten carbene **2.1** was prepared in two steps according to a modification of the procedure reported by Wulff (Scheme 2.2).[45] A dry Schlenk flask was charged with a Teflon stir bar, cis-1-bromo-1-propene (1.35 mL, 15.9 mmol), and diethyl ether (Et_2O, 100 mL) before cooling the solution to -78 °C for 10 minutes. Tert-

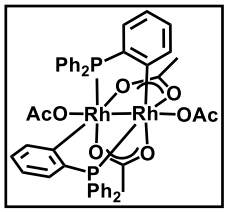
Scheme 2.2. Synthesis of 2.1



2.1

butyllithium (1.5 M in pentane, 21 mL, 31.7 mmol) was added dropwise, and the reaction was stirred at -78 °C for 1.5 hours. In a separate Schlenk flask, a suspension of tungsten hexacarbonyl (8.35 g, 23.8 mmol) in THF (100 mL) and Et_2O (100 mL) was cooled to -78 °C for 15 minutes. The cold propenyl lithium solution was then cannula transferred to this suspension under a flow of N_2. Following complete addition of the lithiate, the reaction mixture was warmed to room temperature with stirring over the course of 2.5 hours. The solvent was evaporated under vacuum, and triethyloxonium tetrafluoroborate (7.52 g, 39.6 mmol) was added to the resultant residue in a mixture of hexanes/water (11:4 v/v). The mixture was stirred at room temperature for 10 minutes, extracted with hexanes (3 x 50 mL), washed with water (3 x 50 mL), and dried over sodium sulfate. The crude product was purified via silica gel chromatography (hexanes as eluent). The isolated material (1.32 g, 2.7 mmol) was stirred with cyclopentadiene (5 mL, 59 mmol) for 2 hours at room temperature. The excess cyclopentadiene was evaporated in vacuo, and the crude product was purified via silica gel chromatography (hexanes as eluent) to afford **2.1** as an orange solid (0.84 g, 11% yield). Characterization data were in agreement with previous reports.[45] Consistent with previous reports, **2.1** was obtained as a mixture of diastereomers (80:20 *endo:exo*) that could not be further separated (Figure 2.21 and Figure 2.22).[45]

Synthesis of **2.5** for CO Detection



Rh complex **2.5** was prepared via an adapted procedure from Sancenón.[46,47] A dry Schlenk flask was charged with a Teflon stir bar, rhodium (II) acetate dimer (75 mg, 0.17 mmol), and triphenylphosphine (89 mg, 0.34 mmol). Glacial acetic acid (5 mL) was degassed via three freeze-pump-thaw cycles and added to the reaction vessel. The reaction was stirred at reflux (120 °C) for 2 hours under N_2. The reaction was cooled to room temperature, diluted with water (5 mL), and the product was extracted with $CHCl_3$ (3 x 10 mL). Excess triphenylphosphine was crystallized away using methanol. The product was obtained as a purple solid (95 mg, 58% yield). Characterization data were in agreement with previous reports (Figure 2.1, Figure 2.14, Figure 2.23 and Figure 2.24).[48]

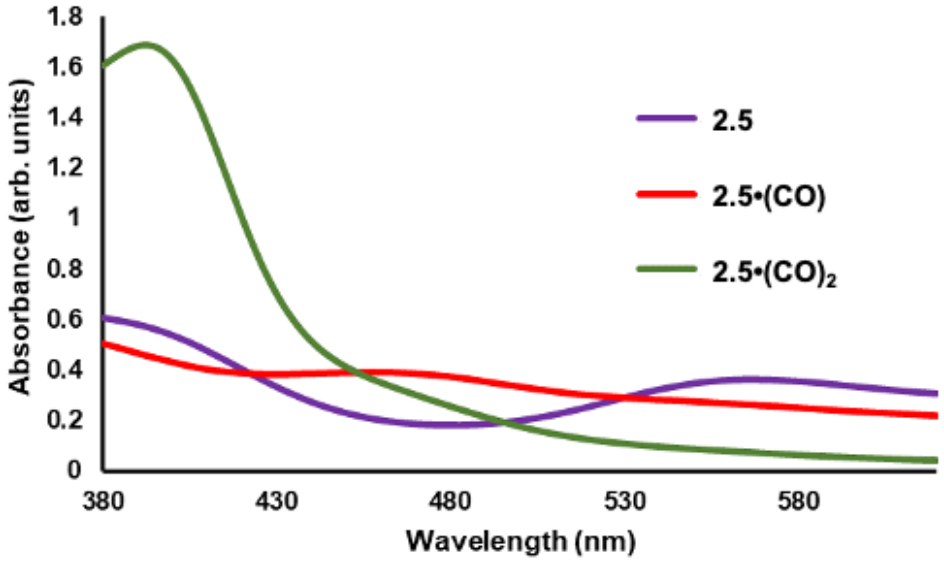
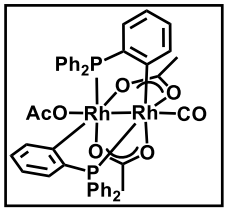
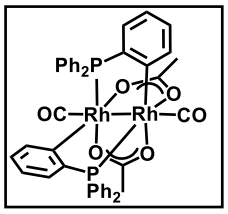


Figure 2.1. UV-vis Profiles for **2.5** (violet), **2.5•(CO)** (red), and **2.5•$(CO)_2$** (green)



2.5•(CO) was prepared via an adapted procedure from Sancenón.[46,47] $CO_{(g)}$ was generated *ex situ* by adding formic acid (3.6 µL, 85%, 0.0811 mmol) to sulfuric acid (1 mL, 18.4 M) and bubbled through a solution of **2.5** (4.46 mg, 4.6 µmol) in CD_2Cl_2 using the apparatus shown in Figure 2.18. The solution of **2.5** changed from violet to orange, and ^{1}H NMR spectroscopic analysis was consistent with complete conversion to **2.5•(CO)**. Characterization data were in agreement with previous reports (Figure 2.1, Figure 2.15, Figure 2.25 and Figure 2.26).[46,47]



2.5•(CO)$_2$ was prepared via an adapted procedure from Sancenón[46,47] by bubbling a large excess of $CO_{(g)}$ through a solution of **2.5** in CD_2Cl_2 for several minutes. Characterization data were in agreement with previous reports (Figure 2.1, Figure 2.16, Figure 2.27 and Figure 2.28).[46,47]

General Polymerization Procedure

In a N_2 filled glovebox, a stock solution of **2.4** was prepared in methylene chloride (CH_2Cl_2, 3.98 mM) and cooled to -35 °C. A solution of **2.1** in CH_2Cl_2 (0.025 M) was added to a vial and cooled to -35 °C for 10 minutes, after which an aliquot of the catalyst stock solution was added. The amount of catalyst solution added depended upon the desired $[\mathbf{2.1}]_0$:$[\mathbf{2.4}]_0$ ratios (Table 2.1). Polymerizations were conducted at -35 °C for 3 hours unless otherwise noted in Table 2.1. Polymerizations were quenched with benzaldehyde, and the resultant polymeric material was precipitated from methanol twice. SEC data for the isolated polymers are reported in Figure 2.2. ^{1}H and ^{13}C NMR spectra for the precipitated material were collected in $CDCl_3$ (Figure 2.30 and Figure 2.31, respectively). IR spectroscopic analysis of **2.P1** was consistent with incorporation of $W(CO)_5$ fragments into the polymer (Figure 2.3).

Synthesis of Block Copolymers with Norbornene

In a N_2 filled glovebox, a solution of **2.1** (54.9 mg, 0.11 mmol) in CH_2Cl_2 (4 mL, 0.025 M) was cooled to -35 °C, and a solution of **2.4** (0.15 mL, 6.88 mM in CH_2Cl_2) was added. The polymerization was conducted at -35 °C for 2 hours, after which time an aliquot (0.25 mL) was removed for analysis by SEC (Scheme 2.3). Norbornene (50.6 mg, 0.54 mmol) was added as a solution in CH_2Cl_2 (2 mL) to the reaction vessel and allowed to react at -35 °C for 2 hours. The polymerization was quenched with benzaldehyde, and the resultant copolymer was

Table 2.1. Selected Molecular Weight Data for **2.P1**

Entry	M_n[a]	Target M_n[b]	DP	Đ[c]	Yield (%)
1[d]	17,800	24,400	36	1.23	96
2[e]	43,500	48,800	90	1.15	95
3[d]	131,100	244,000	268	1.29	59
4[f]	234,500	488,000	480	1.32	55
5[g]	405,400	488,000	830	1.28	52

[a]Measured by SEC. [b]Calculated using $[2.1]_0$:[$2.4]_0$ × 488.15. [c]Calculated using M_w/M_n. [d]Conditions: −35 °C; $[2.1]_0$ = 0.025 M (0.102 mmol total); 3.5 h. [e]Conditions: −35 °C; $[2.1]_0$ = 0.025 M (2.40 mmol total); 3.5 h. [f]Conditions: −35 °C; $[2.1]_0$ = 0.05 M (0.102 mmol total); 5 h. [g]Conditions: −35 °C; $[2.1]_0$ = 0.1 M (0.102 mmol total); 5 h.

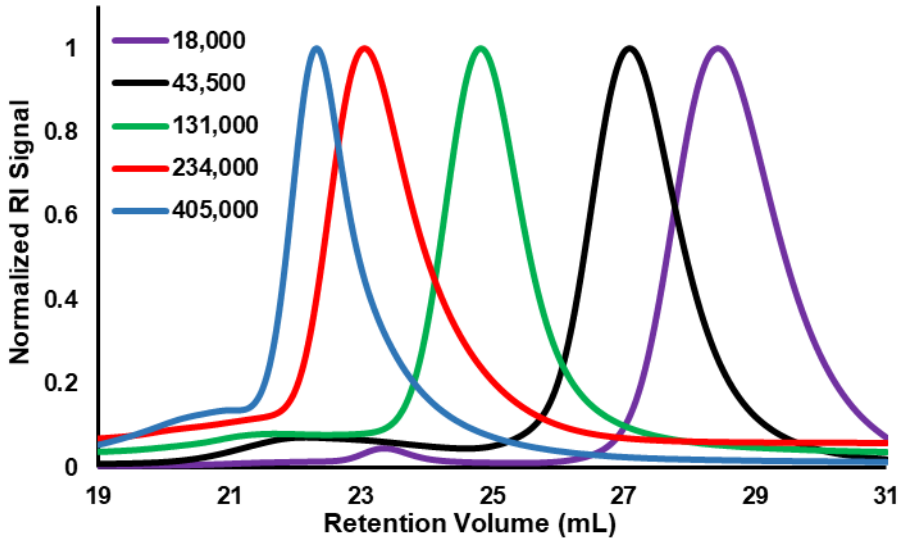


Figure 2.2. SEC Data for **2.P1** with THF as Eluent

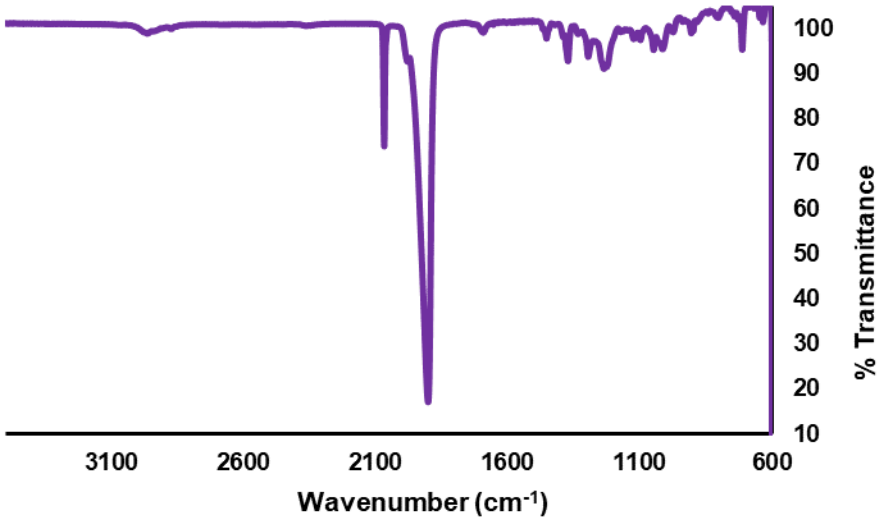
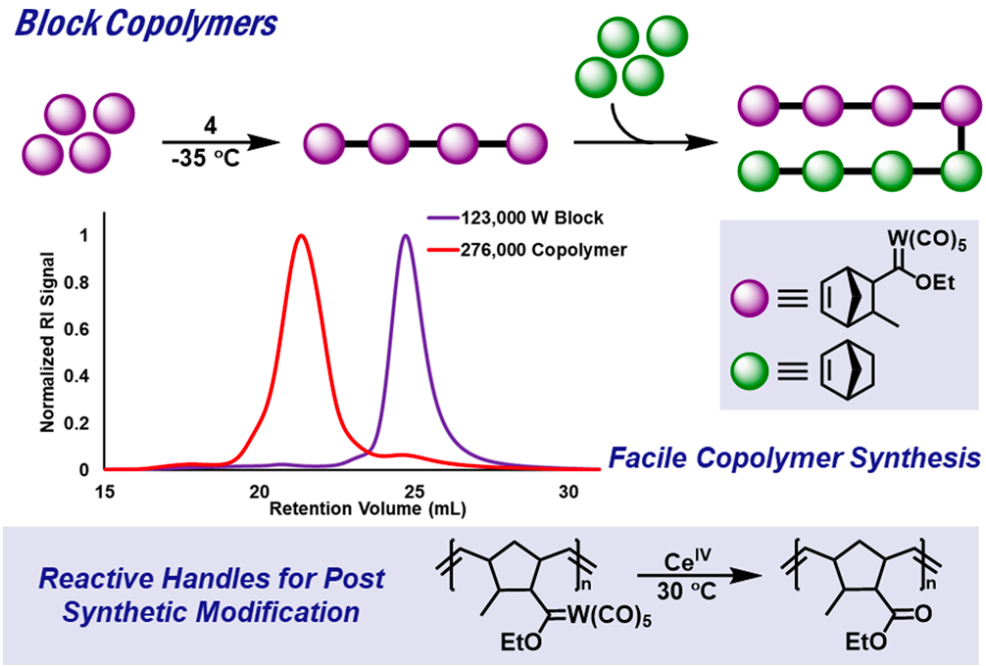


Figure 2.3. Representative IR Spectrum for 2.P1

Scheme 2.3. Synthetic Utility of Metallocarbene Polymers



precipitated from methanol twice. The isolated copolymer (65.8 mg; 62% yield) was analyzed via ^{1}H NMR spectroscopy (Figure 2.32) and SEC (Scheme 2.3).

Oxidative Demetallation of **2.P1**

A 1 dram vial was charged with a Teflon stir bar, **2.P1** (39.5 mg; 0.08 mmol), and THF (0.5 mL). A solution of ceric ammonium nitrate (75.2 mg; 0.14 mmol) in H_2O (0.1 mL) was added dropwise to the solution of **2.P1** at room temperature. The reaction was mixed by inversion, the sides of the vial were washed with THF (0.1 mL), and the reaction was stirred at room temperature for 1 h. A second portion of ceric ammonium nitrate (75.2 mg; 0.14 mmol) was added as a solution in H_2O (0.1 mL). The reaction was mixed by inversion, the sides of the vial were washed with THF (0.1 mL), and the reaction was stirred at 30 ºC for 16 h. Volatiles were removed under reduced pressure, and the yellow residue was washed with THF (3 × 0.5 mL). The residue was then washed with H_2O (1.0 mL) and centrifuged. The aqueous supernatant was decanted, and the pellet was dissolved in THF (1.0 mL). All organic washings were combined and filtered through a 0.45 μm syringe filter and concentrated under reduced pressure. The concentrated solution was then added to MeOH (2.0 mL) and the precipitated solid was collected. The precipitate was washed with H_2O (3 × 0.5 mL), MeOH (3 × 0.5 mL), and then dried *in vacuo* to afford a white powder (7.2 mg; 51% yield). ^{1}H NMR spectroscopic analysis confirmed complete consumption of the carbene moieties (Figure 2.33).

Results and Discussion

Polymerization Studies and Material Characterization

Tungsten carbene **2.1** was selected for our initial polymerization studies (Scheme 2.1).[45] We surmised that, in addition to providing a handle for metathesis, the norbornyl substituent of **2.1** would enhance the solubility of the final metallopolymer. Polymerization of **2.1** was initially attempted using Ru catalysts (**2.2a**, **2.2b**, and **2.3**)[49,50] due to their ease of handling and established ubiquity in ROMP (Scheme 2.1).[51–53] In general, a solution of **2.1** in deuterated chloroform ($CDCl_3$, 0.5 mL) was added to a J-Young tube and frozen. Solid catalyst (**2.2a**, **2.2b**, or **2.3**; [**2.1**]$_0$:[Catalyst]$_0$ ratios indicated in Table 2.2) was added to the frozen solution, and the sides of the tube were rinsed with additional $CDCl_3$ (0.2 mL). The frozen mixture was subjected to three freeze-pump-thaw cycles, and allowed to warm to room

Table 2.2. Initial Catalyst Screen for Polymerization of **1**

Entry	Catalyst	$[1]_0$:$[Catalyst]_0$	Time	Temp	Atmosphere	Conversion
1	2.2a	40:1	3 h	20 °C	N_2	0%
2	2.2a	40:1	1.5 h	30 °C	N_2	0%
3	2.2a	74:1	18 h	50 °C	N_2	0%
4	2.2a	74:1	18 h	60 °C	N_2	0%
6	2.2a	40:1	18 h	70 °C	N_2	Decomp
7	2.2a	83:1	18 h	20 °C	CO	0%
8	2.2a	83:1	6 h	50 °C	CO	0%
9	2.2a	83:1	4 h	60 °C	CO	0%
10	2.2a	83:1	12 h	70 °C	CO	Decomp
11	2.2a	40:1	2 wks	20 °C	N_2	0%
12	2.2b	39:1	1 h	20 °C	N_2	0%
13	2.3	38:1	1 h	20 °C	N_2	0%
14	2.3	38:1	1.5 h	30 °C	N_2	0%
15	2.3	38:1	18 h	70 °C	N_2	Decomp
16	2.3	38:1	2 wks	20 °C	N_2	0%
17	2.4	43:1	2 h	20 °C	N_2	100%

temperature under an atmosphere of N_2. Polymerization progress at a variety of temperatures was monitored using ^{1}H NMR spectroscopy (Table 2.2). However, no polymer was observed under a variety of reaction conditions (even after extended reaction periods of 2 weeks; Table 2.3 and Table 2.2).[54] To circumvent potential deligation of CO from **2.1**, polymerizations were also attempted under an atmosphere of CO (Table 2.2). In each case, no reaction (or monomer decomposition) was observed (Table 2.2 entries 1-15).

We note that Ru catalysts are known to decompose to catalytically inactive species in the presence of CO.[55–58] To explore whether or not this could explain the lack of reactivity observed with **2.1**, **2.2a** (16.7 mg, 0.02 mmol) was added to a J-Young tube, dissolved in deuterated methylene chloride (CD_2Cl_2, 0.8 mL), and analyzed by ^{1}H NMR spectroscopy (Figure 2.4, red). **2.1** (12.6 mg, 0.034 mmol) was then added to the reaction vessel, the solution was degassed via three freeze-pump-thaw cycles, and the reaction was warmed to room temperature under N_2 over the course of 5 min. The sample was analyzed by ^{1}H NMR spectroscopy (Figure 2.4, green) which indicated no reaction had occurred. After 4 hours at room temperature, the sample was analyzed via ^{1}H NMR spectroscopy (Figure 2.4, teal). The aromatic region showed the formation of new species that were consistent with CO-induced decomposition of **2.2a**[56] (also confirmed by comparison to a sample of **2.2a** that was independently exposed to excess CO; Figure 2.4, purple). We speculate that slow (or reversible) insertion of Ru catalysts into **2.1**, combined with poisoning of the catalysts by CO, is at least partially responsible for the lack of reactivity we observe (Table 2.2 and Figure 2.29). Polymerization of **2.1** was observed, however, using catalyst **2.4**. In a N_2 filled glovebox, solid catalyst **2.4** was added to a solution of **2.1** in CD_2Cl_2, and the polymerization progress was monitored via ^{1}H NMR spectroscopy. Initial experiments yielded high dispersity polymers with M_n's that exceeded the expected value. Cooling and diluting the polymerization lowered the dispersity and yielded polymers with M_n's more consistent with the expected value. (Table 2.3, entries 1-8). The optimized conditions for polymerization of **2.1** were determined to be 0.025 M, at -35 °C for 3.5 hours (Table 2.3, entry 9).

In contrast, rapid polymerization of **2.1** was achieved using Schrock-type catalyst **2.4** (Table 2.4).[59] Polymerizations conducted at 20 °C (0.15 M) reached complete conversion within 10 min, as determined by ^{1}H NMR spectroscopy. The reaction mixture was quenched

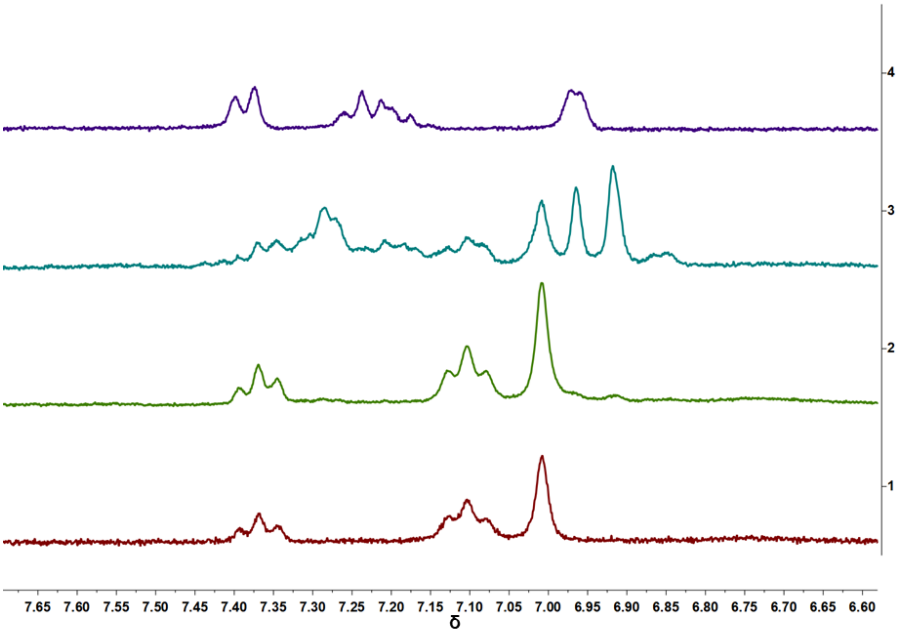


Figure 2.4. ^{1}H NMR Spectra from Analysis of **2.2a** Poisoning. **2.2a** (red), **2.2a** 5 Minutes after 1 Equivalent of **2.1** Added (green), **2.2a** 4 Hours after Addition of **2.1** (teal), and **2.2a** after Exposure to $CO_{(g)}$ (purple)

Table 2.3. Optimization of Polymerizaation of **2.1** Using Catalyst **2.4**

Entry	$[\mathbf{2.1}]_0$[a] (M)	Catalyst Addition	$[\mathbf{2.1}]_0$: $[\mathbf{2.4}]_0$	Time (h)	Temp (°C)	Expected M_n	M_n	Đ
1	0.1	Solid	41:1	2	20	20,000	320,000	3.05
2	0.1	Solid	206:1	0.33	20	100,500	465,000	1.60
3	0.25	Solid	29:1	0.33	20	14,000	102,700	2.27
4	0.05	Solid	35:1	0.33	20	17,000	122,200	2.12
5	0.025	Solid	51:1	0.33	20	25,000	283,300	4.29
6	0.025	Solid	46:1	1	0	22,500	66,600	2.21
7	0.025	Solid	30:1	3	0	14,500	49,300	1.82
8	0.025	Solid	33:1	1.5	-35	16,000	72,100	1.33
9	0.025	Solution[b]	49:1	3.5	-35	24,000	17,500	1.36

(a) Solution in CH_2Cl_2

(b) $[\mathbf{2.4}]_0$ = 3.98 mM in CH_2Cl_2

Table 2.4. Catalyst Screening for Polymerization of **2.1**

Entry	Catalyst[a]	Time	Temperature	Atmosphere	Conversion
1	2.2a	3 h	20 ºC	N_2	0%
2	2.2a	2 weeks	20 ºC	N_2	0%
3	2.2b	1 h	20 ºC	N_2	0%
4	2.3	1 h	20 ºC	N_2	0%
5	2.4	10 min	20 ºC	N_2	100%

[a]See Scheme 2.1.

with benzaldehyde and added to methanol to precipitate any polymer, and the isolated material was analyzed using size exclusion chromatography (SEC). The polymer displayed high dispersity (Đ = 2.27), and the calculated number-average molecular weight (M_n) far exceeded the targeted value (c.f. 102,700 versus 19,500 Da). These data suggested that deleterious secondary metathesis reactions could be operative; thus, we hypothesized that conducting polymerizations at reduced temperatures and under higher dilution might mitigate these issues.[60] Indeed, polymerization of **2.1** at lower concentrations (0.025 M) and temperatures (−35 °C) afforded the desired metallocarbene-containing polymer, **2.P1**, with low dispersity and calculated M_n values that agreed with the theoretical values (Table 2.3).

Having established general reaction conditions, we successfully prepared materials exhibiting a wide range of molecular weights (M_n = 17,870−405,400 Da; Đ < 1.4) in modest to excellent yield (52−96%; Table 2.1). Given the relatively high molecular weight of the monomer, we emphasize that the M_n values determined by SEC correspond to high degrees of polymerization (DP = 36−830). We also note that access to high DP materials required more concentrated conditions (although this was accompanied by premature precipitation of the polymer in some cases; see Table 2.4). As anticipated, these metallopolymers were soluble in common organic solvents (e.g., chloroform, tetrahydrofuran, methylene chloride). Since these materials were easily processed, we sought to characterize some of their physical properties in more detail. Thermogravimetric analysis (TGA) revealed a relatively high decomposition onset temperature of 135 °C (Figure 2.5).[41,42] The 12% mass change at 135 ºC is consistent with the mass loss observed after loss of 2 CO per repeat unit. The mechanical properties of **2.P1** were also investigated using dynamic mechanical analysis (DMA), but films of the brittle material yielded at low strain (< 1%; Figure 2.6). The modulus of these materials was determined to be 1.7 GPa, which is significantly higher than unfunctionalized polynorbornene (0.09 GPa) and similar to polystyrene and polymethylmethacrylate.[61]

Block Copolymer Synthesis and Post Polymerization Modifications

We also explored the more general utility of our carbene materials. For example, block copolymers of **2.1** and norbornene were easily prepared by sequential monomer addition (Scheme 2.3). The resultant copolymer was isolated in good yield (62%), and we observed nearly quantitative chain extension via SEC (Scheme 2.3). This result suggests that **2.1** may

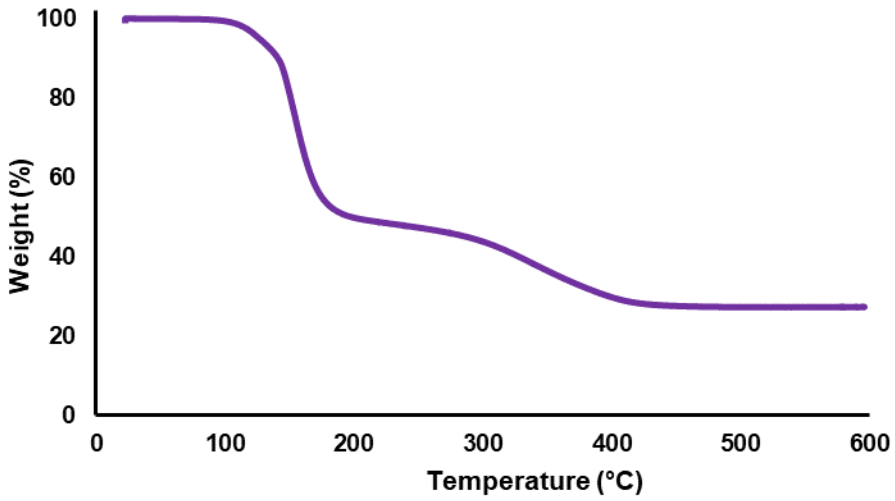


Figure 2.5. Representative TGA Thermogram of **2.P1** (Ramp Rate of 10 °C/min in N_2)

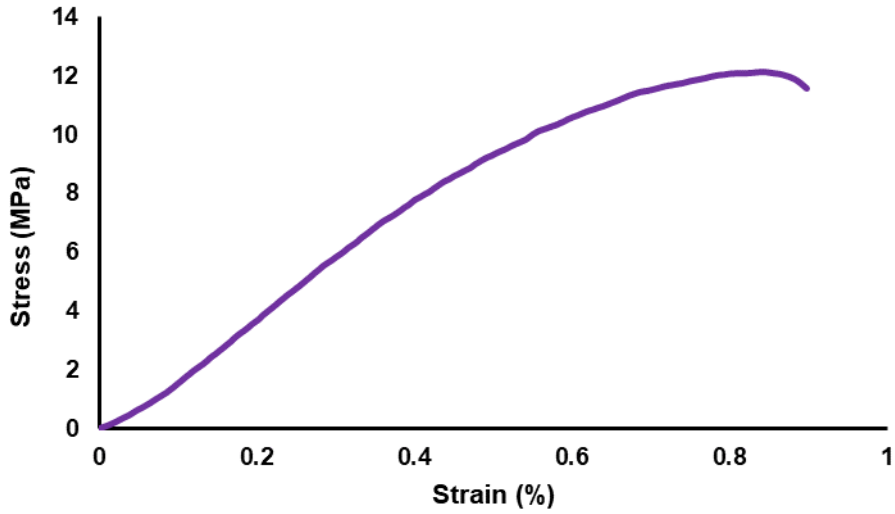


Figure 2.6. Representative DMA Stress Strain Plot for **2.P1** (0.1% strain/min)

be compatible with common ROMP monomers, which is critical for creating hybrid organic/inorganic materials with precisely tailored microstructures. The carbene moieties of **2.P1** could also be leveraged for post-synthetic modifications (Scheme 2.3). For example, demetallation with ceric ammonium nitrate proceeded smoothly to afford ester-containing polymers (Figure 2.7 and Figure 2.33).[62] IR analysis revealed the carbene CO stretches were no longer present in the material, and a new stretch at 1734 cm^{-1} (consistent with the formation of ester moieties) was observed (Figure 2.7). This reactivity is in agreement with known demetallations of Fischer carbenes using ceric ammonium nitrate.[62] The ability to engage the carbene center and install orthogonal functional groups (which could, in turn, be elaborated through further synthetic manipulations) suggests that metallocarbene-containing polymers could be powerful platforms for developing tunable materials.

CO Release Experiments

Given the abundance of $W(CO)_5$ fragments in **2.P1**, we hypothesized it could exhibit selectively triggered carbon monoxide (CO) release. The potent antimalarial[63] and antimicrobial[64] properties of CO have long been known; however, recent studies have demonstrated that CO can limit reperfusion injury[65] and aid recovery following organ transplants.[66] As such, CO-releasing materials (CORMs), which represent alternatives to gaseous CO, have emerged as promising platforms for developing CO therapy.[67] In contrast to the behavior of chromium Fischer carbenes,[68,69] CO extrusion from tungsten carbenes is rare.[70] Agostic interactions between tungsten and alkoxy substituents, however, have been reported to facilitate expulsion of CO,[71] and we envisioned that analogous stabilization within **2.P1** could enable CO release. Since TGA revealed negligible mass loss below the decomposition temperature of **2.P1** (Figure 2.5), we decided to explore photolytic CO release.

SEC Analysis of Irradiated Polymer

2.P1 was analyzed by SEC in $CHCl_3$ (M_n = 86,690 Da; Figure 2.8). **2.P1** was then dissolved in THF (10 mg/mL) and irradiated for 3 hours at 20 °C (*vide supra*). The solvent was removed under vacuum, and the material was dissolved in $CHCl_3$ and analyzed by SEC (M_n = 78,010 Da; Figure 2.8). The change in mass of 8,680 Da corresponds to 10% of the total mass of the polymer. A mass loss of 12% corresponds to loss of 2 CO moieties from each repeat unit, and 6% mass loss correspond to loss of 1 CO moiety from each repeat unit.

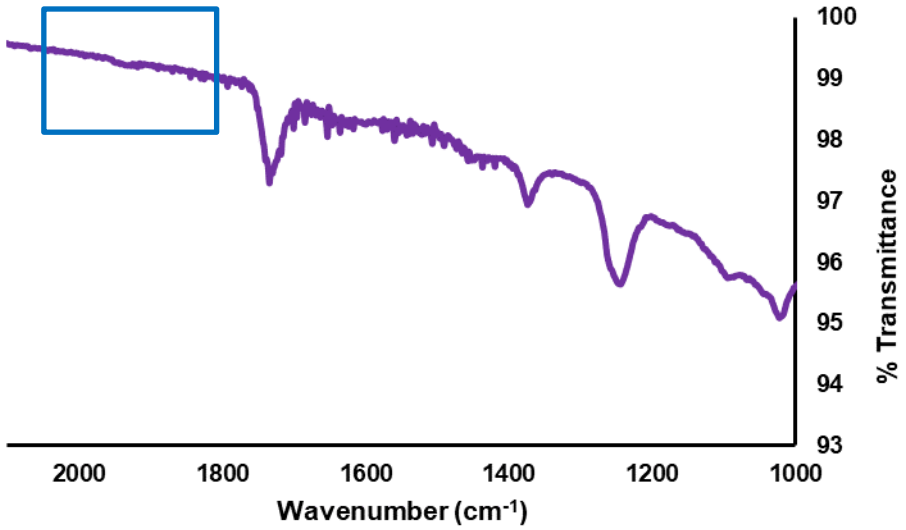


Figure 2.7. IR Spectrum for **2.P1** Following Demetallation. Blue Box Indicates Region Where Initial CO Stretches Appeared.

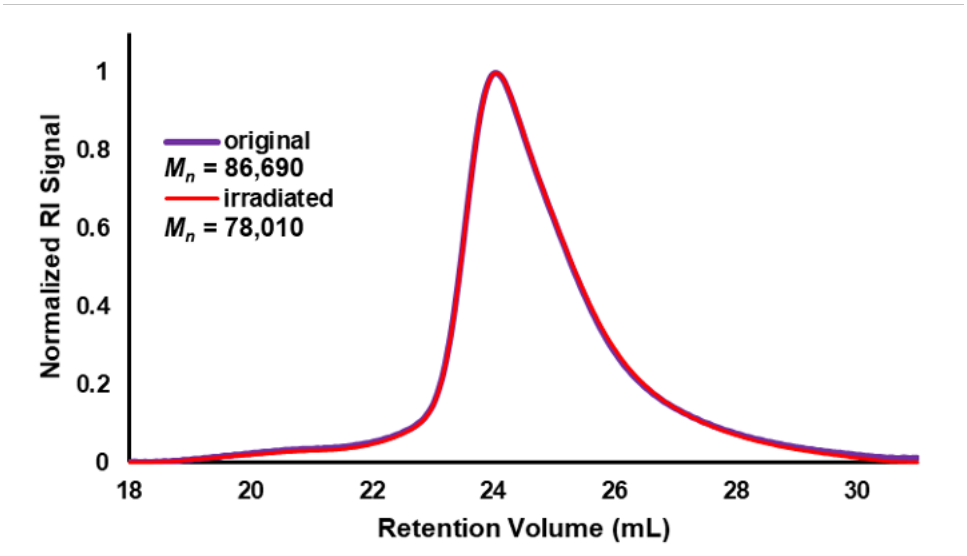


Figure 2.8. SEC Traces of **2.P1** before (violet) and after (red) Irradiation

Infrared Spectroscopy Measurements

Initially, we sought to quantify CO extrusion using infrared (IR) spectroscopy. The CO stretching frequencies of the carbene motif (1967 and 1944 cm^{-1}) were monitored at various **2.P1** concentrations (0.096–1.0 mg/mL in tetrahydrofuran (THF); 0.98–10 mM CO), and a calibration curve was constructed using the band at 1944 cm^{-1} and the Beer–Lambert Law (which afforded a linear correlation; Figure 2.9A).[72] A validation sample of **2.P1** (0.801 mg/mL in THF, 8.2 mM CO) was analyzed using IR spectroscopy (Figure 2.9A), after which the sample was irradiated using a 33 W compact fluorescent lamp (CFL; emission spectrum is shown in Figure 2.19) placed 6" from the sample for 3 hours. The sample was kept at 20 °C to preclude thermal contributions to CO release. The post-irradiated sample was analyzed using IR spectroscopy, and the measured change in the CO absorbance was consistent with loss of ~ 1.8 equivalents of CO per repeat unit (Figure 2.9A). As expected, the intensity of the CO stretches decreased upon irradiation, and the calculated change in CO concentration was consistent with a loss of ~1.8 equiv of CO per repeat unit (Figure 2.9A). This value was in good agreement with the measured change in M_n for a post-irradiated sample of **2.P1** (ΔM_n = 8,680 Da; Figure 2.8).

Demonstration of CO Release from **2.P1** using **2.5**

Given that it is unusual for tungsten carbenes to release CO,[70,71] we sought to further validate this observation. Rhodium complex **2.5**, which exhibits a colorimetric response to CO binding,[46,47] was selected to confirm CO release from our polymers using UV–vis spectroscopy (Figure 2.9B; Figure 2.1, Figure 2.10-Figure 2.13). In general, a **2.P1** sample was added to a septum-capped vial and dissolved in THF ($[CO]_0$ = 0.85 M). In a separate cuvette, **2.5** was dissolved in $CHCl_3$ (2.1 μmol), and analyzed using UV-vis spectroscopy. The two vessels were then connected with a glass manifold as shown in Figure 2.18. The **2.P1** sample was irradiated for 3 h (*vide supra*), after which the headspace in the vial was transferred to the cuvette using a gentle stream of N_2 for 3 minutes. The $CHCl_3$ solution was then analyzed using UV-vis spectroscopy to identify the relative amounts of **2.5, 2.5•(CO), and 2.5•$(CO)_2$**, (which is consistent with the known CO-binding properties of **2.5**;[47] Figure 2.9B, Figure 2.1, Figure 2.10-Figure 2.13). Microsoft Excel was used to obtain relative percentages of each species by

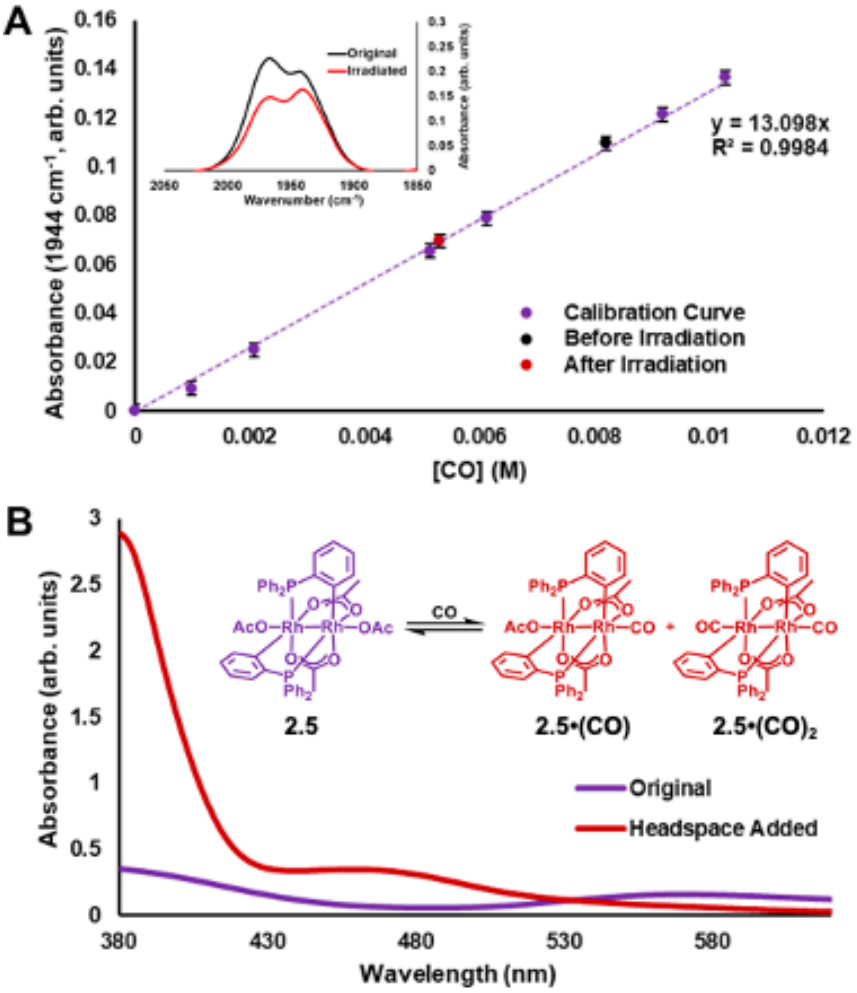


Figure 2.9. Determination of CO Release from **2.P1**. (A) Calibration curve for CO release measurement via IR spectroscopy. Inset shows the CO stretching frequencies of a **2.P1** sample before (black) and after (red) irradiation. (B) UV–vis spectra for CO sensor **2.5** (violet) showing binding of CO released from **2.P1** (red).

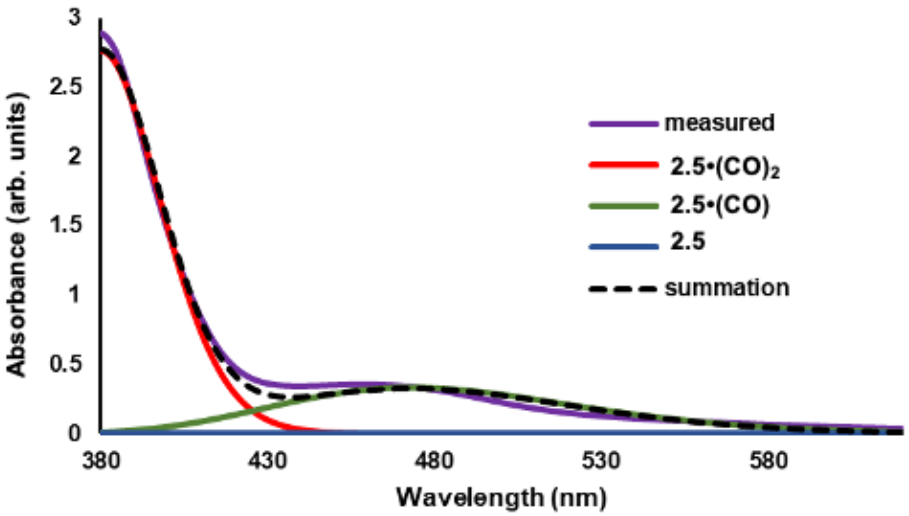


Figure 2.10. Deconvoluted UV-vis Spectrum of **2.5** after Transfer of Headspace from **2.P1** Solution Irradiated under Aerobic Conditions. Spectrum is Consistent with an 81:19 Mixture of **2.5•(CO)** and **2.5•(CO)$_2$**

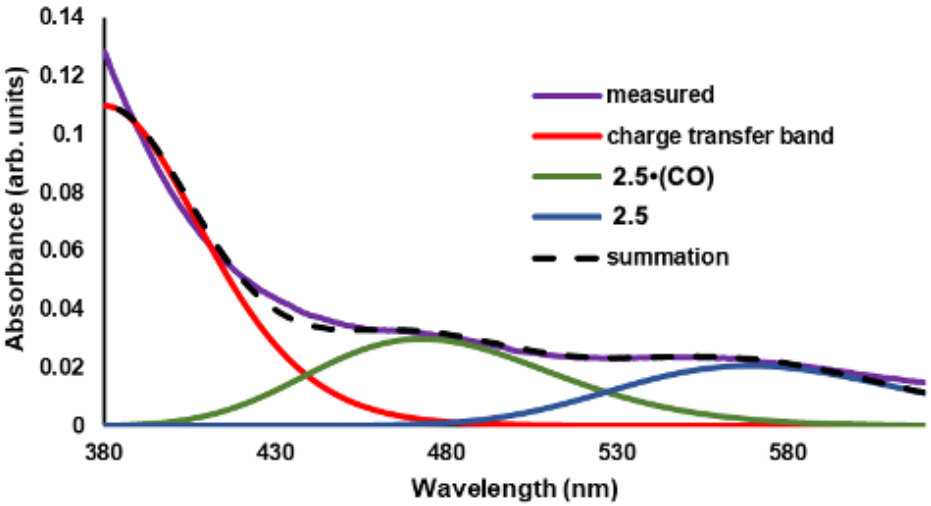


Figure 2.11. Deconvoluted UV-vis Spectrum of **2.5** after Transfer of Headspace from **2.P1** Solution Irradiated under Anaerobic Conditions. Spectrum is Consistent with 71:29 Mixture of **2.5•(CO)** and **2.5**

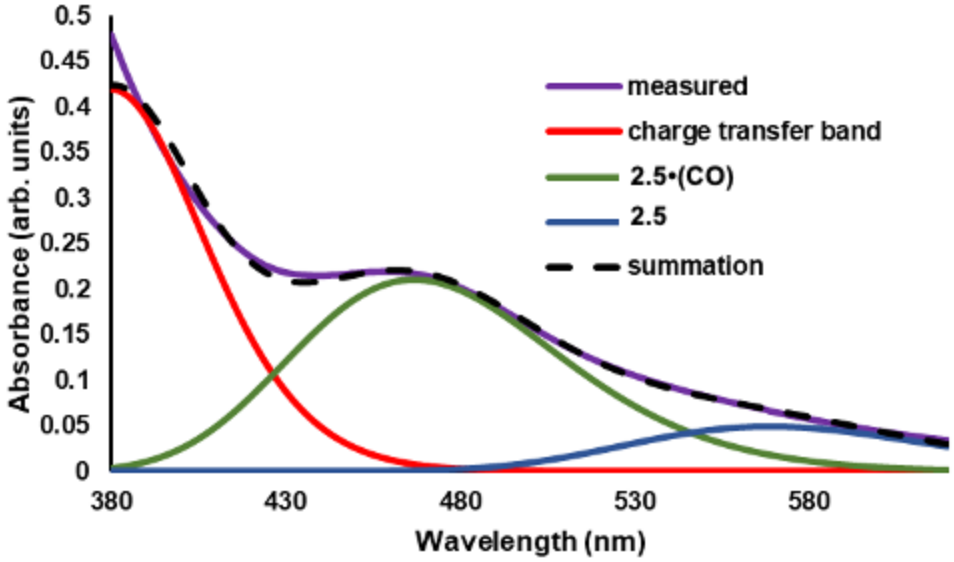


Figure 2.12. Deconvoluted UV-vis Spectrum of **2.5** after Transfer of Headspace from **2.P1** Solution Kept in the Dark under Aerobic Conditions. Spectrum is Consistent with 85:15 mixture of **2.5•(CO)** and **2.5**

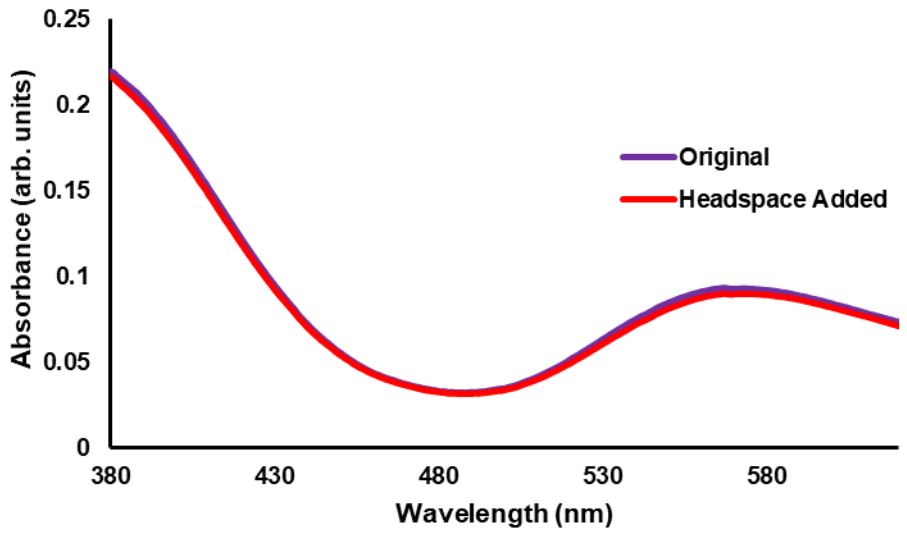


Figure 2.13. UV-vis Spectrum of **2.5** after Transfer of Headspace from **2.P1** Solution Kept in the Dark under Anaerobic Conditions. Overlay of **2.5** before (purple) and after (red) Transfer of Headspace Shows No Change

deconvolution of the UV-vis spectra.[73] The band width and λ_{max} were held constant (determined using data in Figure 2.1), and the fitting was calculated by minimizing the residuals with a X^2 analysis using the solver function.

Irradiation of **2.P1** under Aerobic Conditions

In air, **2.P1** (162.9 mg, M_n = 86,690 Da) was dissolved in THF (3 mL) and connected to a cuvette containing a solution of **2.5** (2.05 mg, 2.1 μmol) in $CHCl_3$ (3 mL) using a glass manifold (Figure 2.18). The solution of **2.P1** was held at 20 °C and irradiated 3 hours (*vide supra*). After irradiation, N_2 was bubbled through the apparatus for 3 minutes to transfer any CO from the headspace of the solution of **2.P1** to the solution of **2.5**. The UV-vis absorption profile of **2.5** following this treatment was measured and compared to the initial spectrum (Figure 2.10). Deconvolution of the spectrum (Figure 2.10) was consistent with conversion of **2.5** to a mixture of **2.5•(CO)** (81%) and **2.5•$(CO)_2$** (19%).

Irradiation of **2.P1** under Anaerobic Conditions

In a N_2 filled glovebox, **2.P1** (21.6 mg, 86,690 Da) was dissolved in THF (3 mL). The **2.P1** solution was held at 20 °C and irradiated for 3 hours (*vide supra*). After irradiation, the vessel containing the **2.P1** solution was connected to a cuvette containing a solution of **2.5** (0.441 mg, 0.46 μmol) in $CHCl_3$ (2.5 mL) using a glass manifold (Figure 2.18). N_2 was bubbled through the apparatus for 3 minutes to aid transfer of CO from the **2.P1** solution to the solution of **2.5**. The UV-vis absorption profile of **2.5** following this treatment was measured and compared to the initial spectrum. Deconvolution of the spectrum (Figure 2.11) was consistent with conversion of **2.5** to a mixture of **2.5** (29%) and **2.5•(CO)** (71%).

Determination of CO Release from **2.P1** under Aerobic Conditions without Irradiation

In air, **2.P1** (151.9 mg, 86,690 Da) was dissolved in THF (3 mL). The **2.P1** solution was wrapped tightly with aluminum foil to eliminate exposure to light, and the vial was held at 20 °C for 3 hours. After 3 hours, the vessel containing the **2.P1** solution was connected to a cuvette containing a solution of **2.5** (1.793 mg, 1.9 μmol) in $CHCl_3$ (3 mL) using a glass manifold (Figure S14). N_2 was bubbled through the apparatus for 3 minutes to aid transfer of CO from the headspace of the **2.P1** solution to the solution of **2.5**. The UV-vis absorption profile of the solution of **2.5** was then measured and compared to the profile obtained before

the headspace treatment. Deconvolution of the spectrum (Figure 2.12) was consistent with conversion of **2.5** to a mixture of **2.5** (15%) and **2.5•(CO)** (85%).

Measurement of CO Release from **2.P1** under Anaerobic Conditions without Irradiation

In a N_2 filled glovebox, **2.P1** (10.0 mg, 86,690 Da) was dissolved in THF (3 mL). The **2.P1** solution was wrapped tightly with aluminum foil to eliminate exposure to light, and the sample was held at 20 °C for 3 hours. After 3 hours, the vessel containing the **2.P1** solution was connected to a cuvette containing a solution of **2.5** (1.124 mg, 1.1 μmol) in $CHCl_3$ (3 mL) using a glass manifold (Figure 2.18). N_2 was bubbled through the apparatus for 3 minutes to aid transfer of CO from the headspace of the **2.P1** solution to the solution of **2.5**. The UV-vis absorption profile of the solution of **2.5** was then measured and compared to the profile obtained before the headspace treatment. No change was observed between the two spectra (Figure 2.13).

Control experiments revealed negligible CO release in the absence of light under an inert atmosphere. Interestingly, however, aerobic conditions were found to induce CO release (even without irradiation; Figure 2.12). The mechanism of CO release under aerobic conditions is unclear at present, as the stimulus could be either H_2O or O_2.[74] Collectively, these data support the conclusion that our tungsten carbene polymers expel CO under the action of light or molecular oxygen. Although such behavior is unusual for tungsten carbenes (and is the subject of ongoing investigation), the ability to trigger CO release using orthogonal stimuli could afford new avenues of exploration in CORMs.

Summary

In sum, we have demonstrated the successful preparation of well-defined, metallocarbene-containing polymers using a metathesis polymerization strategy. These unique materials exhibited stimuli responsive behavior (e.g., CO release), were readily integrated with other polymeric scaffolds, and could be leveraged for post-synthetic modifications. Moreover, these polymers could address limitations in current methodologies for synthesizing metallopolymers (e.g., controllable incorporation of metal species, enhanced thermal stability and solubility, tunable metal sites). As such, we envision these results will serve as inspiration for the development of related functional materials.

Appendix

UV-vis absorbance data for CO release studies

Data corresponding to **2.5** and additional support for CO release experiments are shown in Figure 2.14 - Figure 2.20.

Thermomechanical Data

Representative thermomechanical data for **2.P1** (M_n = 116,000 Da) are shown in Figure 2.5 and Figure 2.6. The TGA thermogram of a powdered sample indicated an initial decomposition onset temperature of 135 °C (Figure 2.5). Negligible mass loss was observed below this temperature. A rectangular film of the same polymer was cast from $CHCl_3$ (20 w% P1) and analyzed using DMA (with a film tension clamp). The Young's modulus of the material was found to be ~ 1.7 GPa, and the material yielded at 0.86% strain (Figure 2.6).

Determination of Molar Absorptivity of **2.5•(CO)**

CO release from **2.P1** was demonstrated using UV-vis spectroscopy. Known CO detector **2.5** exhibits unique absorption profiles upon binding of CO.[46,47] These profiles can be directly correlated to the number of CO ligands bound to the metal (Figure 2.1). Although **2.5** has been reported to selectively bind CO, the change in Lewis acidity after binding one CO ligand [which affords **2.5•(CO)**] significantly decreases the binding affinity for the second CO ligand; thus, conversion of **5** to the bis-CO adduct **2.5•$(CO)_2$** requires a large excess of CO.[46,47] The molar absorptivity (ε) of **2.5•(CO)** has not previously been reported; **2.5•(CO)** was prepared as described above (*vide supra*), and the molar absorptivity was determined using the Beer-Lambert Law ($\varepsilon_{5\bullet(CO)}$ = 325 M^{-1} cm^{-1}; Figure 2.17). Each data point in Figure 2.17 was collected in triplicate.

UV-vis Spectroscopic Analysis of **2.1** and **2.P1**

The UV-vis absorption profile of **2.1** was obtained in THF and compared to the profile of **2.P1** (55,000 Da in THF; Figure 2.20). The observed UV-vis spectrum from **2.P1** is consistent with the SEC UV-vis profile of the material at the elution volume of the polymer (Figure 2.20 inset).

NMR Spectra

All NMR spectra for compounds listed in the chapter are shown in Figure 2.21 - Figure 2.33.

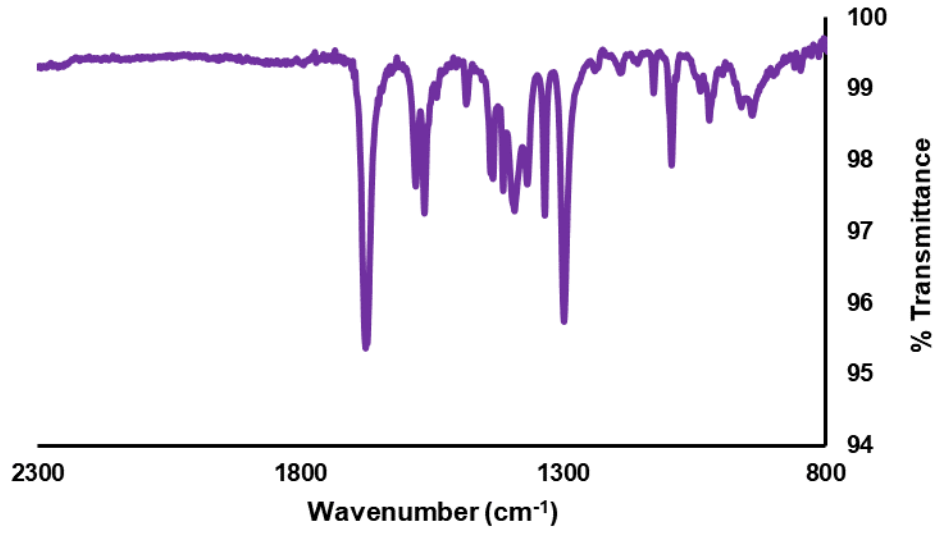


Figure 2.14. IR Spectrum for 2.5

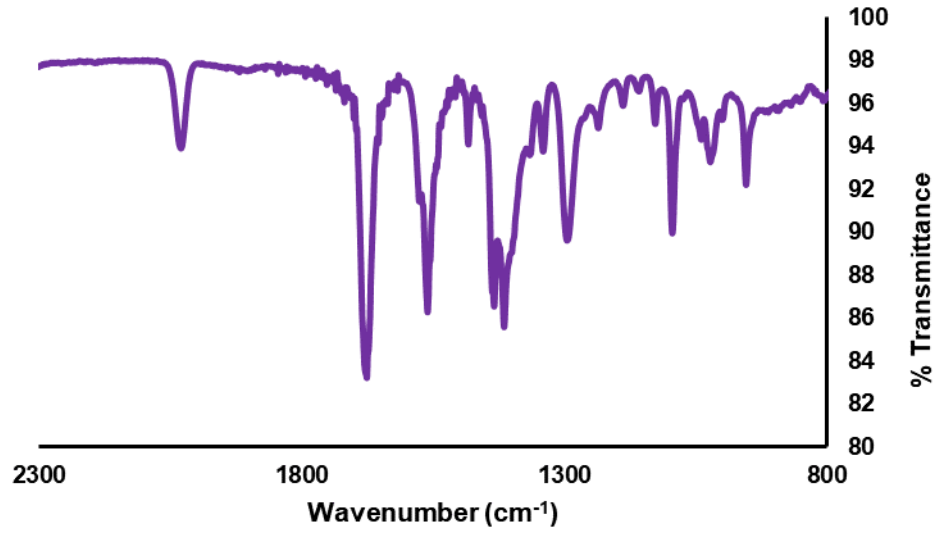


Figure 2.15. IR Spectrum for 2.5•(CO)

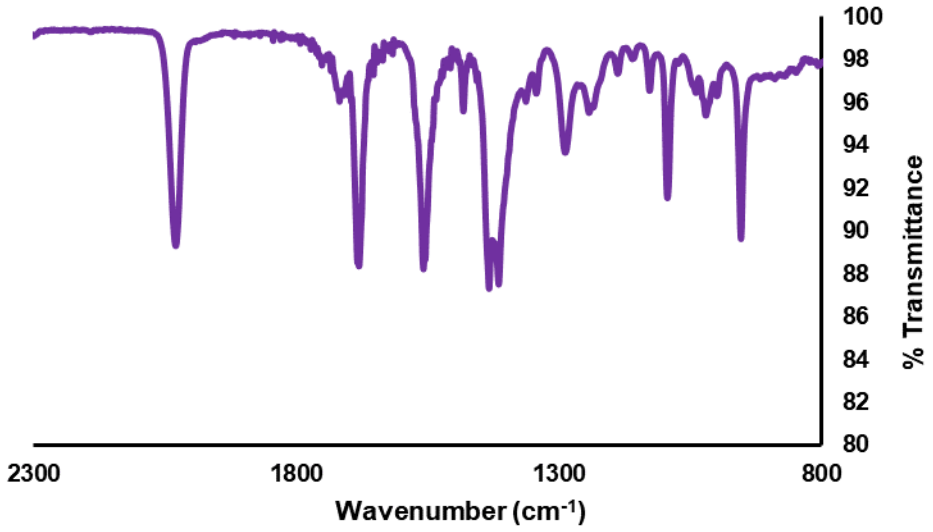


Figure 2.16. IR Spectrum for **2.5•(CO)$_2$**

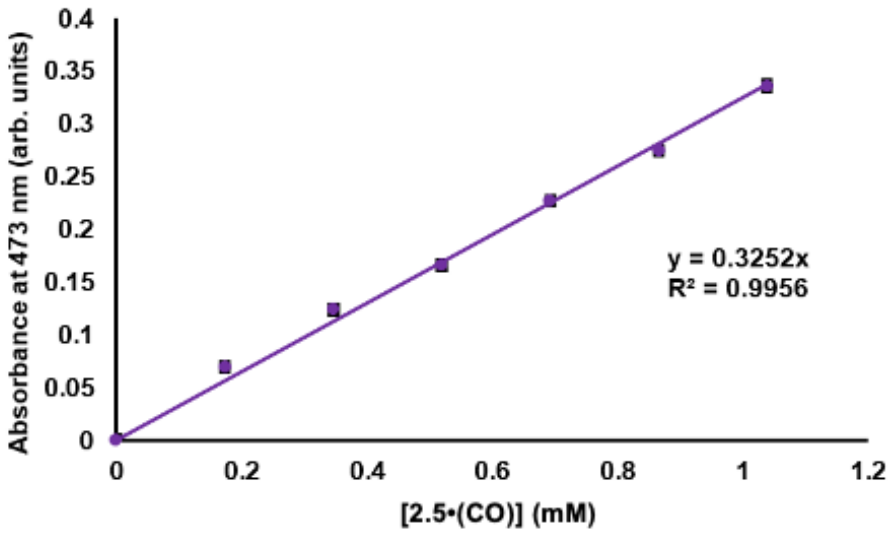


Figure 2.17. Calibration Curve for Determining Molar Absorptivity of **2.5•(CO)**



Figure 2.18. Apparatus for Irradiation of **2.P1** and Transfer of CO from Headspace to a Solution of **2.5**

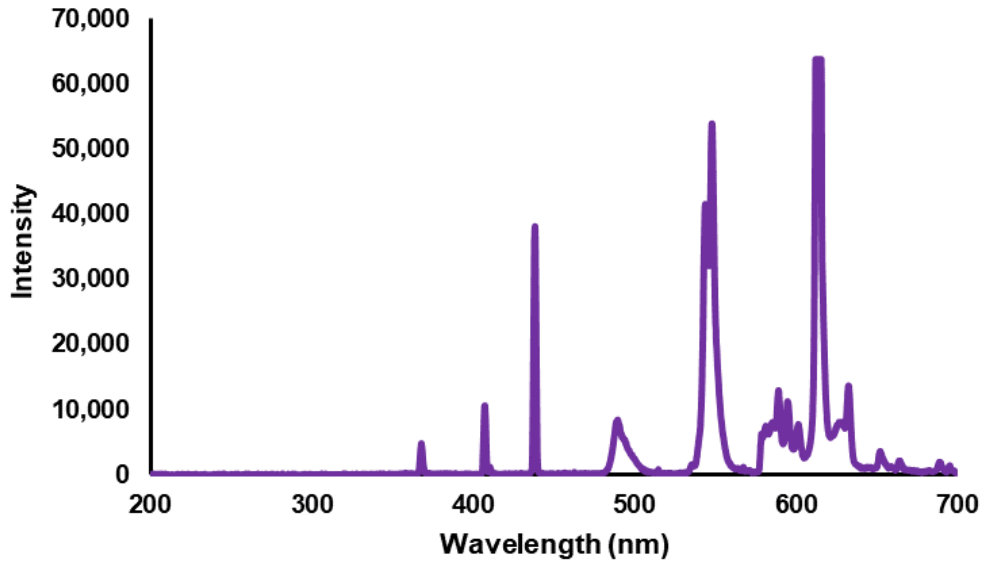


Figure 2.19. Emission Spectrum of 33 W Compact Fluorescent Lamp

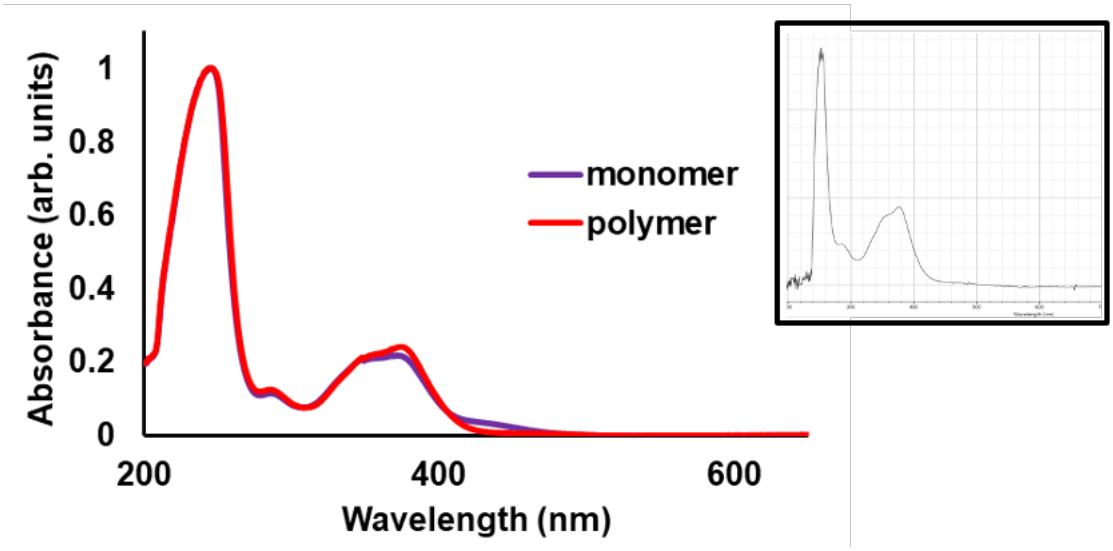


Figure 2.20. UV-vis Overlay of **2.1** & **2.P1**, λ_{max} = 246 nm. Inset: UV-vis profile from SEC of **2.P1** with $CHCl_3$ as Eluent (M_n = 341,000 Da; 23.17 mL retention volume)

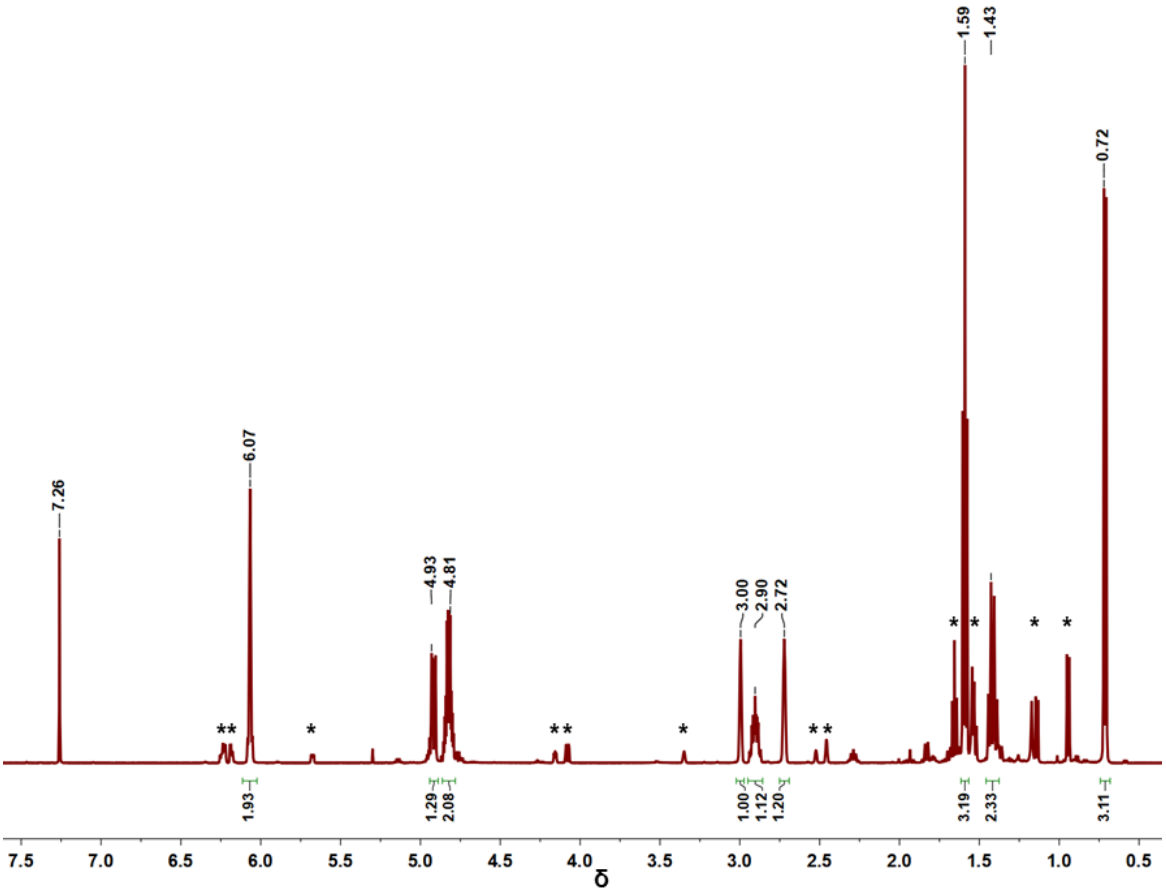


Figure 2.21. ^{1}H NMR Spectrum for **2.1**. Peaks for Major Diastereomer are Picked and Integrated. Minor Diastereomers are Labelled with *.

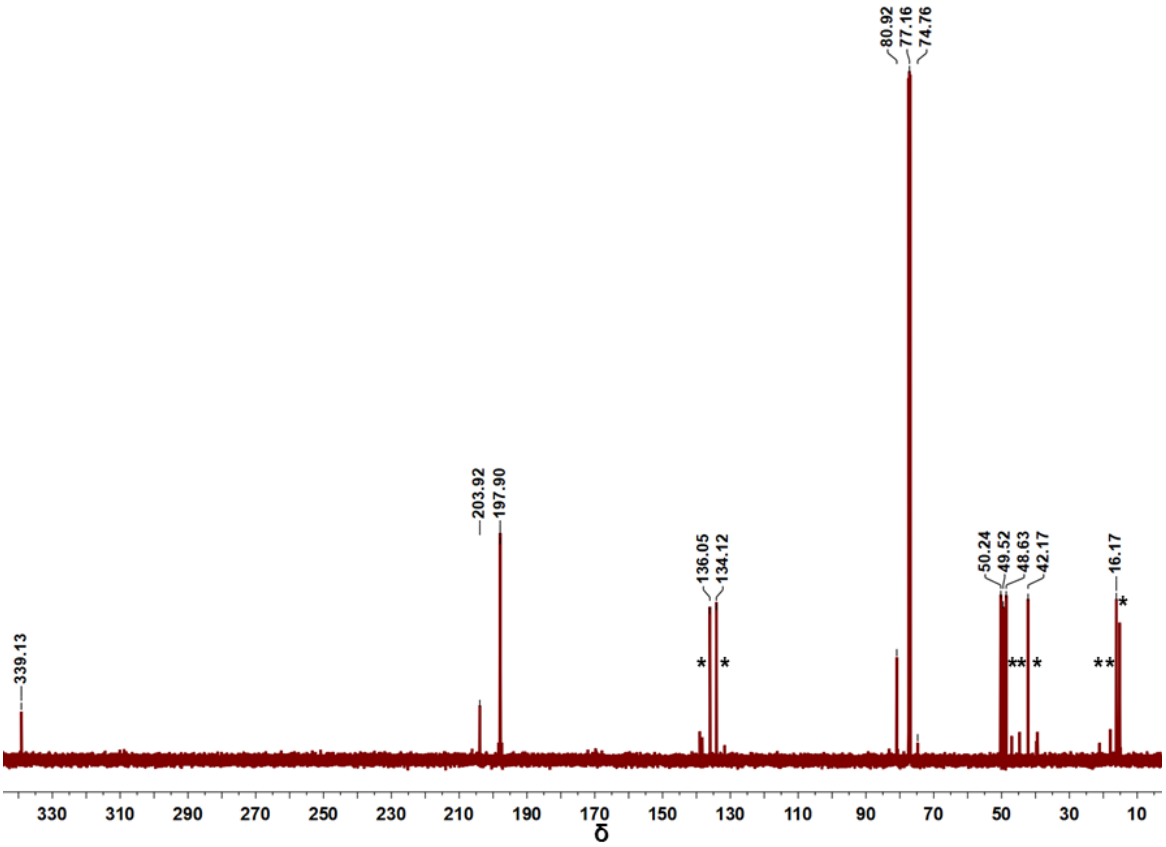


Figure 2.22. ^{13}C NMR Spectrum for **2.1**. Peaks for Major Diastereomer are Picked and Integrated. Minor Diastereomers are Labelled with *.

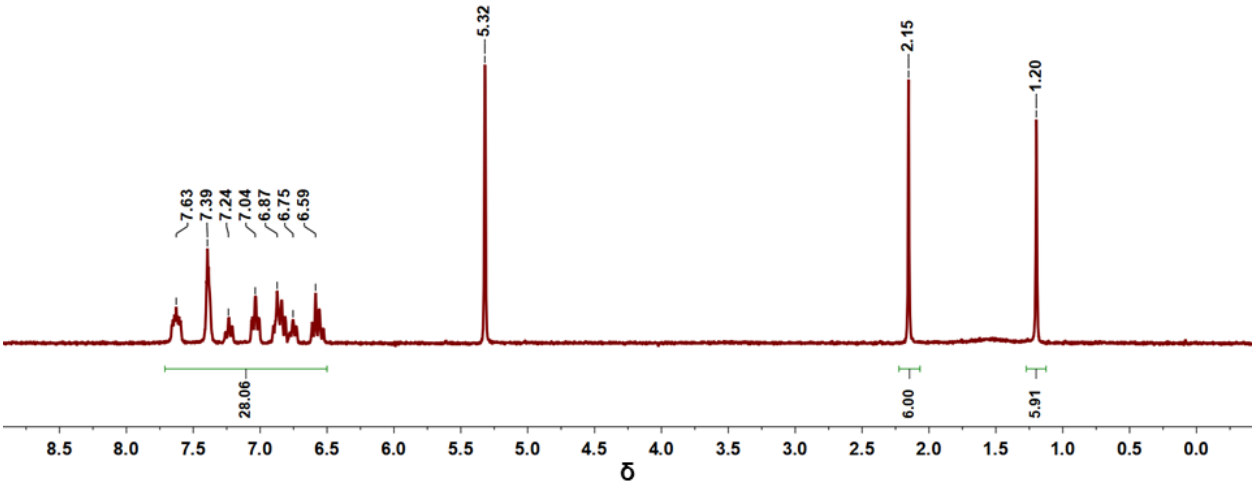


Figure 2.23. ^{1}H NMR Spectrum for **2.5.**

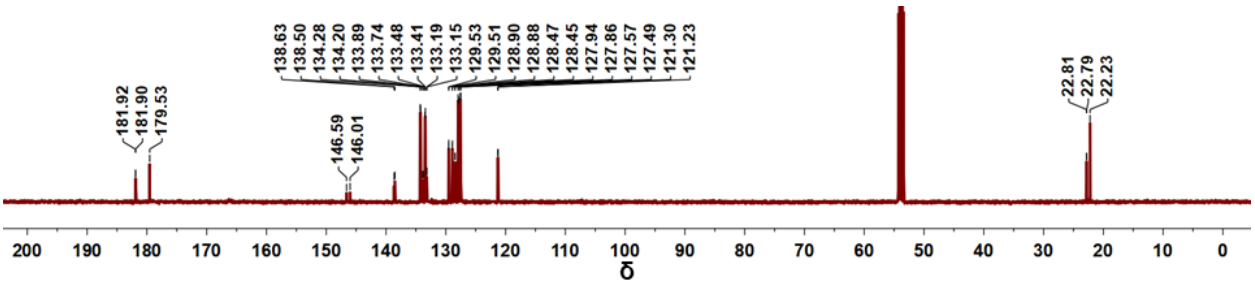


Figure 2.24. ^{13}C NMR Spectrum for **2.5.**

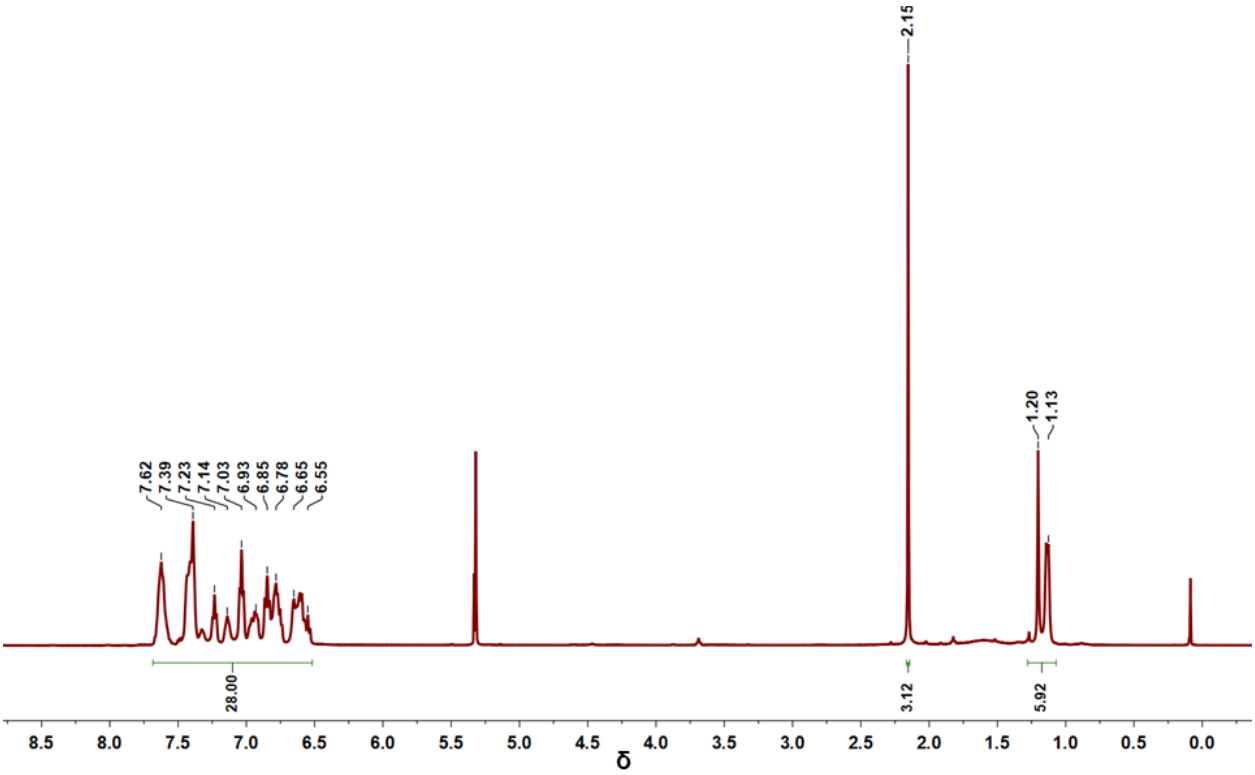


Figure 2.25. ^{1}H NMR Spectrum for **2.5•(CO)**.

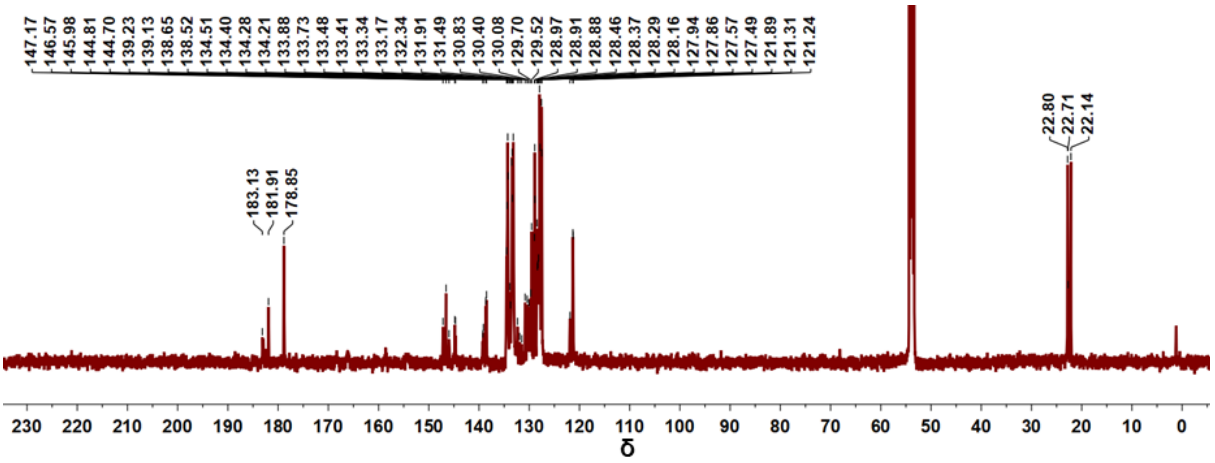


Figure 2.26. ^{13}C NMR Spectrum for **2.5•(CO)**.

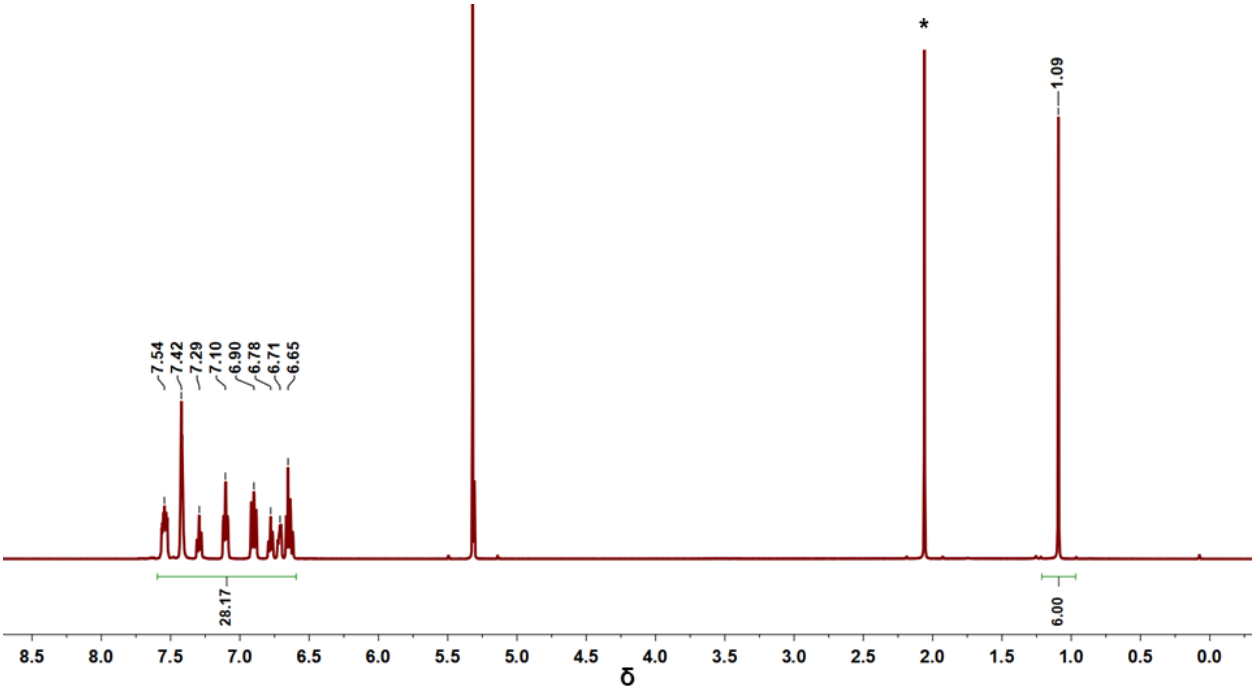


Figure 2.27. ^{1}H NMR Spectrum for **2.5•(CO)$_2$**. * Denotes Acetic Acid.

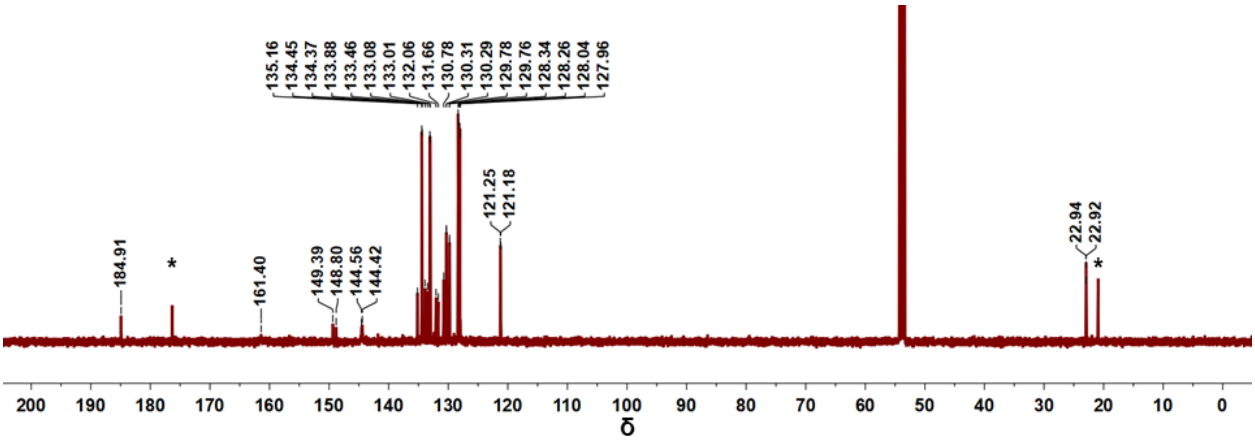


Figure 2.28. ^{13}C NMR Spectrum for **2.5•(CO)$_2$**. * Denotes Acetic Acid.

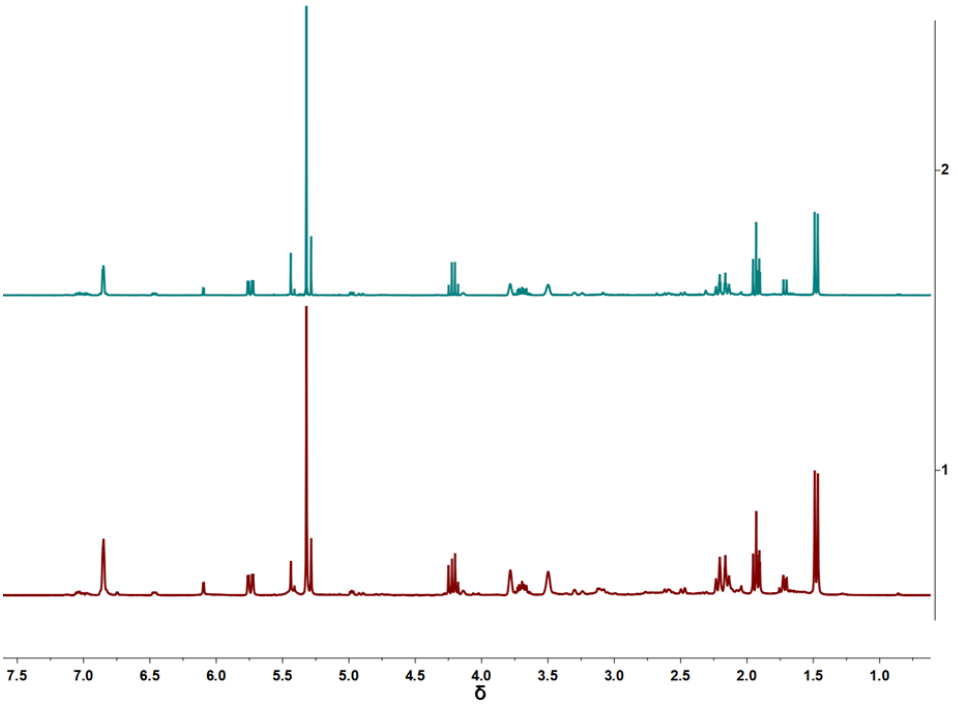


Figure 2.29. ^{1}H NMR Spectrum for Polymerization of **2.1** with **2.2a** initially (teal) and after two weeks (red).

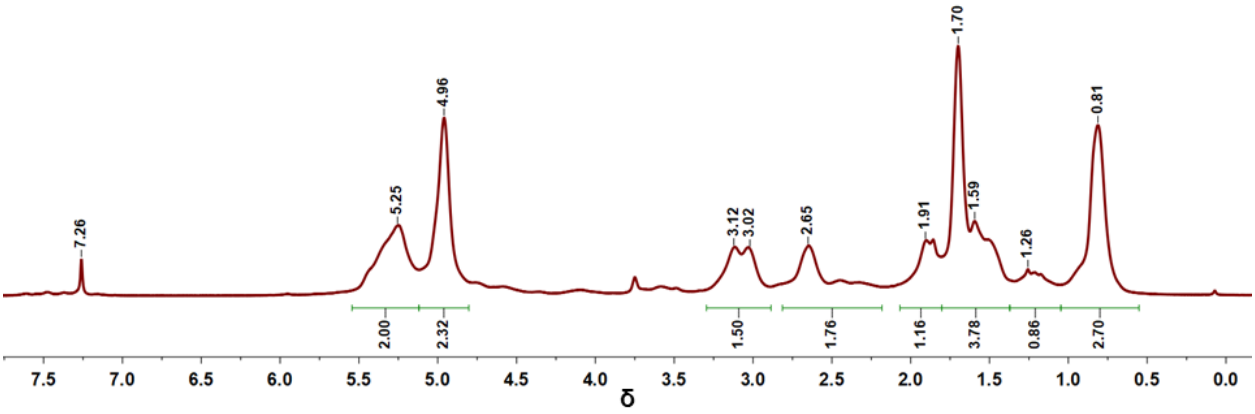


Figure 2.30. ^{1}H NMR Spectrum for **2.P1.**

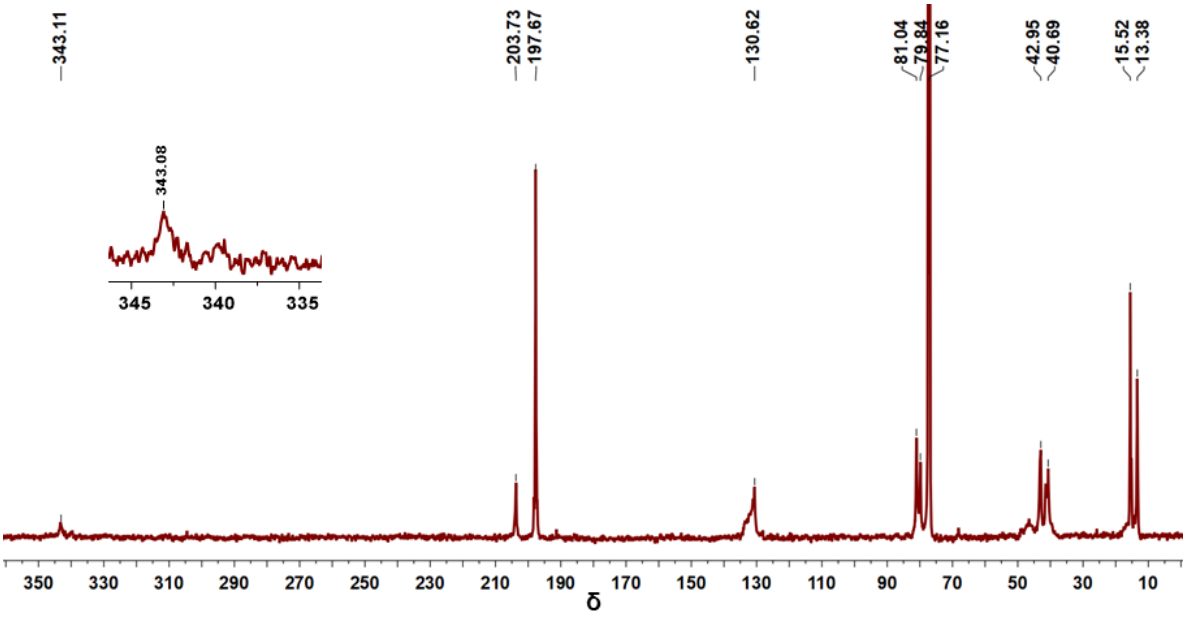


Figure 2.31. ^{13}C NMR Spectrum for **2.P1.**

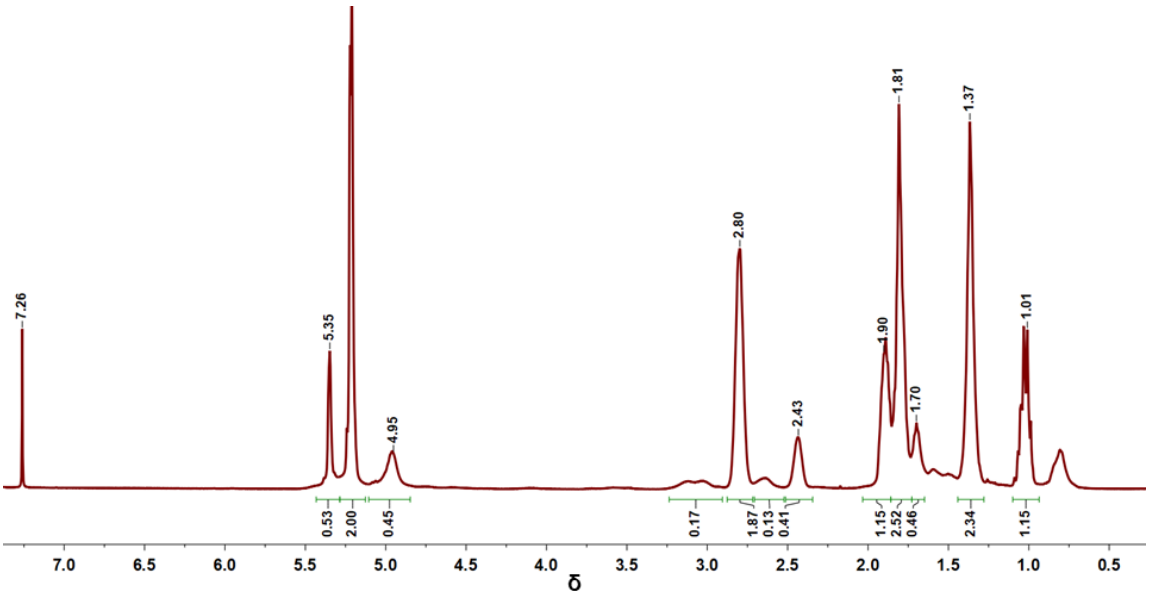


Figure 2.32. ^{1}H NMR Spectrum for Block Copolymer Consisting of a Tungsten Block and Norbornene Block.

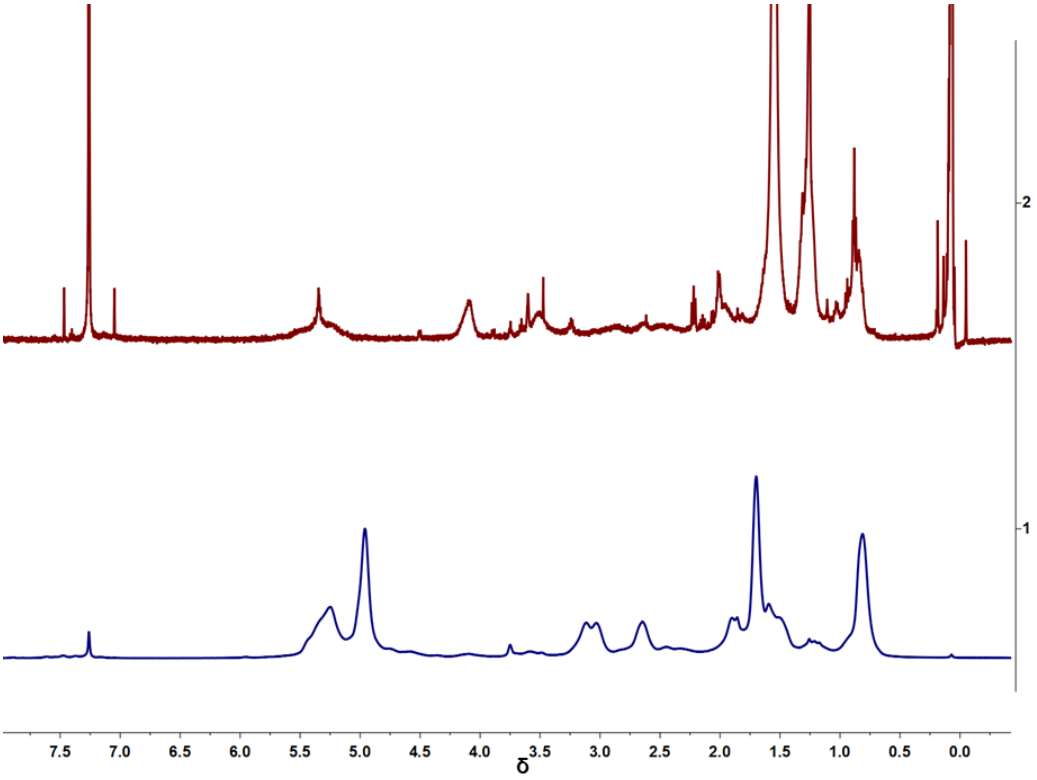


Figure 2.33. ^{1}H NMR Spectrum for Demetallation of **2.P1** (red) with Starting Polymer (blue).

References

(1) Fréchet, J. M. J. Functional Polymers and Dendrimers: Reactivity, Molecular Architecture, and Interfacial Energy. *Science* **1994**, *263* (5154), 1710–1715.

(2) Stuart, M. A. C.; Huck, W. T. S.; Genzer, J.; Müller, M.; Ober, C.; Stamm, M.; Sukhorukov, G. B.; Szleifer, I.; Tsukruk, V. v.; Urban, M.; Winnik, F.; Zauscher, S.; Luzinov, I.; Minko, S. Emerging Applications of Stimuli-Responsive Polymer Materials. *Nature Materials* **2010**, *9* (2), 101–113. https://doi.org/10.1038/nmat2614.

(3) Abd-El-Aziz, A.; Agatemor, C.; Etkin, N. Functional Materials Based on Metal-Containing Polymers. In *Functional Metallosupramolecular Materials*; Hardy, J., Schacher, F., Eds.; 2015; pp 87–119.

(4) Rüttiger, C.; Appold, M.; Didzoleit, H.; Eils, A.; Dietz, C.; Stark, R. W.; Stühn, B.; Gallei, M. Structure Formation of Metallopolymer-Grafted Block Copolymers. *Macromolecules* **2016**, *49*, 3415–3426. https://doi.org/10.1021/acs.macromol.6b00577.

(5) Liu, X.; Ling, Q.; Zhao, L.; Qiu, G.; Wang, Y.; Song, L.; Zhang, Y.; Ruiz, J.; Astruc, D.; Gu, H. New ROMP Synthesis of Ferrocenyl Dendronized Polymers. *Macromolecular Rapid Communications* **2017**, *38* (19), 1700448. https://doi.org/10.1002/marc.201700448.

(6) Musgrave, R. A.; Russell, A. D.; Hayward, D. W.; Whittell, G. R.; Lawrence, P. G.; Gates, P. J.; Green, J. C.; Manners, I. Main-Chain Metallopolymers at the Static–Dynamic Boundary Based on Nickelocene. *Nature Chemistry* **2017**, *9* (8), 743–750. https://doi.org/10.1038/nchem.2743.

(7) Bentz, K. C.; Cohen, S. M. Supramolecular Metallopolymers: From Linear Materials to Infinite Networks. *Angewandte Chemie International Edition* **2018**, *57* (46), 14992–15001. https://doi.org/10.1002/anie.201806912.

(8) Liu, S.; Zhang, K.; Lu, J.; Zhang, J.; Yip, H.-L.; Huang, F.; Cao, Y. High-Efficiency Polymer Solar Cells via the Incorporation of an Amino-Functionalized Conjugated Metallopolymer as a Cathode Interlayer. *J. Am. Chem. Soc.* **2013**, *135*, 15326–15329. https://doi.org/10.1021/ja408363c.

(9) Gu, H.; Ciganda, R.; Castel, P.; Moya, S.; Hernandez, R.; Ruiz, J.; Astruc, D. Tetrablock Metallopolymer Electrochromes. *Angewandte Chemie International Edition* **2018**, *57* (8), 2204–2208. https://doi.org/10.1002/anie.201712945.

(10) Xiang, J.; Ho, C.-L.; Wong, W.-Y. Metallopolymers for Energy Production, Storage and Conservation. *Polymer Chemistry* **2015**, *6* (39), 6905–6930. https://doi.org/10.1039/C5PY00941C.

(11) Rüttiger, C.; Pfeifer, V.; Rittscher, V.; Stock, D.; Scheid, D.; Vowinkel, S.; Roth, F.; Didzoleit, H.; Stühn, B.; Elbert, J.; Ionescu, E.; Gallei, M. One for All: Cobalt-Containing Polymethacrylates for Magnetic Ceramics, Block Copolymerization, Unexpected Electrochemistry, and Stimuli-Responsiveness. *Polymer Chemistry* **2016**, *7* (5), 1129–1137. https://doi.org/10.1039/C5PY01845E.

(12) Gu, H.; Mu, S.; Qiu, G.; Liu, X.; Zhang, L.; Yuan, Y.; Astruc, D. Redox-Stimuli-Responsive Drug Delivery Systems with Supramolecular Ferrocenyl-Containing Polymers for Controlled Release. *Coordination Chemistry Reviews* **2018**, *364*, 51–85. https://doi.org/10.1016/J.CCR.2018.03.013.

(13) Zhang, K. Y.; Liu, S.; Zhao, Q.; Huang, W. Stimuli–Responsive Metallopolymers. *Coordination Chemistry Reviews* **2016**, *319*, 180–195. https://doi.org/10.1016/J.CCR.2016.03.016.

(14) de Bettencourt-Dias, A.; Rossini, J. S. K. Ligand Design for Luminescent Lanthanide-Containing Metallopolymers. *Inorganic Chemistry* **2016**, *55*, 9954–9963. https://doi.org/10.1021/acs.inorgchem.6b00946.

(15) Arsenault, A. C.; Míguez, H.; Kitaev, V.; Ozin, G. A.; Manners, I. A Polychromic, Fast Response Metallopolymer Gel Photonic Crystal with Solvent and Redox Tunability: A Step Towards Photonic Ink (P-Ink). *Advanced Materials* **2003**, *15* (6), 503–507. https://doi.org/10.1002/adma.200390116.

(16) Mauro, M.; Bellemin-Laponnaz, S.; Cebrián, C. Metal-Containing Polymers as Light-Emitting and Light-Responsive Materials and Beyond. *Chemistry - A European Journal* **2017**, *23* (70), 17626–17636. https://doi.org/10.1002/chem.201702936.

(17) Vandermeulen, G. W. M.; Kim, T. K.; Wang, Z.; Manners, I. Metallopolymer–Peptide Conjugates: Synthesis and Self-Assembly of Polyferrocenylsilane Graft and Block

Copolymers Containing a β-Sheet Forming Gly-Ala-Gly-Ala Tetrapeptide Segment. *Biomacromolecules* **2006**, *7* (4), 1005–1010. https://doi.org/10.1021/BM050732P.

(18) Wang, Y.; Astruc, D.; Abd-El-Aziz, A. S. Metallopolymers for Advanced Sustainable Applications. *Chemical Society Reviews* **2019**, *48* (2), 558–636. https://doi.org/10.1039/C7CS00656J.

(19) Ahmed, R.; Hsiao, M.-S.; Matsuura, Y.; Houbenov, N.; Faul, C. F. J.; Manners, I. Redox-Active Mesomorphic Complexes from the Ionic Self-Assembly of Cationic Polyferrocenylsilane Polyelectrolytes and Anionic Surfactants. *Soft Matter* **2011**, *7* (21), 10462–10471. https://doi.org/10.1039/c1sm06374j.

(20) Schmidt, B. V. K. J.; Elbert, J.; Scheid, D.; Hawker, C. J.; Klinger, D.; Gallei, M. Metallopolymer-Based Shape Anisotropic Nanoparticles. *ACS Macro Lett.* **2015**, *4*, 731–735. https://doi.org/10.1021/acsmacrolett.5b00350.

(21) Ruttiger, C.; Hubner, H.; Schottner, S.; Winter, T.; Cherkashinin, G.; Kuttich, B.; Stuhn, B.; Gallei, M. Metallopolymer-Based Block Copolymers for the Preparation of Porous and Redox-Responsive Materials. *ACS Appl. Mater. Interfaces* **2018**, *10*, 4018–4030. https://doi.org/10.1021/acsami.7b18014.

(22) Bode, S.; Zedler, L.; Schacher, F. H.; Dietzek, B.; Schmitt, M.; Popp, J.; Hager, M. D.; Schubert, U. S. Self-Healing Polymer Coatings Based on Crosslinked Metallosupramolecular Copolymers. *Advanced Materials* **2013**, *25* (11), 1634–1638. https://doi.org/10.1002/adma.201203865.

(23) Burnworth, M.; Tang, L.; Kumpfer, J. R.; Duncan, A. J.; Beyer, F. L.; Fiore, G. L.; Rowan, S. J.; Weder, C. Optically Healable Supramolecular Polymers. *Nature* **2011**, *472* (7343), 334–337. https://doi.org/10.1038/nature09963.

(24) Ramakers, G.; D'Incal, C.; Gagliardi, M.; Molin, D. G. M.; Junkers, T. Synthesis of Functional Polymer Particles from Morita-Baylis-Hillman Polymerization. *Macromolecular Rapid Communications* **2018**, 1800678. https://doi.org/10.1002/marc.201800678.

(25) Qiu, H.; Gilroy, J. B.; Manners, I. DNA-Induced Chirality in Water-Soluble Poly(Cobaltoceniumethylene). *Chem. Commun.* **2013**, *49*, 42–44. https://doi.org/10.1039/c2cc37026c.

(26) Astruc, D.; Ornelas, A.; Ruiz, J. Metallocenyl Dendrimers and Their Applications in Molecular Electronics, Sensing, and Catalysis. *Accounts of Chemical Research* **2008**, *41*, 841–856. https://doi.org/10.1021/ar8000074.

(27) Zhang, J.; Chen, Y. P.; Miller, K. P.; Ganewatta, M. S.; Bam, M.; Yan, Y.; Nagarkatti, M.; Decho, A. W.; Tang, C. Antimicrobial Metallopolymers and Their Bioconjugates with Conventional Antibiotics against Multidrug-Resistant Bacteria. *J. Am. Chem. Soc.* **2014**, *136*, 4873–4876. https://doi.org/10.1021/ja5011338.

(28) Fischer, E. O.; Maasböl, A. On the Existence of a Tungsten Carbonyl Carbene Complex. *Angewandte Chemie International Edition* **1964**, *3* (8), 580–581. https://doi.org/10.1002/anie.196405801.

(29) Klabunde, U.; Fischer, E. O. Two New Chromium Carbonyl Carbene Complexes. *J Am Chem Soc* **1967**, 7141–7142.

(30) Fischer, E. O.; Beck, H.-J. Transfer of Methoxyphenylcarbene Ligands from Molybdenum to Iron and Nickel. *Angewandte Chemie International Edition in English* **1970**, *9* (1), 72–73. https://doi.org/10.1002/anie.197000721.

(31) Hegedus, L. S.; Schultze, L. M.; Toro, J.; Yijun, C. Photolytic Reaction of Chromium and Molybdenum Carbene Complexes with Imines. *Tetrahedron* **1985**, *41* (24), 5833–5838. https://doi.org/10.1016/S0040-4020(01)91422-X.

(32) Barluenga, J.; Vicente, R.; López, L.; Rubio, E.; Tomás, M.; Álvarez-Rúa, C. New Fischer Carbene Complexes of Rhodium(I): Preparation and 2-Cyclopentenone Ring Synthesis by Annelation to Alkynes. *J. Am. Chem. Soc.* **2004**, *126* (2), 470–471. https://doi.org/10.1021/JA038817Q.

(33) Brookhart, M.; Timmers, D.; Tucker, J. R.; Williams, G. D. Enantioselective Cyclopropane Synthesis Using the Chiral Carbene Complexes (SFeSc)- and = (RFeSc)-(C5H5)(CO)(Ph2R*P)Fe=CHCH3+ (R* (S)-2-Methylbutyl). Role of Metal vs. Ligand Chirality in the Optical Induction. *J. Am. Chem. Soc.* **1983**, *105*, 6721–6723.

(34) Powell, A. B.; Bielawski, C. W.; Cowley, A. H. Synthesis, Study, and Applications of Polymeric N-Heterocyclic Carbenes. *Comments on Inorganic Chemistry* **2010**, *31* (3–4), 75–82. https://doi.org/10.1080/02603594.2010.517459.

(35) Yao, Q. A Soluble Polymer-Bound Ruthenium Carbene Complex: A Robust and Reusable Catalyst for Ring-Closing Olefin Metathesis. *Angewandte Chemie* **2000**, *39* (21), 3896–3898. https://doi.org/10.1002/1521-3773(20001103)39:21<3896::AID-ANIE3896>3.0.CO;2-8.

(36) Schönfelder, D.; Nuyken, O.; Weberskirch, R. Heck and Suzuki Coupling Reactions in Water Using Poly(2-Oxazoline)s Functionalized with Palladium Carbene Complexes as Soluble, Amphiphilic Polymer Supports. *Journal of Organometallic Chemistry* **2005**, *690* (21–22), 4648–4655. https://doi.org/10.1016/J.JORGANCHEM.2005.07.053.

(37) Kim, J.-H.; Kim, J.-W.; Shokouhimehr, M.; Lee, Y.-S. Polymer-Supported N-Heterocyclic Carbene-Palladium Complex for Heterogeneous Suzuki Cross-Coupling Reaction. *Journal of Organic Chemistry* **2005**, *70*, 6714–6720. https://doi.org/10.1021/jo050721m.

(38) Raubenheimer, H. G. Fischer Carbene Complexes Remain Favourite Targets, and Vehicles for New Discoveries. *Dalton Trans.* **2014**, *43* (45), 16959–16973. https://doi.org/10.1039/C4DT01943A.

(39) Maiorana, S.; Seneci, P.; Rossi, T.; Baidoli, C.; Ciraco, M.; de Magistris, E.; Licandro, Emanuela.; Papagni, Antonio.; Provera, S. Synthesis of Polymer-Bound Fischer Chromium Alkoxy and Aminocarbene Complexes. *Tetrahedron Letters* **1999**, *40*, 3635–3638.

(40) Barluenga, J.; Prado, A. de; Santamaria, J.; Tomas, M. Polymer-Bound Fischer Tungsten Carbene Complexes: Synthesis and Reactivity. *Organometallics* **2005**, *24*, 3614–3617. https://doi.org/10.1021/om0503186.

(41) Macomber, D. W.; Hung, M. H.; Liang, M.; Verma, A. G.; Madhukar, P. New Organometallic Polymers Containing Tungsten Carbene Complexes. *Macromolecules* **1988**, *21* (4), 1187–1189. https://doi.org/10.1021/ma00182a061.

(42) Nomura, R.; Watanabe, K.; Masuda, T. Synthesis of Metal - Carbene Containing Polymers by Polycondensation of a Bifunctional Alkoxycarbene with Diamines. *Macromolecules* **2000**, *33*, 1936–1939. https://doi.org/10.1021/ma990599r.

(43) Sültemeyer, J.; Dötz, K. H.; Hupfer, H.; Nieger, M. Reactions of Complex Ligands: Part 91. Application of Ring Closing Metathesis to Fischer-Type Carbene Complexes:

Synthesis and Structure of Medium-Sized Chromium Oxacycloalkenylidenes. *Journal of Organometallic Chemistry* **2000**, *606* (1), 26–36. https://doi.org/10.1016/S0022-328X(00)00095-4.

(44) Haase, W.-C.; Nieger, M.; Dötz, K. H. Furanosylidene and Iminofuranosylidene Complexes: Synthesis by Stoichiometric Olefin Metathesis and Ring-Opening/Mitsunobu-Recyclization Sequence. *Chemistry European Journal* **1999**, *5* (7), 2014–2024. https://doi.org/10.1002/(SICI)1521-3765(19990702)5:7<2014::AID-CHEM2014>3.0.CO;2-N.

(45) Wulff, W. D.; Bauta, W. E.; Kaesler, R. W.; Lankford, P. J.; Miller, R. A.; Murray, C. K.; Yang, D. C. Chromium and Tungsten Pentacarbonyl Groups as Reactivity Auxiliaries in the Diels-Alder Reactions of Alkenyl Carbene Complexes with 1,3-Dienes. *J Am Chem Soc* **1990**, *112* (9), 3642–3659. https://doi.org/10.1021/ja00165a060.

(46) Moragues, M. E.; Esteban, J.; Ros-lis, V.; Marcos, M. D.; Martínez, M.; Soto, J.; Sancenon, F. Sensitive and Selective Chromogenic Sensing of Carbon Monoxide via Reversible Axial CO Coordination in Binuclear Rhodium Complexes. *J. Am. Chem. Soc.* **2011**, *133*, 15762–15772. https://doi.org/10.1021/ja206251r.

(47) Esteban, J.; Ros-Lis, J. V.; Martínez-Máñez, R.; Marcos, M. D.; Moragues, M.; Soto, J.; Sancenón, F. Sensitive and Selective Chromogenic Sensing of Carbon Monoxide by Using Binuclear Rhodium Complexes. *Angewandte Chemie International Edition* **2010**, *49* (29), 4934–4937. https://doi.org/10.1002/anie.201001344.

(48) Chakravarty, A. R.; Cotton, F. A.; Tocher, D. A.; Tocher, J. H. Structural and Electrochemical Characterization of the Novel Ortho-Metalated Dirhodium(II) Compounds Rh2(OzCCH3)2[(C6H5)2P(C6H4)]2-2L. *Organometallics* **1985**, *4*, 8–13. https://doi.org/10.1021/om00120a003.

(49) Scholl, M.; Ding, S.; Woo Lee, C.; Grubbs, R. H. Synthesis and Activity of a New Generation of Ruthenium-Based Olefin Metathesis Catalysts Coordinated with 1,3-Dimesityl-4,5-Dihydroimidazol-2-Ylidene Ligands. *Organic Letters* **1999**, *1* (6), 953–956. https://doi.org/10.1021/ol990909q.

(50) Garber, S. B.; Kingsbury, J. S.; Gray, B. L.; Hoveyda, A. H. Efficient and Recyclable Monomeric and Dendritic Ru-Based Metathesis Catalysts. *J. Am. Chem. Soc.* **2000**, *122* (34), 8168–8179. https://doi.org/10.1021/JA001179G.

(51) Bielawski, C. W.; Grubbs, R. H. Highly Efficient Ring-Opening Metathesis Polymerization (ROMP) Using New Ruthenium Catalysts Containing N-Heterocyclic Carbene Ligands. *Angewandte Chemie* **2000**, *39* (16), 2903–2906. https://doi.org/10.1002/1521-3773(20000818)39:16<2903::AID-ANIE2903>3.0.CO;2-Q.

(52) Haigh, D. M.; Kenwright, A. M.; Khosravi, E. Ring Opening Metathesis Polymerisations of Norbornene and Norbornadiene Derivatives Containing Oxygen: A Study on the Regeneration of Grubbs Catalyst. *Tetrahedron* **2004**, *60* (34), 7217–7224. https://doi.org/10.1016/J.TET.2004.06.065.

(53) Maynard, H. D.; Okada, S. Y.; Grubbs, R. H. Synthesis of Norbornenyl Polymers with Bioactive Oligopeptides by Ring-Opening Metathesis Polymerization. *Macromolecules* **2000**, *33*, 6239–6248. https://doi.org/10.1021/ma000460c.

(54) CO is known to poison Ru metathesis catalysts, and we speculate this is the origin of the inactivity we observe for **2.2a**, **2.2b**, and **2.3** (see Figure 2.4). See: (a) Diver, S. T. Ruthenium Vinyl Carbene Intermediates in Enyne Metathesis. Coord. Chem. Rev. **2007**, 251, 671. (b) Galan, B. R.; Gembicky, M.; Dominiak, P. M.; Keister, J. B.; Diver, S. T. Carbon Monoxide-Promoted Carbene Insertion into the Aryl Substituent of an N-Heterocyclic Carbene Ligand: Buchner Reaction in a Ruthenium Carbene Complex. J. Am. Chem. Soc. **2005**, 127, 15702. (c) Nelson, D. J.; Manzini, S.; Urbina-Blanco, C. A.; Nolan, S. P. Key Processes in Ruthenium-Catalysed Olefin Metathesis. Chem. Commun. **2014**, 50, 10355. (d) Poater, A.; Ragone, F.; Correa, A.; Cavallo, L. Exploring the Reactivity of Ru-Based Metathesis Catalysts with a π-Acid Ligand Trans to the Ru−Ylidene Bond. J. Am. Chem. Soc. **2009**, 131, 9000.

(55) Diver, S. T. Ruthenium Vinyl Carbene Intermediates in Enyne Metathesis. *Coordination Chemistry Reviews* **2007**, *251* (5–6), 671–701. https://doi.org/10.1016/J.CCR.2006.09.008.

(56) Galan, B. R.; Gembicky, M.; Dominiak, P. M.; Keister, J. B.; Diver, S. T. Carbon Monoxide-Promoted Carbene Insertion into the Aryl Substituent of an N-Heterocyclic Carbene

Ligand: Buchner Reaction in a Ruthenium Carbene Complex. *J. Am. Chem. Soc.* **2005**, *127* (45), 15702–15703. https://doi.org/10.1021/JA0545618.

(57) Nelson, D. J.; Manzini, S.; Urbina-Blanco, C. A.; Nolan, S. P. Key Processes in Ruthenium-Catalysed Olefin Metathesis. *Chemical Communications* **2014**, *50* (72), 10355–10375. https://doi.org/10.1039/C4CC02515F.

(58) Poater, A.; Ragone, F.; Correa, A.; Cavallo, L. Exploring the Reactivity of Ru-Based Metathesis Catalysts with a π-Acid Ligand Trans to the Ru−Ylidene Bond. *J Am Chem Soc* **2009**, *131* (25), 9000–9006. https://doi.org/10.1021/ja902552m.

(59) Fox, H. H.; Lee, J. K.; Park, L. Y.; Schrock, R. R. Synthesis of Five- and Six-Coordinate Alkylidene Complexes of the Type Mo(CHR)(NAr)[OCMe(CF3)2]2Sxand Their Use as Living ROMP Initiators or Wittig Reagents. *Organometallics* **1993**, *12* (3), 759–768. https://doi.org/10.1021/om00027a028.

(60) Odian, G. G. *Principles of Polymerization*; 2004.

(61) Mark, J. *Polymer Data Handbook*, 2nd ed.; Mark, J., Ed.; Oxford University Press, 2009.

(62) Chan, K. S.; Wulff, W. 1,3-Dipolar Cycloaddition Reactions of Transition-Metal Carbene Complexes and the Formal [3 + 2 + 1] Pyridinannulation of the Cycloadducts. *J. Am. Chem. Soc.* **1986**, *108*, 5229–5236.

(63) Pena, A. C.; Penacho, N.; Mancio-Silva, L.; Neres, R.; Seixas, J. D.; Fernandes, A. C.; Romão, C. C.; Mota, M. M.; Bernardes, G. J. L.; Pamplona, A. A Novel Carbon Monoxide-Releasing Molecule Fully Protects Mice from Severe Malaria. *Antimicrob Agents Chemother* **2012**, *56* (3), 1281–1290. https://doi.org/10.1128/AAC.05571-11.

(64) Desmard, M.; Foresti, R.; Morin, D.; Dagouassat, M.; Berdeaux, A.; Denamur, E.; Crook, S. H.; Mann, B. E.; Scapens, D.; Montravers, P.; Boczkowski, J.; Motterlini, R. Differential Antibacterial Activity Against Pseudomonas Aeruginosa by Carbon Monoxide-Releasing Molecules. *Antioxidants & Redox Signaling* **2012**, *16* (2), 153–163. https://doi.org/10.1089/ars.2011.3959.

(65) Stein, A. B.; Bolli, R.; Dawn, B.; Sanganalmath, S. K.; Zhu, Y.; Wang, O.-L.; Guo, Y.; Motterlini, R.; Xuan, Y.-T. Carbon Monoxide Induces a Late Preconditioning-Mimetic Cardioprotective and Antiapoptotic Milieu in the Myocardium. *Journal of Molecular and*

Cellular Cardiology **2012**, *52* (1), 228–236. https://doi.org/10.1016/J.YJMCC.2011.11.005.

(66) Motterlini, R.; Otterbein, L. E. The Therapeutic Potential of Carbon Monoxide. *Nature Reviews Drug Discovery* **2010**, *9* (9), 728–743. https://doi.org/10.1038/nrd3228.

(67) Brückmann, N. E.; Wahl, M.; Reiß, G. J.; Kohns, M.; Wätjen, W.; Kunz, P. C. Polymer Conjugates of Photoinducible CO-Releasing Molecules. *European Journal of Inorganic Chemistry* **2011**, 4571–4577. https://doi.org/10.1002/ejic.201100545.

(68) Fischer, H.; Fischer, E. O.; Werner, H. Ubergangsmetall-Carben-Komplex LXXHI*. Kinetik Und Mechanismus Der Isomerisierung von Cis- Und Trans- Tetracarbonyl-Methoxymethylcarben-Phophin-Chrom(0)-Komplexen. *Journal of Organometallic Chemistry* **1974**, *73*, 331–342.

(69) Hegedus, L. Chromium Carbene Complex Photochemistry in Organic Synthesis. *Tetrahedron* **1997**, *53* (12), 4105–4128.

(70) Foley, H.; Strubinger, L.; Targos, T.; Geoffroy, G. Photochemistry of [W(CO)5{C(OMe)Ph}]. Formation of Alkyne-Carbene Complexes and Studies of Their Decomposition Reactions. *J. Am. Chem. Soc.* **1983**, *105* (10), 3064–3073.

(71) Gut, H.-P.; Welte, N.; Link, U.; Fischer, H.; Steiner, U. E. Formation and Reactions of Tetracarbonyl Intermediates of the Fischer Carbene Complex (CO) 5 WdC(OMe)Ph. A Laser Flash Photolysis Study Using Time-Resolved Infrared and UV/Vis Spectroscopy. *Organometallics* **2000**, *19*, 2354–2364. https://doi.org/10.1021/om990708q.

(72) Qiu, K.; Song, X.; Lai, Y.; Wu, L.; Tang, G.; Min, S. Comparison of ATR/Transmittance FTIR Combined with Beer's Law and PLS to Determine Fipronil in Matrine Formulation. *Analytical Methods* **2013**, *5* (18), 4790. https://doi.org/10.1039/c3ay40406d.

(73) Billo, E. J. *Excel for Chemists: A Comprehensive Guide*, 2nd ed.; Wiley: Chestnut Hill, 2001.

(74) For discussion of further experiments to gain a deeper understanding of the stimuli-responsive behavior of these polymers, see Chapter 6.

CHAPTER 3: ELUCIDATING THE ORIGIN OF DIVERGENT ROMP ACTIVITY IN METALLOCARBENE MONOMERS

This chapter is currently in preparation for peer review to be published by Breana J. Kyker, Brett A. Smith, Konstantinos D. Vogiatzis, and Johnathan N. Brantley. All experimentation and data analysis was conducted by Breana J. Kyker and all computational work was completed by Brett A. Smith. The manuscript was compiled through efforts from all authors.

Abstract

Ring opening metathesis polymerization (ROMP) is one of the preeminent methodological tools available to polymer scientists. As such, a detailed understanding of the factors that promote (or suppress) ROMP activity is critical for designing next-generation catalysts and materials. Ruthenium- and molybdenum based ROMP catalysts typically exhibit substrate selectivity, which is governed by a combination of factors. We previously reported lack of activity with ruthenium catalysts when polymerizing tungsten monomers, despite achieving synthesis with a molybdenum catalyst. However, we have observed polymerization of chromium monomers with ruthenium catalysts. Intrigued by this observation, we wanted to understand the origin of this divergent behavior. Through a combination of experimental and computational efforts, we were able to identify key interactions explaining why ruthenium polymerization is inactive with tungsten carbenes. Steric congestion during propagation hinders the insertion of additional monomers. Furthermore, we were able to exploit these interactions to design a monomer that would enable polymerization by adding a methylene spacer and eliminating steric congestion between the monomer and the ruthenium center.

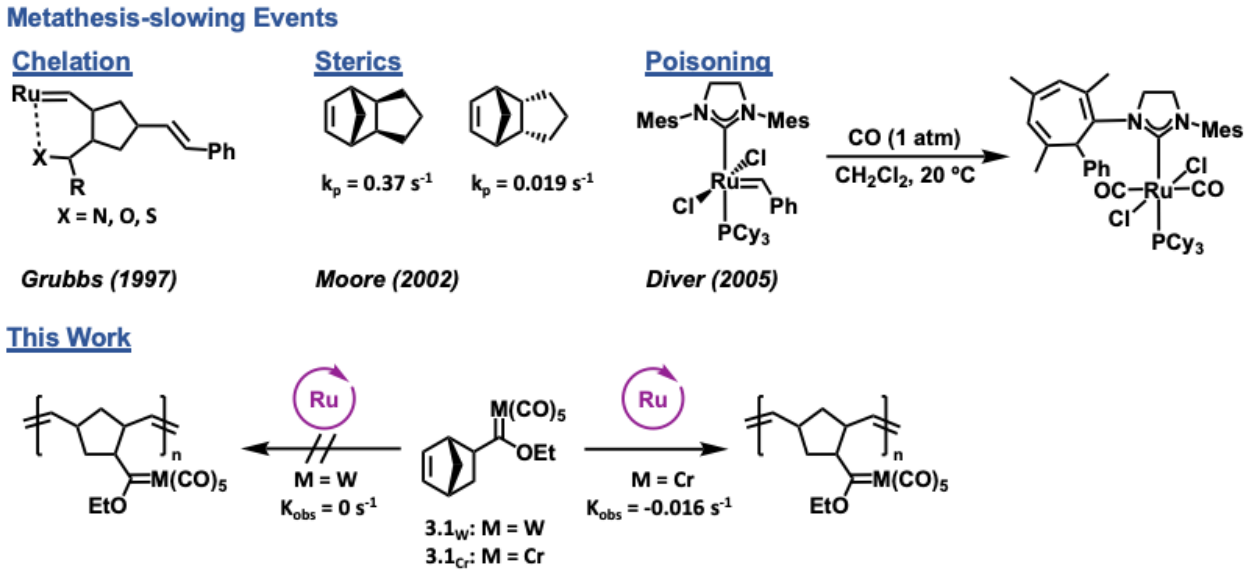
Introduction

Olefin metathesis has emerged as one of the preeminent C–C bond forming strategies available to synthetic chemists. Indeed, a wide range of transformations (e.g., ethenolysis,[1–4] cross metathesis,[5–8] acyclic diene metathesis,[9–12] ring closing metathesis,[8,13–15] and ring opening metathesis[16–19]) involve olefin metathesis processes along their reaction coordinates. The ubiquity (and, perhaps more importantly, the reliability) of olefin metathesis has enabled significant advancements across fields that range from total synthesis[20,21] and drug discovery[22–24] to polymer synthesis.[25–29] As such, understanding the mechanistic nuances of olefin metathesis is imperative for facilitating access to next-generation materials.

Although reports of olefin metathesis first emerged in the 1950s, Calderon was the first to determine that metathesis fundamentally involved the cleavage and reformation olefinic bonds.[30,31] Detailed mechanistic studies by Chauvin,[32] Grubbs,[33] Katz,[34–42] Schrock,[41,42] and others[43–48] soon followed, and these efforts were crucial to the design of more effective catalysts. Since this time, further studies on the mechanism of olefin metathesis have been widely reported,[49–51] and many well-defined materials can be achieved through utilization of metathesis chemistry. The wealth of knowledge provided by these studies has allowed for the improvement of catalyst design. Reliable catalysts that can be used to make well-defined materials have been produced. For example, variation of ligands in the ruthenium type catalysts allowed for investigation of initiation rate and its effect on polymer properties.[52] In addition, controlling the stereoselectivity of ROMP catalysts has been accomplished through the implementation of rigid ligands that direct the orientation of incoming monomers.[53]

Ring opening metathesis polymerization (ROMP) has caused the rapid expansion of the scope of polymer synthesis, and exponentially more so with the reports of well-defined metathesis catalysts by Schrock and Grubbs. Schrock-type catalysts are highly active but must be handled in an inert and dry atmosphere, while Grubbs-type catalysts exhibit high functional group compatibility and can be handled on the benchtop. Though these catalysts are quite different and exhibit different selectivities, they operate under the same mechanism reported by Chauvin. Knowing the impact of various factors on polymerization initiation and propagation allows for the synthesis of controlled materials of varying microstructures. Catalyst activity can be reduced via functional group chelation[50,54–57] steric effects,[58,59] and poisoning (Scheme 3.1).[60–63] Although steric effects are known to influence polymerization rate in ROMP, there is no clear steric barrier for ROMP monomers,[59] in contrast with vinyl addition polymerization, in which there is a clear difference between the polymerization rates of *endo*- and *exo*- isomers, to the point that polymerization of purely *endo*- isomers can be unachievable.[64] In consideration of our observation and the difference between these two mechanisms, we sought to conduct a similar analysis of the reaction coordinate for ROMP, as understanding the structure-property relationships in the context of ROMP is critical for synthesis of next-generation materials.

Scheme 3.1. Examples of Factors Affecting Polymerization Rate with Ruthenium Catalysts



Results and Discussion

We previously found that **3.1w** did not polymerize (starting material recovered) under the action of Grubbs-type catalysts (i.e., G1, G2, G3, GZ, or HG2); however, polymerization of **2.1** was observed with Schrock's molybdenum catalyst (see Chapter 2). For example, when **2.1** (0.05 mmol) was reacted with G3 (0.001 mmol), no polymerization was observed via ^{1}H NMR spectroscopy or SEC analysis. As we have previously shown that **2.P1** releases CO, we hypothesized that CO-poisoning of catalyst was responsible for the lack of ROMP activity.[67] However, polymerizations conducted in the dark under N_2 (which should avoid CO release from **2.1**; Chapter 2) also yielded no polymer. As pyridines can also induce CO-release from Fischer-type carbenes upon coordination,[68,69] we suspected this might provide an alternative mechanism by which CO could be released from **3.1w** to poison the catalyst. Specifically, the deligation of 3-bromopyridine from G3 (which is necessary for polymerization to occur) could promote CO release even in the absence of light. To test this hypothesis, **3.1** was dissolved in DCM (0.011 mmol, 0.011 mM), and the reaction vessel was foiled prior to sparging with N_2 for 30 seconds. To test for background CO-release, the headspace of the vessel was transferred to a UV-vis cell containing a solution of **2.5** [70,71] in DCM (0.011 mmol, 0.004 mM). Analysis of the resulting solution by UV-vis absorbance spectroscopy revealed no detectable CO. 3-bromopyridine (0.011 mmol) was then added to the foiled solution of **3.1**, and the reaction headspace was again transferred to the solution of **2.5** after 30 min. Analysis of the resulting solution via UV-vis spectroscopy revealed no detectable release of CO (Figure 3.1). Furthermore, ^{1}H NMR spectral studies supported the conclusion that the exogenously added 3-bromopyridine was not binding to **3.1**, as equimolar mixtures of **3.1** and 3-bromopyridine in $CDCl_3$ resulted in negligible changes to the heteroaromatic proton resonances (δ = 7.17 vs 7.22; Figure 3.3). Collectively, these experiments suggested that CO poisoning was most likely not responsible for our inability to polymerize **3.1w** with Grubbs-type catalysts.

We next sought to ascertain whether or not **3.1cr** would exhibit analogous recalcitrance toward ROMP with G3. A sample of **3.1cr** (0.15 mmol, 0.15 mM) was prepared in $CDCl_3$, and G3 (0.003 mmol) was added to the solution at 20 °C in the dark under N_2. To our surprise, ^{1}H NMR spectral analysis of the reaction mixture revealed complete consumption of the vinyl protons in **3.1cr** (δ = 5.69) occurred within 5 min, and new vinyl resonances consistent with

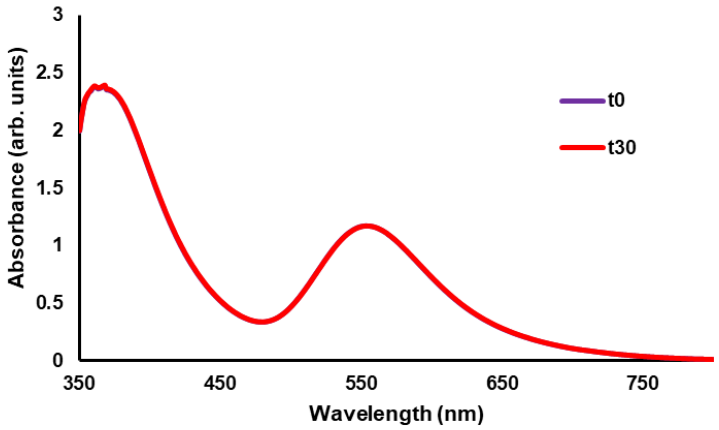


Figure 3.1. UV-vis overlay of **2.5** before addition of 3-bromopyridine to **3.1w** (purple) and after addition of 3-bromopyridine to **3.1w** (red).

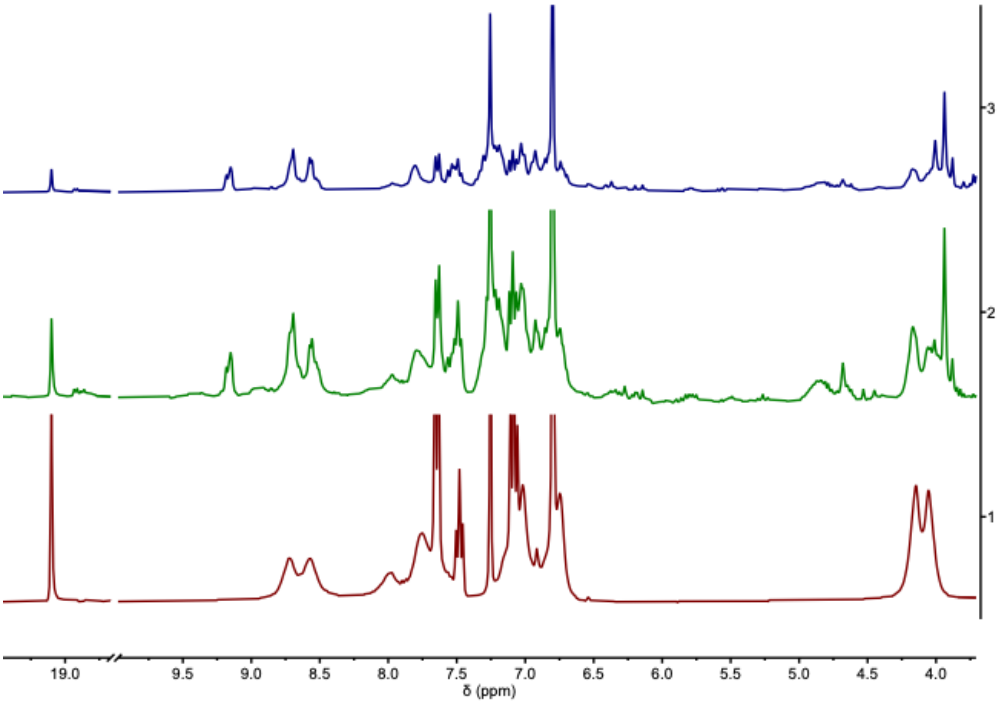


Figure 3.2. ^{1}H NMR spectra for stoichiometric experiment between **3.1w** and G3. 1) G3 only, 2) G3 plus **3.1w**, t_0, 3) G3 plus **3.1w**, t_{60}

polymerization (δ = 5.07) were observed. Furthermore, precipitation of the sample from methanol provided yellow polymeric material (M_n = 57,000; Đ = 2.70; Figure 3.2) in 62% yield. Surprised by this difference in reactivity, we set out to understand the origin of this phenomenon in greater detail.

Having established that catalyst poisoning via CO-release was an unlikely explanation for the inability to polymerize **3.1$_W$**, we sought to determine if off-cycle species were forming during initiation or propagation. In an initial study, a mixture of G3 (0.01 mmol) and **3.1$_W$** (0.01 mmol) in $CDCl_3$ was analyzed by ^{1}H NMR spectroscopy. The sample was held under N_2 in the dark to prevent CO-release during the experiment. The ruthenium carbene resonance (δ = 19.11 ppm) drastically decreased after 1 h, and the NMR spectrum itself became so complex as to preclude more detailed analysis (Figure 3.3). Further, a new signal that could be attributed to the ring-opened product could be observed at 4.87 ppm while the vinyl signals from **3.1$_W$** (6.14 and 5.69 ppm) were completely consumed. In another experiment, **3.1$_W$** (0.009 mmol, 0.012 mM) was dissolved in $CDCl_3$ with G3 (0.009 mmol) and analyzed via ^{1}H NMR, followed by iterative sequential addition of single equivalents of **3.1$_W$** (4 total equivalents of **3.1$_W$**). These spectra indicated the same drastic decrease in the ruthenium carbene resonance (δ = 19.11 ppm), suggesting catalyst decomposition, however, signals consistent with insertion of the catalyst into the olefin were also present (Figure 3.4). In comparison, an analogous experiment with **3.1$_{Cr}$** was conducted, in which **3.1$_{Cr}$** (0.01 mmol, 0.015 mM) was dissolved in $CDCl_3$ with G3 (0.01 mmol). The ruthenium carbene signal (19.11 ppm) remained consistent throughout the experiment, and the vinyl signals from **3.1$_{Cr}$** (6.14 and 5.66 ppm) disappeared and the signal for the ring opened product (5.09 ppm) appeared (Figure 3.5), consistent with control experiments between norbornene and G3 (Figure 3.18). The differences in these spectra suggest that the decomposition pathway present in **3.1$_W$** is inactive with **3.1$_{Cr}$**.

We also sought to determine if these monomers were having adverse effects on propagation. **3.1$_W$** (0.011 mmol; 0.016 mM) was dissolved in $CDCl_3$ with G3 (0.011 mmol) and a ^{1}H NMR spectrum was collected to confirm initiation. An aliquot of this sample (0.0016 mmol) was added to an additional 40 equivalents of **3.1$_W$** in $CHCl_3$ and the solution was held in the dark at 20 °C under N_2 for 1 h. The solution was quenched with ethyl vinyl ether added

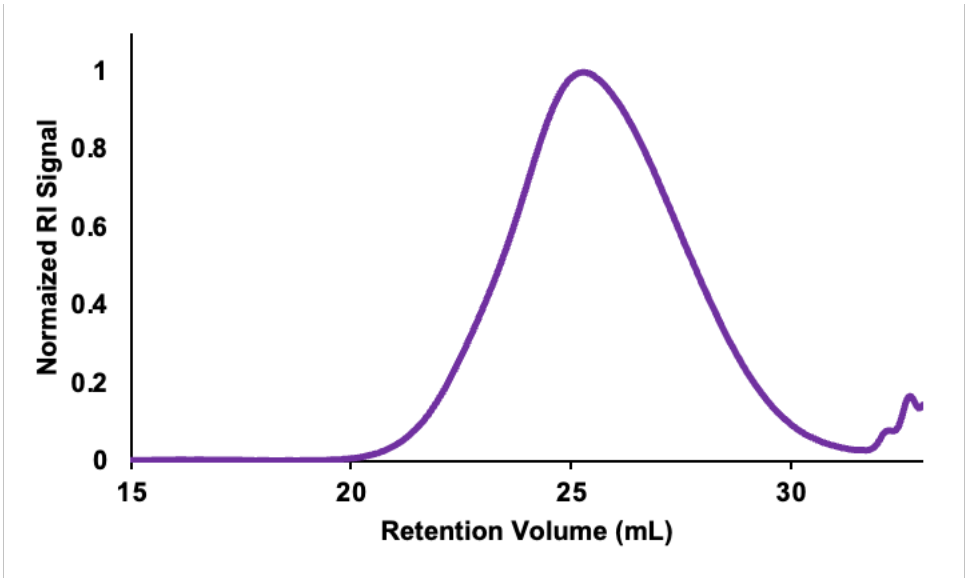


Figure 3.2. SEC data for **3.P1**$_{cr}$ from triple detection

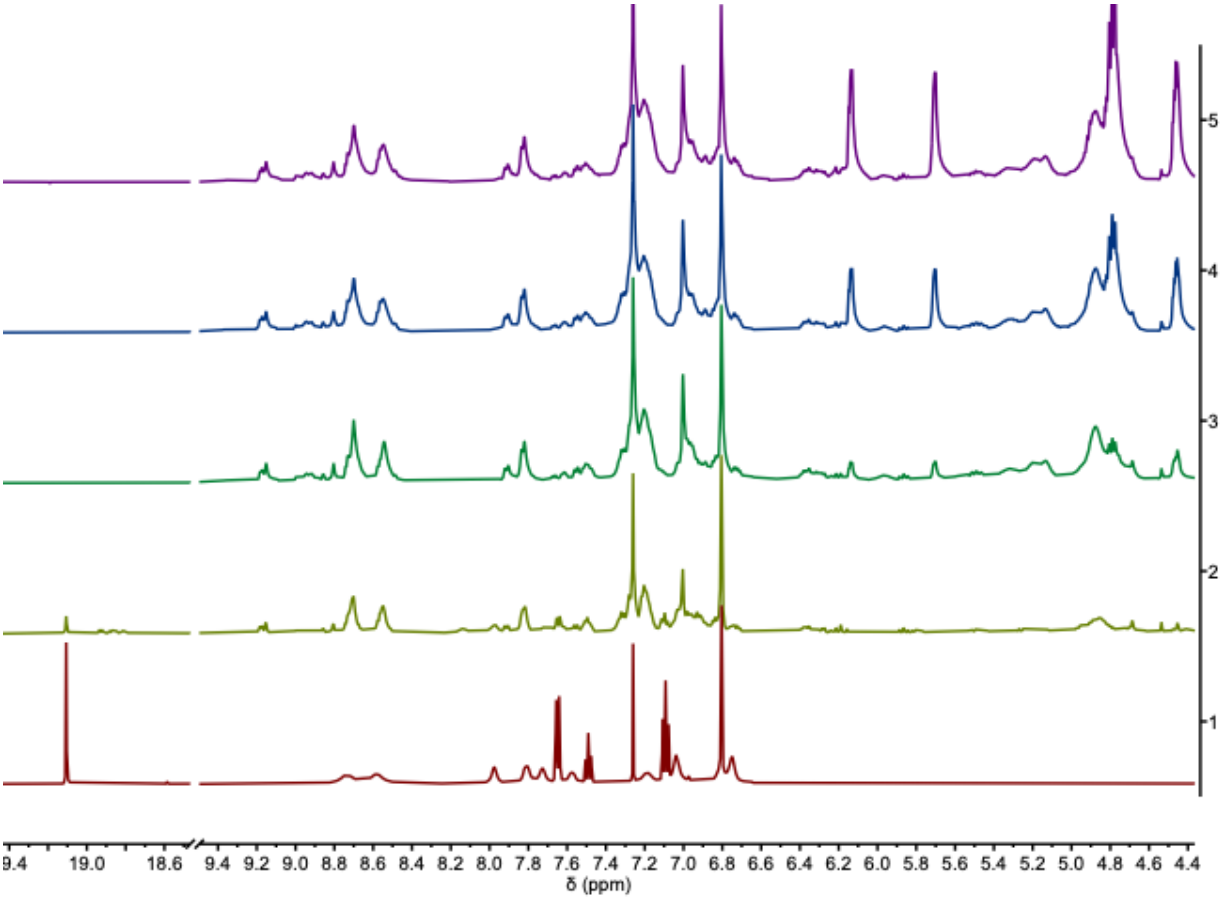


Figure 3.4. ^{1}H NMR spectra for Iterative stoichiometric addition of **3.1$_W$** to G3. 1) G3 only, 2) G3 plus 1 equivalent **3.1$_W$**, 3) G3 plus 2 equivalents **3.1$_W$**, 4) G3 plus 3 equivalents **3.1$_W$**, 5) G3 plus 4 equivalents **3.1$_W$**.

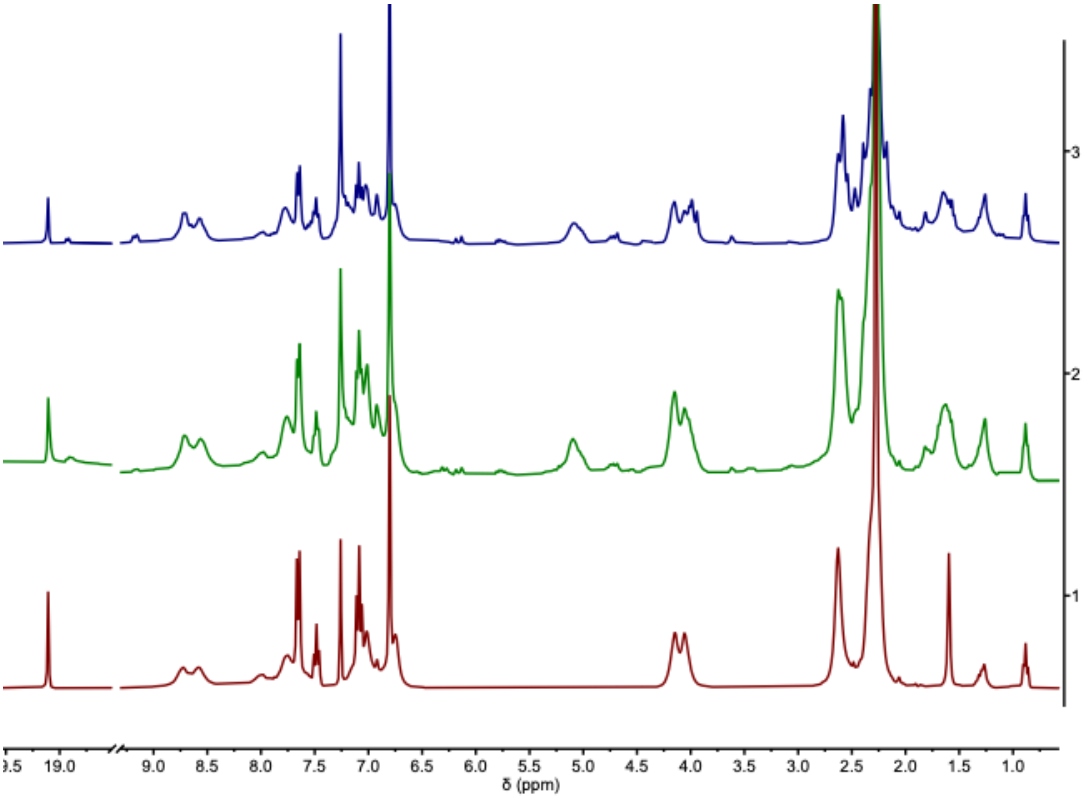


Figure 3.5. ^{1}H NMR spectra for stoichiometric experiment between G3 and **3.1$_{Cr}$**. 1) G3 only, 2) G3 plus **3.1$_{Cr}$**, t_0, 3) G3 plus **3.1$_{Cr}$**, t_{60}.

to methanol to precipitate any polymeric material (9% recovery; Figure 3.6A). SEC analysis of the isolated material indicated poor control over the polymerization as well as large amounts of oligomeric species. An analogous experiment with **3.1$_{Cr}$** provided well-defined polymeric material as observed by SEC in 40% recovery (Figure 3.6B). These data suggest that the barrier to insertion of additional monomers is much higher with **3.1$_{W}$** than with **3.1$_{Cr}$**. To confirm that we were not inadvertently making an inactive species, an experiment between **3.1$_{W}$** and norbornene was conducted. **3.1$_{W}$** (0.01 mmol, 0.015 mM) was dissolved in $CDCl_3$ with G3 (0.01 mmol) and a ^{1}H NMR spectrum was collected to confirm initiation, followed by addition of the sample to a solution of norbornene (1.18 mmol). The reaction was held in the dark at 20 ºC under N_2 for 20 minutes before precipitation from methanol. Polymeric material was isolated via filtration in 53% recovery and analyzed by SEC and UV-vis to reveal incorporation of the UV profile consistent with **3.1$_{W}$** had been incorporated into the polymer (M_n = 77,700 Da, Đ = 1.96; Figure 3.7). While promising, this data does not conclusively prove whether **3.1$_{W}$** is located at the chain end or incorporated throughout the polymer.

Kinetic analyses for the polymerizations of **3.1$_{W}$** and **3.1$_{Cr}$** were initially conducted using variable temperature (VT)-NMR (-35 to +5 °C). ^{1}H NMR spectra were collected prior to adding catalyst solution, and additional spectra were collected over the course of the polymerization (Figure 3.8). The vinyl signals for **3.1** (δ = 5.69) were monitored over the course of the polymerization, and the observed change in integration was used for determination of K_{obs}.[72] The observed rate was consistent with first order kinetics and K_{obs} for **3.1$_{Cr}$** was determined to be -0.016 s^{-1}, while K_{obs} for tungsten monosubstituted was determined to be 0. The kinetics data was also used to construct an Eyring plot in order to determine the activation parameters for the polymerization of **3.1$_{Cr}$** ($\Delta H^{\ddagger}_{Cr}$ = 18.45 kcal mol^{-1}; $\Delta S^{\ddagger}_{Cr}$ = -0.003 kcal mol^{-1}, Figure 3.9). As no polymerization was observed for **3.1$_{W}$** across our selected temperature range, we could not determine activation parameters for this monomer.

To gain a deeper understanding of the observed phenomena, we turned our attention to computational studies. All quantum chemical calculations were carried out using density functional theory (DFT) in the ORCA 5.0 software package.[73,74] The accuracy of DFT calculations is inherently dependent on the approximation employed in the density functional. The Becke-Perdew density functional (BP86)[75,76] was utilized with Grimme's D3 dispersion

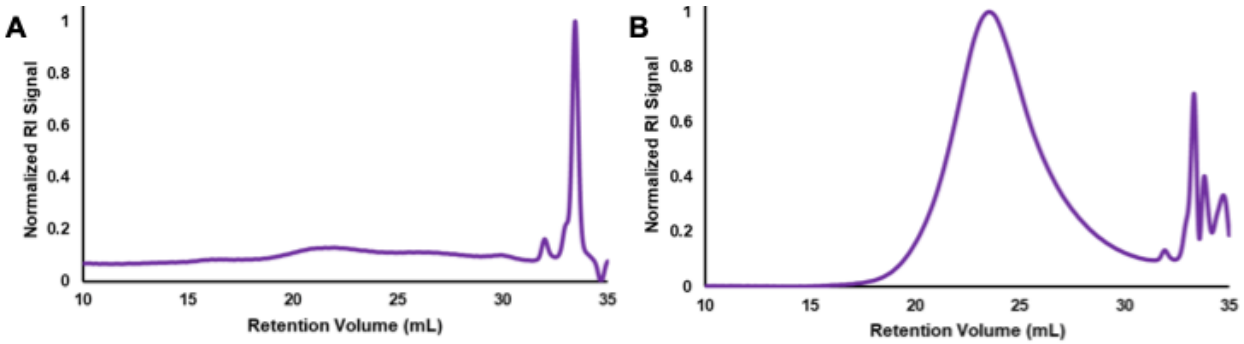


Figure 3.6. SEC data for A) initiation with **3.1$_W$** followed by chain extension with **3.1$_W$** and B) initiation with **3.1$_{Cr}$** followed by chain extension with **3.1$_{Cr}$**.

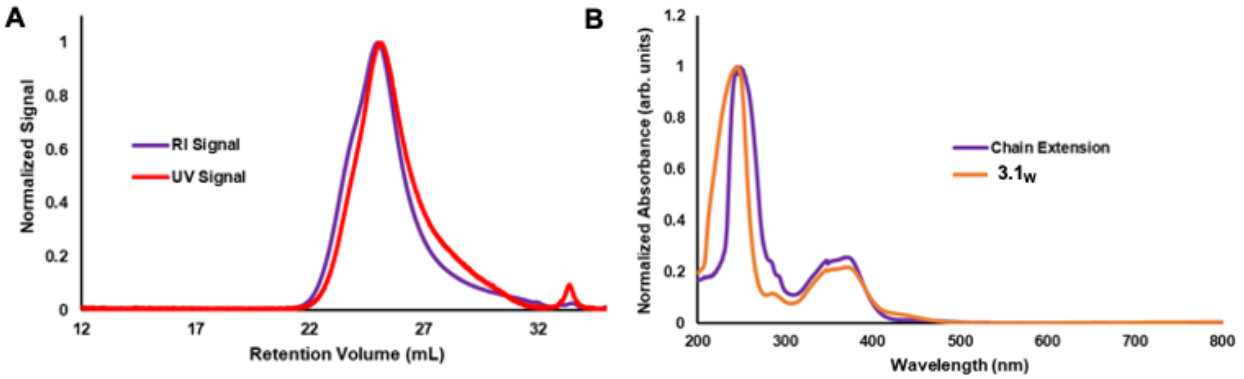


Figure 3.7. Chain extension with norbornene from ruthenium initiated **3.1$_W$**. A) SEC data for chain-extended material exhibiting UV-signal, B) UV-vis absorbance profile of **3.1$_W$** overlay with chain-extended material.

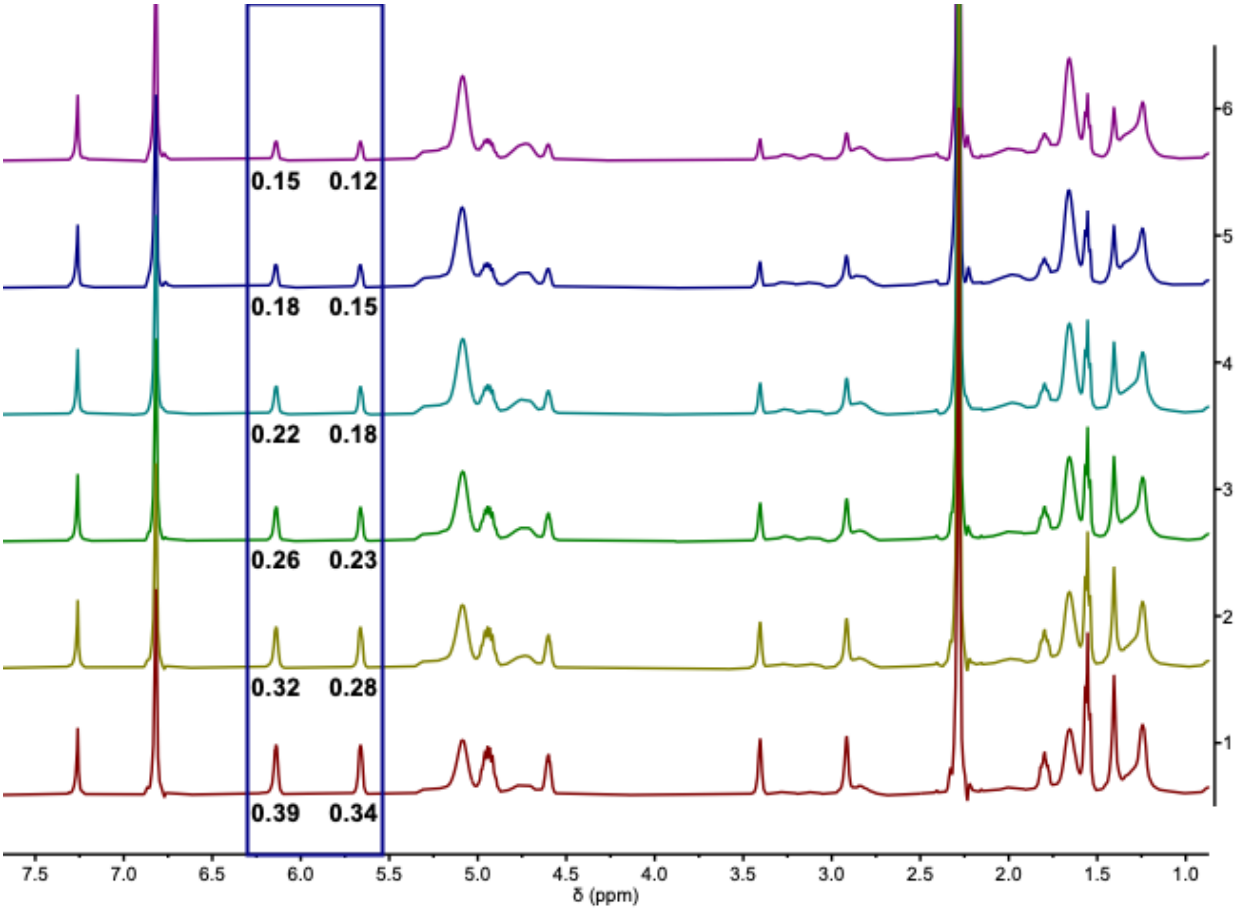


Figure 3.8. Representative ^{1}H NMR kinetics data for polymerization of **3.1**$_{Cr}$ (collected at -5 °C). Highlighted area indicates vinyl resonances of **3.1**$_{Cr}$; selected spectra are at 90-second intervals between 4:30 minutes and 12 minutes.

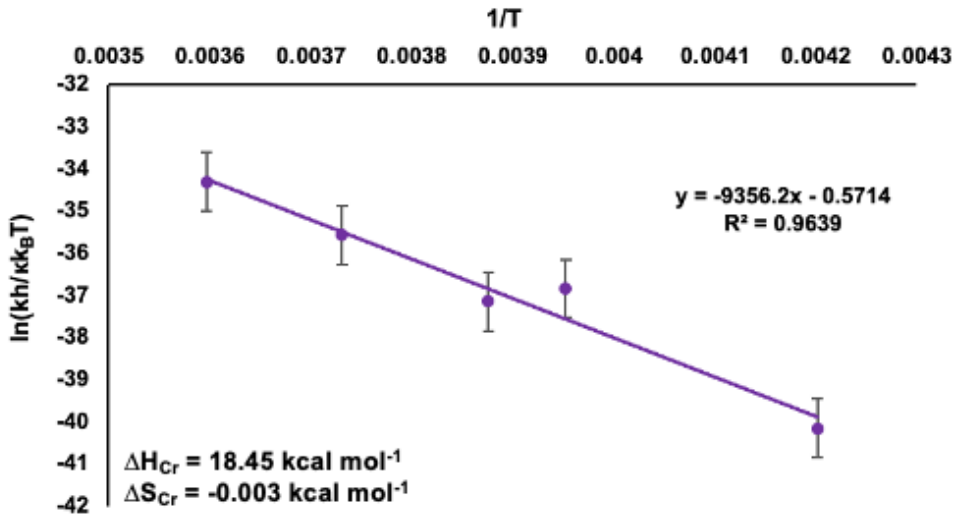


Figure 3.9. Eyring plot for **3.1**$_{Cr}$. Each data point is measured in triplicate.

correction and the Becke-Johnson damping (D3-BJ)[77] for all geometry optimizations and calculation of the analytic Hessian. Single point calculations were carried out after optimization with B3LYP-D3(BJ).[78] Single point calculations employed the conductor-like polarizable continuum model (CPCM)[79] using the chloroform solvent potential. All optimizations utilized the def2-SVP basis and all single points utilized the def2-TZVPP basis set.[80] All optimizations utilized the resolution of identity (RI) approximation,[81] and single points utilized the RIJ-chain of spheres (RIJCOSX) approximation.[82] The relative free energies shown in Figure 3.10, are all obtained using the thermal corrections from BP86-D3(BJ) and the electronic energy from CPCM-B3LYP-D3(BJ). This level of theory was chosen based on a study using G3.[83] Calculation of transition state energies for propagation steps revealed similar values for insertion of additional monomers for both metals (Figure 3.10). Throughout the initiation process, the difference in energy between **3.1$_W$** and **3.1$_{Cr}$** remains the same, with **3.1$_W$** being lower in energy throughout this process. However, upon insertion of a second monomer unit into the initiated chain end, the energetic barrier increases, and **3.1$_W$** is observed to become higher in energy (PTS1; Figure 3.10). The calculated activation parameters from both experimental and computational studies are in agreement (experimental: $\Delta G^{\ddagger}_{Cr}$ = 19.33 kcal mol^{-1} vs. theoretical: $\Delta G^{\ddagger}_{Cr}$ = 16.85 kcal mol^{-1}; $\Delta G^{\ddagger}_{W}$ = 18.32 kcal mol^{-1}). Further investigation into the origin of the difference between these two complexes is needed. Our hypothesis remains that there is steric encumbrance preventing propagation with tungsten carbenes.

Based on our computational results, we postulate that sterics are responsible for the observed phenomenon, in addition to deleterious side reactions with between **3.1$_W$** and G3. With respect to this hypothesis, we sought to find the root of the difference between the Grubbs-type and Schrock-type catalysts. With respect to both catalysts, the tacticity of the polymer is driven by chain end control.[84] The Schrock-type catalysts are well known to exhibit stereogenic metal control to favor one isomer and tacticity per monomer (cis-syndiotactic), while the ruthenium catalysts in question do not provide this same selectivity.[85] The barrier to rotation of the carbene around the Ru=C bond has been calculated previously, and was determined to be extremely low, leading to a lack of preference for one isomer over the

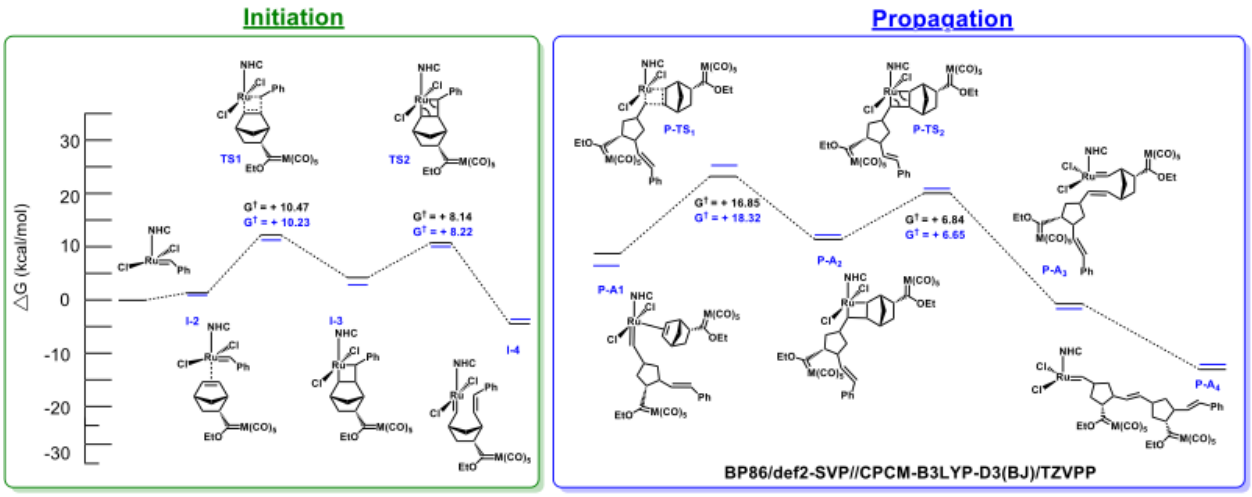


Figure 3.10. Initiation and Propagation Energies for G3 with **3.1**. Blue represents **3.1**$_W$, while black represents **3.1**$_{Cr}$.

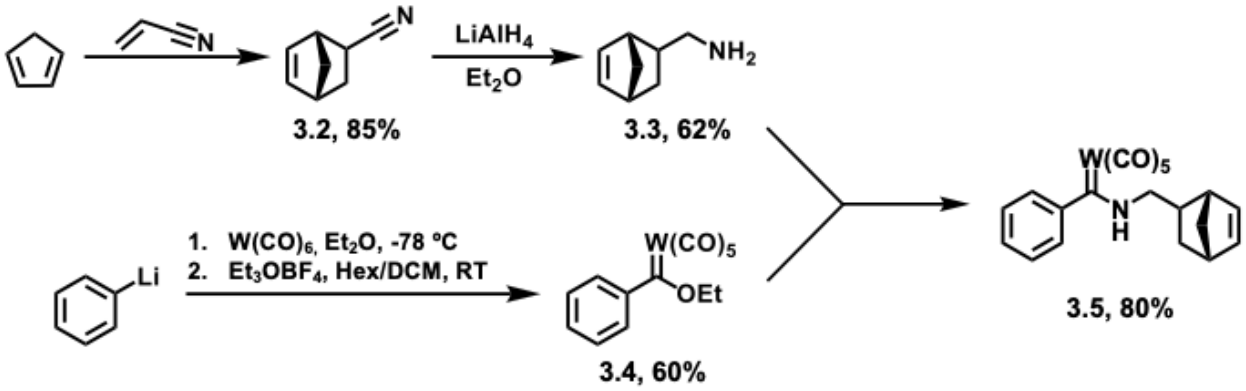
other.[72] We postulate that due to the cis-syndiotactic nature of addition provided by the Schrock catalyst, the steric hindrance from the buttressing carbenes is eliminated. In order to test the computational predictions, we surmised that we could simply reduce the steric penalty by moving the tungsten farther from the ruthenium center. We hypothesized that the importance of steric congestion with these monomers could be tested and thus designed monomer **3.5** (Scheme 3.2). A Diels-Alder reaction between acrylonitrile and cyclopentadiene at 20 ºC for 16 h affords the norbornene carbonitrile (**3.2**, 76% yield, 50% endo), which was purified via silica column with 95:5 hexanes:EtOAc in 93% purity. The carbonitrile was then reduced to the amine with $LiAlH_4$ (**3.3**, 81%). Finally, **3.3** was condensed with the phenyl ethoxy carbene (**3.4**) to provide the desired aminocarbene (**3.5**). We then subjected **3.5**$_W$ (0.11 mmol) to polymerization with G3 (0.002 mmol) at room temperature for 1 h and observed polymeric material following precipitation from methanol (72% yield, 161,400 Da, 1.10 Đ, Figure 3.11). While nitrogen containing monomers are commonly difficult to polymerize due to their chelation to the ruthenium center, we speculate that the bulkiness of the tungsten blocks the chelation and allows for polymerization activation.

Materials and Methods

General Considerations

Unless otherwise noted, solvents were dried on an MBraun solvent purification system with 3Å molecular sieves and degassed via three freeze-pump-thaw cycles. All other reagents were obtained from commercial sources and used without further purification. Oxygen and water sensitive manipulations were performed in a nitrogen filled MBraun glovebox or using standard Schlenk techniques. Polymerizations were performed in an N_2-filled glovebox or in an NMR spectrometer. ^1H and ^{13}C NMR data were collected on a Varian 300 MHz NMR or a Bruker 500 MHz NMR spectrometer. Chemical shifts (δ) are reported in ppm using the residual solvent as reference. IR spectra were collected on a Bruker Alpha II FT-IR with Platinum ATR accessory. UV-visible absorbance spectra were recorded using an Agilent Cary 100 series UV-Vis spectrophotometer. Thermogravimetric analysis (TGA) was performed on a TA Instruments TGA Q500 and Dynamic Mechanical Analysis (DMA) data was collected on a TA Instruments DMA Q800 with a film tension clamp. Size Exclusion Chromatography (SEC)

Scheme 3.2. Synthesis of **3.5**



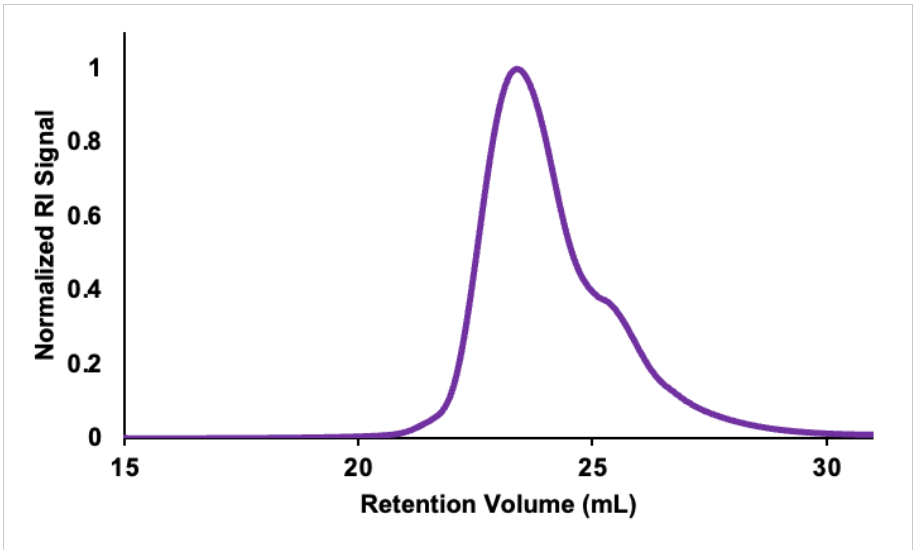


Figure 3.11. SEC data from triple detection for initial polymerization of **3.5**

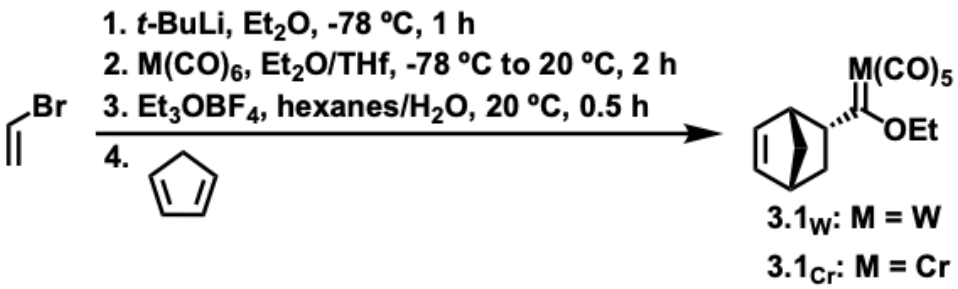
data were collected on an Omnisec Resolve and Omnisec Reveal System using triple detection or conventional calibration with detectors in series: UV, light scattering, viscometer, and refractive index and three Viscotek styrene divinylbenzene copolymer columns (in series: T3000, T4000, and T5000) at a flow rate of 1 mL/min and thermostatted to 30 °C using tetrahydrofuran (THF) as the eluent. Molecular weight and dispersity data are reported using triple detection or conventional calibration against polystyrene standards.

Synthetic Considerations

*Synthesis of **3.1***

Tungsten and chromium carbenes **3.1** were prepared in two steps according to a modification of the procedure reported by Wulff (Scheme 3.3).[65] A dry Schlenk flask was charged with a Teflon stir bar, vinyl bromide (15.9 mmol), and diethyl ether (Et_2O, 100 mL) before cooling the solution to -78 °C for 10 minutes. Tert-butyllithium (1.5 M in pentane, 21 mL, 31.7 mmol) was added dropwise, and the reaction was stirred at -78 °C for 1 hour. In a separate Schlenk flask, a suspension of metal carbonyl (8.35 g, 23.8 mmol) in and Et_2O (100 mL) was cooled to -78 °C for 15 minutes. The cold vinyl lithium solution was then cannula transferred to the suspension of metal carbonyl under a flow of N_2. Following complete addition of the lithiate, the reaction mixture was warmed to room temperature with stirring over the course of 2.5 hours. The solvent was evaporated under vacuum, and triethyloxonium tetrafluoroborate (7.52 g, 39.6 mmol) was added to the resultant residue in a mixture of hexanes/water (11:4 v/v). The mixture was stirred at room temperature for 10 minutes, and dried over sodium sulfate. The crude product was used without purification and stirred with cyclopentadiene (5 mL, 59 mmol) for 0.5 hours at room temperature. The excess cyclopentadiene was evaporated in vacuo, and the crude product was purified via silica gel chromatography (hexanes as eluent) to afford **3.1** as an orange solid (0.84 g, 11% yield). Characterization data were in agreement with previous reports. Consistent with previous reports, **3.1** was obtained as a mixture of diastereomers (90:10 endo:exo) that could not be further separated (Figure 3.12).

Scheme 3.3. Synthesis of 3.1



*Synthesis of **3.2***

A pressure flask was equipped with stir bar and dicyclopentadiene (9.30 g, 70.3 mmol) was added followed by acrylonitrile (9.5 mL, 145 mmol) and heated to 170 °C for 16 h. The reaction was cooled to room temperature and purified on silica column with 95/5 hexanes/EtOAc. The reaction resulted in a 50:50 mixture of *endo*- and *exo*- isomers that could be separated via column in > 94% purity with some mixed fractions. *Endo*-: 4.108 g, > 95% pure by NMR. *Exo*-: 2.8609 g, > 95% pure by NMR. Mixed: 4.9154 g. total yield 11.8843 g, 71% yield. ^{1}H NMR spectra are consistent with previous reports (Figure 3.13-Figure 3.14).

*Synthesis of **3.3***

The norbornene carbonitrile (pure isomer) was subjected to reduction via lithium aluminum hydride ($LiAlH_4$). A dry Schlenk flask was charged with stir bar, $LiAlH_4$ (2.2171 g, 55.5 mmol), and Et_2O (100 mL). Norbornene carbonitrile (5.7261 g, 48.1 mmol) was added dropwise and the reaction was allowed to stir at room temperature overnight. The reaction was then cooled to 0 °C and H_2O (2.5 mL) was added slowly, followed by NaOH (15% by mass, 2.5 mL), then H_2O (7.5 mL). The reaction was stirred for 15 minutes at room temperature, then sodium sulfate was added and the mixture was stirred another 15 minutes. The reaction was filtered to remove solids and concentrated under vacuum. The amine product was distilled under vacuum (85 °C, 30 mmHg) to yield 4.8027 g (81%) of clear, colorless liquid. NMR spectra are consistent with previous reports.

*Synthesis of **3.4***

3.4 was prepared following an adapted procedure reported by Fischer.[66] Metal hexacarbonyl (3.0313 g, 8.6 mmol) was added to a dry Schlenk flask with stir bar and Et_2O (40 mL) and cooled to -78 °C. Phenyllithium (4.6 mL, 1.9 M) was added dropwise, and the reaction was allowed to stir at -78 °C for 1 h. The solvent was evaporated under vacuum and triethyloxonium tetrafluoroborate (1.6217 g, 8.5 mmol) was added with a mixture of hexanes and water (20 mL, 50/50 mixture) and stirred vigorously for 10 min. The product was extracted with hexanes (2 x 20 mL) and washed with brine (2 x 20 mL), followed by purification via silica gel chromatography with hexanes to give 2.8274 g (72% yield) of red solid. NMR spectra were in agreement with previous reports (Figure 3.5).

Synthesis of **3.5**

The phenyl amino carbene was synthesized by adding the **3.4** (1.2259 g, xx mmol) to a vial with DCM (5 mL) and adding the **3.3** (403.1 mg). The reaction was stirred at 30 °C for 3 h. The solvent was evaporated under vacuum and the product was purified via silica gel chromatography with 95/5 hexanes/EtOAc. Starting material was recovered as the first compound off the column, followed by the product which was isolated as mixture of two rotamers. 995.3 mg, 69% yield. A representative ^{1}H NMR spectrum is provided in Figure 3.16.

Polymerization Studies and Material Characterization

General Polymerization Kinetics Collection and Analysis Procedures

In an N_2 filled glovebox, **3.1** was dissolved in $CDCl_3$ and mesitylene was added as an internal standard and added to a septa capped NMR tube, sealed with electrical tape. The sample was allowed to equilibrate at the appropriate temperature in the spectrometer and an initial spectrum was collected. A stock solution of Grubbs 3rd Generation Catalyst was prepared in $CDCl_3$. An aliquot of catalyst solution was injected into the sample and ^{1}H NMR spectra of the reaction were collected at appropriate intervals for 30-50 minutes. Monomer consumption was monitored via integration of vinyl peaks in the monomer compared to the aromatic peak in mesitylene.

Chain Extension Experiments with Carbenes from Carbene Initiated Chain Ends

Grubbs 3rd generation catalyst (11.0 mg) was added to an NMR tube with $CDCl_3$ (0.7 mL) and mesitylene (1 µL) as an internal standard and an NMR spectrum was taken. A solution of monosubstituted chromium carbene in $CDCl_3$ (3.6 mg in 0.1 mL) was added and a spectrum was taken. The sample was kept away from light and held at 20 °C for 1 h and another spectrum was taken. An aliquot (0.1 mL) was taken from the NMR sample and added to a DCM solution of chromium monosubstituted carbene (31.1 mg in 0.3 mL) and held at 20 °C for 1 h. The sample was quenched with ethyl vinyl ether and concentrated to minimal volume before precipitation from MeOH to yield 11.8 mg of yellow-orange polymer. SEC of this material indicates that propagation occurs from the active chain end when initiated with chromium carbene and additional chromium carbene is added.

CO Detection Control – Addition of Pyridine to ***3.1***$_{Cr}$

Rhodium complex was added to a quartz UV-vis cell with septa cap and sparged with N_2, followed by collection of a UV-vis spectrum. Chromium monosubstituted was added to a septa cap vial with DCM and foiled to keep away from light and sparged with N_2. The two containers were connected with a glass manifold and 3-bromopyridine (1 equiv.) was added. The sample was held at 20 °C for 1 h, sparged with N_2 for 30 sec and a UV-vis spectrum was collected. The experiment was repeated with the tungsten carbene.

Summary

In conclusion, we have provided a fundamental study on metathesis chemistry which could have far-reaching impacts. Probing the steric barrier to polymerization with ruthenium catalysts has been conducted with metallocarbenes. We have discovered that a steric wall does in fact exist for ruthenium metathesis catalysts, as supported by both experimental and computational data. Our work also provides insight into simple design elements that can be considered for turning on metathesis when bulky groups are used.

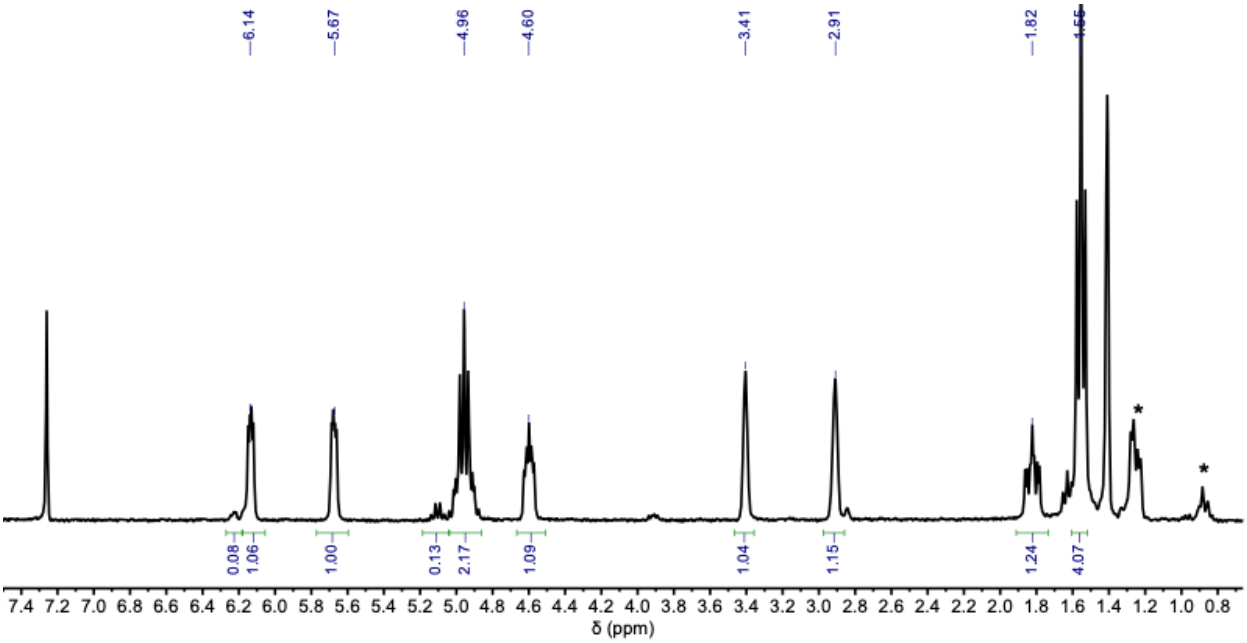


Figure 3.12. Representative ^{1}H NMR spectrum for **3.1$_{Cr}$**. * denotes grease

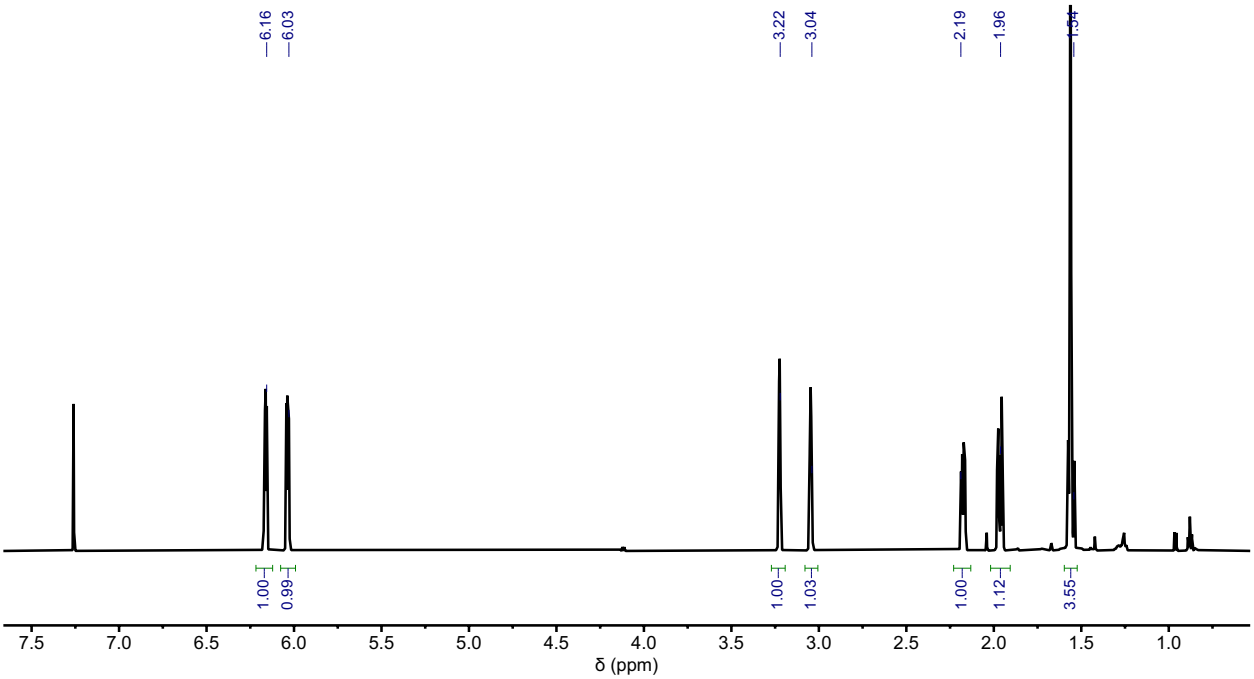


Figure 3.13. Representative ^{1}H NMR spectrum for **3.2** *exo*

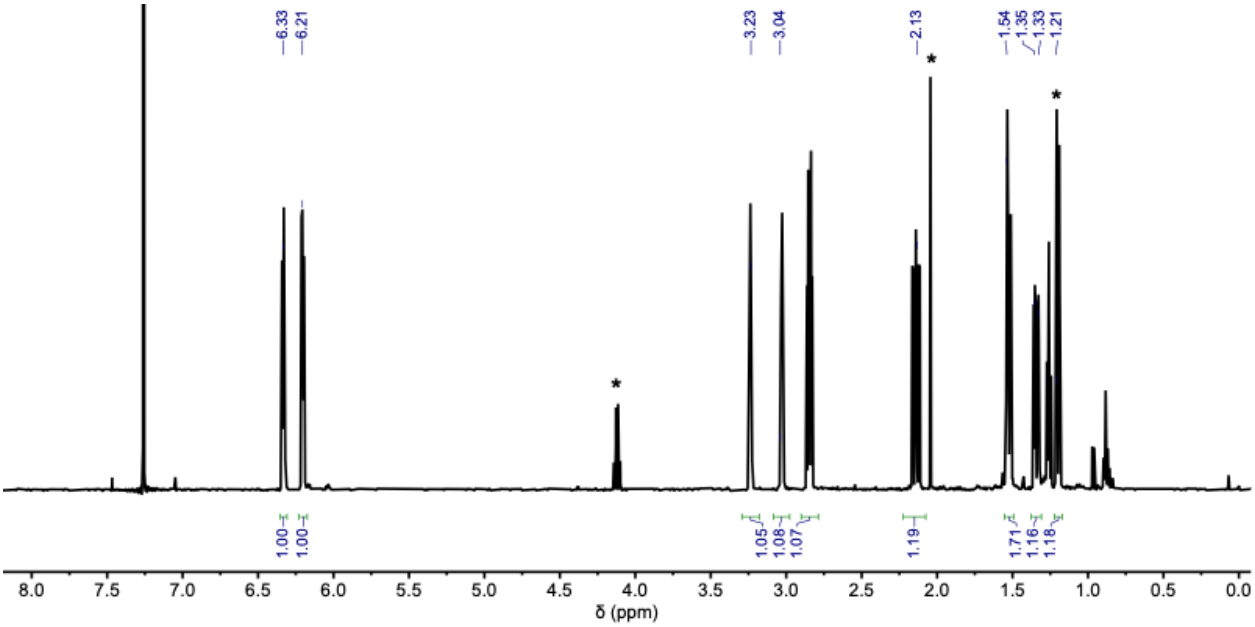


Figure 3.14. Representative ^{1}H NMR spectrum for **3.2** ***endo.*** ***** denotes ethyl acetate

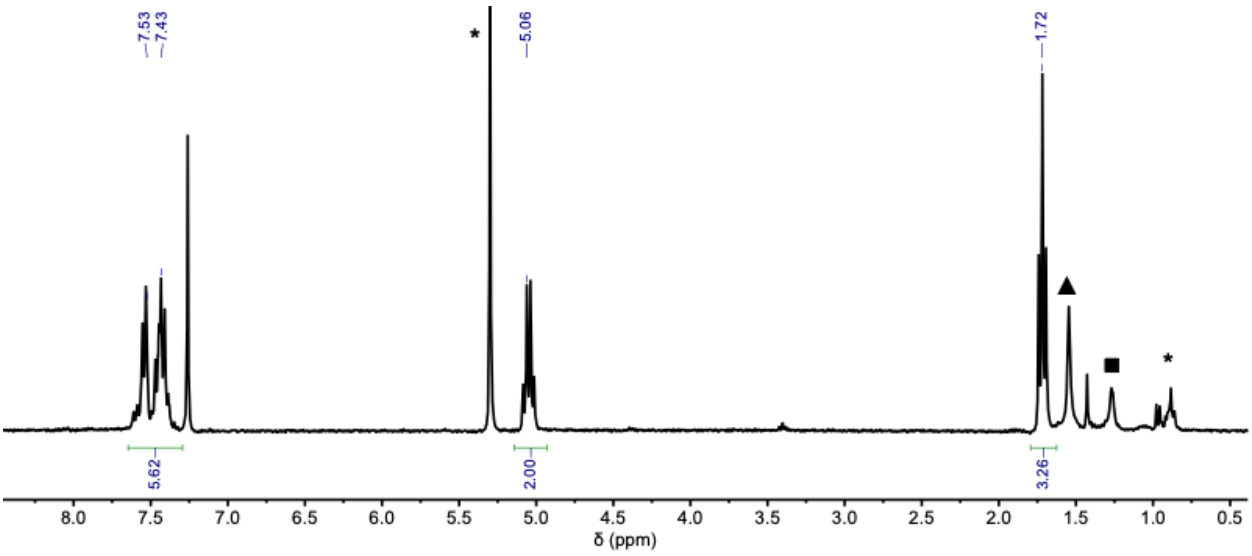


Figure 3.15. ^{1}H NMR spectra for **3.4**$_{W}$**.** ***** denotes DCM, ▲ denotes water, and ■ denotes grease

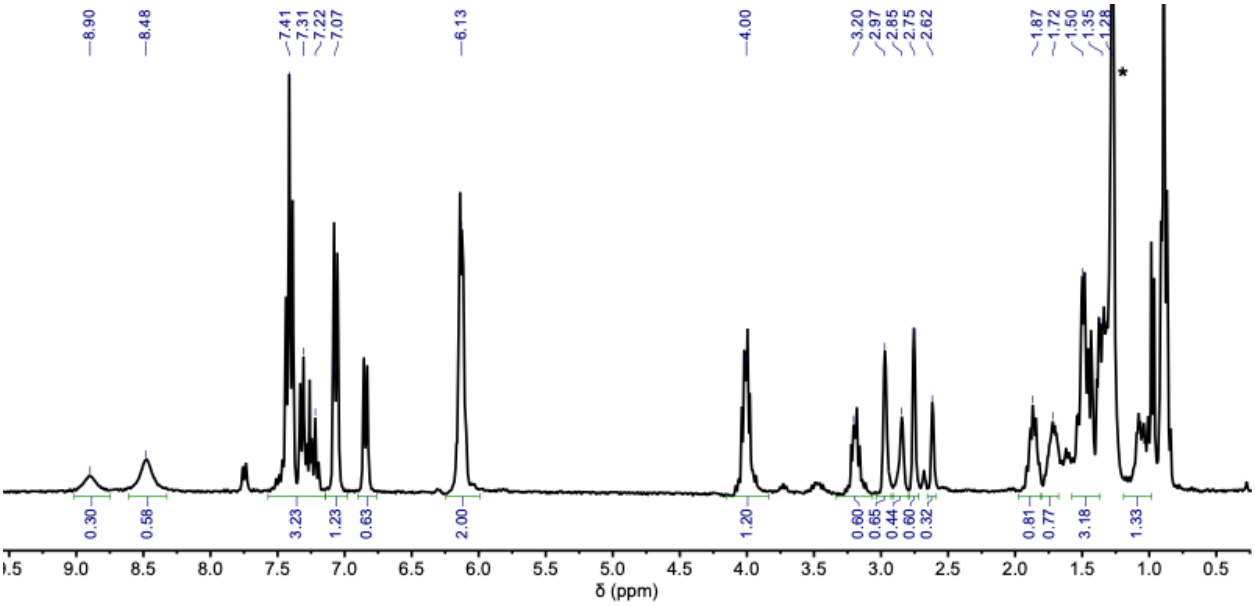


Figure 3.16. ^{1}H NMR spectrum for **3.5$_{W}$.** * denotes grease

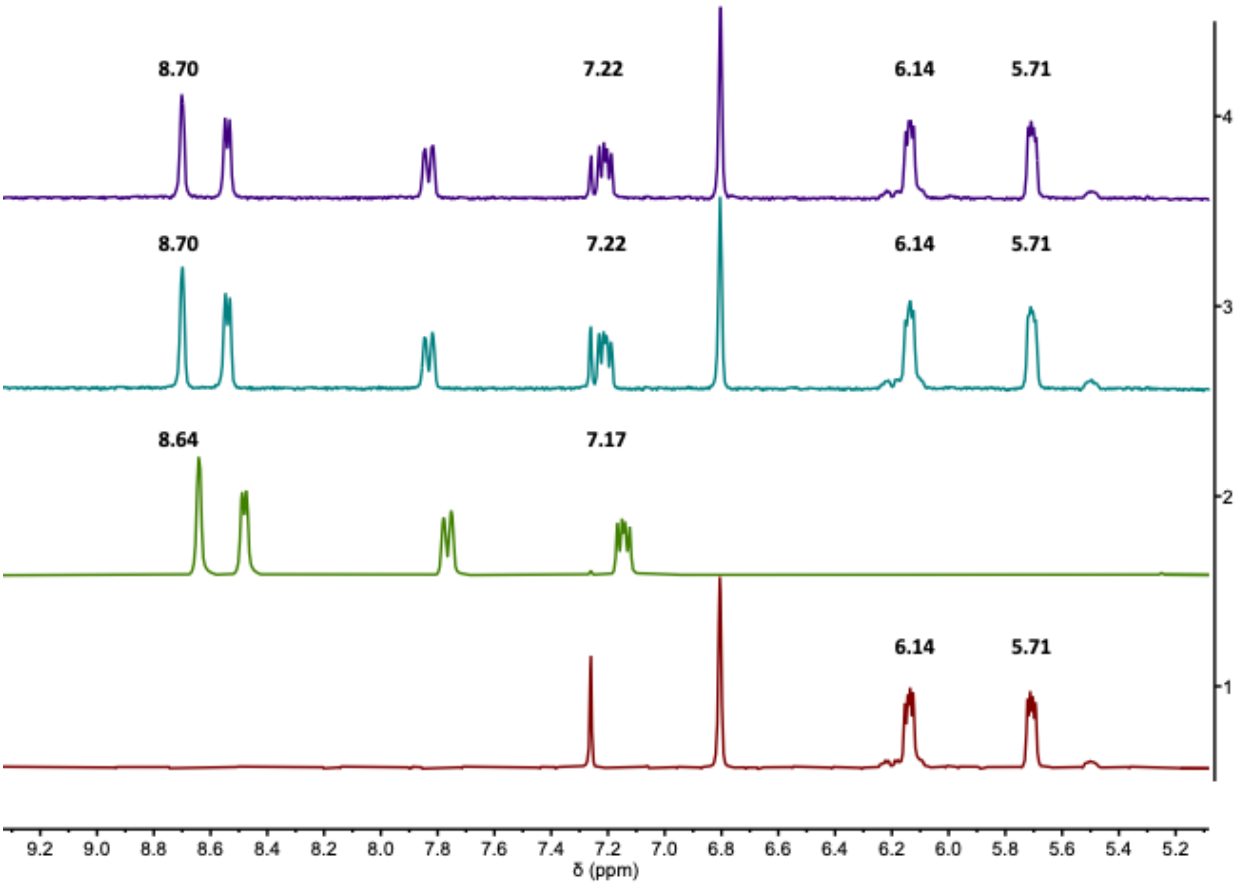


Figure 3.17. ^{1}H NMR spectra for the addition of pyridine to **3.1$_W$**. 1) **3.1$_W$** only, 2) 3-bromopyridine only, 3) **3.1$_W$** plus 3-bromopyridine, t_0, 4) **3.1$_W$** plus 3-bromopyridine, t_{60}

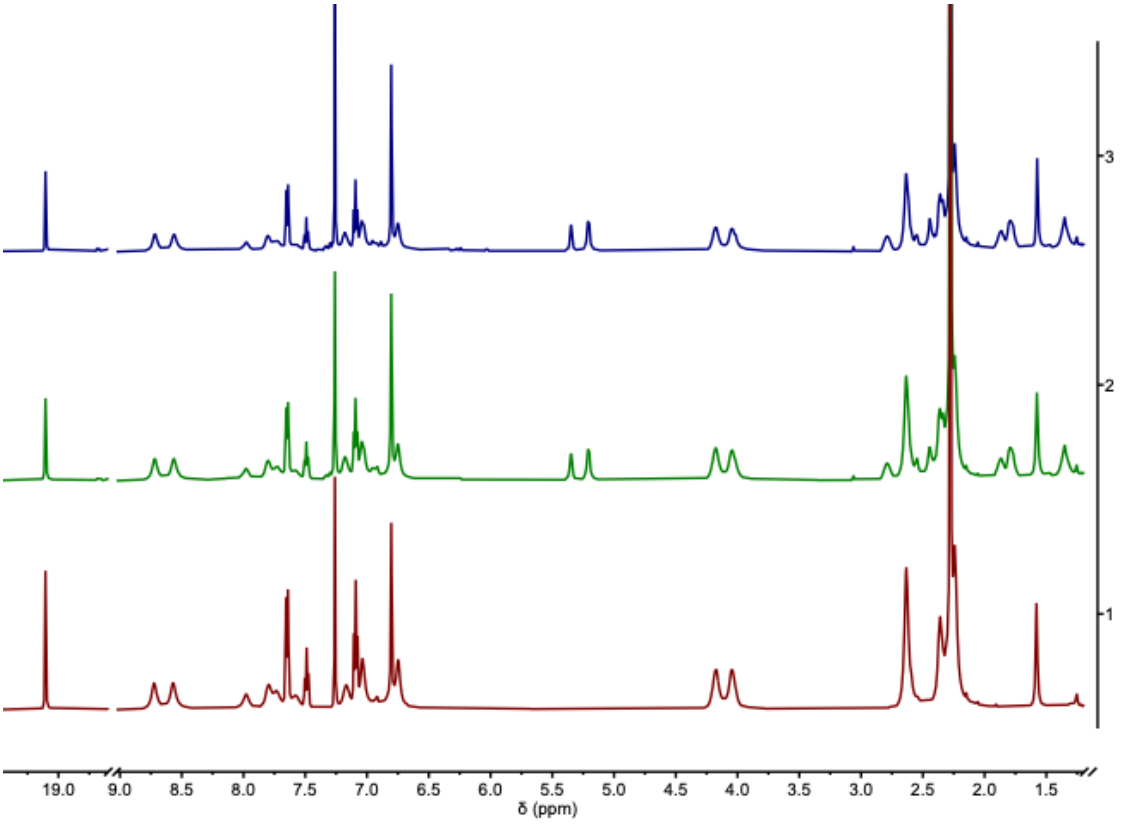


Figure 3.18. ^{1}H NMR spectra for control experiment between G3 and norbornene. 1) G3 only, 2) G3 plus norbornene, t0, 3) G3 plus norbornene, t60.

References

(1) Marinescu, S. C.; Schrock, R. R.; Mü, P.; Hoveyda, A. H. Ethenolysis Reactions Catalyzed by Imido Alkylidene Monoaryloxide Monopyrrolide (MAP) Complexes of Molybdenum. *J Am Chem Soc* **2009**, *131*, 10840–10841. https://doi.org/10.1021/ja904786y.

(2) Burdett, K. A.; Harris, L. D.; Margl, P.; Maughon, B. R.; Mokhtar-Zadeh, T.; Saucier, P. C.; Wasserman, E. P. Renewable Monomer Feedstocks via Olefin Metathesis: Fundamental Mechanistic Studies of Methyl Oleate Ethenolysis with the First-Generation Grubbs Catalyst. *Organometallics* **2004**, *23*, 2027–2047. https://doi.org/10.1021/om0341799.

(3) Thomas, R. M.; Keitz, B. K.; Champagne, T. M.; Grubbs, R. H. Highly Selective Ruthenium Metathesis Catalysts for Ethenolysis. *J. Am. Chem. Soc* **2011**, *133*, 7490–7496. https://doi.org/10.1021/ja200246e.

(4) Rybak, A.; Fokou, P. A.; Meier, M. A. R. Metathesis as a Versatile Tool in Oleochemistry. *Eur. J. Lipid Sci. Technol* **2008**, *110*, 797–804. https://doi.org/10.1002/ejlt.200800027.

(5) Chatterjee, A. K.; Sanders, D. P.; Grubbs, R. H. Synthesis of Symmetrical Trisubstituted Olefins by Cross Metathesis. *Organic Letters* **2002**, *4*, 1939–1942. https://doi.org/10.1021/ol0259793.

(6) Blackwell, H. E.; O'leary, D. J.; Chatterjee, A. K.; Washenfelder, R. A.; Bussmann, D. A.; Grubbs, R. H. New Approaches to Olefin Cross-Metathesis. *J Am Chem Soc* **2000**, *2000*, 58–71. https://doi.org/10.1021/ja993063u.

(7) Connon, S. J.; Blechert, S. Cross-Metathesis of Olefins Recent Developments in Olefin Cross-Metathesis. *Angew. Chem. Int. Ed* **2003**, *42*, 1900–1923. https://doi.org/10.1002/anie.200200556.

(8) Sinclair, F.; Alkattan, M.; Prunet, J.; Shaver, M. P. Olefin Cross Metathesis and Ring-Closing Metathesis in Polymer Chemistry. *Polymer Chemistry* **2017**, *8*, 3398. https://doi.org/10.1039/c7py00340d.

(9) Rybak, A.; Meier, M. A. R. Acyclic Diene Metathesis with a Monomer from Renewable Resources: Control of Molecular Weight and One-Step Preparation of Block Copolymers. *ChemSusChem* **2008**, *1*, 542–547. https://doi.org/10.1002/cssc.200800047.

(10) Mutlu, H.; Montero De Espinosa, L.; Meier, M. A. R. Acyclic Diene Metathesis: A Versatile Tool for the Construction of Defined Polymer Architectures. *Chem. Soc. Rev* **2011**, *40*, 1404–1445. https://doi.org/10.1039/b924852h.

(11) Wagener, K. B.; Boncella, J. M.; Nel, J. G. Acyclic Diene Metathesis (ADMET) Polymerization. *Macromolecules* **1991**, *24*, 2649–2657.

(12) Brzezinska, K.; Wolfe, P. S.; Watson, M. D.; Wagener, K. B. Acyclic Diene Metathesis (ADMET) Polymerization Using a Well-Defined Ruthenium Based Metathesis Catalyst. *Macromolecular Chemistry and Physics* **1996**, *197* (6), 2065–2074. https://doi.org/10.1002/MACP.1996.021970622.

(13) Kirkland, T. A.; Lynn, D. M.; Grubbs, R. H. Ring-Closing Metathesis in Methanol and Water. *J. Org. Chem.* **1998**, *63*, 9904–9909. https://doi.org/10.1021/jo981678o.

(14) Grubbs, R. H.; Miller, S. J.; Fu, G. C. Ring-Closing Metathesis and Related Processes in Organic Synthesis. *Acc. Chem. Res* **1995**, *28*, 446–452.

(15) Cink, R. D.; Lukin, K. A.; Bishop, R. D.; Zhao, G.; Pelc, M. J.; Towne, T. B.; Gates, B. D.; Ravn, M. M.; Hill, D. R.; Ding, C.; Cullen, S. C.; Mei, J.; Leanna, M. R.; Henle, J.; Napolitano, J. J.; Nere, N. K.; Chen, S.; Sheikh, A.; Kallemeyn, J. M. Development of the Enabling Route for Glecaprevir via Ring-Closing Metathesis. *Org. Process Res. Dev* **2020**, *24*, 183–200. https://doi.org/10.1021/acs.oprd.9b00469.

(16) Kotha, S.; Pulletikurti, S.; Dommaraju, Y. Ring-Opening Metathesis of n-Alkenyl β-Lactams. *Heterocycles* **2019**, *98* (1), 79–87. https://doi.org/10.3987/COM-18-S(F)81.

(17) Slugovc, C. The Ring Opening Metathesis Polymerisation Toolbox. *Macromolecular Rapid Communications* **2004**, *25*, 1283–1297. https://doi.org/10.1002/marc.200400150.

(18) Tallarico, J. A.; Bonitatebus, P. J.; Snapper, M. L. Ring-Opening Metathesis. A Ruthenium Catalyst Caught in the Act. *J Am Chem Soc* **1997**, *119*, 7157–7158.

(19) Frenzel, U.; Nuyken, O. Ruthenium-Based Metathesis Initiators: Development and Use in Ring-Opening Metathesis Polymerization. *Journal of Polymer Science Part A: Polymer Chemistry* **2002**, *40*, 2895–2916. https://doi.org/10.1002/pola.10324.

(20) Yang, Z.; He, Y.; Vourloumis, D.; Vallberg, H.; Nicolaou, K. C. Total Synthesis of Epothilone A: The Olefin Metathesis Approach. *Angewandte Chemie International Edition in English* **1997**, *36* (1–2), 166–168. https://doi.org/10.1002/ANIE.199701661.

(21) Smith III, A. B.; Kozmin, S. A.; Adams, C. M.; Paone, D. v. Assembly of (-)-Cylindrocyclophanes A and F via Remarkable Olefin Metathesis Dimerizations. *J Am Chem Soc* **2000**, *122*, 4984. https://doi.org/10.1021/ja000430p.

(22) Colombo, M.; Peretto, I. Chemistry Strategies in Early Drug Discovery: An Overview of Recent Trends. *Drug Discovery Today* **2008**, *13* (15–16), 677–684. https://doi.org/10.1016/J.DRUDIS.2008.03.007.

(23) Hughes, D.; Wheeler, P.; Ene, D. Olefin Metathesis in Drug Discovery and Development - Examples from Recent Patent Literature. *Organic Process Research and Development* **2017**, *21*, 1938–1962. https://doi.org/10.1021/acs.oprd.7b00319.

(24) Piscopio, A. D.; Robinson, J. E. Recent Applications of Olefin Metathesis to Combinatorial Chemistry This Review Comes from a Themed Issue on Combinatorial Chemistry. *Current Opinion in Chemical Biology* **2004**, *8*, 245–254. https://doi.org/10.1016/j.cbpa.2004.04.001.

(25) Song, J.-A.; Peterson, G. I.; Bang, K.-T.; Ahmed, T. S.; Sung, J.-C.; Grubbs, R. H.; Choi, T.-L. Ru-Catalyzed, Cis-Selective Living Ring-Opening Metathesis Polymerization of Various Monomers, Including a Dendronized Macromonomer, and Iplications to Enhanced Shear Stability. *J. Am. Chem. Soc* **2020**, *142*, 10438–10445. https://doi.org/10.1021/jacs.0c02785.

(26) Cho, I. New Ring-Opening Polymerizations for Copolymers Having Controlled Microstructures. *Progress in Polymer Science* **2000**, *25*, 1043–1087.

(27) Elling, B. R.; Xia, Y. Living Alternating Ring-Opening Metathesis Polymerization Based on Single Monomer Additions. *J Am Chem Soc* **2015**, *137*, 9922–9926. https://doi.org/10.1021/jacs.5b05497.

(28) Chen, Y.; Mehawed Abdellatif, M.; Nomura, K. Olefin Metathesis Polymerization: Some Recent Developments in the Precise Polymerizations for Synthesis of Advanced

Materials (by ROMP, ADMET). *Tetrahedron* **2018**, *74*, 619–643. https://doi.org/10.1016/j.tet.2017.12.041.

(29) Bielawski, C. W.; Grubbs, R. H. Living Ring-Opening Metathesis Polymerization. *Progress in Polymer Science* **2007**, *32* (1), 1–29. https://doi.org/10.1016/J.PROGPOLYMSCI.2006.08.006.

(30) Calderon, N.; Chen, H. Y.; Scott, K. W. Olefin Metathesis - A Novel Reaction for Skeletal Transformations of Unsaturated Hydrocarbons. *Tetrahedron Letters* **1967**, *8* (34), 3327–3329. https://doi.org/10.1016/S0040-4039(01)89881-6.

(31) Calderon, N.; Ofstead, E. A.; Ward, J. P.; Judy, W. A.; Scott, K. W. Olefin Metathesis. I. Acyclic Vinylenic Hydrocarbons. *J Am Chem Soc* **1968**, *93*, 4133–4140.

(32) Herisson, J.-L.; Chauvin, Y. Catalyse de Transformation Des Oléfines Par Les Complexes Du Tungstène. *Die Makromolekulare Chemie* **1971**, *141*, 161–176.

(33) Grubbs, R. H.; Burk, P. L.; Carr, D. D. Consideration of the Mechanism of the Olefin Metathesis Reaction. *J Am Chem Soc* **1975**, *97*, 3265–3267.

(34) Katz, T. J.; McGinnis, J. The Mechanism of the Olefin Metathesis Reaction. *J Am Chem Soc* **1975**, *97*, 1592–1594.

(35) Katz, T. J.; Sivavec, T. M. Metal-Catalyzed Rearrangement of Alkene-Alkynes and the Stereochemistry of Metallacyclobutene Ring Opening. *J Am Chem Soc* **1985**, *107*, 737–738.

(36) Katz, T. J.; Lee, S. J. Initiation of Acetylene Polymerizaiton by Metal Carbenes. *J Am Chem Soc* **1980**, *102*, 422–424.

(37) Katz, T. J.; McGinnis, J.; Altus, C. Metathesis of a Cyclic Trisubstituted Alkene. Preparation of Polyisoprene from 1-Metylcyclobutane. *J Am Chem Soc* **1976**, *98*, 606–608.

(38) McGinnis, J.; Katz, T. J.; Hurwitz, S. Selectivity in the Olefin Metathesis of Unsymmetrically Substituted Ethylenes. *J Am Chem Soc* **1976**, *98*, 605–606.

(39) Lee, S. J.; McGinnis, J.; Katz, T. J. Directional Specificity and Stereoselectivity in the Metathesis of a Trisubstituted Olefin. *J Am Chem Soc* **1976**, *98*, 7818–7819.

(40) Katz, T. J.; Lee, S. J.; Nair, M.; Savage, E. B. Induction of Olefin Metathesis by Acetylenes. *J Am Chem Soc* **1980**, *102*, 7942–7944.

(41) Wengrovius, J. H.; Sancho, J.; Schrock, R. R. Metathesis of Acetylenes by Tungsten(VI)-Alkylidene Complexes. *J Am Chem Soc* **1981**, *103*, 3932–3934.

(42) Schrock, R. R. An "Alkylcarbene" Complex of Tantalum by Intramolecular a-Hydrogen Abstraction. *J Am Chem Soc* **1974**, *96*, 6796–6797.

(43) Cardin, D. J.; Cetinkaya, B.; Doyle, M. J.; Lappert, M. F. The Chemistry of Transition-Metal Carbene Complexes and Their Role as Reaction Intermediates. *Chemical Society Reviews* **1973**, *2*, 99–144.

(44) Cardin, D. J.; Doyle, M. J.; Lappert, M. F. Rhodium(I)-Catalysed Dismutation of Electron-Rich Olefins : Rhodium(I) Carbene Complexes as Intermediates. *Journal of the Chemical Society, Chemical Communications* **1972**, 927–928.

(45) Casey, C. P.; Burkhardt, T. J. (Diphenylcarbene)Pentacarbonyltungsten(0). *J Am Chem Soc* **1973**, *95*, 5833–5834.

(46) Casey, C. P.; Burkhardt, T. J. Reactions of (Diphenylcarbene)Pentacarbonyltungsten(0) with Alkenes. Role of Metal-Carbene Complexes in Cyclopropantation and Olefin Metathesis Reactions. *J Am Chem Soc* **1974**, *96*, 7808–7809.

(47) Casey, C. P.; Burkhardt, T. J.; Bunnell, C. A.; Calabrese, J. C. Synthesis and Crystal Structure of Diphenylcarbene(Pentacarbonyl)Tungsten(0). *J Am Chem Soc* **1977**, *99*, 2127–2128.

(48) Masuda, T.; Sasako, N.; Higashimura, T. Polymerization of Phenylacetylenes. III. Structure and Properties of Poly(Phenylacetylene)s Obtained by WCl6 or MoCl5. *Macromolecules* **1975**, *8*, 717–721.

(49) Patra, S. G.; Das, N. K. Recent Advancement on the Mechanism of Olefin Metathesis by Grubbs Catalysts: A Computational Perspective. *Polyhedron* **2021**, *200*, 115096. https://doi.org/10.1016/J.POLY.2021.115096.

(50) Wolf, W. J.; Lin, T. P.; Grubbs, R. H. Examining the Effects of Monomer and Catalyst Structure on the Mechanism of Ruthenium-Catalyzed Ring-Opening Metathesis Polymerization. *J Am Chem Soc* **2019**, *141* (44), 17796–17808. https://doi.org/10.1021/JACS.9B08835/SUPPL_FILE/JA9B08835_SI_002.CIF.

(51) Schrock, R. R. Recent Advances in Olefin Metathesis by Molybdenum and Tungsten Imido Alkylidene Complexes. *Journal of Molecular Catalysis A: Chemical* **2004**, *213* (1), 21–30. https://doi.org/10.1016/J.MOLCATA.2003.10.060.

(52) Walsh, D. J.; Lau, S. H.; Hyatt, M. G.; Guironnet, D. Kinetic Study of Living Ring-Opening Metathesis Polymerization with Third-Generation Grubbs Catalysts. *J Am Chem Soc* **2017**, *139* (39), 13644–13647. https://doi.org/10.1021/JACS.7B08010/SUPPL_FILE/JA7B08010_SI_002.CIF.

(53) Keitz, B. K.; Endo, K.; Patel, P. R.; Herbert, M. B.; Grubbs, R. H. Improved Ruthenium Catalysts for Z-Selective Olefin Metathesis. *J Am Chem Soc* **2012**, *134* (1), 693–699. https://doi.org/10.1021/JA210225E/SUPPL_FILE/JA210225E_SI_002.CIF.

(54) Maughon, B. R.; Grubbs, R. H. Ruthenium Alkylidene Initiated Living Ring-Opening Metathesis Polymerization (ROMP) of 3-Substituted Cyclobutenes. *Macromolecules* **1997**, *30*, 3459–3469.

(55) Kuanr, N.; Gilmour, D. J.; Gildenast, H.; Perry, M. R.; Schafer, L. L. Amine-Containing Monomers for Ring-Opening Metathesis Polymerization: Understanding Chelate Effects in Aryl-and Alkylamine-Functionalized Polyolefins. *Macromolecules* **2022**. https://doi.org/10.1021/acs.macromol.1c02664.

(56) Hyatt, M. G.; Walsh, D. J.; Lord, R. L.; Andino Martinez, J. J.; Guironnet, D. Mechanistic and Kinetic Studies of the Ring Opening Metathesis Polymerization of Norbornenyl Monomers by a Grubbs Third Generation Catalyst. *J Am Chem Soc* **2019**, *141*, 17918–17925. https://doi.org/10.1021/jacs.9b09752.

(57) Pawar, G. M.; Weckesser, J.; Blechert, S.; Buchmeiser, M. R. Ring Opening Metathesis Polymerization-Derived Block Copolymers Bearing Chelating Ligands: Synthesis, Metal Immobilization and Use in Hydroformylation under Micellar Conditions. *Beilstein Journal of Organic Chemistry* **2010**, *6*. https://doi.org/10.3762/BJOC.6.28.

(58) Silva, T. B.; Camargo, R. S.; Lima-Neto, B. S. Electronic vs. Steric Hindrance Effects in Amine Ligands to Ru-Based Initiators for ROMP. *J. Braz. Chem. Soc* **2014**, *25* (12), 2425–2432. https://doi.org/10.5935/0103-5053.20140269.

(59) Rule, J. D.; Moore, J. S. ROMP Reactivity of Endo- and Exo-Dicyclopentadiene. *Macromolecules* **2002**, *35* (21), 7878–7882. https://doi.org/10.1021/MA0209489/SUPPL_FILE/MA0209489_S.PDF.

(60) Diver, S. T. Ruthenium Vinyl Carbene Intermediates in Enyne Metathesis. *Coordination Chemistry Reviews* **2007**, *251* (5–6), 671–701. https://doi.org/10.1016/J.CCR.2006.09.008.

(61) Galan, B. R.; Gembicky, M.; Dominiak, P. M.; Keister, J. B.; Diver, S. T. Carbon Monoxide-Promoted Carbene Insertion into the Aryl Substituent of an N-Heterocyclic Carbene Ligand: Buchner Reaction in a Ruthenium Carbene Complex. *J. Am. Chem. Soc.* **2005**, *127* (45), 15702–15703. https://doi.org/10.1021/JA0545618.

(62) Nelson, D. J.; Manzini, S.; Urbina-Blanco, C. A.; Nolan, S. P. Key Processes in Ruthenium-Catalysed Olefin Metathesis. *Chemical Communications* **2014**, *50* (72), 10355–10375. https://doi.org/10.1039/C4CC02515F.

(63) Poater, A.; Ragone, F.; Correa, A.; Cavallo, L. Exploring the Reactivity of Ru-Based Metathesis Catalysts with a π-Acid Ligand Trans to the Ru−Ylidene Bond. *J Am Chem Soc* **2009**, *131* (25), 9000–9006. https://doi.org/10.1021/ja902552m.

(64) Tsai, S. D.; Register, R. A. Endo/Exo Reactivity Ratios in Living Vinyl Addition Polymerization of Substituted Norbornenes. *Macromolecular Chemistry and Physics* **2018**, *219* (11), 1–7. https://doi.org/10.1002/macp.201800059.

(65) Wulff, W. D.; Bauta, W. E.; Kaesler, R. W.; Lankford, P. J.; Miller, R. A.; Murray, C. K.; Yang, D. C. Chromium and Tungsten Pentacarbonyl Groups as Reactivity Auxiliaries in the Diels-Alder Reactions of Alkenyl Carbene Complexes with 1,3-Dienes. *J Am Chem Soc* **1990**, *112* (9), 3642–3659. https://doi.org/10.1021/ja00165a060.

(66) Fischer, E. O.; Schubert, U.; Fischer, H. Carbene Complexes Obtained by Nucleophilic Substitution. Pentacarbonyl [(Dimethylamino)Phenylmethylene]Tungsten(0). In *Inorganic Syntheses*; Shriver, D. F., Ed.; Inorganic Syntheses; John Wiley & Sons, Inc.: Hoboken, NJ, USA, 1979; Vol. 19, pp 169–171. https://doi.org/10.1002/9780470132500.

(67) Wilson, B. J.; Brantley, J. N. Synthesis and Reactivity of Metallocarbene-Containing Polymers. *J Am Chem Soc* **2019**, *141* (32), 12453–12457. https://doi.org/10.1021/jacs.9b04077.

(68) Dötz, K. H.; Stendel, J. Fischer Carbene Complexes in Organic Synthesis : Metal-Assisted and Metal-Templated Reactions. *Chem Rev* **2009**, *109*, 3227–3274. https://doi.org/https://doi.org/10.1021/cr900034e.

(69) Raubenheimer, H. G. Fischer Carbene Complexes Remain Favourite Targets, and Vehicles for New Discoveries. *Dalton Trans.* **2014**, *43* (45), 16959–16973. https://doi.org/10.1039/C4DT01943A.

(70) Esteban, J.; Ros-Lis, J. V.; Martínez-Máñez, R.; Marcos, M. D.; Moragues, M.; Soto, J.; Sancenón, F. Sensitive and Selective Chromogenic Sensing of Carbon Monoxide by Using Binuclear Rhodium Complexes. *Angewandte Chemie International Edition* **2010**, *49* (29), 4934–4937. https://doi.org/10.1002/anie.201001344.

(71) Moragues, M. E.; Esteban, J.; Ros-lis, V.; Marcos, M. D.; Martínez, M.; Soto, J.; Sancenon, F. Sensitive and Selective Chromogenic Sensing of Carbon Monoxide via Reversible Axial CO Coordination in Binuclear Rhodium Complexes. *J. Am. Chem. Soc.* **2011**, *133*, 15762–15772. https://doi.org/10.1021/ja206251r.

(72) Flook, M. M.; Gerber, L. C. H.; Debelouchina, G. T.; Schrock, R. R. Z-Selective and Syndioselective Ring-Opening Metathesis Polymerization (ROMP) Initiated by MonoAryloxidePyrrolide (MAP) Catalysts. *Macromolecules* **2010**, *43* (18), 7522. https://doi.org/10.1021/MA101375V.

(73) Neese, F. Software Update: The ORCA Program System—Version 5.0. *Wiley Interdiscip. Rev. Comput. Mol. Sci.* **2022**, e1606.

(74) Neese, F. The ORCA Program System. *WIREs Comput. Mol. Sci.* **2012**, *2* (1), 73–78.

(75) Becke, A. D. Density-Functional Thermochemistry. III. The Role of Exact Exchange. *J. Chem. Phys.* **1993**, *98* (7), 5648–5652.

(76) Becke, A. D. Density-Functional Exchange-Energy Approximation with Correct Asymptotic Behavior. *Phys. Rev. A* **1988**, *38* (6), 3098. https://doi.org/10.1103/PhysRevA.38.3098.

(77) Grimme, S.; Antony, J.; Ehrlich, S.; Krieg, H. A Consistent and Accurate Ab Initio Parametrization of Density Functional Dispersion Correction (DFT-D) for the 94 Elements H-Pu. *J. Chem. Phys.* **2010**, *132* (15), 154104.

(78) Grimme, S.; Ehrlich, S.; Goerigk, L. Effect of the Damping Function in Dispersion Corrected Density Functional Theory. *J. Comput. Chem.* **2011**, *32* (7), 1456–1465.

(79) Barone, V.; Cossi, M. Quantum Calculation of Molecular Energies and Energy Gradients in Solution by a Conductor Solvent Model. *J. Phys. Chem. A* **1998**, *102* (11), 1995–2001.

(80) Weigend, F.; Ahlrichs, R. Balanced Basis Sets of Split Valence, Triple Zeta Valence and Quadruple Zeta Valence Quality for H to Rn: Design and Assessment of Accuracy. *Phys. Chem. Chem. Phys.* **2005**, *7* (18), 3297–3305. https://doi.org/10.1039/B508541A.

(81) Weigend, F.; Häser, M.; Patzelt, H.; Ahlrichs, R. RI-MP2: Optimized Auxiliary Basis Sets and Demonstration of Efficiency. *Chem. Phys. Lett.* **1998**, *294* (1–3), 143–152.

(82) Neese, F.; Wennmohs, F.; Hansen, A.; Becker, U. Efficient, Approximate and Parallel Hartree–Fock and Hybrid DFT Calculations. A 'Chain-of-Spheres' Algorithm for the Hartree–Fock Exchange. *Chem. Phys.* **2009**, *356* (1–3), 98–109.

(83) Hyatt, M. G.; Walsh, D. J.; Lord, R. L.; Andino Martinez, J. G.; Guironnet, D. Mechanistic and Kinetic Studies of the Ring Opening Metathesis Polymerization of Norbornenyl Monomers by a Grubbs Third Generation Catalyst. *J. Am. Chem. Soc.* **2019**, *141* (44), 17918–17925.

(84) Schrock, R. R. Synthesis of Stereoregular ROMP Polymers Using Molybdenum and Tungsten Imido Alkylidene Initiators. *Dalton Transactions* **2011**, *40* (29), 7484–7495. https://doi.org/10.1039/C1DT10215J.

(85) Straub, B. F. Ligand Influence on Metathesis Activity of Ruthenium Carbene Catalysts: A DFT Study. *Adv. Synth. Catal.* **2007**, *349*, 204–214. https://doi.org/10.1002/adsc.200600465.

CHAPTER 4: POLYMER SCAFFOLD EDITING VIA BROWN ALLYLATIONS

This chapter is currently in preparation for peer review to be published by Breana J. Kyker and Johnathan N. Brantley. All experimentation and data analysis was conducted by Breana J. Kyker and the manuscript was compiled through the efforts of all authors.

Abstract

Chemoselective editing of soft materials through post-synthetic manipulations is a powerful strategy for tailoring polymer properties. The expanding sphere of chemical space that can be accessed through modern synthetic methodologies is an undeniably attractive frontier for polymer modification studies. However, there also exists an untapped wealth of established synthetic methods that are routinely underutilized with polymeric substrates (despite holding promise as selective editing tools). The Brown allylation reaction has left an indelible mark on synthetic chemistry, but this highly reliable transformation has not be explored within the context of post polymerization modification. Here, we report that allylic boronate esters can be readily incorporated within soft polymers in moderate yield (55-75%) across a range of molecular weights (12,000 Da – 75,000 Da). The resultant materials are competent substrates in the Brown allylation, and they readily react with exogenous aldehydes to afford homoallylic alcohols in excellent yield (50-95%).

Introduction

Design of functional polymers remains an area of active exploration in materials science. Many advances have been made in the synthesis of these materials, and post polymerization modifications are at the forefront of polymer functionalization methods.[1,2] These modifications allow for the synthesis of soft materials without the need for designing new monomers. Utilization of the powerful synthetic tools available for small molecule systems can allow polymer chemists to achieve new materials with previously inaccessible functionalities due to their incompatibility with current polymerization technologies. The post-polymerization modification of polymers can occur at various sites within the material such as the end group, side chain, or backbone, however, functionalization of soft materials can be difficult to implement in many cases as the incorporation of synthetic handles remains a challenge. There have been many reports that overcome the difficulty in implementation of

post-polymerization functionalization. Leibfarth has reported C-H activation methodologies with a variety of substrates, allowing for the upcycling of polyolefin materials.[3–6] We have recently reported the Skattebøl rearrangement in polymer architectures as a method of polymer backbone editing.[7] Zhukhovitskiy has reported skeletal editing of polymers via sigmatropic rearrangements,[8,9] providing insight into how retrosynthesis can be applied to polymeric materials. Despite these advances, there is still room for expansion of the post-synthetic modification toolkit. Transformations that readily modify both the polymer backbone and side chains are underutilized, and many chemo- and stereoselective reactions have been overlooked despite the structure-property relationship held by polymeric materials.

Brown allylations remain among the powerful synthetic transformations imparted by boron-containing substrates. This methodology allows for the conversion of allylic boronate systems to homoallylic alcohols.[10–12] Brown allylations are amenable to a variety of substrates and have been utilized in many total syntheses to date, further exemplifying their broad utility.[13] Despite these reports, use of Brown allylations in polymer chemistry has been overlooked. Due to the broad functional group compatibility intrinsic to the Brown allylation, many new motifs could be easily installed into polymeric architectures. Furthermore, these reactions implement the use of aldehydes to provide alcohols in the final product. The intrinsic reactivity of aldehydes makes polymerization of these functional groups difficult, however the abundance of aldehyde reagents would allow for a library of functionalized polymers to be synthesized. In addition to their ability to add structural complexity to molecular scaffolds, Brown allylations can proceed in an asymmetric fashion with high enantioselectivity. However, application of this transformation to polymeric architectures would require a polyaldehyde or a polyallylic boronate. The former is difficult to synthesize, while the latter has yet to be reported. The recent advances that incorporate boron-containing functionalities into polymeric materials provide a benchmark for further exploration. [14–17]

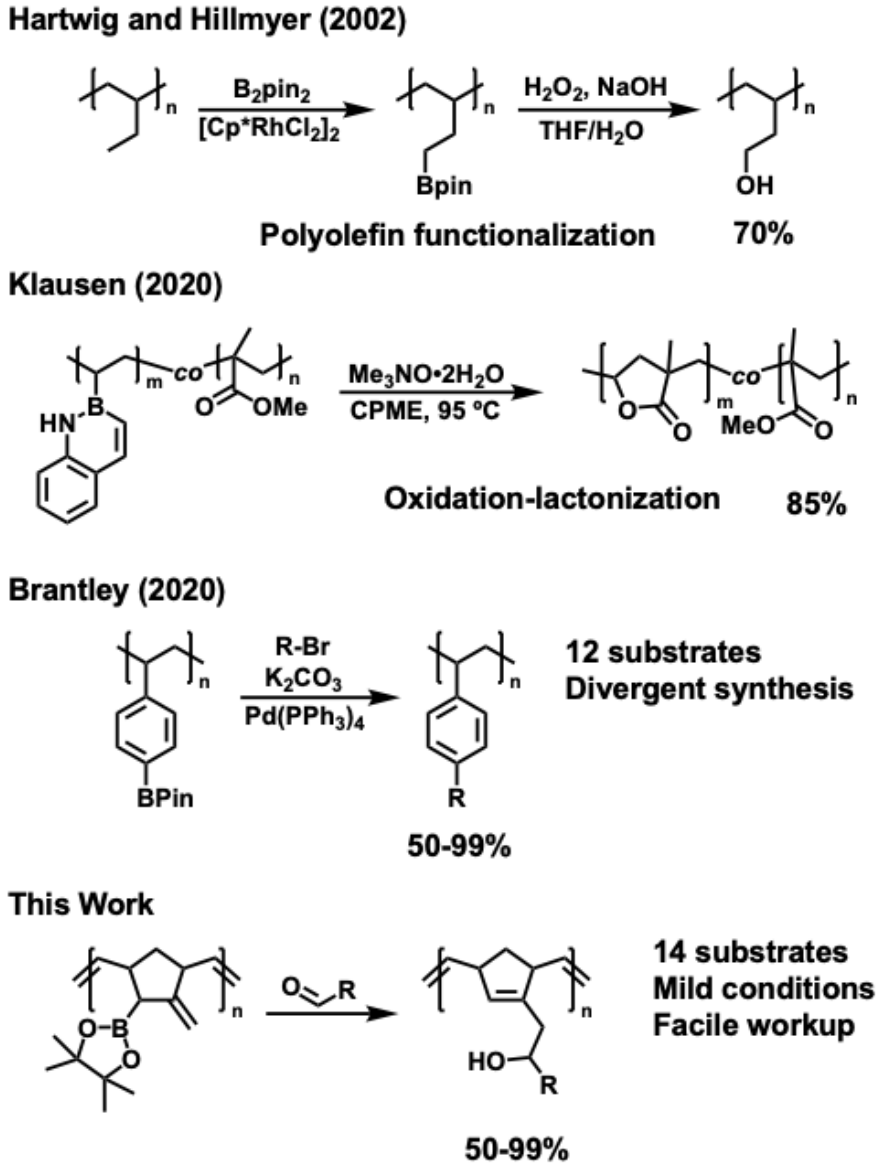
Boron-containing materials can impart various properties and applications for soft materials (e.g. sensors[17,18] or vitrimers[19,20]). However, there is significant potential for expansion of post-polymerization methodologies as well, such as multicomponent,[21,22] cross coupling,[23,24] and cyclization reactions,[25,26] among others.[27–29] Given this potential, studies have shown that application of these transformations to soft materials holds great promise for the

expansion of polymer chemical space. For example, Hartwig and Hillmyer reported the hydroboration-oxidtion of polyolefins (Scheme 4.1).[30] Klausen has reported the oxidation-lactonization of borylated polymers (Scheme 4.1).[31] Beyond these, our group has reported Suzuki-Miyaura cross coupling in styrenyl boronates has reported as a means of joining divergent synthesis with polymer chemistry (Scheme 4.1).[32] Combining these advances with the advantages imparted by Brown allylations would allow for the generation of a library of new materials. We have focused on the synthesis of a polyallylic boronate as our polymer scaffold for implementation of this transformation.

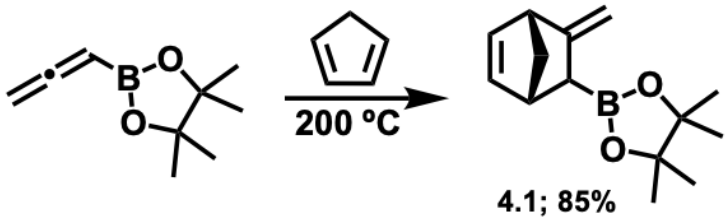
Careful design of our target scaffold was required, as radical and ionic polymerizations are difficult to achieve with allylic systems.[33–35] In contrast, ROMP catalysts are well-known to be compatible with monomers containing allylic functional groups. Thus, we envisioned chemoselective polymerization of a norbornadiene (wherein one of the olefins was part of the allylic boronate system) could be achieved, provided the boronate was sufficiently bulky. Our initial target for such a monomer was prepared through the Diels-Alder reaction between allenyl Bpin and cyclopentadiene (200 ºC for 4 h), which afforded **4.1** in excellent yield (80%; Scheme 4.2).[36] With our target monomer in hand, we then undertook a preliminary reactivity screen with established ROMP catalysts (G1, G2, G3, HG2). G3 was selected, as it provided the best control over molecular weight and dispersity (Table 4.1 and Figure 4.1). A variety of molecular weights could be achieved through polymerization of **4.1** (xx% yield, 12,000 – 75,000 Da, Đ = 2.40), and **4.P1** is soluble in common organic solvents (DCM, THF, toluene, $CHCl_3$, etc). ^1H and ^{11}B NMR spectroscopic characterization of the resultant polymer was consistent with the presence of the expected allylic boronate motifs in the repeating unit (δ = 1.18 ppm).

Having synthesized our target scaffold, we turned our attention to preliminary reactivity studies with exogenous aldehydes. We selected benzaldehyde as our model substrate due to its characteristic ^1H NMR resonances (δ = 7.86, 7.61, 7.51) and UV-Vis absorbance profile (λ_{max} = 254 nm), both of which facilitated monitoring of reaction progress. Initial studies combined **4.P1** (0.086 mmol) and benzaldehyde (0.1 mmol) in anhydrous toluene (0.08 mM) at 120 °C[37] for 3 h under N_2, but little conversion was observed via ^1H NMR spectroscopy. After the addition of molecular sieves (either powdered or spherical) to the reaction,[38,39] full

Scheme 4.1. Synthetic manipulations of boron-containing polymers



Scheme 4.2. Synthesis of **4.1**



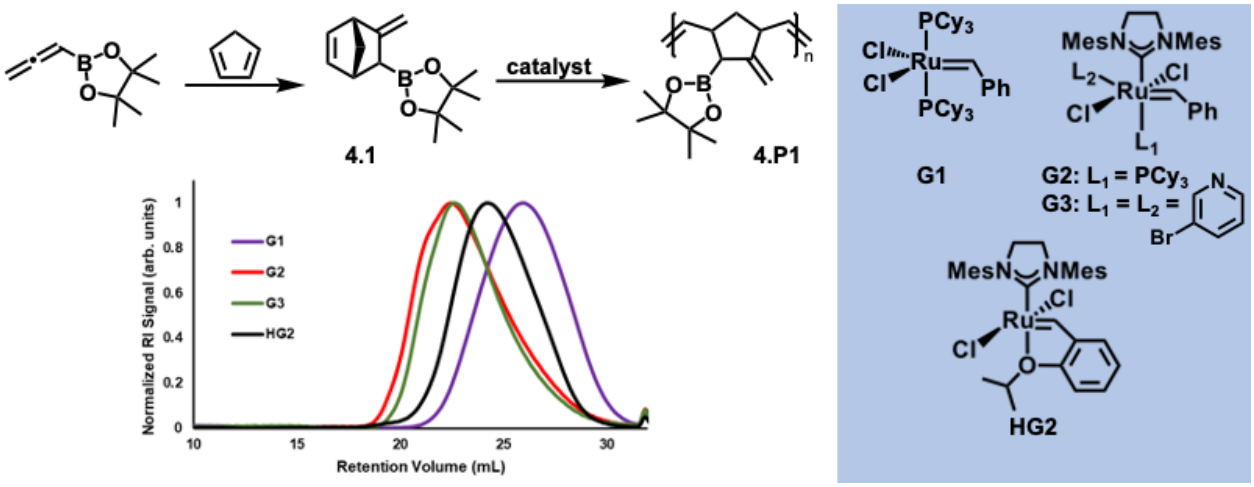


Figure 4.1. Catalyst screening for the polymerization of **4.1**

Table 4.1. SEC data for catalyst screening for the polymerization of **4.1**

Entry	Catalyst	Theoretical M_n	Measured M_n	Đ	Yield
1	G1	34,800 Da	12,500 Da	2.09	65%
2	G2	35,900 Da	47,800 Da	2.78	70%
3	G3	37,000 Da	43,000 Da	2.29	56%
4	HG2	17,600 Da	30,000 Da	2.25	44%

consumption of the exocyclic vinyl signals (δ = 4.89-4.63) was observed after 3.5 h. As both spherical and powdered sieves afforded similar conversion to the desired product, we selected spherical sieves for all subsequent studies (as they simplified our workup procedure; *vide infra*).

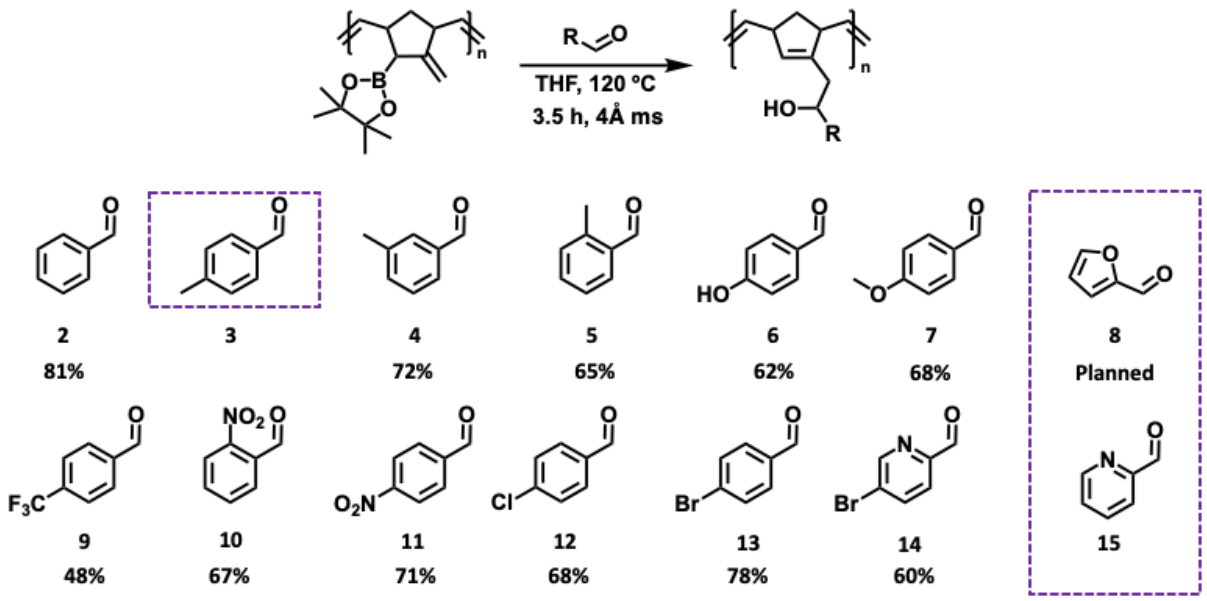
Following the reaction period, the solution was cooled to 20 °C for workup, which proved difficult. Initially, we utilized direct acidolysis via addition of 0.1 M HCl, 10% acetic acid in THF, or precipitation from acidic (0.1 M HCl) methanol caused the materials to turn brown-black and become insoluble. Subsequently, filtration of the material over silica with THF mediated the workup, however significant reduction in mass recovery was observed, and full cleavage of the boronate was not achieved. We ultimately discovered that we could successfully hydrolyze the boronate ester conducting the reaction in THF and adding this solution to excess 0.1 M HCl to afford a precipitate, which was stirred vigorously for 0.5 h prior to centrifugation. The residue was redissolved in THF and precipitated from hexanes at -78 °C. Analysis of the resultant material via ^{1}H NMR spectroscopy revealed that all pinacol was removed from the system (δ = 1.12 ppm). Additionally, analysis of ^{11}B NMR spectra indicated that any boron-containing functionalities had been removed.

After establishing optimal conditions with our model system, we sought to determine the scope of aldehyde coupling partners compatible with this system. We selected a variety of aromatic aldehydes with varying electron densities (Scheme 4.3). Overall, screening of these aldehydes revealed that conversion from the boronic ester to the homoallylic alcohols proceeded with moderate-to-high conversion (70-95%) and good mass recovery (50-82%). Electron rich aldehydes (e.g., **4.3**-**4.7**) provided higher mass recovery and conversion when compared to electron poor aldehydes (e.g., **4.9**-**4.14**). Investigation of how sterics affect the conversion was observed in substrates **4.3**-**4.5** and **4.10**-**4.11**, by changing the substitution of the aromatic ring. We observed a decrease in conversion with sterically hindered substrates. Heteroaromatic substrates furfural (**4.8**) and pyridine carbaldehydes (**4.14**-**4.15**) are planned, which could give rise to further functionalization such as Diels-Alder or sensing materials (pH-responsive).

Materials and Methods

General Considerations

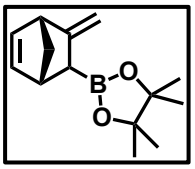
Scheme 4.3. Substrate Scope for Post-Polymerization Brown Allylation



Unless otherwise noted, solvents were dried on an MBraun solvent purification system with 3Å molecular sieves and degassed with three freeze-pump-thaw cycles. All other reagents were obtained from commercial sources and used without further purification. Oxygen and water sensitive manipulations were performed in a nitrogen (N_2) filled MBraun glovebox or using standard Schlenk techniques. All polymerizations were performed in a N_2 filled glovebox. ^1H and ^{13}C NMR data were collected on a Bruker 500 MHz, Varian 500 MHz or Varian 300 MHz NMR spectrometer. Chemical shifts (δ) are reported in ppm using the residual solvent as reference. IR spectra were collected on a Bruker Alpha II FT-IR with Platinum ATR accessory. Thermogravimetric analysis (TGA) was performed on a TA Instruments TGA Q500 and Dynamic Mechanical Analysis (DMA) data were collected on a TA Instruments DMA Q800 with a film tension clamp. Size Exclusion Chromatography (SEC) data were collected on an Omnisec Resolve and Omnisec Reveal System using triple detection or conventional calibration with detectors in series: UV, light scattering, viscometer, and refractive index and three Viscotek styrene divinylbenzene copolymer columns (in series T3000, T4000, and T5000) at a flow rate of 1 mL/min and thermostatted to 30 °C using tetrahydrofuran (THF) as the eluent. Molecular weight data are reported using either triple detection or conventional calibration relative to polystyrene standards.

Synthetic Considerations

Synthesis of **4.1**



4.1 was synthesized according to a modified procedure by Pelegrinet et al.[36] Allenyl boronic acid pinacol ester (1 g, 6 mmol) was added to a pressure flask with Teflon stir bar, toluene (20 mL), BHT (66.3 mg, 0.3 mmol), and cyclopentadiene (2.5 mL, 30 mmol). The reaction was heated to 180 °C for 4 h. The solution was concentrated under vacuum, followed by vacuum distillation at 130 °C to produce the pure material as a colorless liquid consisting of a mixture of diastereomers (50:50 endo:exo) in 80% yield. Characterization data were in agreement with previous reports (Figure 4.8).

Polymerization Optimization and Considerations

Polymerization of **4.1** was initially attempted with Ru catalysts (G1, G2, G3, HG2). The results of the catalyst screen are shown in Table 4.1. G3 was selected to carry out further

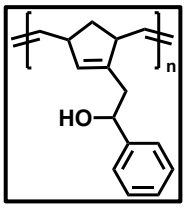
polymerization studies. The exocyclic boronic ester was polymerized via ROMP with Grubbs 3rd generation catalyst. **4.1** (160 mg, 0.69 mmol) was added to a vial with DCM (6.5 mL) and degassed via 3 FPT cycles. Grubbs 3rd generation catalyst (5.4 mg, 0.0067 mmol) was added and the reaction was allowed to stir at room temperature for 1 h. The polymerization was quenched with ethyl vinyl ether and precipitated from MeOH twice. The polymeric material was isolated in 49% yield. ^{1}H NMR spectra are provided in Figure 4.9.

Brown allylation Methodology and Substrate Scope

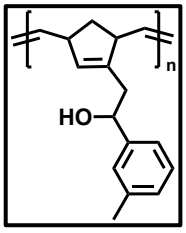
General Procedure for Post Polymerization Brown allylation

4.P1 was added to a septa capped vial with 4 Å molecular sieves, and Teflon stir bar. Solid aldehydes were added at this time. The atmosphere was evacuated and replaced with N_2. THF was added to the vial. Liquid aldehydes were added after the solvent. The reactions were heated at 120 °C for 3 h. After cooling to 20 °C, the reaction mixture was concentrated to minimal volume and precipitated from 0.1 M HCl. The residue was redissolved in THF and precipitated from hexanes at -78 ºC. The solid polymer was isolated and dried in vacuo for 1 h for spectral characterization and then dissolved in THF for storage.

Substrate Scope and Characterization



4.P2: Using the protocol above, benzaldehyde was employed as the aldehyde. SEC data is provided in Figure 4.2 (14,800 Da; Đ = 4.60). ^{1}H and ^{13}C NMR spectra are provided in Figure 4.10 and Figure 4.11, respectively.



4.P4: Using the protocol above, *m*-tolualdehyde was employed as the aldehyde. ^{1}H spectra are provided in Figure 4.12.

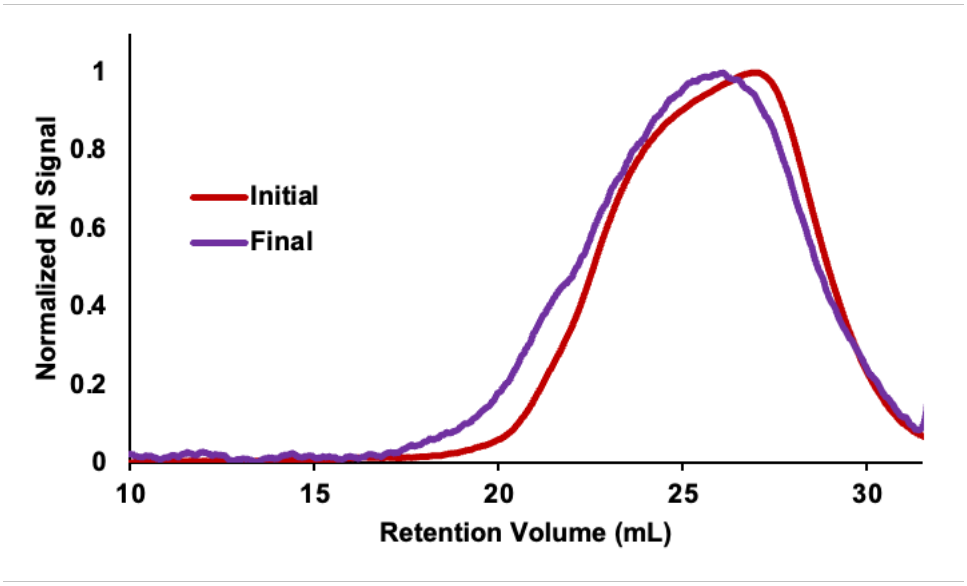
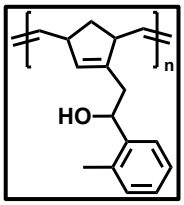
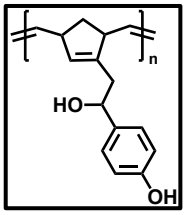


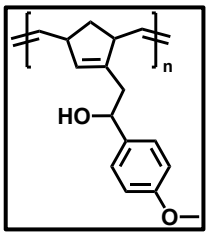
Figure 4.2. SEC data for Brown allylation with benzaldehyde. Red indicates **4.P1**, and purple indicates **4.P2.**



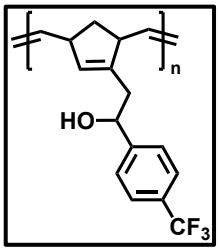
4.P5: Using the protocol above, *o*-tolualdehyde was employed as the aldehyde. Although this experiment was conducted, the final product was insoluble in common organic solvents, and therefore SEC and NMR data were not collected.



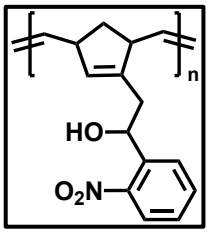
4.P6: Using the protocol above, *p*-hydroxybenzaldehyde was employed as the aldehyde. Although this experiment was conducted, the final product was insoluble in common organic solvents, and therefore SEC and NMR data were not collected.



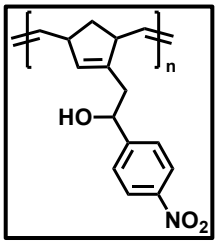
4.P7: Using the protocol above, *p*-anisaldehyde was employed as the aldehyde. SEC data is provided in Figure 4.3. ^{1}H NMR spectra are provided in Figure 4.13.



4.P9: Using the protocol above, *p*-trifluoromethylbenzaldehyde was employed as the aldehyde. SEC data is provided in Figure 4.4. ^{1}H and ^{13}C NMR spectra are provided in Figure 4.14 and Figure 4.15, respectively.



4.P10: Using the protocol above, *o*-nitrobenzaldehyde was employed as the aldehyde. SEC data is provided in Figure 4.5. ^{1}H and ^{13}C NMR spectra are provided in Figure 4.16 and Figure 4.17, respectively.



4.P11: Using the protocol above, *p*-nitrobenzaldehyde was employed as the aldehyde. SEC data is provided in Figure 4.6.

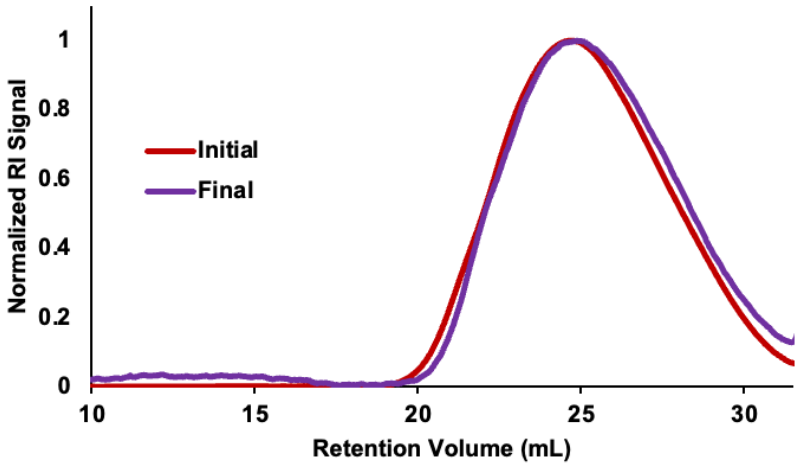


Figure 4.3. SEC data for Brown allylation with anisaldehyde. Red indicates **4.P1**, and purple indicates **4.P8**.

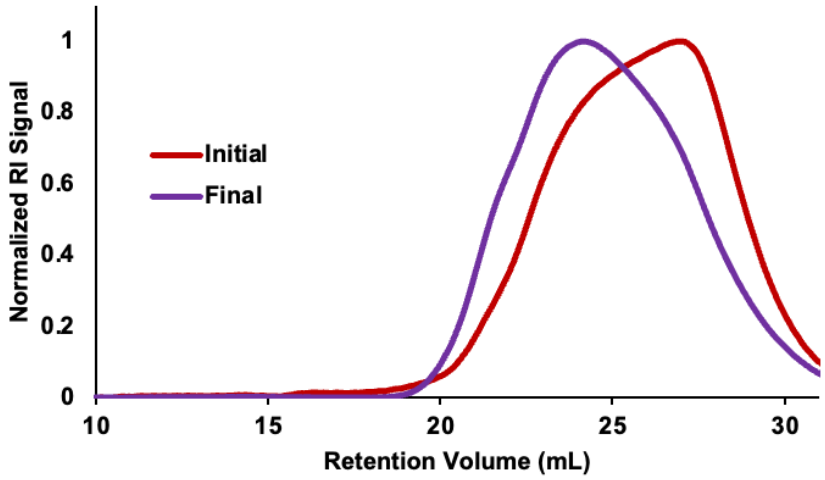


Figure 4.4. SEC data for brown allylation with p-trifluoromethylbenzaldehyde. Red indicates **4.P1** and purple indicates **4.P9.**

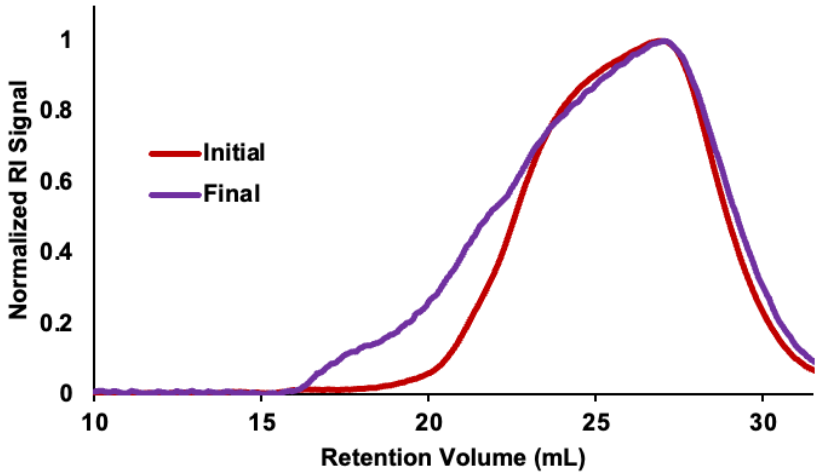


Figure 4.5. SEC data for Brown allylation with o-nitrobenzaldehyde. Red indicates **4.P1,** and purple indicates **4.P10.**

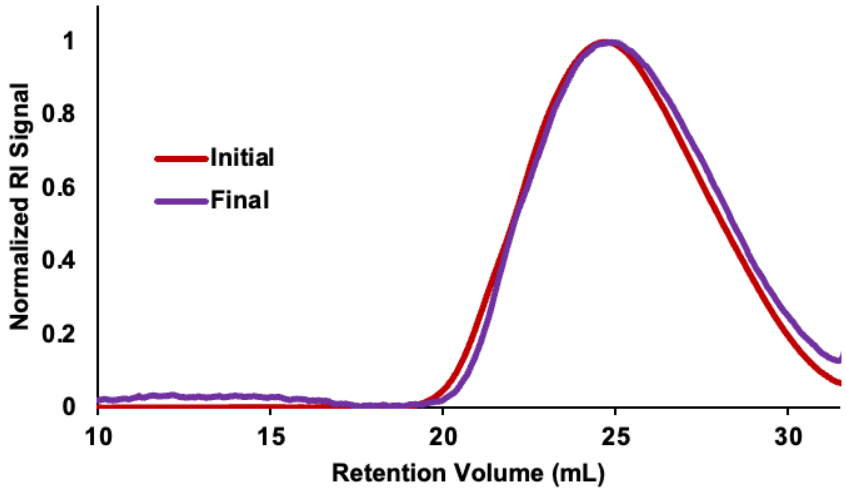
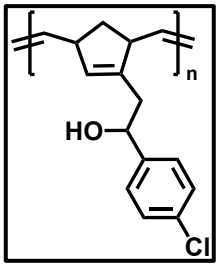
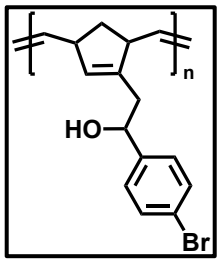


Figure 4.6. SEC data for Brown allylation with p-nitrobenzaldehyde. Red indicates **4.P1**, and purple indicates **4.P11**



4.P12: Using the protocol above, *p*-chlorobenzaldehyde was employed as the aldehyde. Although this experiment was conducted, the final product was insoluble in common organic solvents, and therefore SEC and NMR data were not collected.



4.P13: Using the protocol above, *p*-bromobenzaldehyde was employed as the aldehyde. SEC data is provided in Figure 4.7. ^{1}H and ^{13}C NMR spectra are provided in Figure 4.18 and Figure 4.19, respectively.

Summary

Development of post-polymerization technologies that allow for the modification of soft materials requires robust reactions compatible with a variety of substrates. Harnessing these reactions to selectively edit polymer scaffolds to generate chemo- and stero- diversity could allow for the development of new materials. We have found that allylic boronates can be readily incorporated into polymers, and these motifs undergo brown allylations with a wide range of (hetero)aromatic aldehydes. We anticipate that our work will inspire the design of other intrinsically tunable materials.

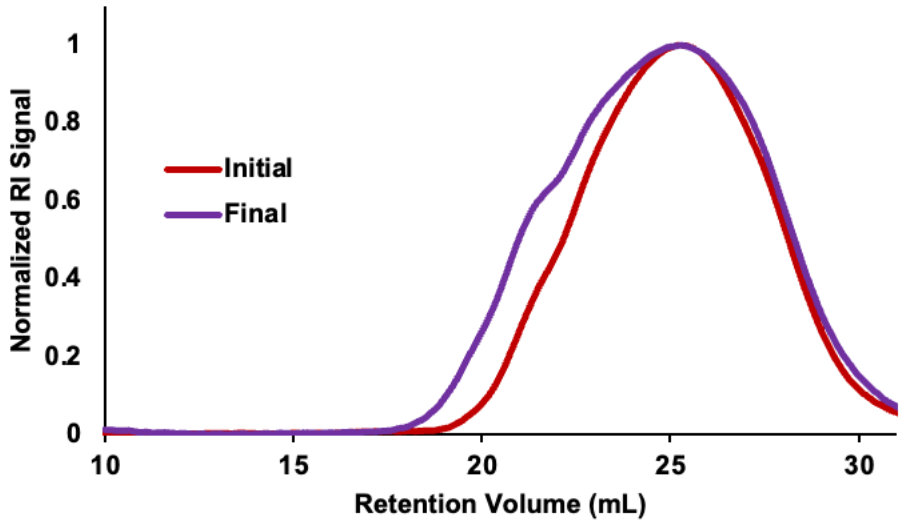


Figure 4.7. SEC data for Brown allylation with p-bromobenzaldehyde. Red indicates **4.P1**, and purple indicates **4.P13**

Appendix

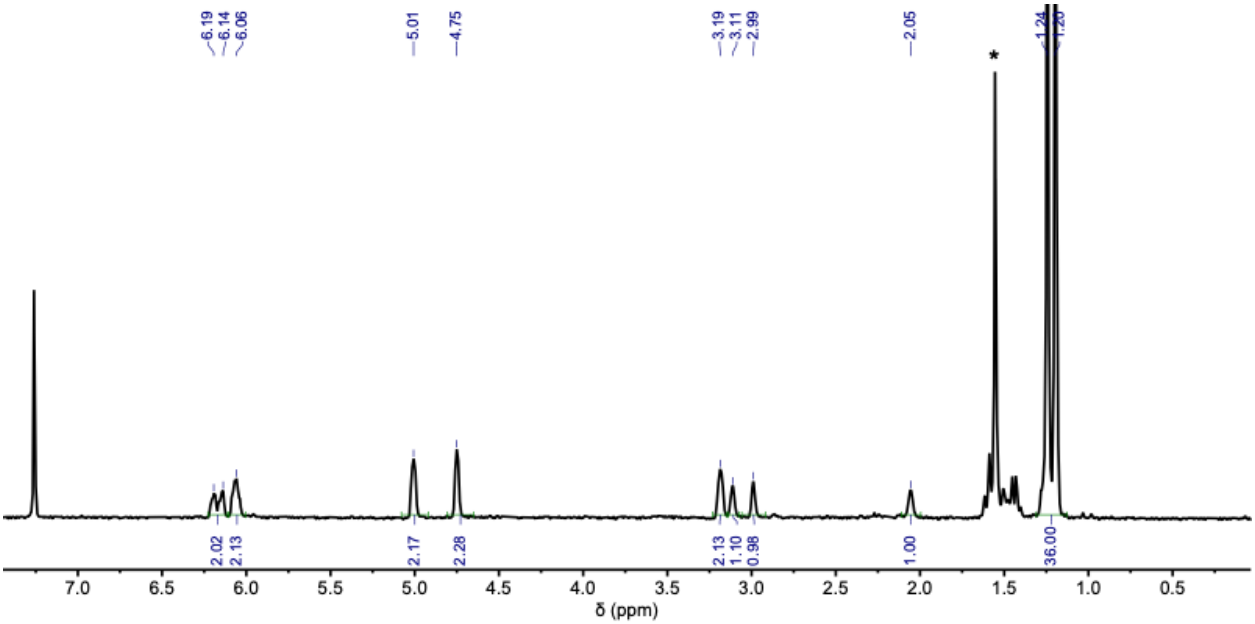


Figure 4.8. ^{1}H NMR spectrum for **4.1.** * denotes water

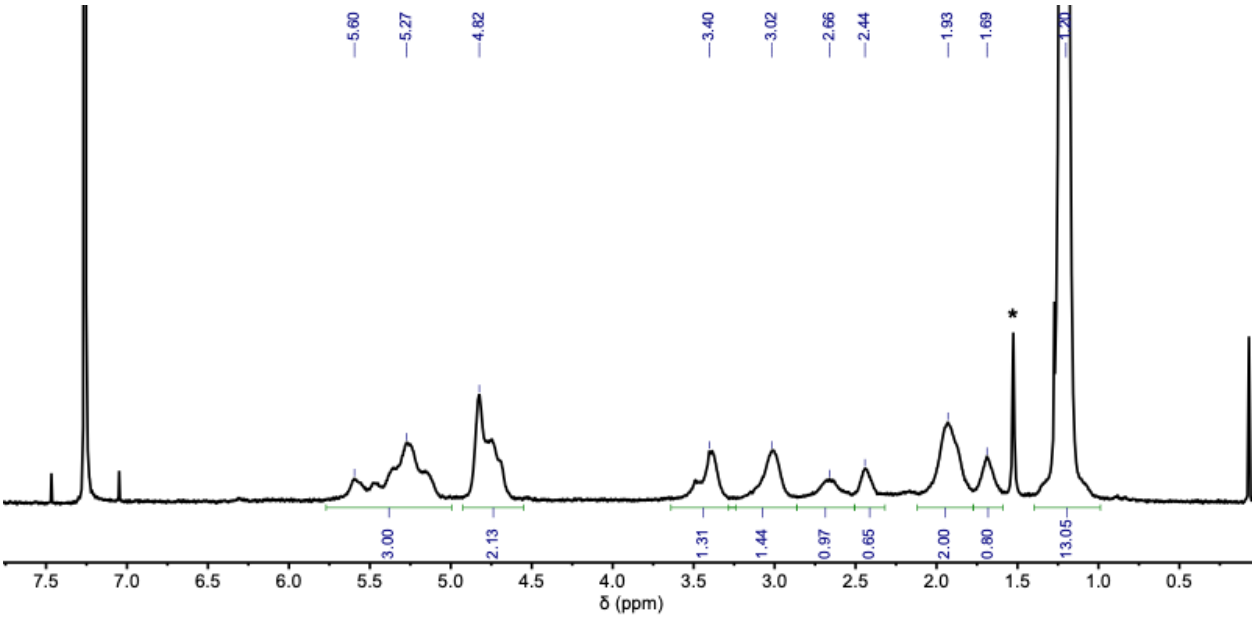


Figure 4.9. ^{1}H NMR spectrum for **4.P1** in $CDCl_3$

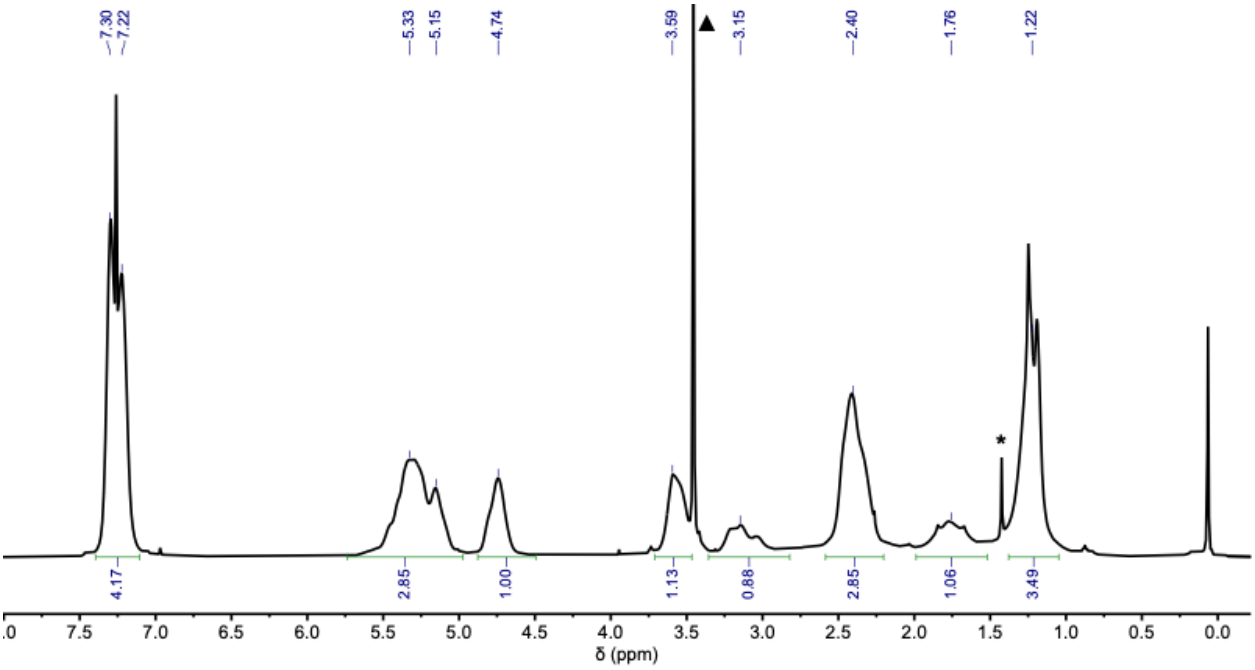


Figure 4.10. ^{1}H NMR spectrum for **4.P2** in $CDCl_3$. ▲ denotes methanol. * denotes water.

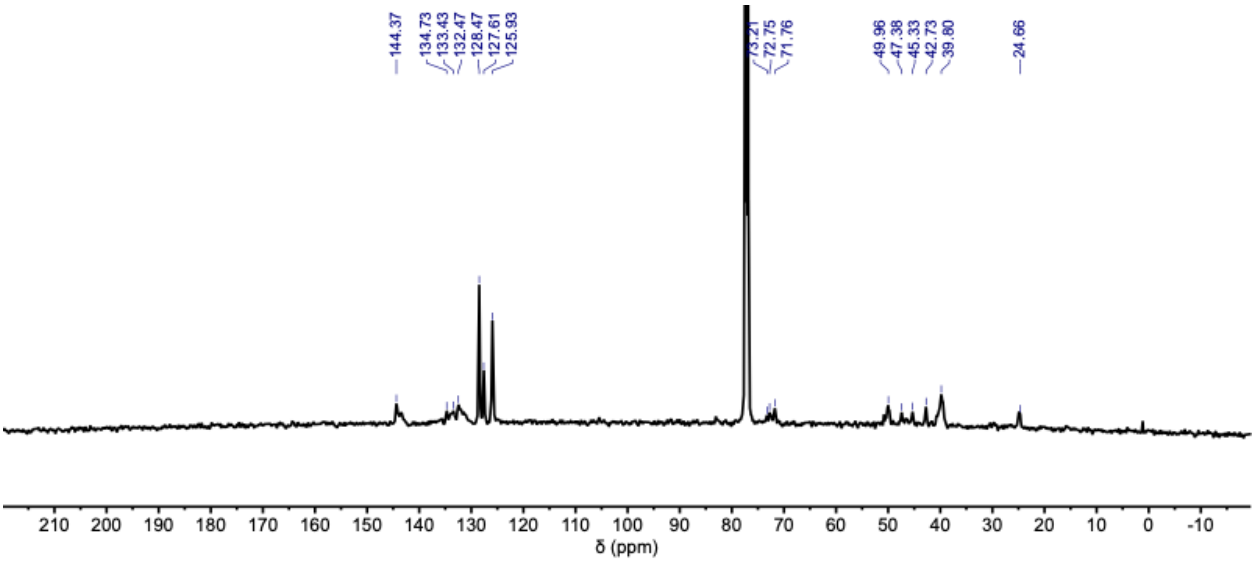


Figure 4.11. ^{13}C NMR spectrum for **4.P2** in $CDCl_3$.

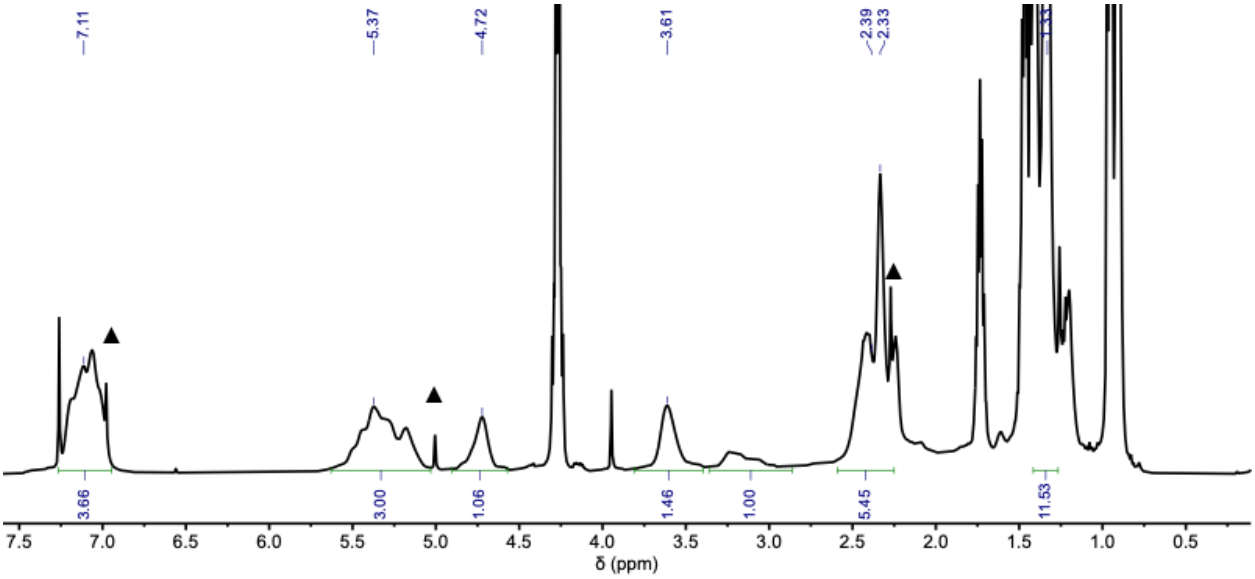


Figure 4.12. ^{1}H NMR spectrum for **4.P4** in $CDCl_3$. ▲ denotes BHT.

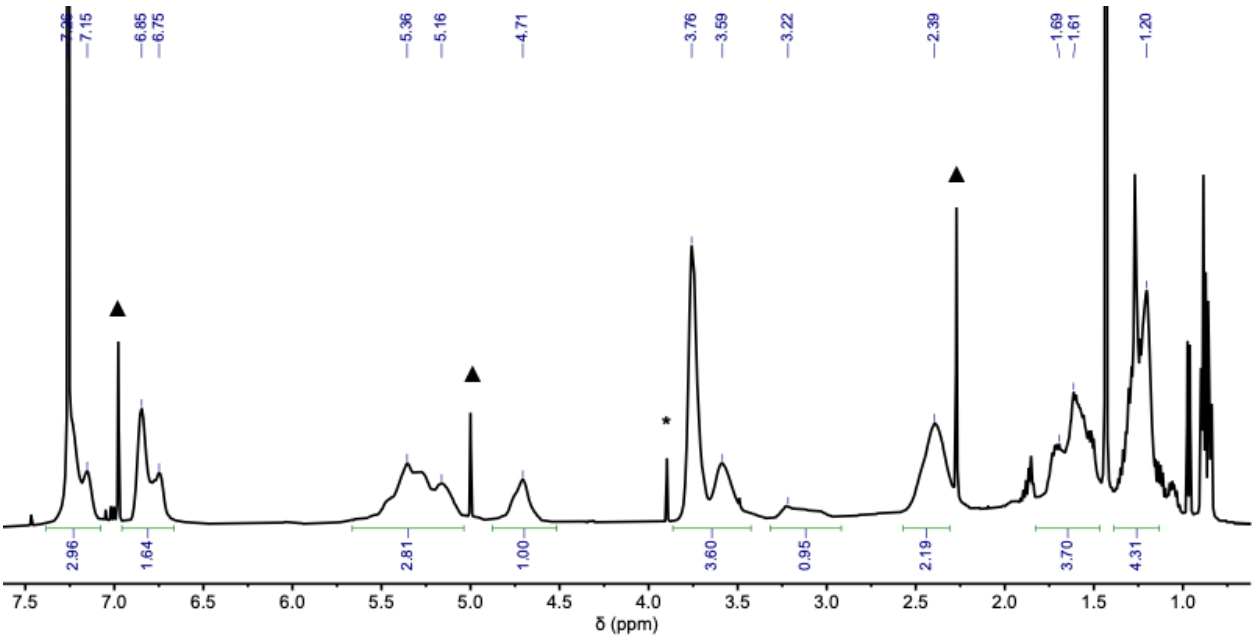


Figure 4.13. ^{1}H NMR spectrum for **4.P7** in $CDCl_3$. ▲ denotes BHT. * denotes methanol.

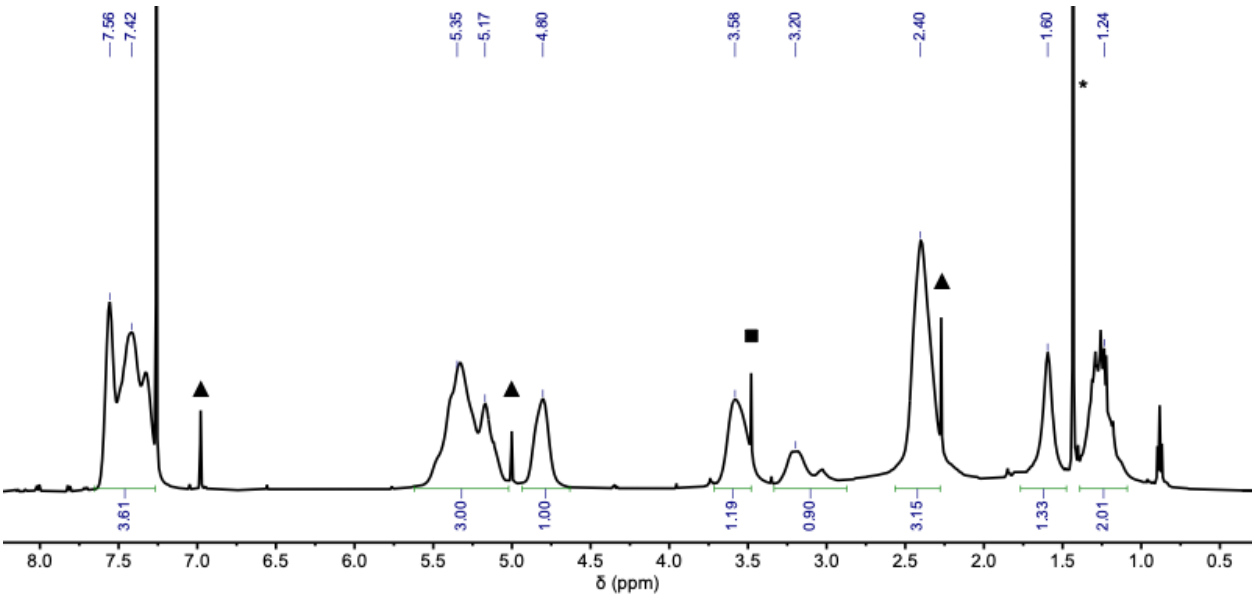


Figure 4.14. ^{1}H NMR spectrum for **4.P9** in $CDCl_3$. ▲ denotes BHT. ■ denotes methanol. * denotes water.

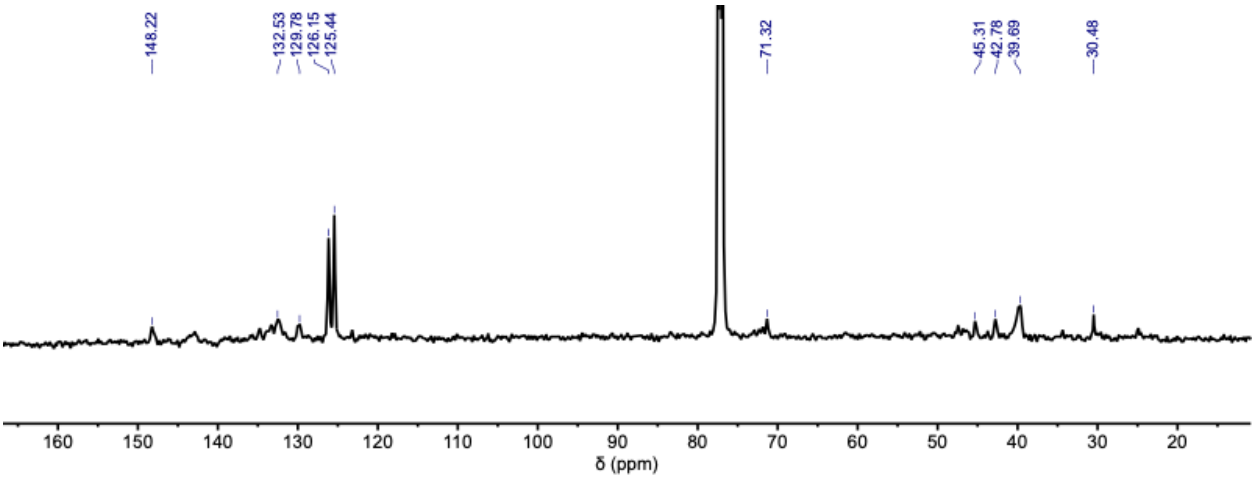


Figure 4.15. ^{13}C NMR spectrum for **4.P9** in $CDCl_3$.

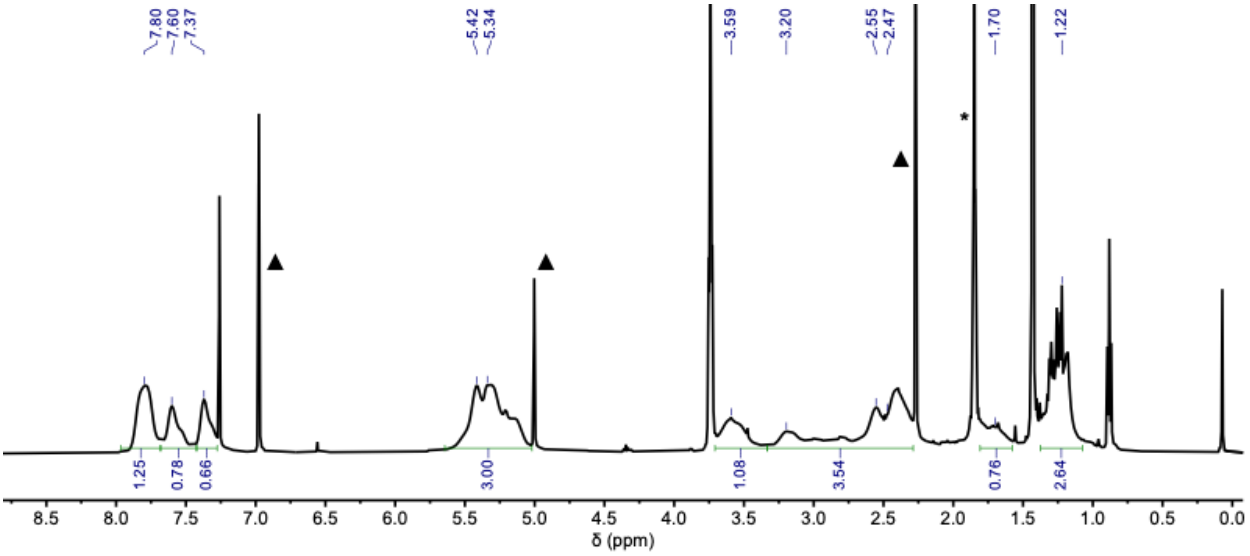


Figure 4.16. ^{1}H NMR spectrum for **4.P10** in $CDCl_3$. ▲ denotes BHT. * denotes water.

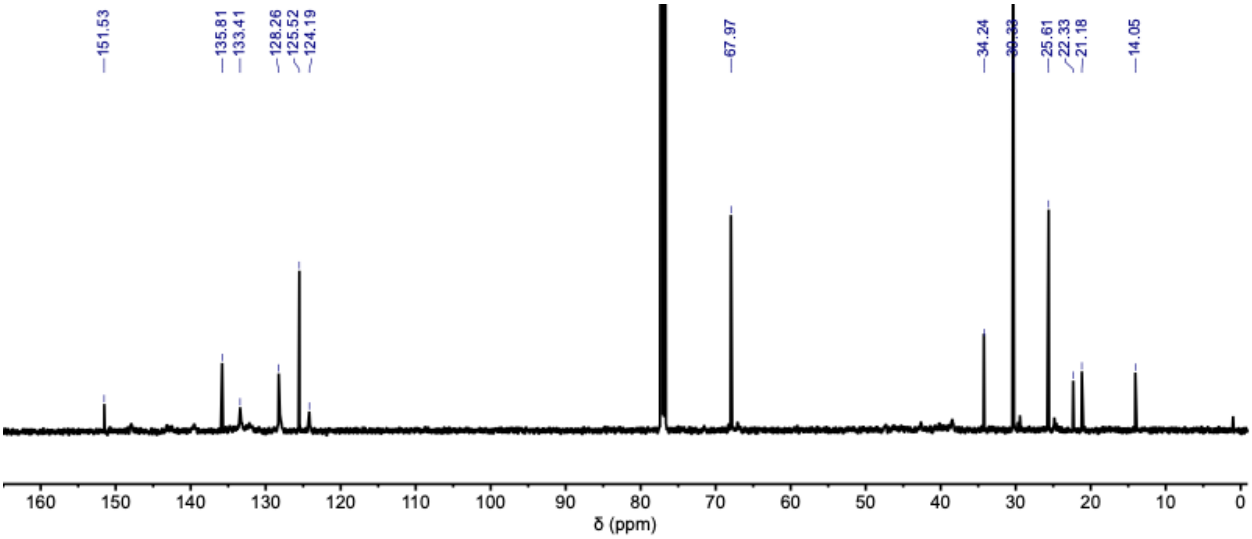


Figure 4.17. ^{13}C NMR spectrum for **4.P10** in $CDCl_3$.

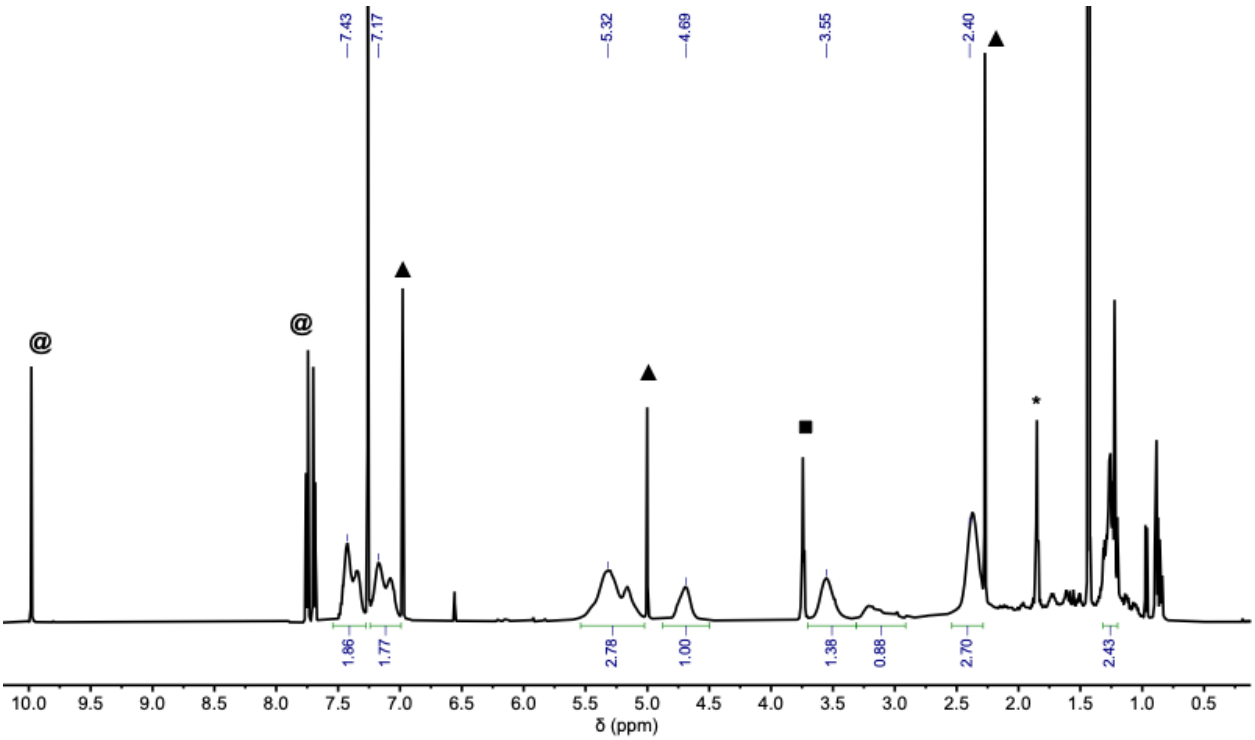


Figure 4.18. ^{1}H NMR spectrum for **4.P13** in $CDCl_3$. @ denotes residual xxxx. ▲ denotes BHT. ■ denotes methanol. * denotes water.

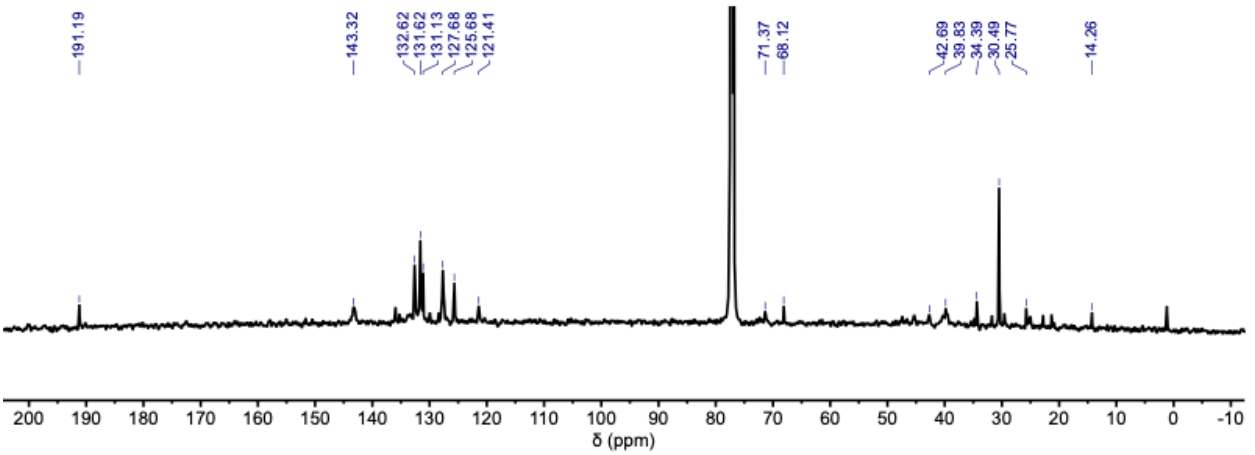


Figure 4.19. ^{13}C NMR spectrum for **4.P13** in $CDCl_3$.

References

(1) Günay, K. A.; Theato, P.; Klok, H.-A. Standing on the Shoulders of Hermann Staudinger: Post-Polymerization Modification from Past to Present. *Journal of Polymer Science Part A: Polymer Chemistry* **2013**, *51* (1), 1–28. https://doi.org/10.1002/pola.26333.

(2) Boaen, N. K.; Hillmyer, M. A. Post-Polymerization Functionalization of Polyolefins. *Chemical Society Reviews* **2005**, *34* (3), 267–275. https://doi.org/10.1039/B311405H.

(3) Lewis, S. E.; Wilhelmy, B. E.; Leibfarth, F. A. Upcycling Aromatic Polymers through C–H Fluoroalkylation. *Chemical Science* **2019**, *10* (25), 6270–6277. https://doi.org/10.1039/C9SC01425J.

(4) Williamson, J. B.; Czaplyski, W. L.; Alexanian, E. J.; Leibfarth, F. A. Regioselective C–H Xanthylation as a Platform for Polyolefin Functionalization. *Angewandte Chemie International Edition* **2018**, *57* (21), 6261–6265. https://doi.org/10.1002/ANIE.201803020.

(5) Williamson, J. B.; Lewis, S. E.; Johnson, R. R.; Manning, I. M.; Leibfarth, F. A. C–H Functionalization of Commodity Polymers. *Angewandte Chemie International Edition* **2019**, *58* (26), 8654–8668. https://doi.org/10.1002/ANIE.201810970.

(6) Fazekas, T. J.; Alty, J. W.; Neidhart, E. K.; Miller, A. S.; Leibfarth, F. A.; Alexanian, E. J. Diversification of Aliphatic C-H Bonds in Small Molecules and Polyolefins through Radical Chain Transfer. *Science (1979)* **2022**, *375* (6580), 545–550. https://doi.org/10.1126/SCIENCE.ABH4308/SUPPL_FILE/SCIENCE.ABH4308_SM.PDF.

(7) Galan, N. J.; Brantley, J. N. General Access to Allene-Containing Polymers Using the Skattebøl Rearrangement. *ACS Macro Letters* **2020**, *13*, 1662–1666. https://doi.org/10.1021/ACSMACROLETT.0C00745/SUPPL_FILE/MZ0C00745_SI_001.PDF.

(8) Ratushnyy, M.; Zhukhovitskiy, A. v. Polymer Skeletal Editing via Anionic Brook Rearrangements. *J Am Chem Soc* **2021**, *143* (43), 17931–17936.

https://doi.org/10.1021/JACS.1C06860/ASSET/IMAGES/LARGE/JA1C06860_0005.JPEG.

(9) Ditzler, R. A. J.; Zhukhovitskiy, A. v. Sigmatropic Rearrangements of Polymer Backbones: Vinyl Polymers from Polyesters in One Step. *J Am Chem Soc* **2021**, *143* (48), 20326–20331. https://doi.org/10.1021/JACS.1C09657/ASSET/IMAGES/LARGE/JA1C09657_0004.JPEG.

(10) Brown, H. C.; Racherla, U. S. Chiral Synthesis via Organoboranes. 27. Remarkably Rapid and Exceptionally Enantioselective (Approaching 100% Ee) Allylboration of Representative Aldehyde at -100 °C under New Salt-Free Conditions. *Journal of Organic Chemistry* **1991**, *56*, 401–404.

(11) Brown, H. C.; Bhat, K. S. Chiral Synthesis via Organoboranes. 7. Diastereoselective Enantioselective Synthesis of Erythro- and Threo-B-Methylhomoallyl Alcohols via Enantiomeric (Z)- and (E)-Crotylboranes. *J Am Chem Soc* **1986**, *108* (19), 5919–5923.

(12) Brown, H. C.; Jadhav, P. K. Asymmetric Carbon-Carbon Bond Formation via B-Allyldiisopinocampheylborane. Simple Synthesis of Secondary Homoallylic Alcohols with Excellent Enantiomeric Purities. *J Am Chem Soc* **1983**, *105*, 2092–2093.

(13) Boiarska, Z.; Braga, T.; Silvani, A.; Passarella, D. Brown Allylation: Application to the Synthesis of Natural Products. *European Journal of Organic Chemistry* **2021**, *2021* (22), 3214–3222. https://doi.org/10.1002/EJOC.202100258.

(14) Chauhan, N. P. S.; Hosmane, N. S.; Mozafari, M. Boron-Based Polymers: Opportunities and Challenges. *Materials Today Chemistry* **2019**, *14*, 100184. https://doi.org/10.1016/J.MTCHEM.2019.08.003.

(15) Cheng, F.; Jäkle, F. Boron-Containing Polymers as Versatile Building Blocks for Functional Nanostructured Materials. *Polymer Chemistry* **2011**, *2* (10), 2122–2132. https://doi.org/10.1039/C1PY00123J.

(16) Cambre, J. N.; Sumerlin, B. S. Biomedical Applications of Boronic Acid Polymers. *Polymer (Guildf)* **2011**, *52* (21), 4631–4643. https://doi.org/10.1016/J.POLYMER.2011.07.057.

(17) Mellerup, S. K.; Wang, S.; Zhou, W.-X.; Soren, S.; Mellerup, K.; Mellerup Ab, S. K. Boron-Based Stimuli Responsive Materials. *Chemical Society Reviews* **2019**, *48* (13), 3537–3549. https://doi.org/10.1039/C9CS00153K.

(18) Roy, D.; Cambre, J. N.; Sumerlin, B. S. Triply-Responsive Boronic Acid Block Copolymers: Solution Self-Assembly Induced by Changes in Temperature, PH, or Sugar Concentration. *Chemical Communications* **2009**, *0* (16), 2106. https://doi.org/10.1039/b900374f.

(19) Zhang, X.; Wang, S.; Jiang, Z.; Li, Y.; Jing, X. Boronic Ester Based Vitrimers with Enhanced Stability via Internal Boron−Nitrogen Coordination. *J Am Chem Soc* **2020**, *142*, 21852–21860. https://doi.org/10.1021/jacs.0c10244.

(20) Zhang, X.; Zhao, Y.; Wang, S.; Jing, X. Cross-Linked Polymers Based on B–O Bonds: Synthesis, Structure and Properties. *Materials Chemistry Frontiers* **2021**, *5* (15), 5534–5548. https://doi.org/10.1039/D1QM00514F.

(21) Wu, P.; Givskov, M.; Nielsen, T. E. Reactivity and Synthetic Applications of Multicomponent Petasis Reactions. *Chemical Reviews* **2019**, *119* (20), 11245–11290. https://doi.org/10.1021/ACS.CHEMREV.9B00214/ASSET/IMAGES/MEDIUM/CR9B00214_0046.GIF.

(22) Armstrong, R. J.; Aggarwal, V. K. 50 Years of Zweifel Olefination: A Transition-Metal-Free Coupling. *Synthesis (Stuttg)* **2017**, *49* (15), 3323–3336. https://doi.org/10.1055/S-0036-1589046.

(23) Singh Gujral, S.; Khatri, S.; Riyal, P. Suzuki Cross Coupling Reaction- A Review. *Indo Global Journal of Pharmaceutical Sciences* **2012**, *2* (4), 351–367.

(24) Lennox, A. J. J.; Lloyd-Jones, G. C. Selection of Boron Reagents for Suzuki–Miyaura Coupling. *Chemical Society Reviews* **2013**, *43* (1), 412–443. https://doi.org/10.1039/C3CS60197H.

(25) Ren, S. C.; Zhang, F. L.; Qi, J.; Huang, Y. S.; Xu, A. Q.; Yan, H. Y.; Wang, Y. F. Radical Borylation/Cyclization Cascade of 1,6-Enynes for the Synthesis of Boron-Handled Hetero- and Carbocycles. *J Am Chem Soc* **2017**, *139* (17), 6050–6053. https://doi.org/10.1021/JACS.7B01889/SUPPL_FILE/JA7B01889_SI_003.ZIP.

(26) Issaian, A.; Tu, K. N.; Blum, S. A. Boron-Heteroatom Addition Reactions via Borylative Heterocyclization: Oxyboration, Aminoboration, and Thioboration. *Accounts of Chemical Research* **2017**, *50* (10), 2598–2609. https://doi.org/10.1021/ACS.ACCOUNTS.7B00365/ASSET/IMAGES/LARGE/AR-2017-00365X_0025.JPEG.

(27) Zweifel, G.; Brown, H. C. Hydration of Olefins, Dienes, and Acetylenes via Hydroboration. *Organic Reactions* **2011**, 1–54. https://doi.org/10.1002/0471264180.OR013.01.

(28) Burkhardt, E. R.; Matos, K. Boron Reagents in Process Chemistry: Excellent Tools for Selective Reductions. *Chemical Reviews* **2006**, *106* (7), 2617–2650. https://doi.org/10.1021/CR0406918/ASSET/IMAGES/LARGE/CR0406918H00044.JPEG.

(29) Yeung, K.; Mykura, R. C.; Aggarwal, V. K. Lithiation–Borylation Methodology in the Total Synthesis of Natural Products. *Nature Synthesis* **2022**, *1* (2), 117–126. https://doi.org/10.1038/s44160-021-00012-1.

(30) Kondo, Y.; García-Cuadrado, D.; Hartwig, J. F.; Boaen, N. K.; Wagner, N. L.; Hillmyer, M. A. Rhodium-Catalyzed, Regiospecific Functionalization of Polyolefins in the Melt. *J Am Chem Soc* **2002**, *124* (7), 1164–1165. https://doi.org/10.1021/JA016763J/SUPPL_FILE/JA016763J_S1.PDF.

(31) Ji, Y.; Zhou, T.; van de Wouw, H. L.; Klausen, R. S. Organoborane Strategy for Polymers Bearing Lactone, Ester, and Alcohol Functionality. *Macromolecules* **2020**, *53*, 249–255. https://doi.org/10.1021/acs.macromol.9b02201.

(32) Jacobs, B. P.; Brantley, J. N. Exploring Combinatorial Approaches to Polymer Diversification. *Macromolecules* **2020**, *53* (21), 9287–9293. https://doi.org/10.1021/ACS.MACROMOL.0C01538/ASSET/IMAGES/LARGE/MA0C01538_0004.JPEG.

(33) Zubov, V. P.; Kumar, M. V.; Asterova, M. N. M.; Kabanov, V. A. Reactivity of Allyl Monomers in Radical Polymerization. *Journal of Macromolecular Science: Part A - Chemistry* **1979**, *13* (1), 111. https://doi.org/10.1080/00222337908058160.

(34) Maurice Morton. *Anionic Polymerization: Principles and Practice*, 1st ed.; Academic Press Inc.: New York, New York, 1983.

(35) Bywater, S. Structure and Mechanism in Anionic Polymerization. *Progress in Polymer Science* **1994**, *19* (2), 287–316. https://doi.org/10.1016/0079-6700(94)90008-6.

(36) Labadie, N.; Ramos Marchena, J. M.; Medrán, N. S.; Pellegrinet, S. C. Allenylboronic Acid Pinacol Ester: A Selective Partner for [4 + 2] Cycloadditions. *Organic Letters* **2021**, *23* (13), 5081–5085. https://doi.org/10.1021/ACS.ORGLETT.1C01609/SUPPL_FILE/OL1C01609_SI_001.PDF.

(37) Additionally, the polymers possess a T_d of 300 °C.

(38) Keck, G. E.; Tarbet, K. H.; Geraci, L. S. Catalytic Asymmetric Allylation of Aldehydes. *J Am Chem Soc* **1993**, *115* (2), 8467–8468.

(39) Luisa Costa, A.; Piazza, M. G.; Tagliavini, E.; Trombini, C.; Umani-Ronchi, A. Catalytic Asymmetric Synthesis of Homoallylic Alcohols. *J. Am. Chem. Soc* **1993**, *115*, 7001–7002.

CHAPTER 5: ELECTROEDITING OF SOFT POLYMER BACKBONES

A version of this chapter was originally published by Alan D. Fried, Breana J. Wilson, Nicholas J. Galan, and Johnathan N. Brantley: Fried, A. D.; Wilson, B. J.; Galan, N. G.; Brantley, J. N. Electroediting of Soft Polymer Backbones. J. Am. Chem. Soc. 2022, 144, 8885-8891. DOI: 10.1021/jacs.2c02098

Minor text revisions and figure placement changes have been made. All experimentation and data collection was completed by Alan D. Fried, Breana J. Wilson, and Nicholas J. Galan as well as writing of the document in conjunction with Dr. Johnathan N. Brantley, the PI for this work.

This work was completed in memory of Dr. Alan D. Fried, who passed away on March 4th, 2022.

Abstract

Synthetic methods that edit soft polymer back-bones are critical technologies for tailoring the structures and properties of macromolecules. Developing strategies that leverage underexplored reaction manifolds are vital for accessing new chemical (and functional) space in soft materials. Here, we report a mild electrochemical approach that enables both degradation and functionalization of synthetic polymers. We found that bulk electrolysis (under either homogeneous or heterogenous conditions) promoted facile, chemoselective chain scission in a variety of olefin-containing materials. Polymer degradation could also be coupled with functionalization (e.g., azidation) to afford new species that could serve as macromonomers.

Introduction

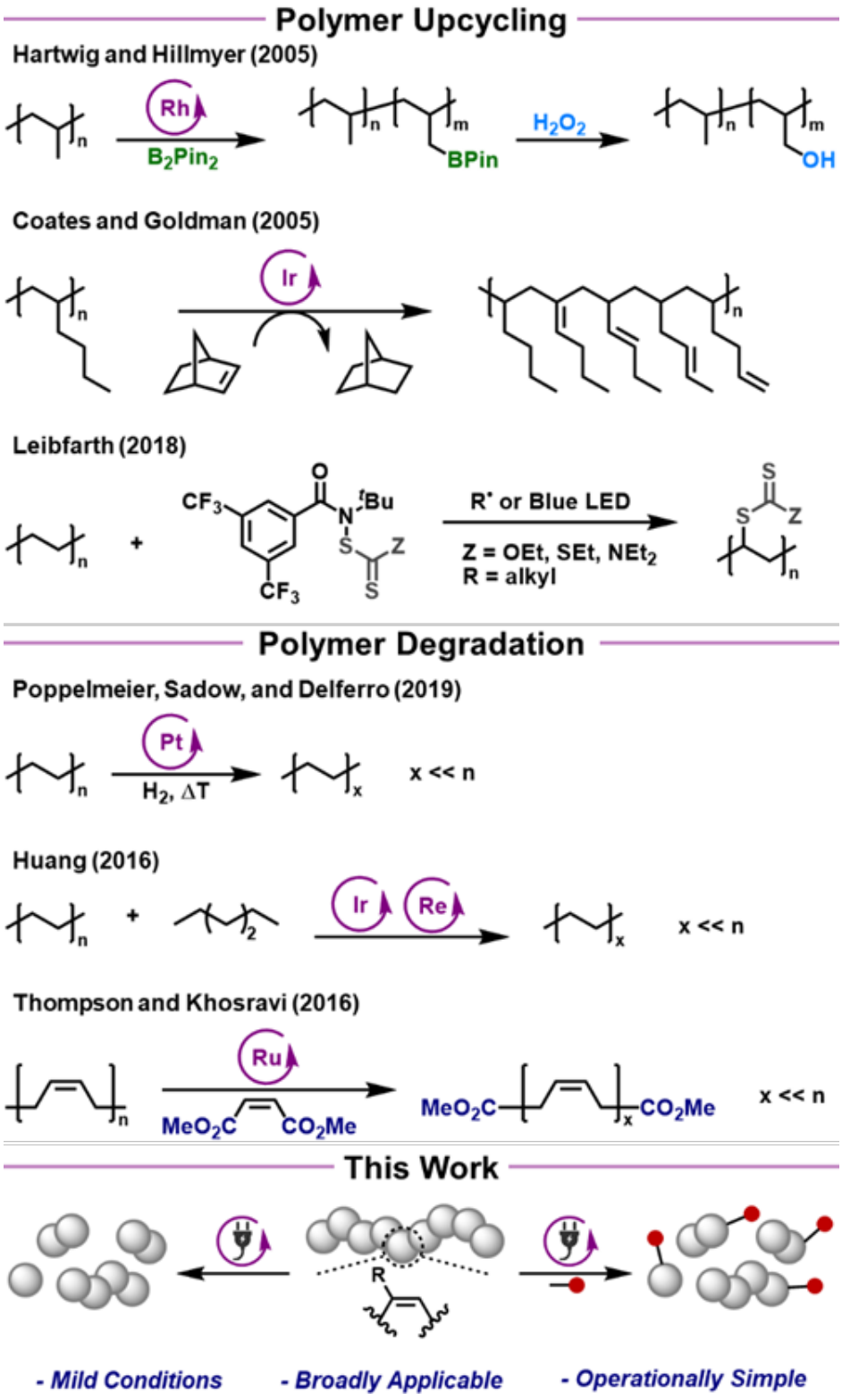
Synthetic macromolecules have revolutionized nearly every aspect of human society since their discovery by Staudinger.[1–3] The inextricable link between polymer structure and bulk material properties has long served as the impetus for exploring new chemical space for monomer design. However, there is growing interest in developing synthetic tools that directly edit the structures of polymeric substrates (thereby circumventing the need to design esoteric monomers to achieve functionality). In practice, however, many such transformations can be

difficult to implement on macromolecules. As such, there is a critical need to expand the repertoire of reaction manifolds that facilitate editing of soft polymers.

Notwithstanding this synthetic challenge, there have been significant achievements toward the direct chemical tailoring of polymer scaffolds (both via functionalization and chain scission; Despite this somewhat limited scope of exploration, electrochemistry could unlock new chemical space in soft polymer backbone editing. For example, anodic oxidation of electron rich olefins is known to generate radical cations that can participate in a variety of transformations (e.g., nucleophile trapping,[21,37,38] cyclizations,[21,38–40] Scheme 5.1). In a seminal report, Hartwig and Hillmyer disclosed the rhodium catalyzed borylation of branched polyolefins.[4,5] Similarly pioneering work from Coates and Goldman demonstrated that iridium pincer complexes could embed reactive alkenes throughout branched polyolefins via catalytic dehydrogenation.[6,7] More recently, Leibfarth has reported C-H activation strategies for the functionalization of polyolefins.[8–10] Advancements have also been realized in polymer deconstruction technologies. Pyrolysis is the most widely used method for de-grading soft materials;[11–14] however, this approach exhibits low energy efficiency and poor chemoselectivity. As such, alternative processes that leverage catalytic manifolds are increasingly the focal points of intense research (Despite this somewhat limited scope of exploration, electrochemistry could unlock new chemical space in soft polymer backbone editing. For example, anodic oxidation of electron rich olefins is known to generate radical cations that can participate in a variety of transformations (e.g., nucleophile trapping,[21,37,38] cyclizations,[21,38–40] Scheme 5.1). Elegant examples of polyolefin hydrogenolysis have been reported by Basset,[15] Delferro and colleagues,[16] and Scott.[17] More recent efforts have also explored polymer chain scission through metathesis. Huang and coworkers reported a tandem dehydrogenation/cross metathesis strategy to convert polyethylene to short hydrocarbons.[18] Similarly, Pilard and Khosravi described the degradation of polybutadiene and polyisoprene via cross metathesis using Grubb's 2nd generation catalyst.[19,20]

While promising, the narrow scope of reaction manifolds represented in these precedents highlight the lingering opportunities to explore new chemical space in polymer editing. Indeed, exploring methods that leverage underutilized chemistries could significantly advance efforts toward tailoring the structures and properties of soft materials.

Scheme 5.1. Selected Examples of Modern Polymer Upcycling and Degradation Strategies



Electrosynthetic methods are emerging as attractive tools for mediating chemical transformations, and mild electrochemical conditions for selective functionalizations are well established.[21–24] Surprisingly, however, the application of electrosynthesis toward polymer modification is somewhat limited. While Matyjaszewski has reported electrochemically-mediated atom transfer radical polymerization (eATRP),[25,26] examples of electrochemically modifying synthetic polymers are limited to chlorinations or cyanations of π-conjugated scaffolds in the film state.[27–36]

Despite this somewhat limited scope of exploration, electrochemistry could unlock new chemical space in soft polymer backbone editing. For example, anodic oxidation of electron rich olefins is known to generate radical cations that can participate in a variety of transformations (e.g., nucleophile trapping,[21,37,38] cyclizations,[21,38–40] cycloadditions,[21,37,38] and β-scission[41–44]). This reactivity compliments the more traditional olefin chemistry that is routinely used for polymer modification (e.g., via additions,[45–47] thiol-ene chemistry,[48] ozonolysis,[49] and others[50,51]); thus, electrochemical modifications hold enormous potential for tailoring materials. We hypothesized that entropic factors would favor β-scission pathways in a macromolecular substrate, thereby driving backbone cleavage. We also surmised that any reactive intermediates following the initial oxidation step could be trapped with exogenous reagents to prepare functionalized materials. Thus, electrosynthesis would represent a unified approach for backbone editing of olefin-containing polymers.

Results and Discussion

To explore these ideas, we selected polynorbornene (**5.1**; prepared via ring-opening metathesis polymerization (ROMP)) as the model substrate for our preliminary studies. We synthesized samples of **5.1** using a Z-selective Grubbs catalyst,[52] as the high cis-olefin content was anticipated to simplify subsequent characterization. Cyclic voltammetry revealed that oxidation of **5.1** occurred at 2.2 V (1.1 V vs Fc/Fc^+), consistent with the oxidation potential of unactivated olefins.[53] To test whether chain scission accompanied oxidation, a solution of **5.1** (0.039 M in DCM) was initially electrolyzed in an undivided cell under a constant, unreferenced potential (E_{cell} = 2.5 V) for 1 h. Following electrolysis, the reaction was filtered through a short silica plug and concentrated to dryness. The electrolyzed polymer was isolated

as a white solid with good mass recovery (84%). Consistent with our hypothesis, analysis of the isolated material by size exclusion chromatography (SEC) revealed a significant reduction in the calculated number average molecular weight (ΔM_n = -982 kDa; Figure 5.1). A brief survey of electrode materials revealed that a graphite/zinc (anode/cathode) combination afforded large reductions in molecular weight after electrolysis for 1 h.[54]

To better understand the degradation behavior of our model system, we monitored molecular weight as a function of electrolysis time. A solution of **5.1** (0.036 M in DCM) was stirred under constant potential (E_{cell} = 2.5 V), and 0.1 mL aliquots were removed every 10 min over the course of 1 h for SEC analysis (Figure 5.2A). As expected, the retention volume increased with increasing electrolysis time; however, we also observed the growth of a high M_n species (which we attributed to interchain radical recombination). This conclusion was further supported by a Mark-Houwink analysis, which was consistent with branch formation in the degraded polymer samples (Figure 5.3). A plot of M_n vs electrolysis time showed a monotonic decrease in molecular weight, which suggested that chain scission occurred randomly along the polymer backbone (Figure 5.4). Thus, we surmised that the rate of chain cleavage could be calculated according to Equation 5.1 developed by Malhotra and coworkers:[55,56] where $K' = k_{obs}/M_0$, M_0 is the molecular weight of the repeat unit, M_i is the initial M_z of the polymer, M_t is the M_z following electrolysis for time t, and k_{obs} is the rate constant of polymer cleavage. A representative plot of $1/M_t - 1/M_i$ vs electrolysis time is shown in Figure 5.2B, and we were delighted to observe the expected linear correlation (k_{obs} = 2.82 x 10^{-3} min^{-1} ± 9.42 x 10^{-4} min^{-1}).

Equation 5.1:

$$\frac{1}{M_t} = \frac{1}{M_i} + K't$$

We hypothesized that the addition of a hydrogen atom transfer reagent would quench the anodically generated radical cation, thereby inhibiting chain scission. As expected, the addition of excess 9,10-dihydroanthracene[57] significantly decreased the rate of polymer degradation (k_{obs} = 6.59 x 10^{-4} min^{-1} ± 2.82 x 10^{-4} min^{-1}; Figure 5.5).[58] Additionally, ^{1}H NMR spectral analysis of electrolyzed **5.1** revealed the presence of aldehydic end groups (δ = 9.61),

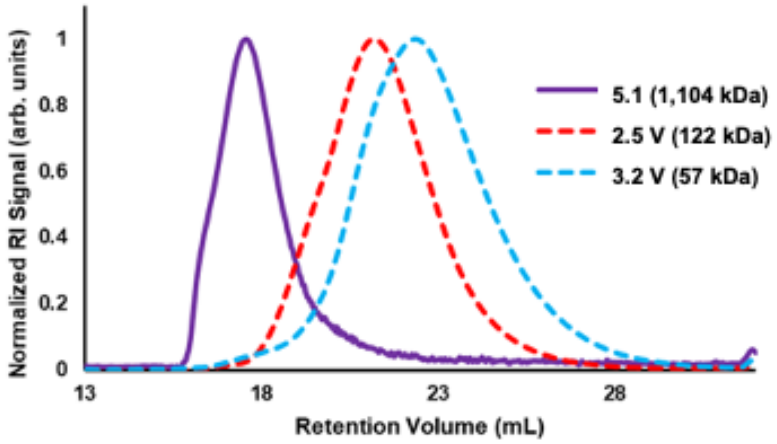


Figure 5.1. SEC data from conventional calibration for electrochemical degradation of **5.1**. Solid trace represents polymer before electrolysis. Dotted traces represent polymer after electrolysis at 2.5 V (red) and 3.2 V (blue).

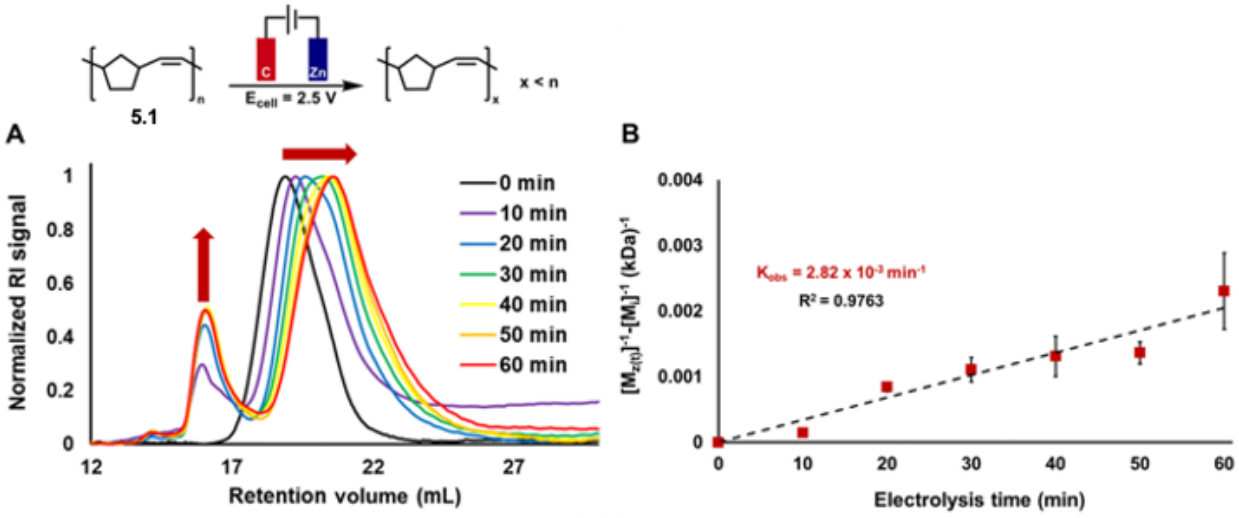


Figure 5.2. Electrochemical degradation study using **5.1**. (A) Molecular weight evolution as a function of electrolysis time (as determined by SEC). (B) Representative kinetic plot for the electrochemical degradation of **5.1**.

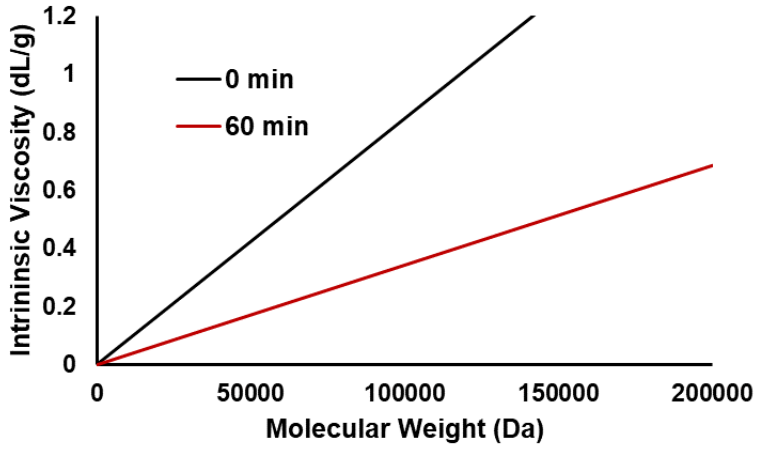


Figure 5.3. Mark-Houwink plot from triple detection for material following electrochemical degradation of **5.1**. The black line represents **5.1** prior to electrolysis and the red line represents the polymer following 60 min of electrolysis.

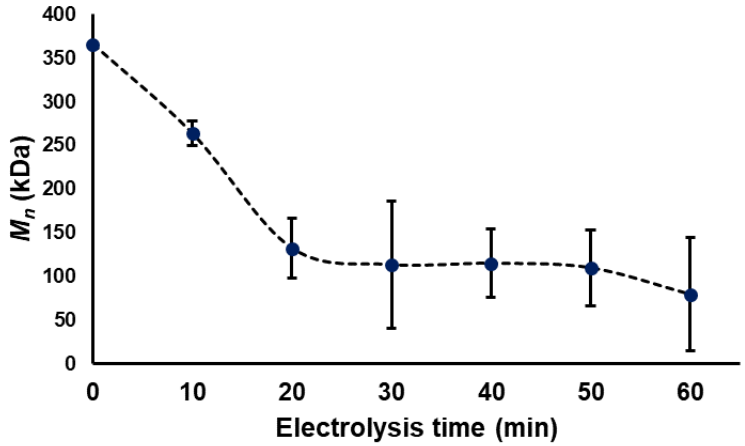


Figure 5.4. M_n (determined by triple detection SEC) as a function of electrolysis time during the electrochemical degradation of **5.1**.

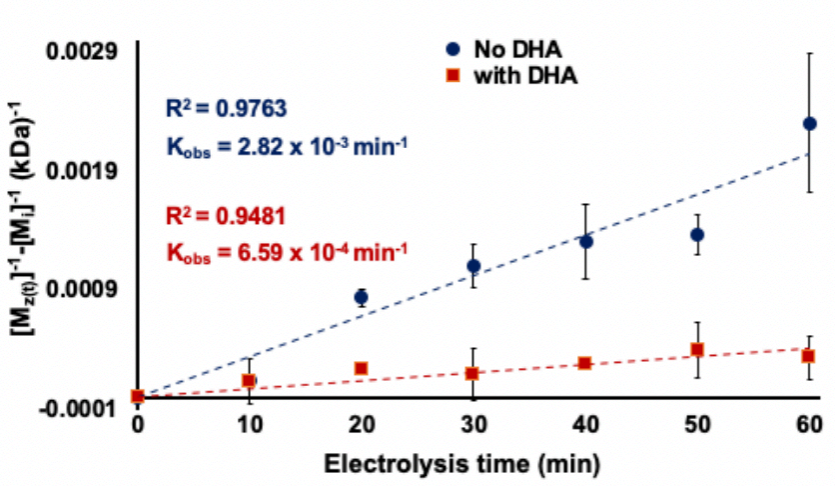


Figure 5.5. Overlayed kinetic plot using data from the electrochemical degradation of **5.1** in the presence of DHA (red) and absence of DHA (blue).

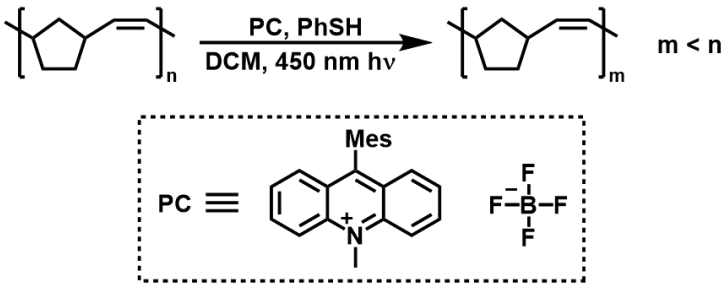
which would be consistent with water addition to the expected cationic chain end following β-scission of a radical cation (Figure 5.53). To further implicate radical cation intermediates in the observed process, we also explored the impact of chemical oxidants on polymer M_n. Specifically, we employed organic photoredox catalysts (e.g., 9-mesityl-10-methyl acridinium salts) that have been shown to oxidize unactivated olefins to radical cations in their excited state (Scheme 5.2).[59] Consistent with our mechanistic hypothesis, a significant reduction in molecular weight (ΔM_n = -696 kDa; Figure 5.6) was observed when a sample of **5.1** was irradiated in the presence of an acridinium photooxidant. Collectively, these data implicate the intermediacy of radical cations along the reaction coordinate for polymer chain scission.

Having established the electrochemical degradation of **5.1**, we sought to determine if our method could be generalized to other olefin-containing polymers. A solution of *cis*-1,4-polyisoprene (0.062 M in DCM) was stirred under the optimized conditions described above.[60] SEC analysis following electrolysis for 1 h revealed a significant reduction in molecular weight (cf. ΔM_n = -546 kDa; Figure 5.7). Furthermore, *cis*-1,4-polybutadiene also exhibited a reduction in molecular weight (ΔM_n = -147 kDa; Figure 5.8) despite requiring longer reaction time (16 h). Finally, poly(cyclooctene) (prepared via ROMP) could be electrolytically degraded (ΔM_n = -25 kDa; Figure 5.9), albeit at higher voltage (E_{cell} = 3.2 V).

As the E_{ox} of C(sp^3)–H bonds is significantly higher than that of C(sp^2)–C(sp^2) bonds (cf. ~3.0 V vs. ~2.2 V),[53] we hypothesized that polymers with saturated backbones would remain unperturbed under our reaction conditions (which could be leveraged for chemoselective modifications). To test this, a solution of **5.1** and polystyrene (1:1 by mass) was subjected to bulk electrolysis for 2 h. An aliquot was then removed from the reaction and analyzed by SEC (Figure 5.10). Gratifyingly, we observed a reduction in the M_n of **5.1** with minimal change in the M_n of polystyrene. Furthermore, visualization of the SEC data using UV-detection at 261 nm (a λ_{max} of polystyrene) revealed that no detectable polystyrene had coupled to the degraded **5.1** (Figure 5.11).

Encouraged by these successes with homogenous systems, we also explored heterogeneous electrochemical degradations. As **5.1** exhibited negligible solubility in MeCN, this solvent was selected for a preliminary experiment. Stirring a solid sample of **5.1** in MeCN

Scheme 5.2. Photoredox-mediated degradation of 5.1



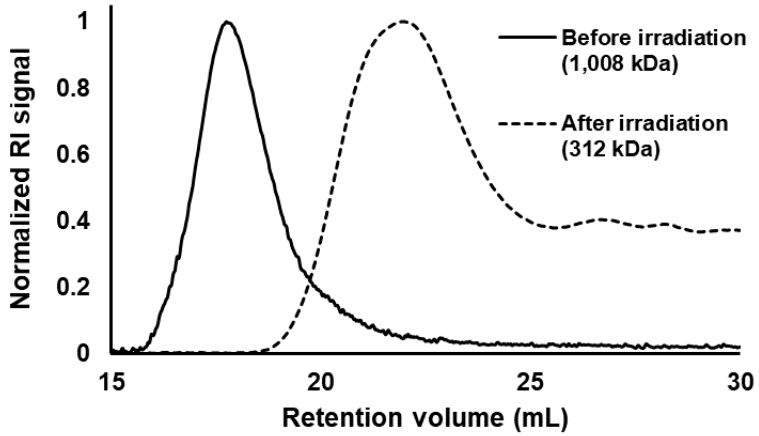


Figure 5.6. SEC data from triple detection for photoredox-mediated degradation of 5.1. Solid trace represents polymer pre-irradiation and dotted trace represents polymer post-irradiation.

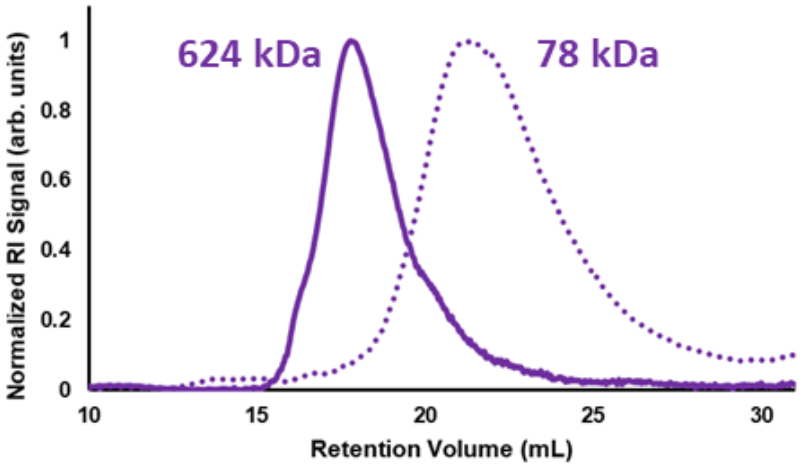


Figure 5.7. SEC data from conventional calibration for the electrochemical degradation of *cis*-1,4-polyisoprene at 2.5 V. Solid trace represents polymer before electrolysis and dotted trace represents polymer after electrolysis.

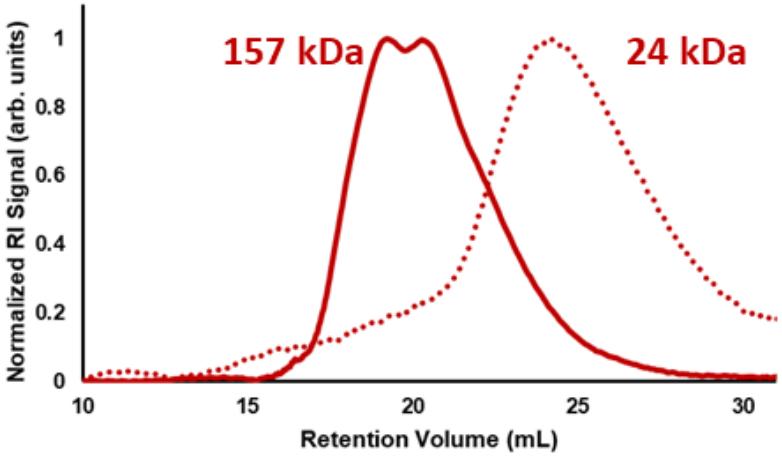


Figure 5.8. SEC data from conventional calibration for the electrochemical degradation of *cis*-1,4-polybutadiene at 2.5 V. Solid trace represents polymer before electrolysis and dotted trace represents polymer after electrolysis.

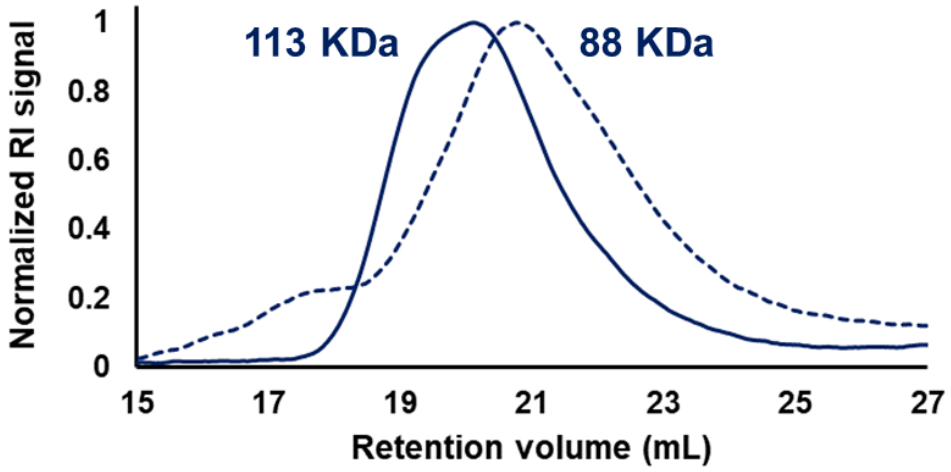


Figure 5.9. SEC data from triple detection for the electrochemical degradation of poly(cyclooctene) at 3.2 V. Solid trace represents polymer before electrolysis and dotted trace represents polymer after electrolysis.

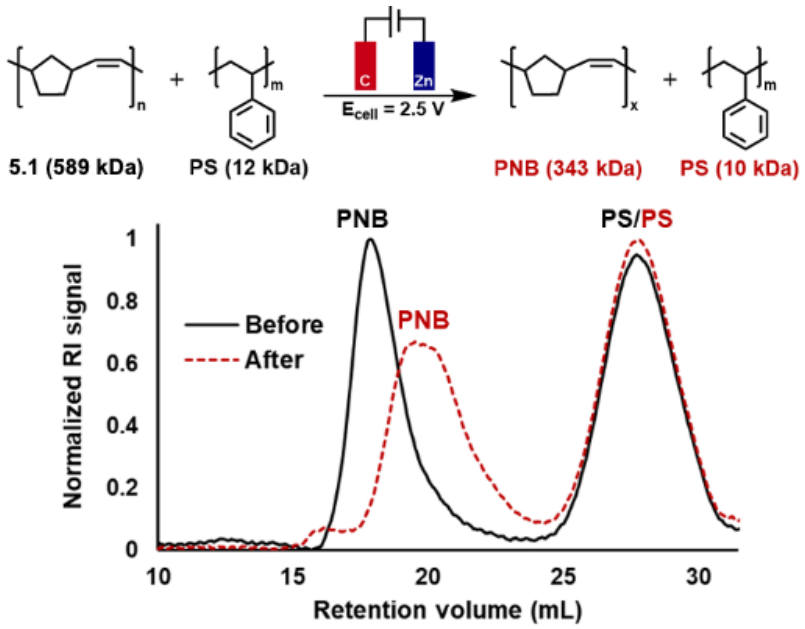


Figure 5.10. Chemoselective degradations of polymer mixtures. SEC analysis of a polymer mixture (polynorbornene and polystyrene; black) showing selective degradation of polynorbornene following electrolysis (red).

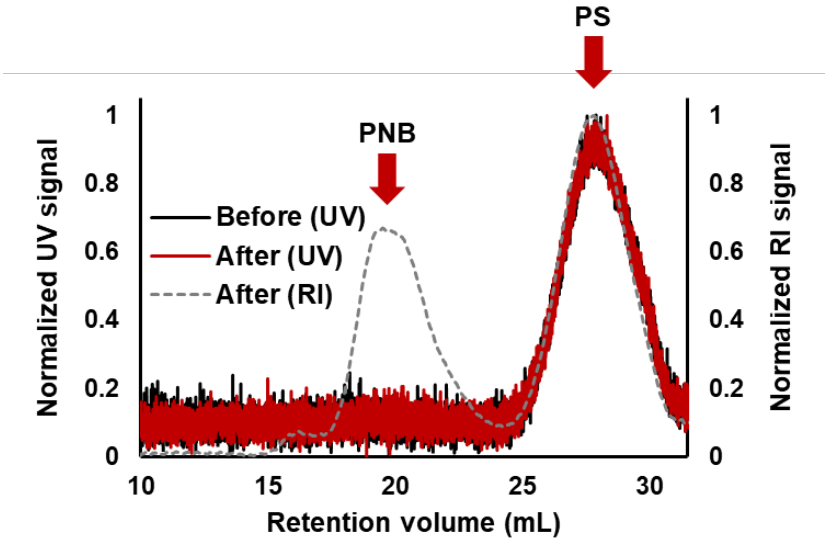


Figure 5.11. UV visualization (294 nm) of SEC data for selective electrochemical degradation of 5.1. UV visualization of the SEC data for a mixed polymer sample prior to electrolysis (black)

under constant potential and temperature (3.2 V and 23 °C) resulted in a clear reduction in molecular weight after 16 h (ΔM_n = -207 kDa; Figure 5.12). As with our homogenous experiments, longer electrolysis times (up to 63 h) resulted in higher degrees of degradation (ΔM_n = -1,402 kDa). To confirm the heterogenous nature of this reaction, a solid sample of **5.1** was stirred in MeCN-d_3 for 63 h at 23 °C. The mixture was then separated by filtration, and the filtrate was analyzed by ^{1}H NMR spectroscopy (which did not reveal any detectable **5.1**; Figure 5.13).

Coupling chemical modification to degradation could also afford new products with intrinsic value (e.g., as macromonomers or macroinitiators for accessing new polymeric species). Recently, the Lin lab demonstrated that unactivated olefins could be azidated under mild, electrochemical conditions.[61] We envisioned that azidating the products of chain scission would create privileged scaffolds for further reactivity (e.g., 1,3-dipolar cycloadditions,[62,63] Staudinger ligations,[64] aza-Wittig reactions,[65] and others[66]). To explore this concept, **5.1** (0.04 M in DCM) was initially electrolyzed in an undivided cell (E_{cell} = 3.2 V) in the presence of $MnBr_2$ (20 mol%) and trimethylsilyl azide (TMS–N_3; 7.0 equiv.).[67]

Following electrolysis for 1 h, the reaction mixture was filtered through neutral alumina and added dropwise to MeOH to precipitate any polymeric material. The resultant white solid, **5.2**, was recovered following centrifugation in excellent yield (98%). Analysis of **5.2** by IR spectroscopy revealed a new stretch consistent with azidation (c.f. 2099 cm^{-1}; ΔM_n = -773 kDa; Figure 5.14).

Control experiments performed in the absence of (i) $MnBr_2$ or (ii) electrolysis afforded negligible functionalization. While other azide sources (e.g., NaN_3 or $N(Bu)_4N_3$) proved ineffectual under our reaction conditions, a variety of electrode combinations were found to facilitate azidation. We ultimately selected an RVC/platinum (anode/cathode) electrode combination, given that ^{1}H NMR conversion was greatest with this combination (Figure 5.15 and Table 5.1). As with electrochemical degradation, the selected conditions were suitable to azidate a variety of olefin-containing polymer substrates (Figure 5.16-Figure 5.21). To estimate the degree of azidation, a low molecular weight sample of **5.1** (prepared using Grubbs 3rd generation catalyst;[68,69] M_n = 6,800 Da) was subjected to azidation under the conditions described above.[67] The ^{1}H NMR spectrum of the precipitated material (**5.2**)

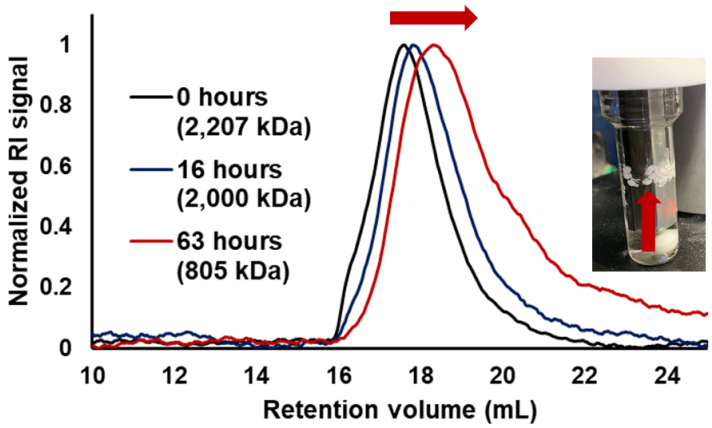


Figure 5.12. Heterogeneous degradation of **5.1**. SEC analysis following heterogenous polymer electroactivation showed a clear reduction in molecular weight with increasing electrolysis time. Inset picture shows a representative experiment with the insoluble polymer highlighted by a red arrow.

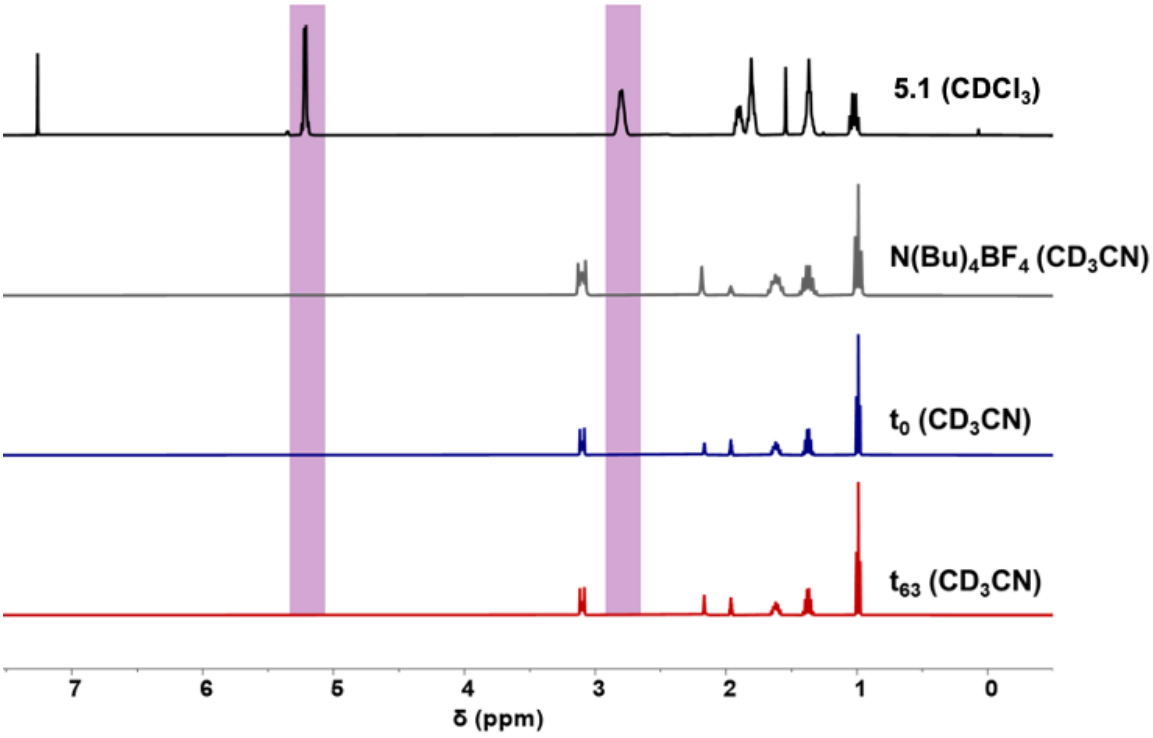


Figure 5.13. ^{1}H NMR spectra for heterogeneous degradation of **5.1**. Black: **5.1** in $CDCl_3$. Grey: Electrolyte in CD_3CN. Blue: Aliquot of reaction mixture prior to electrolysis in CD_3CN. Red: Aliquot of reaction mixture post-electrolysis in CD_3CN. Purple highlights represent characteristic chemical shifts of **5.1**.

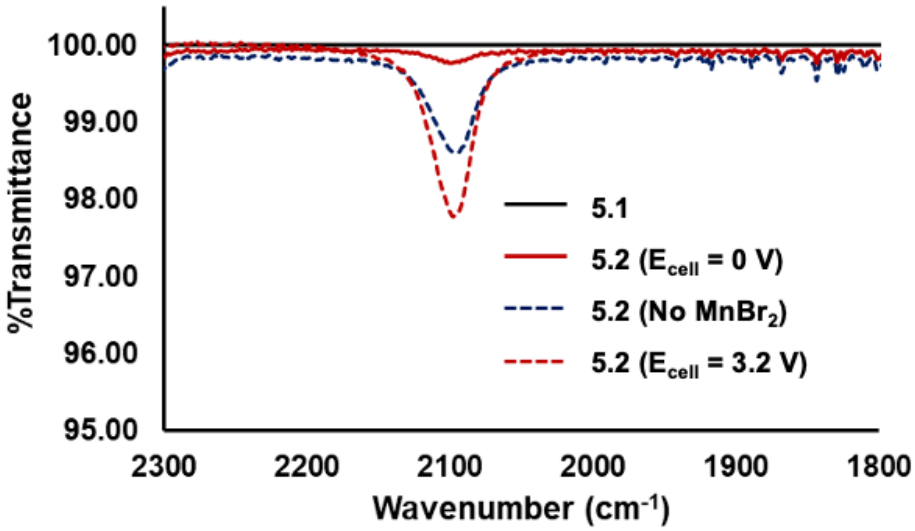


Figure 5.14. Overlayed IR spectra for azidation of **5.1** under various conditions. Spectra for unfunctionalized **5.1** (black), background functionalization in the absence of an applied potential (red), and background functionalization in the absence of $MnBr_2$ (blue, dashed) are shown. The IR spectrum from the material prepared under our standard conditions (red, dashed) has been included for comparison.

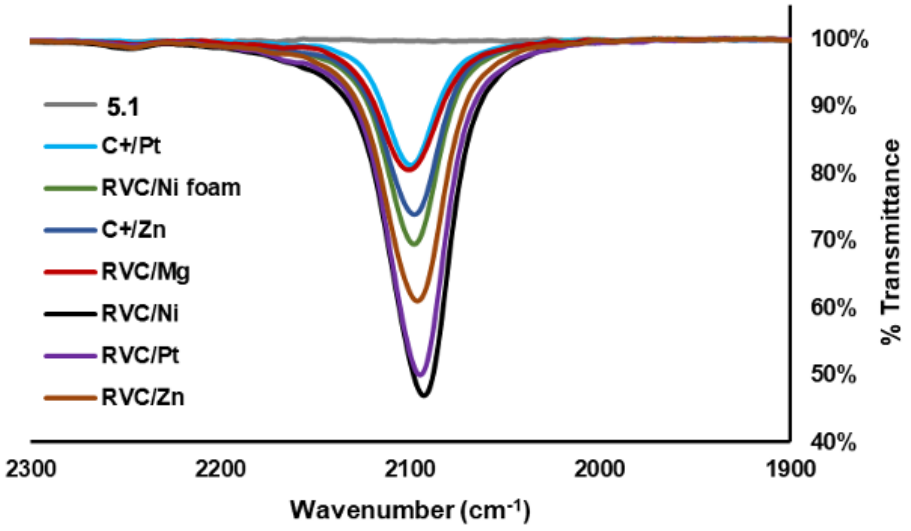


Figure 5.15. IR spectra from the electrode screen for preparing **5.2**. Legend shows electrode combinations in anode/cathode format.

Table 5.1. Electrode screen for electrochemical azidation of **5.1**

Entry	Electrode combination (anode/cathode)	Azidation Observed via IR	Conversion (%)[a]
1	RVC/Pt	yes	20.5
2	RVC/Zn	yes	14.7
3	RVC/Ni	yes	19.8
4	RVC/Mg	yes	14.6
5	RVC/Ni foam	yes	14.2
6	graphite/Zn	yes	4.2
7	graphite/Pt	yes	8.3

[a]Average of two experiments; conversion determined using NMR spectroscopy as described above

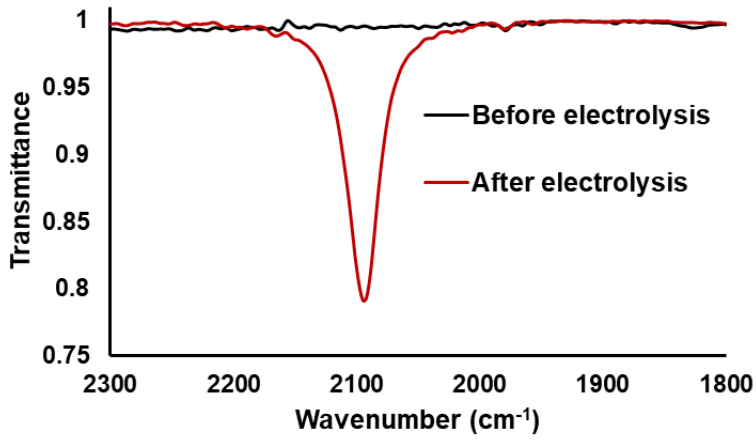


Figure 5.16. IR spectra for the electrochemical azidation of 1,4-polybutadiene. Black line represents polymer before electrolysis. Red line represents solid polymer isolated following electrolysis.

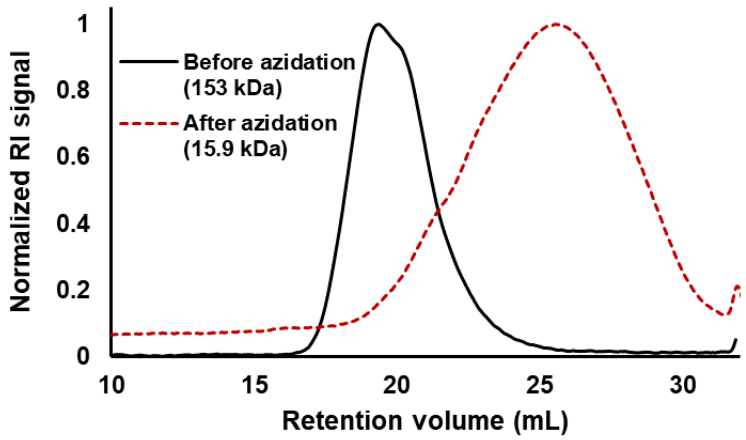


Figure 5.17. SEC data from triple detection for 1,4-polybutadiene before (black trace) and after azidation (dotted red trace).

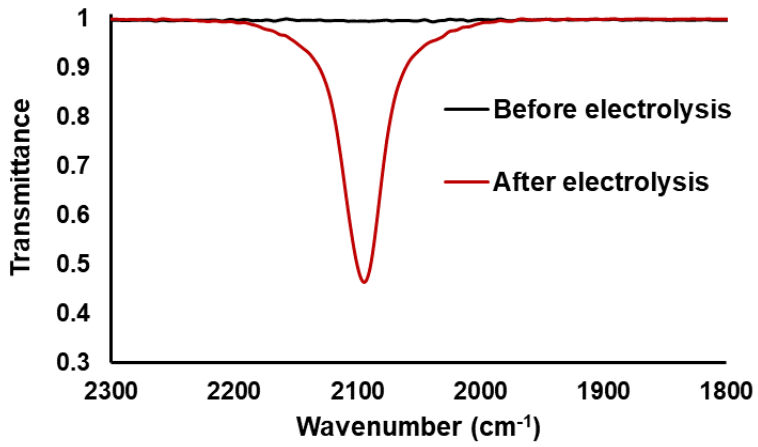


Figure 5.18. IR spectra for the electrochemical azidation of *cis*-1,4-polyisoprene. Black line represents polymer before electrolysis. Red line represents solid polymer isolated after electrolysis.

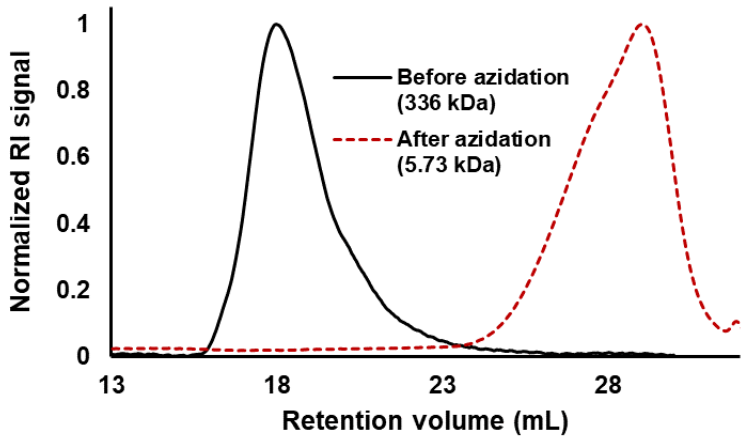


Figure 5.19. SEC data from triple detection for *cis*-1,4-polyisoprene before (black trace) and after azidation (dotted red trace).

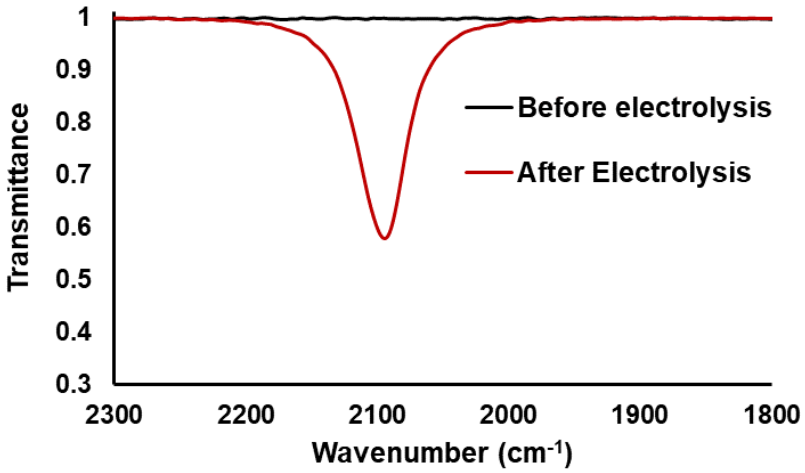


Figure 5.20. IR spectra for the electrochemical azidation of poly(cyclooctene). Black line represents polymer before electrolysis. Red line represents solid polymer isolated after electrolysis.

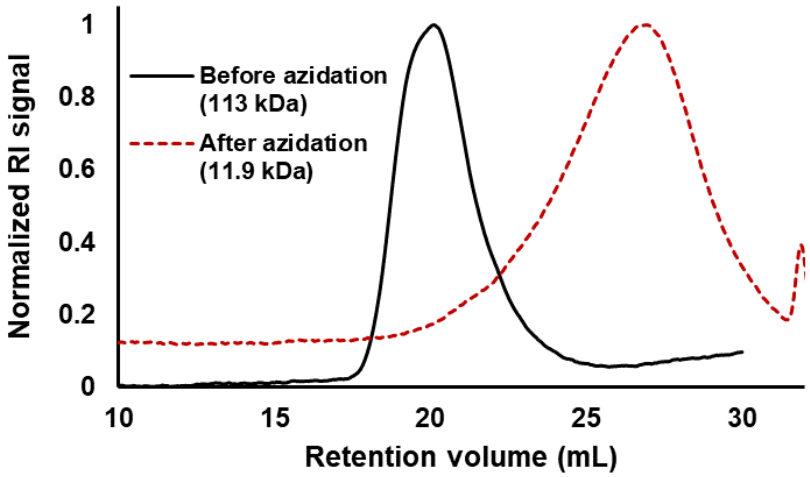


Figure 5.21. SEC data from triple detection for poly(cyclooctene) before (black trace) and after azidation (dotted red trace).

displayed a new broad resonance at δ = 3.84 ppm, which was consistent with the expected methine of the azidated material (Figure 5.64).[61,70] Integration of this signal relative to the unfunctionalized methylenes in the cyclopentyl ring of the repeating unit was consistent with ~30% azidation per polymer chain (Figure 5.72). To corroborate this estimation, **5.2** was reacted with 1-ethynyl pyrene in the presence of CuI to afford triazole-functionalized **5.3** (Figure 5.22 and Figure 5.23). Integration of the new diagnostic aromatic resonance in the ^{1}H NMR spectrum of **5.3** was consistent with ~24% azidation per polymer chain (Figure 5.75). Finally, the total pyrene content of **5.3** was estimated using UV-vis spectroscopy and the Beer-Lambert law, which was consistent with ~29% azidation per polymer chain (Figure 5.24). Averaging these conversions gave a conservative estimate of ~27% azidation per polymer chain under our conditions.

Based on our results, we propose the following mechanism for the observed reactivity (Figure 5.25). Single electron oxidation of the olefin at the anode initially furnishes a radical cation in the polymer backbone. This species subsequently undergoes β-scission, and termination of the resultant radical and cation chain ends could occur via multiple pathways (e.g., hydrogen atom transfer, radical recombination, or nucleophilic trapping).

Materials and Methods

General Considerations

Unless otherwise noted, solvents were dried on an MBraun solvent purification system with 3Å molecular sieves and degassed via three freeze-pump-thaw cycles. Polybutadiene samples (mixture of *cis*- and *trans*- 1,4-polybutadiene (M_w = 200,000-300,000); *cis*-1,4-polybutadiene (M_w = ~200,000 Da); purified by filtration over basic alumina and precipitated from methanol) were purchased from Sigma. All other reagents and materials were obtained from commercial sources and used without further purification unless otherwise noted. Oxygen and water sensitive manipulations were performed in a N_2 filled MBraun glovebox or using standard Schlenk techniques with oven- and flame- dried glassware. ^{1}H and ^{13}C NMR spectral data were collected on a Bruker 500 MHz NMR, Varian 600 MHz NMR, Varian 500 MHz NMR, or Varian 300 MHz NMR spectrometer. Chemical shifts (δ) are reported in ppm using the residual

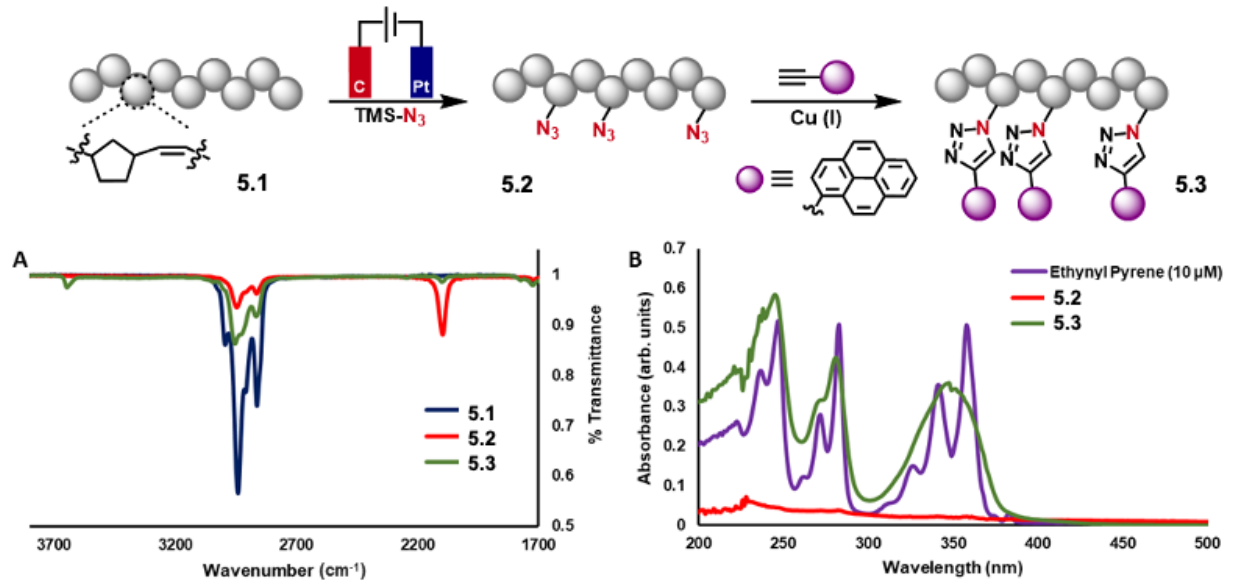


Figure 5.22. Cartoon representation of azidation of a low M_n sample of **5.1** and subsequent Cu-mediated azide/alkyne coupling. A) IR spectra for **5.1** (blue), **5.2** (red), and **5.3** (green). B) UV-vis absorbance spectra of **5.2** (red) and **5.3** (green). The absorbance spectrum of 1-ethynyl pyrene is provided for reference (purple).

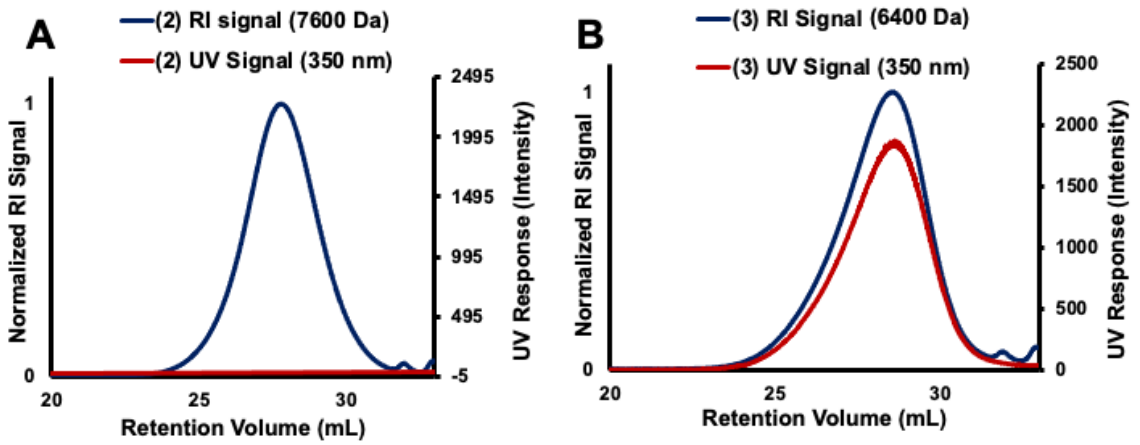


Figure 5.23. SEC data from conventional calibration depicting RI and UV signals (at 350 nm) for **5.2** (A) and **5.3** (B) to confirm presence of pyrene moiety.

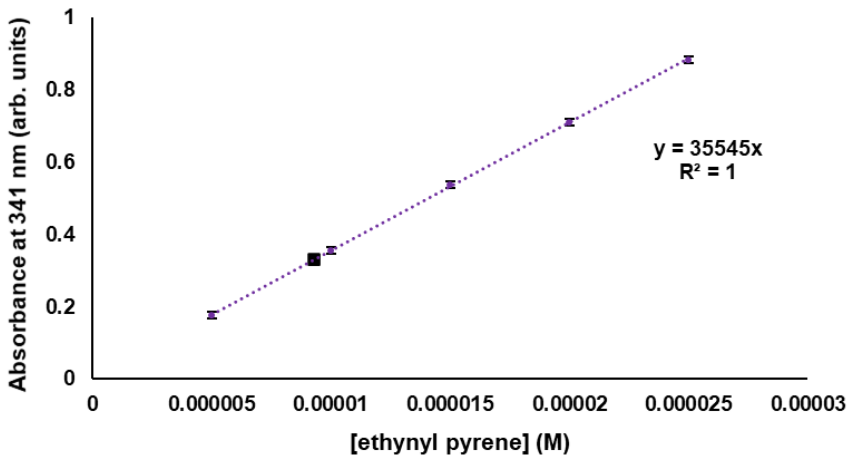


Figure 5.24. UV-vis calibration curve for ethynyl pyrene. Black square represents 9.29 μM with respect to pyrene coupled repeat units in **5.3.**

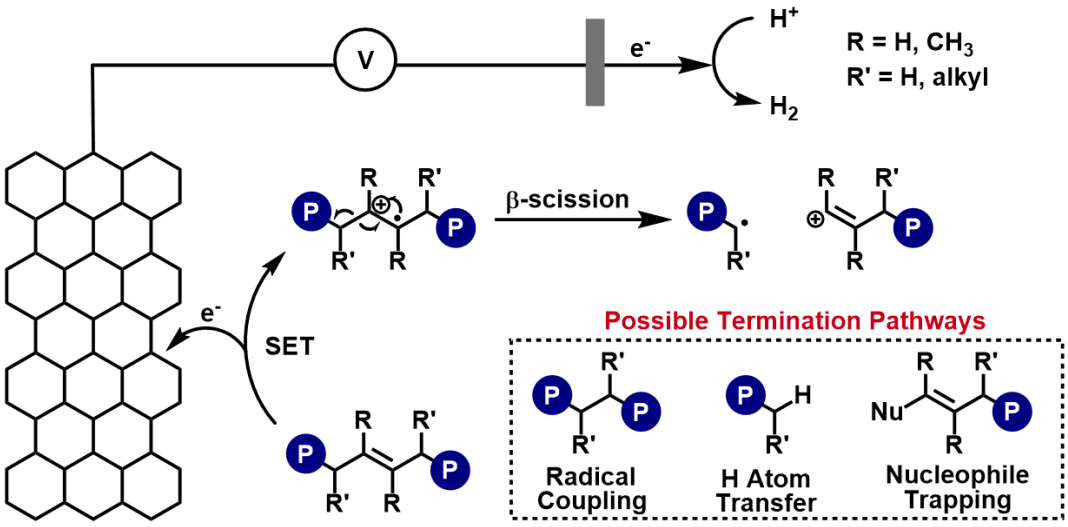


Figure 5.25. Proposed mechanism for electrochemical editing of olefin-containing polymers.

solvent as reference. IR spectra were collected on a Bruker Alpha II FT-IR with Platinum ATR accessory. UV-visible absorbance spectra were recorded using an Agilent Cary 100 series UV-Vis spectrophotometer. Ultra-centrifugation was conducted using a Beckman Coulter Microcentrifuge 16 spun at 16,163 Xg for three 4-min cycles. Size Exclusion Chromatography (SEC) data were collected on an Omnisec Resolve and Omnisec Reveal System using triple detection with detectors in series: UV, light scattering, viscometer, and refractive index and three Viscotek styrene divinylbenzene copolymer columns (in series T3000, T4000, and T5000) at a flow rate of 1 mL/min and thermostatted to 30 °C using tetrahydrofuran (THF) as the eluent. Molecular weight and dispersity data from triple detection or conventional calibration relative to polystyrene standards are reported. Matrix Assisted Laser Desorption Ionization Time of Flight Mass Spectrometry (MALDI-TOF MS) spectra were collected on a Synapt G2-Si MALDI mass spectrometer with a quadrupole time-of-flight mass analyzer. Mass accuracy was achieved by calibration against an external red phosphorus standard. Ionization was performed by a 355 nm laser operating at a firing rate of 2500 Hz. Spectra were averaged over at least 100 scans. Polymer samples were prepared in THF (2-10 mg/mL) with silver trifluoroacetate (AgTFA) as the cation source, and trans-2-[3-(4-tert-Butylphenyl)-2-methyl-2-propenylidene]malononitrile (DCTB) as the matrix. All electrochemical transformations were performed using an IKA ElectraSyn 2.0. Cyclic Voltammetry (CV) measurements were performed on a CH instruments potentiostat using 0.05 mmol compound in 5 mL dichloromethane (DCM) solution (0.01 M) with supporting electrolyte 0.2 M $N(Bu)_4BF_4$ using silver as the reference electrode, along with gold working and tungsten counter electrodes at a scan rate of 50 mVs^{-1}.

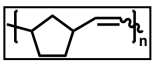
Synthetic Procedures

High M_n cis-polynorbornene

A flame dried 50 mL Schlenk flask was charged with norbornene (316 mg; 3.36 mmol), THF (10 mL), and a Teflon stir bar. The monomer solution was degassed via three cycles of freeze-pump-thaw and cooled to -30 °C. A solution of Z-selective Grubbs catalyst (4.8 mg; 0.008 mmol in 0.25 mL THF) was prepared in an N2 filled glovebox and then added to the monomer solution via syringe. The reaction temperature was maintained between -40 °C and -20 °C

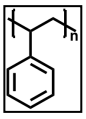
for 4 h, after which the polymerization was quenched with ethyl vinyl ether (0.5 mL; 5.26 mmol) in THF (18 mL). Polymeric material was precipitated from MeOH, collected on a medium porosity fritted funnel, and dried in vacuo. The polymer was dissolved in minimal DCM, precipitated from MeOH a second time, collected via filtration, and dried for 16 h in vacuo. The title material was recovered as a white solid (241 mg, 76.2% yield) SEC data for polymers utilized for electrochemical degradation and azidation studies is provided in Figure 5.26 and Figure 5.27. Spectral data were consistent with literature reports, and representative ^{1}H and ^{13}C NMR spectra are shown in Figure 5.46 and Figure 5.47, respectively. Olefin E:Z ratios were determined based on the relative integrations of the Z (δ = 5.22) and E (δ = 5.35) olefin resonances.

Low M_n polynorbornene



A flame dried 25 mL Schlenk flask was charged with norbornene (500 mg; 5.31 mmol), DCM (20 mL), and a Teflon stir bar. A solution of Grubbs 3rd generation catalyst (140 mg; 0.16 mmol in 1 mL DCM) was added via syringe. The reaction was stirred at 0 °C for 20 min, after which the polymerization was quenched with ethyl vinyl ether and concentrated to minimal volume. The solution was passed over a plug of basic alumina twice and concentrated to minimal volume for precipitation from MeOH before drying in vacuo. The title material was recovered as a white powder (370 mg, 73% yield). SEC data for all polymers utilized for electrochemical degradation and azidation studies is provided in Figure 5.28 and Figure 5.29. Spectral data were consistent with literature reports, and representative ^{1}H and ^{13}C NMR spectra are shown in Figure 5.48 and Figure 5.49, respectively.

Polystyrene



A flame dried 25 mL Schlenk flask was charged with styrene (0.79 mL; 6.91 mmol; uninhibited by passing through a plug of basic alumina), AIBN (recrystallized;[71] 2.2 mg; 0.013 mmol), and THF (5 mL). The reaction solution was degassed via three cycles of freeze-pump-thaw and then stirred at 80 °C for 16 h. The solution was concentrated to minimal volume, and polymeric material was precipitated from MeOH, collected on a fine porosity fritted funnel, and dried for 16 h in vacuo. The title material was recovered as a white powder (160 mg, 22.3% yield; M_n = 4,079 Da; Đ = 1.33 from triple detection). Spectral data

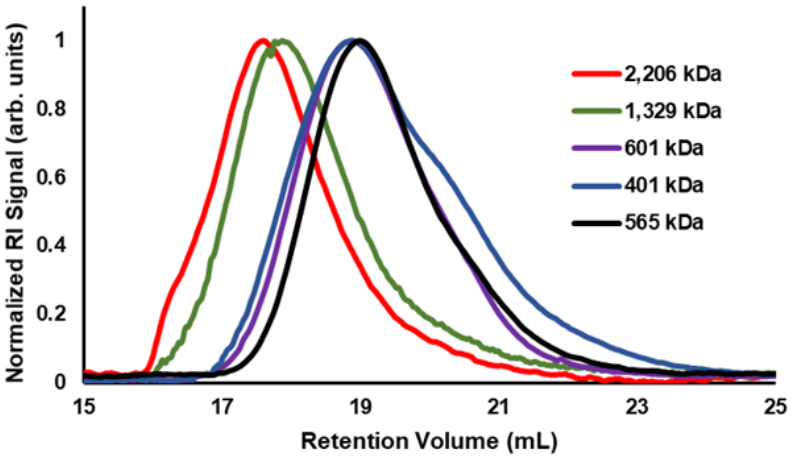


Figure 5.26. SEC data from triple detection for high M_n *cis*-polynorbornenes used in this study.

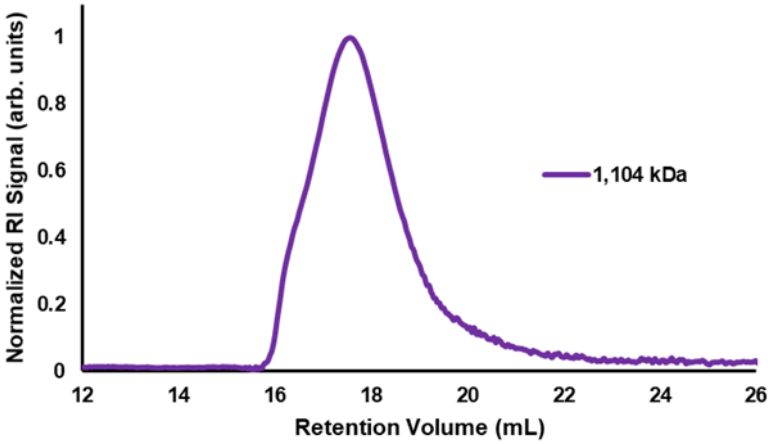


Figure 5.27. SEC data from conventional calibration for high M_n *cis*-polynorbornenes used in this study.

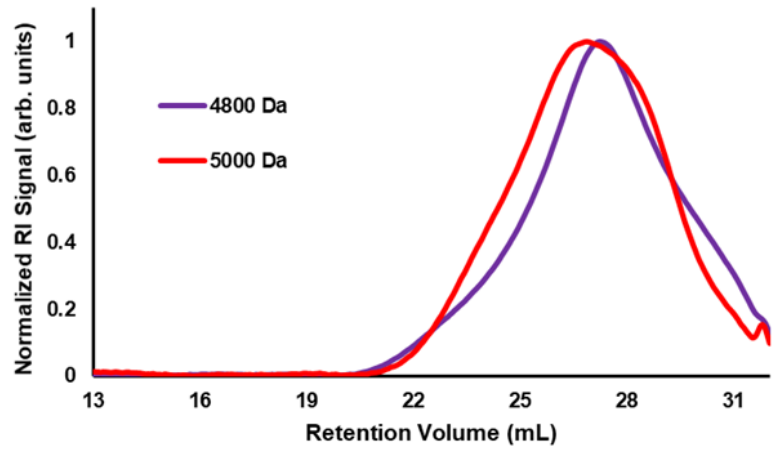


Figure 5.28. SEC data from triple detection for low M_n polynorbornenes used in this study.

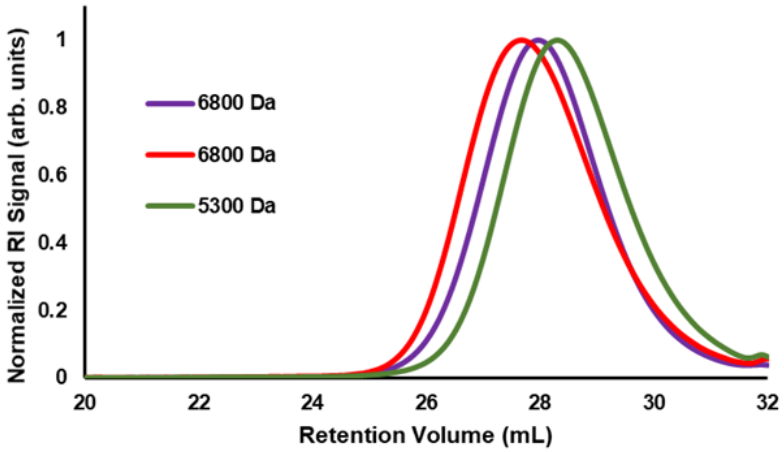
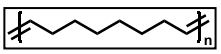


Figure 5.29. SEC data from conventional calibration for low M_n polynorbornenes used in this study.

were consistent with literature reports, and a representative ^{1}H NMR spectrum is shown in Figure 5.50.

Poly(cyclooctene)



A flame dried 25 mL Schlenk flask was charged with *cis*-cyclooctene (204 mg; 1.85 mmol), DCM (2.5 mL), and a Teflon stir bar. The monomer solution was degassed via three cycles of freeze-pump-thaw, and a solution of Grubbs 2nd generation catalyst (3.5 mg; 0.004 mmol in 0.1 mL DCM) was added via syringe. The reaction was stirred at 23 °C for 10 min, after which the polymerization was quenched with ethyl vinyl ether (0.1 mL; 1.05 mmol) and diluted with DCM (10 mL). The reaction mixture was filtered through a plug of basic alumina and then concentrated to dryness. The residue was dissolved in minimal DCM, and polymeric material was precipitated from MeOH, collected on a fine porosity fritted funnel, and dried in vacuo. The polymer was dissolved again in minimal DCM, precipitated from MeOH a second time, collected via filtration, and dried for 16 h in vacuo. The title material was recovered as a white solid, (109 mg, 53.4% yield; M_n = 113.3 kDa; Đ = 1.63 from triple detection) and stored as a 10 mg/mL solution in chloroform ($CHCl_3$). Spectral data were consistent with literature reports, and representative ^{1}H and ^{13}C NMR spectra are shown in Figure 5.51 and Figure 5.52, respectively.

Experiments Related to Homogeneous Electrochemical Degradations of 5.1

Degradation of 1 in the Absence of Electrolysis

A 5 mL ElectraSyn vial was charged with **5.1** (9.0 mg; 0.096 mmol), a Teflon stir bar, and DCM (2.8 mL). The mixture was stirred until all polymer was dissolved, and $N(Bu)_4BF_4$ (47 mg; 0.143 mmol) was added. An ElectraSyn electrode shroud was equipped with electrodes (graphite anode/zinc cathode) and screwed onto the vial. The solution was stirred without any applied potential for 30 min. The reaction mixture was then concentrated to minimal volume, and polymeric material was precipitated from MeOH prior to isolation by centrifugation. The isolated material was then washed with MeOH (2 x 10 mL) and dried for 16 h in vacuo. SEC analysis of the isolated material is shown in Figure 5.30; the change in molecular weight was

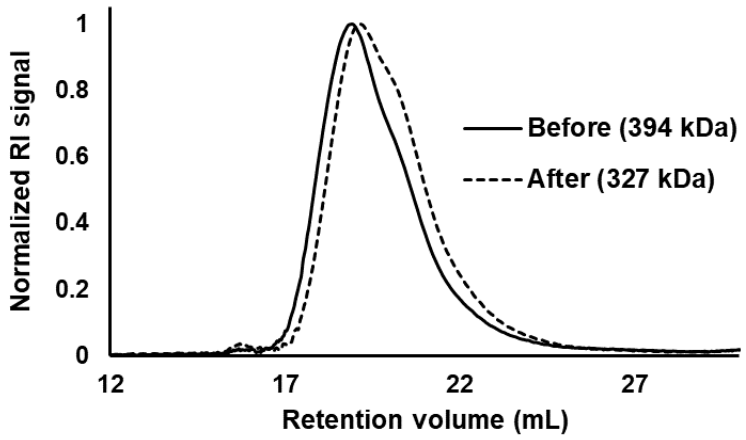


Figure 5.30. SEC data from triple detection for degradation of **5.1** in the absence of electrolysis. Solid trace represents the initial polymer, and the dotted trace represents polymer isolated after the experiment.

minimal under these conditions when compared to experiments conducted with applied potential.

Degradation of 1 using a Referenced Potential (2.18 V)

A 5 mL ElectraSyn vial was charged with **5.1** (5.8 mg; 0.062 mmol), a Teflon stir bar, and DCM (3 mL). The mixture was stirred until all polymer was dissolved then $N(Bu)_4BF_4$ (30 mg; 0.092 mmol) was added. An ElectraSyn electrode shroud was equipped with electrodes (graphite anode/zinc cathode, silver reference electrode) and screwed onto the vial. The solution was electrolyzed using a "Referenced Potential Experiment" at 2.18 V for 1 h. The reaction mixture was then concentrated to minimal volume, and polymeric material was precipitated from MeOH prior to isolation by centrifugation. The isolated material was then washed with MeOH (2 x 10 mL) and dried for 16 h in vacuo. SEC analysis of the isolated material (Figure 5.31) showed a clear reduction in M_n. ^1H and ^{13}C NMR spectra are shown in Figure 5.53 and Figure 5.54, respectively.

*Analysis of **5.1** using Cyclic Voltammetry*

In a N_2-filled glovebox, a 20 mL glass tube (equipped with a gold working electrode, tungsten counter electrode, and silver reference electrode) was charged with **5.1** (4.7 mg; 0.05 mmol), $N(Bu)_4BF_4$ (330 mg; 1.0 mmol), ferrocene (as an internal standard; 9.3 mg; 0.05 mmol), DCM (5 mL), and a Teflon stir bar. The mixture was stirred until homogenous and analyzed using cyclic voltammetry. An irreversible oxidation was observed at 2.18 V. (Figure 5.32; scan rate 50 mVs^{-1}; scan range -1 V to 3.2 V).

*Electrode Screen for Electrochemical Degradation of **5.1***

A 5 mL ElectraSyn vial was charged with **5.1** (10 mg; 0.11 mmol), a Teflon stir bar, and DCM (2.8 mL). The mixture was stirred until all polymer was dissolved, and $N(Bu)_4BF_4$ (54 mg; 0.17 mmol) was added. An ElectraSyn electrode shroud was equipped with various electrodes (Table 5.2) and screwed onto the vial. The solution was electrolyzed using the "Constant Potential" setting at 2.5 V. Following electrolysis for 30 min, the reaction mixture was concentrated to minimal volume, and the polymeric material was precipitated from MeOH and

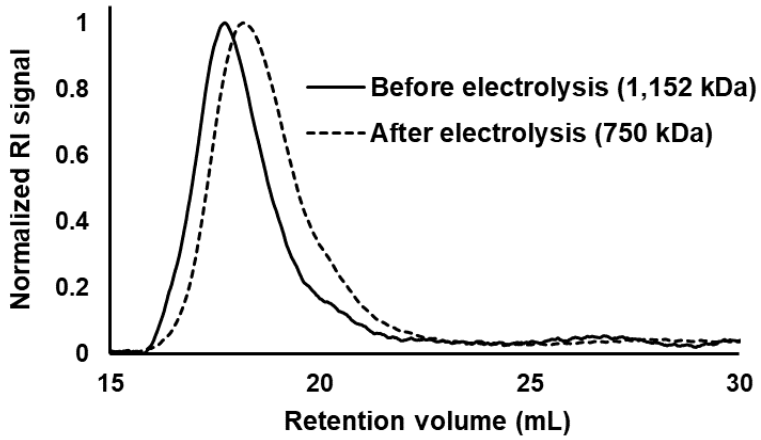


Figure 5.31. SEC data from triple detection for referenced degradation of **5.1** (2.18 V). Solid trace represents polymer before electrolysis and dotted trace represents polymer after electrolysis.

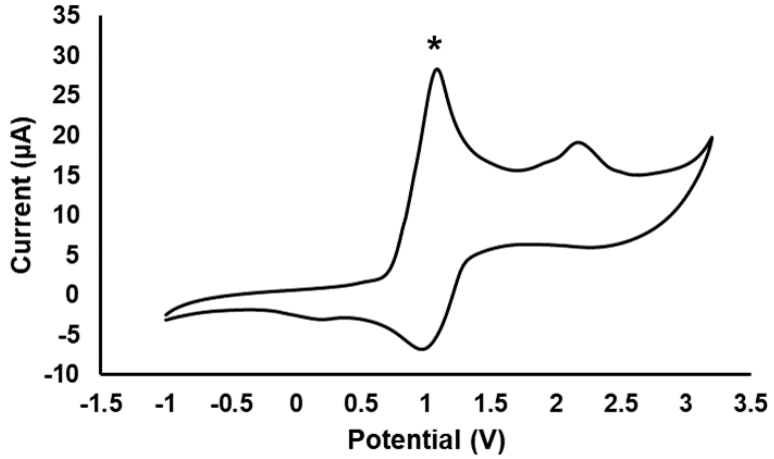


Figure 5.32. Cyclic voltammogram of **5.1** using ferrocene as an internal standard. Oxidation peak associated with ferrocene represented by *.

Table 5.2. Electrode screen for the electrochemical degradation of **5.1**.

Entry	Electrode combination (anode/cathode)	M_n(before) (kDa)	M_n(after) (kDa)
1	RVC/Zn	601	502
2	graphite/graphite	601	488
3[a]	RVC/Pt	601	270; 22
4	graphite/Zn	601	229
5	graphite/Pt	601	172

[a]Resulted in a bimodal trace. Molecular weight data from triple detection is given for each peak.

isolated by centrifugation. This material was then washed with MeOH (2 x 10 mL) and dried for 16 h in vacuo. Results from the electrode screen are shown in Table 5.2. SEC data for the electrolyzed polymers are shown in Figure 5.33.

*Impact of Cell Potential on the Degradation of **5.1***

A 5 mL ElectraSyn vial was charged with **5.1** (20 mg; 0.21 mmol), a Teflon stir bar, and DCM (4.9 mL). The mixture was stirred until all polymer was dissolved, and $N(Bu)_4BF_4$ (104.9 mg; 0.32 mmol) was added. An ElectraSyn electrode shroud was equipped with electrodes (graphite anode/zinc cathode) and screwed onto the vial. The solution was electrolyzed using the "Constant Potential" setting at either 2.5 V or 3.2 V. Following electrolysis for 1 h, the reaction mixture was filtered over a plug of silica and concentrated to dryness. The isolated material was then washed with MeOH (2 x 10 mL) and dried for 16 h in vacuo. Regardless of potential, the electrolyzed polymer was recovered as a white solid in > 80% yield (recovered mass). Although the reduction in molecular weight was higher at 3.2 V, the post-electrolysis material was highly insoluble (which complicated analysis). A lower potential of 2.5 V avoided this issue and was used for subsequent degradation experiments (Figure 5.1).

*Kinetic Analysis of the Electrochemical Degradation of **5.1***

A 10 mL ElectraSyn vial was charged with **5.1** (30 mg; 0.32 mmol), a Teflon stir bar, and DCM (8.8 mL). The mixture was stirred until all polymer was dissolved then $N(Bu)_4BF_4$ (158 mg; 0.48 mmol) was added. An ElectraSyn electrode shroud was equipped with electrodes (graphite anode/zinc cathode) and screwed onto the vial. The solution was electrolyzed using the "Constant Potential" setting at 2.5 V for 1 h. A 0.2 mL aliquot was removed via syringe every 10 min and diluted to 1.0 mL with THF for SEC analysis. SEC data are shown in Figure 5.2A. The rate of chain cleavage was calculated according to Equation 5.1 and found to be $2.35 \times 10^{-6} \pm 6.70 \times 10^{-7}$. A plot of $1 \bullet M_t^{-1} - 1 \bullet M_i^{-1}$ vs electrolysis time is shown in Figure 5.2B. Evolution of M_n, and evolution of M_z over time are shown in Figure 5.4, Figure 5.34 and Table 5.3. The appearance of a high molecular weight species via SEC (Figure 5.2A) was rationalized by the formation of branched species through radical recombination. This conclusion was further supported by Mark-Houwink analysis, which revealed a lower intrinsic viscosity for the electrolyzed material that was consistent with branch formation (Figure 5.3).[72]

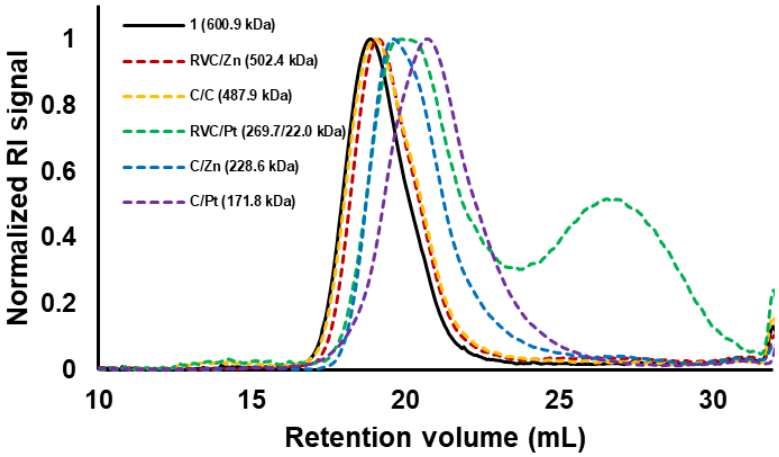


Figure 5.33. SEC data from triple detection for electrochemical degradation of **5.1** electrode screen. Legend shows electrode combinations used for the screen in the format of anode/cathode.

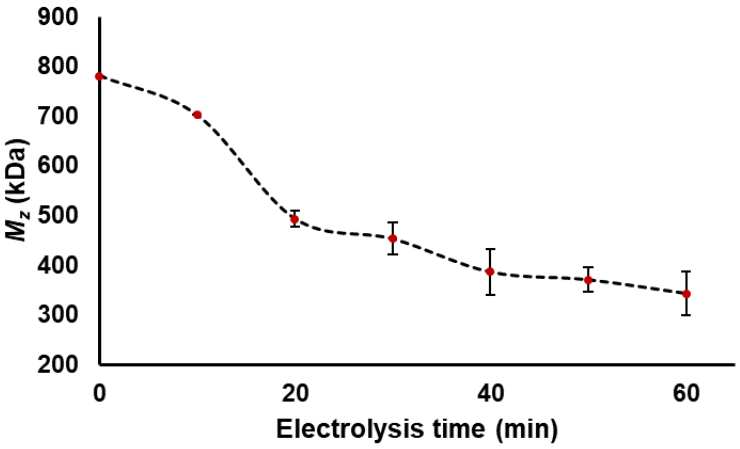


Figure 5.34. M_z (determined by triple detection SEC) as function of electrolysis time during the electrochemical degradation of **5.1**.

Table 5.3. Kinetic study for the electrochemical degradation of **5.1**.

Entry	Electrolysis time (min)	M_n[a] (kDa)	M_z[a] (kDa)
1	0	366	781
2	10	264±14	702±0
3	20	132±34	471±16
4	30	113±73	419±32
5	40	115±39	386±45
6	50	110±43	378±24
7	60	79±65	279±44

*Electrolysis of a Low M_n sample of **5.1***

A 10 mL ElectraSyn vial was charged with low M_n **5.1** (27.1 mg; 0.29 mmol; 5,300 Da; 1.3 Đ), a Teflon stir bar, and DCM (4.9 mL). The mixture was stirred until all polymer was dissolved, and $N(Bu)_4BF_4$ (146 mg; 0.44 mmol) was added. An ElectraSyn shroud was equipped with graphite/zinc (anode/cathode) electrodes and screwed onto the vial. The mixture was electrolyzed using the "Constant Potential" setting at 2.5 V for 1 h. Following electrolysis, the mixture was filtered through neutral alumina and concentrated to minimal volume. Polymeric material was isolated in 83% yield by mass recovery. SEC data before and after electrolysis are shown in Figure 5.35. ^{1}H NMR spectra before and after electrolysis are shown in Figure 5.55. MALDI-TOF analysis of the material isolated following electrolysis is shown in Figure 5.76. End group analysis of MALDI-TOF data was consistent with vinyl and phenyl groups (104 Da), as expected for ROMP polynorbornene synthesized with Grubbs 3rd generation catalyst. The MALDI-TOF signals are separated by an average of 94 Da, which is consistent with the expected repeating unit from ROMP of norbornene. The absence of other repeating units suggests that minimal addition of oxygen or water occurred during the electrolysis.

Experiments to Probe the Scope of Electrochemical Polymer Degradation

Electrochemical Degradation of cis-1,4-Polybutadiene

A 10 mL ElectraSyn vial was charged with *cis*-1,4-polybutadiene (25.1 mg; 0.465 mmol), a Teflon stir bar, and DCM (9.8 mL). The mixture was stirred until all polymer was dissolved, and $N(Bu)_4BF_4$ (229 mg; 0.695 mmol) was added. An ElectraSyn electrode shroud was equipped with electrodes (graphite anode/zinc cathode) and screwed onto the vial. The solution was electrolyzed using the "Constant Potential" setting at 2.5 V for 16 h. At this point, an aliquot (0.1 mL) was removed for analysis by SEC (Figure 5.8). The reaction mixture was filtered over a plug of silica and concentrated to dryness. The material was then washed with MeOH (2 x 10 mL) and dried for 16 h in vacuo to afford 13.1 mg of colorless solid (52% yield by recovered mass). Representative ^{1}H and ^{13}C NMR spectra are shown in Figure 5.56 and Figure 5.57, respectively.

Electrochemical Degradation of cis-1,4-Polyisoprene

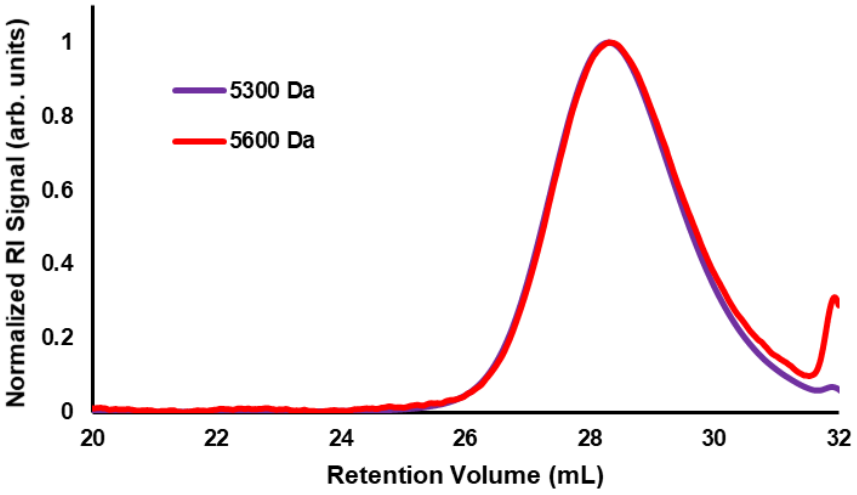


Figure 5.35. SEC data from conventional calibration before (purple) and after (red) electrolysis of low M_n **5.1**.

A 5 mL ElectraSyn vial was charged with *cis*-1,4-polyisoprene (21.3 mg; 0.313 mmol), a Teflon stir bar, and DCM (4.7 mL). The mixture was stirred until all polymer was dissolved, and $N(Bu)_4BF_4$ (154 mg; 0.468 mmol) was added. An ElectraSyn electrode shroud was equipped with electrodes (graphite anode/zinc cathode) and screwed onto the vial. The solution was electrolyzed using the "Constant Potential" setting at 2.5 V for 1 h. At this point, an aliquot (0.1 mL) was removed for analysis by SEC (Figure 5.7). The reaction mixture was filtered over a silica plug and concentrated to dryness. The material was then washed with MeOH (2 x 10 mL) and dried for 16 h in vacuo to afford 17.5 mg of colorless solid (82% yield by recovered mass). Representative ^{1}H and ^{13}C NMR spectra are shown in Figure 5.58 and Figure 5.59, respectively.

Electrochemical Degradation of Poly(cyclooctene)

A 5 mL ElectraSyn vial was charged with a 10 mg/ml solution of poly(cyclooctene) (25 mg; 0.227 mmol) in $CHCl_3$, a Teflon stir bar, and $N(Bu)_4BF_4$ (112 mg; 0.340 mmol). An ElectraSyn electrode shroud was equipped with electrodes (graphite anode/zinc cathode) and screwed onto the vial. The solution was electrolyzed using the "Constant Potential" setting at 3.2 V for 16 h. At this point, an aliquot (0.1 mL) was removed for analysis by SEC (Figure 5.9). The reaction mixture was concentrated to minimal volume, polymeric material was isolated by centrifugation following precipitation from MeOH. The material was then washed with MeOH (2 x 10 mL) and dried for 16 h in vacuo to afford 22.8 mg of colorless solid (91% yield by recovered mass). Representative ^{1}H and ^{13}C NMR spectra are shown in Figure 5.60 and Figure 5.61, respectively.

*Experimental Procedure for Selective Electrochemical Degradation of **5.1** in the Presence of Polystyrene*

A 5 mL ElectraSyn vial was charged with **5.1** (10 mg; 0.11 mmol), polystyrene (10 mg; 0.10 mmol), a Teflon stir bar, and DCM (3 mL). The mixture was stirred until all polymers were dissolved, and $N(Bu)_4BF_4$ (54 mg; 0.17 mmol) was added. An ElectraSyn electrode shroud was equipped with electrodes (graphite anode/zinc cathode) and screwed onto the vial. Prior to electrolysis, a 0.2 mL aliquot was removed via syringe and diluted to 1.0 mL with THF before being analyzed by SEC. The solution was electrolyzed using the "Constant Potential" setting

at 2.5 V for 2 h. Following electrolysis, a 0.2 mL aliquot was removed via syringe and diluted to 1.0 mL with THF for SEC analysis. SEC RI data before and after electrolysis are shown in Figure 5.10, and UV-visualization of this data is shown in Figure 5.11.

Experiments to Confirm Radical Cation Formation

*Electrochemical Degradation of **5.1** in the Presence of 9,10-Dihydroanthracene (DHA)*

A 10 mL ElectraSyn vial was charged with **5.1** (20 mg; 0.21 mmol), a Teflon stir bar, and DCM (8.8 mL). The mixture was stirred until all polymer was dissolved prior to the addition of $N(Bu)_4BF_4$ (105 mg; 0.32 mmol) and DHA (383 mg; 2.1 mmol). An ElectraSyn electrode shroud was equipped with electrodes (graphite anode/zinc cathode) and screwed onto the vial. The solution was electrolyzed using the "Constant Potential" setting at 2.5 V for 1 h. A 0.2 mL aliquot was removed via syringe every 10 minutes and diluted to 1.0 mL with THF for SEC analysis (Figure 5.36). The calculated rate of scission in the presence of DHA (5.65×10^{-7} min^{-1}) was found to be significantly slower than in the absence of DHA (2.35×10^{-6} min^{-1}). Overlayed rates of cleavage, evolution of M_n, and evolution of M_z over time are shown in Figure 5.36-Figure 5.38 and Table 5.4.

Control Experiment: Electrolysis of DHA in the Absence of Polymer

A 10 mL ElectraSyn vial was charged with $N(Bu)_4BF_4$ (105 mg; 0.32 mmol), DHA (383 mg; 2.1 mmol), a Teflon stir bar, and DCM (8.8 mL). An ElectraSyn electrode shroud was equipped with electrodes (graphite/zinc) and screwed onto the vial. The solution was electrolyzed using the "Constant Potential" setting at 2.5 V for 1 h. Following electrolysis, the solution was passed through a plug of silica twice and concentrated to dryness. The recovered solid (96% yield by recovered mass) was analyzed by ^1H NMR spectroscopy (Figure 5.62).

*Photoredox-Mediated Degradation of **5.1***

A 2-dram vial equipped with septum cap was charged with **5.1** (14.2 mg; 0.150 mmol), 9-mesityl-10-methylacridinium tetrafluoroborate (PC; 3 mg; 0.0075 mmol), DCM (0.9 mL), and thiophenol (0.23 mL; 0.03 mmol; 0.13 M in DCM). The mixture was stirred until all polymer was dissolved and then degassed via three freeze-pump-thaw cycles. The reaction mixture

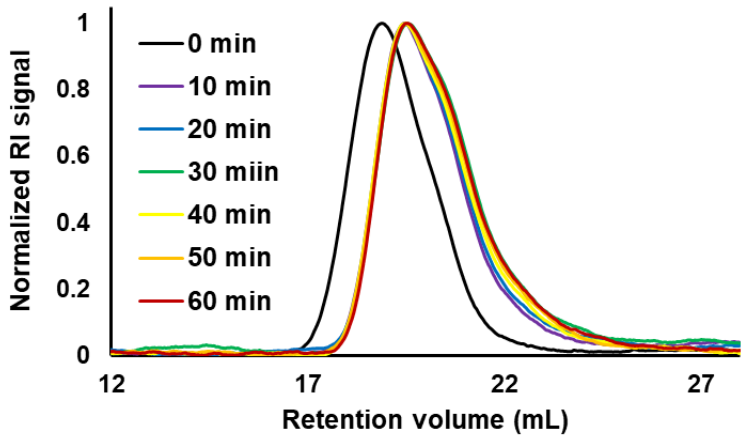


Figure 5.36. SEC data from triple detection showing the evolution of molecular weight as a function of electrolysis time for the electrochemical degradation of **5.1** in the presence of DHA.

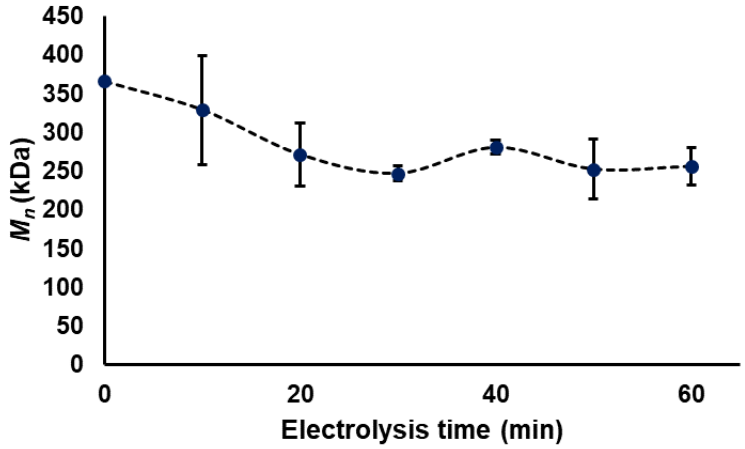


Figure 5.37. M_n (determined by triple detection SEC) as a function of electrolysis time for the electrochemical degradation of **5.1** in the presence of DHA.

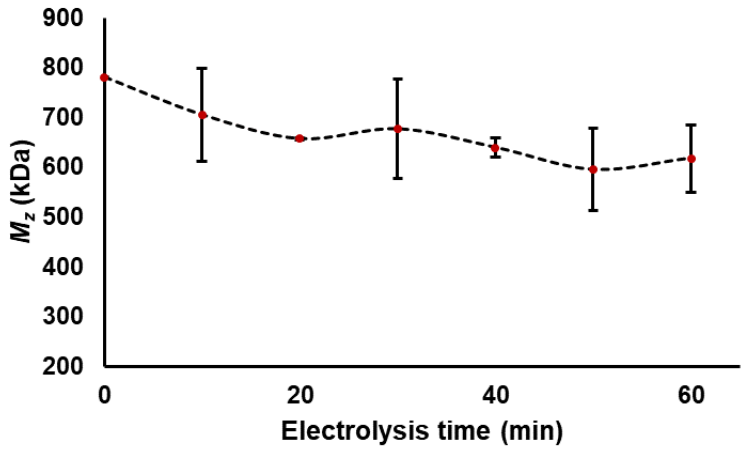


Figure 5.38. M_z (determined by triple detection SEC) as a function of electrolysis time for the electrochemical degradation of **5.1** in the presence of DHA.

Table 5.4. Kinetic data for electrochemical degradation of **5.1** in the presence of DHA.

Entry	Electrolysis time (min)	M_n[a] (kDa)	M_z[a] (kDa)
1	0	366	781
2	10	329±53	705±94
3	20	272±61	657±2.7
4	30	247±41	677±100
5	40	281±18	639±20
6	50	253±40	595±82
7	60	256±17	618±68

[a]Average of two experiments.

was irradiated at 450 nm with stirring for 1 h, after which point the mixture was filtered through a pad of silica and concentrated to minimal volume. Polymeric material was precipitated from MeOH, the mother liquor was decanted, and the remaining solid was washed with MeOH (2 x 10 mL). This material was dried in vacuo for 16 h prior to ^{1}H NMR spectral (Figure 5.63) and SEC (Figure 5.6) analysis.

Experiments Related to Electrochemical Degradations of Heterogenous Samples of 5.1

Heterogenous Electrochemical Degradation of ***5.1***

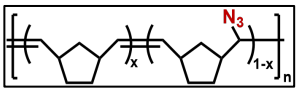
A 5 mL ElectraSyn vial was charged with **5.1** (10 mg; 0.11 mmol), a Teflon stir bar, $N(Bu)_4BF_4$ (54 mg; 0.17 mmol), and acetonitrile (MeCN; 3 mL). An ElectraSyn electrode shroud was equipped with electrodes (graphite anode/zinc cathode) and screwed onto the vial. The suspension was electrolyzed using the "Constant Potential" setting at 3.2 V for 16 hours, at which point a piece of undissolved polymer was removed from the vial and analyzed by SEC. The suspension was stirred further under 3.2 V for another 47 h (total electrolysis time 63 h), at which point the electrolyzed solid was collected by filtration and analyzed using SEC. The bulk solution temperature was monitored using a thermometer, and the observed temperature did not exceed 23 °C. SEC data are shown in Figure 5.12.

Confirmation of Heterogenous Conditions by NMR Spectroscopy

A 5 mL ElectraSyn vial was charged with **5.1** (10 mg; 0.11 mmol), a Teflon stir bar, $N(Bu)_4BF_4$ (54 mg; 0.17 mmol), and CD_3CN (3 mL). A 0.6 mL aliquot of the liquid was removed and analyzed by ^{1}H NMR spectroscopy, and an ElectraSyn electrode shroud equipped with electrodes (graphite anode/zinc cathode) was screwed onto the vial. The mixture was stirred for 63 h at 23 °C without any applied potential. At this point, another 0.6 mL aliquot of the liquid was removed and analyzed by ^{1}H NMR spectroscopy. No proton resonances consistent with **1** were observed in either aliquot (Figure 5.13).

Experiments Related to Electrochemical Polymer Azidation

*Electrochemical Azidation of **5.1***



Using conditions adapted from Lin and coworkers,[61] a 10 mL ElectraSyn vial was charged with **5.1** (20 mg; 0.21 mmol), a Teflon stir bar, and DCM (4.8 mL). The mixture was stirred until all polymer was dissolved, and $N(Bu)_4BF_4$ (104.9 mg; 0.32 mmol) and $MnBr_2$ (9.2 mg; 0.04 mmol) were added. An ElectraSyn shroud was equipped with electrodes (RVC anode/platinum cathode) and screwed onto the vial. The vial was wrapped with foil, and TMS-N_3 (0.2 mL; 1.49 mmol) was added via syringe. The mixture was electrolyzed using the "Constant Potential" setting at 3.2 V for 1 h. Five identical reactions were run in parallel and combined prior to workup. Following electrolysis, the mixture was filtered through a pad of neutral alumina and concentrated to minimal volume. Polymeric material was precipitated from MeOH. Isolated material was dried in vacuo for 16 h to afford 87 mg (87% yield by recovered mass) of the azidated polynorbornene (**5.2**). Proper care should be taken to ensure all electrodes are cleaned prior to use, as improper cleaning can lead to variable results.[73,74] Representative IR spectra before and after azidation are shown in Figure 5.22. Representative SEC data before and after azidation is shown in Figure 5.39 and Figure 5.40. Representative ^1H and ^{13}C NMR spectra are shown in Figure 5.64 and Figure 5.65, respectively.

*Control Experiment: Azidation of **5.1** without Applied Potential*

A 10 mL ElectraSyn vial was charged with **5.1** (10 mg; 0.11 mmol), a Teflon stir bar, and DCM (2.8 mL). The mixture was stirred until all polymer was dissolved, and $N(Bu)_4BF_4$ (54 mg; 0.17 mmol) and $MnBr_2$ (4.3 mg; 0.02 mmol) were added. An ElectraSyn shroud was equipped with electrodes (graphite anode/zinc cathode) and screwed onto the vial. The vial was wrapped with foil, and TMS-N_3 (92 µL; 0.7 mmol) was added via syringe. The mixture was stirred without any applied potential for 30 min, and the mixture was then filtered through a pad of neutral alumina and concentrated to minimal volume. Polymeric material was precipitated from MeOH and isolated by centrifugation. The recovered polymer was washed with MeOH (3 x 10 mL) before being dried in vacuo for 16 h. A very weak N_3 stretch in the IR spectrum (2160-2120 cm^{-1}; Figure 5.14) suggested that azidation occurs as a background process in the

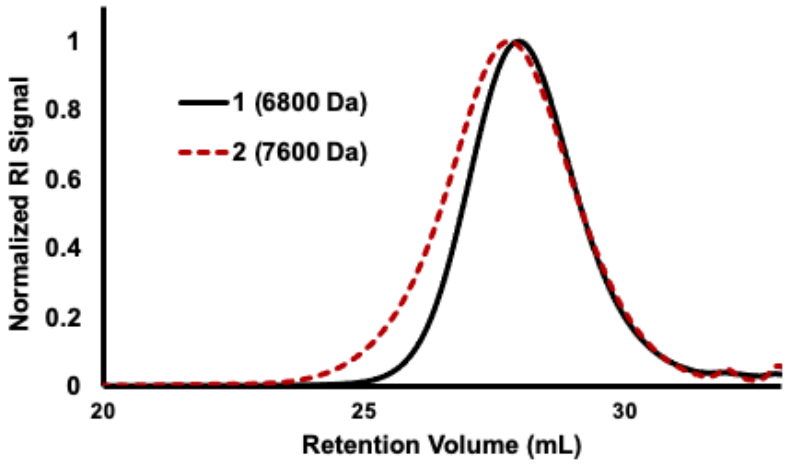


Figure 5.39. SEC data from conventional calibration for a low M_n sample of **5.1** before (black) and after (red) electrochemical azidation.

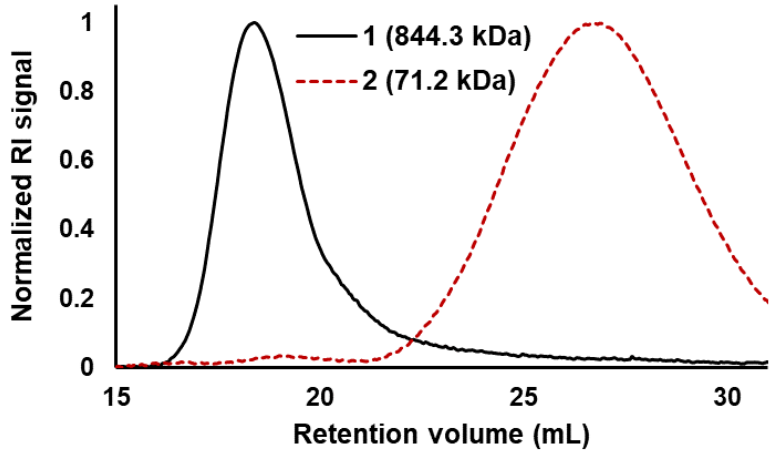


Figure 5.40. SEC data from triple detection for a high M_n sample of **5.1** before (black) and after (red) electrochemical azidation.

presence of $MnBr_2$ with no applied potential. However, the intensity of the N_3 stretch was significantly increased with applied potential, consistent with the observations of Lin and coworkers.[61]

*Control Experiment: Azidation of **5.1** without $MnBr_2$*

A 10 mL ElectraSyn vial was charged with **5.1** (10 mg; 0.11 mmol), a Teflon stir bar, and DCM (2.8 mL). The mixture was stirred until all polymer was dissolved, and $N(Bu)_4BF_4$ (54 mg; 0.17 mmol) was added. An ElectraSyn shroud was equipped with electrodes (graphite anode/zinc cathode) and screwed onto vial. The vial was wrapped with foil, and TMS-N_3 (92 µL; 0.7 mmol) was added via syringe. The mixture was stirred using the "Constant Potential" setting at 3.2 V for 30 min at which point the mixture was filtered through a pad of neutral alumina and concentrated to minimal volume. Polymeric material was precipitated from MeOH and isolated by centrifugation. The recovered polymer was washed with MeOH (3 x 10 mL) before being dried in vacuo for 16 h. When compared to experiments conducted with $MnBr_2$, the N_3 stretch was noticeably weaker in the absence of $MnBr_2$ (Figure 5.14). As such, all following azidation experiments included $MnBr_2$.

*Electrochemical Azidation of **5.1** at Low (2.5 V) and High (3.2 V) Potentials*

A 10 mL ElectraSyn vial was charged with **5.1** (10 mg; 0.11 mmol), a Teflon stir bar, and DCM (2.8 mL). The mixture was stirred until all polymer was dissolved, and $N(Bu)_4BF_4$ (54 mg; 0.17 mmol) and $MnBr_2$ (4.3 mg; 0.02 mmol) were added. An ElectraSyn shroud was equipped with electrodes (graphite anode/platinum cathode) and screwed onto the vial. The vial was wrapped with foil, and TMS-N_3 (92 µL; 0.7 mmol) was added via syringe. The mixture was electrolyzed using the "Constant Potential" setting at either 2.5 V or 3.2 V for 30 min. Following electrolysis, the mixture was filtered through a pad of neutral alumina and concentrated to minimal volume. Polymeric material was precipitated from MeOH, isolated by centrifugation, and washed with MeOH (3 x 10 mL) before being dried in vacuo for 16 h. Regardless of potential, **5.2** was recovered as a white solid in > 95% yield (by recovered mass). As 3.2 V resulted in a stronger apparent N_3 stretch in the IR spectrum (Figure 5.41), this potential was used for all following azidation experiments.

*Electrochemical Azidation of **5.1** with Different Electrode Combinations*

A 5 mL ElectraSyn vial was charged with **5.1** (20 mg; 0.21 mmol), a Teflon stir bar, and DCM (4.9 mL). The mixture was stirred until all polymer was dissolved, and $N(Bu)_4BF_4$ (104.9 mg; 0.32 mmol) and $MnBr_2$ (9.1 mg; 0.04 mmol) were added. An ElectraSyn shroud was equipped with the desired electrode combination (see Table 5.1 for comprehensive list of electrode combinations) and screwed onto the vial. The vial was wrapped with foil, and TMS-N_3 (0.2 mL; 1.49 mmol) was added via syringe. The mixture was electrolyzed using the "Constant Potential" setting at 3.2 V for 1 h. Following electrolysis, the mixture was filtered through a pipet column of neutral alumina and concentrated to minimal volume. Polymeric material was precipitated from MeOH before being dried in vacuo for 16 h. In all cases, polymeric material was isolated in > 80% yield. IR spectra showing results of the electrode screen are provided in Figure 5.15.

Electrochemical Azidation of cis-1,4-Polybutadiene

A 5 mL ElectraSyn vial was charged with 1,4-polybutadiene (31.0 mg; 0.573 mmol), a Teflon stir bar, and DCM (3.1 mL). The mixture was stirred until all polymer was dissolved, and $N(Bu)_4BF_4$ (283 mg; 0.860 mmol) was added followed by $MnBr_2$ (23.6 mg; 0.115 mmol). An ElectraSyn electrode shroud was equipped with electrodes (RVC anode/platinum cathode) and screwed onto the vial. The vial was wrapped with foil, and TMS-N_3 (0.52 mL; 4.0 mmol) was added via syringe. The solution was electrolyzed using the "Constant Potential" setting at 3.2 V for 1 h. Following electrolysis, the mixture was filtered through a pipette column of neutral alumina and concentrated to minimal volume. Polymeric material was precipitated from MeOH, isolated by centrifugation, and washed with MeOH (3 x 10 mL) before being dried in vacuo for 1 h. The azidated polymeric material was isolated as a colorless solid in 63% yield. Representative IR spectra before and after azidation are shown in Figure 5.16. Representative SEC data before and after azidation are shown in Figure 5.17. Representative ^1H and ^{13}C NMR spectra are shown in Figure 5.66 and Figure 5.67, respectively.

Electrochemical Azidation of cis-1,4-Polyisoprene

A 5 mL ElectraSyn vial was charged with *cis*-1,4-polyisoprene (28.0 mg as a 10 mg/mL solution in $CHCl_3$; 0.411 mmol), and a Teflon stir bar. $N(Bu)_4BF_4$ (203 mg; 0.615 mmol) was

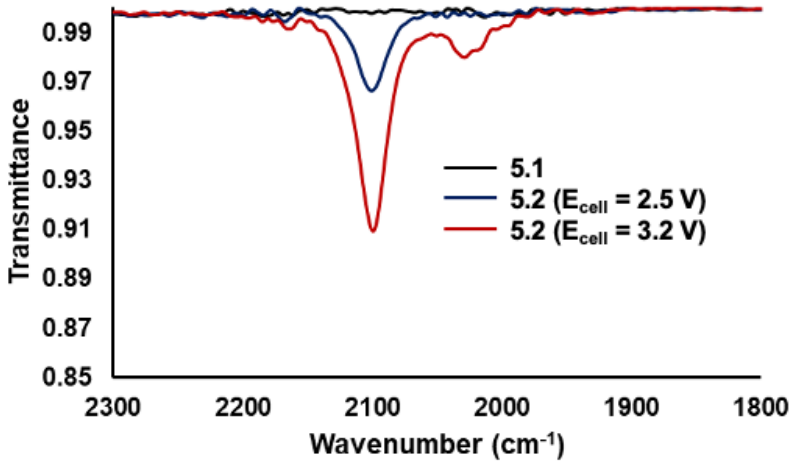


Figure 5.41. IR spectra for the electrochemical azidation of **5.1** at different potentials. Spectra for unfunctionalized **5.1** (black), material following azidation at 2.5 V (blue), and material following azidation at 3.2 V (red) are shown.

added followed by $MnBr_2$ (17.6 mg; 0.082 mmol). An ElectraSyn electrode shroud was equipped with electrodes (RVC anode/platinum cathode) and screwed onto the vial. The vial was wrapped with foil, and TMS-N_3 (0.38 mL, 2.88 mmol) was added via syringe. The solution was electrolyzed using the "Constant Potential" setting at 3.2 V for 1 h. Following electrolysis, the mixture was filtered through a pipette column of neutral alumina and concentrated to minimal volume. Polymeric material was precipitated from MeOH, isolated by centrifugation, and washed with MeOH (3 x 10 mL) before being dried in vacuo for 1 h. The azidated polymeric material was isolated as a pale-yellow solid in 92% yield. Representative IR spectra before and after azidation are shown in Figure 5.18. Representative SEC data before and after azidation are shown in Figure 5.19. Representative ^1H and ^{13}C NMR spectra are shown in Figure 5.68 and Figure 5.69, respectively.

Electrochemical Azidation of Poly(cyclooctene)

A 5 mL ElectraSyn vial was charged with poly(cyclooctene) (28.0 mg as a 10 mg/mL solution in $CHCl_3$; 0.254 mmol), and a Teflon stir bar. $N(Bu)_4BF_4$ (125 mg; 0.381 mmol) was added followed by $MnBr_2$ (10.9 mg; 0.051 mmol). An ElectraSyn electrode shroud was equipped with electrodes (RVC anode/platinum cathode) and screwed onto the vial. The vial was wrapped with foil, and TMS-N_3 (0.23 mL, 1.78 mmol) was added via syringe. The solution was electrolyzed using the "Constant Potential" setting at 3.2 V for 1 h. Following electrolysis, the mixture was filtered through a pipette column of neutral alumina and concentrated to minimal volume. Polymeric material was precipitated from MeOH, isolated by centrifugation, and washed with MeOH (3 x 10 mL) before being dried in vacuo for 1 h. The azidated polymeric material was isolated as a white solid in 98% yield. Representative IR spectra before and after azidation are shown in Figure 5.20. Representative SEC data before and after azidation are shown in Figure 5.21. Representative ^1H and ^{13}C NMR spectra are shown in Figure 5.70 and Figure 5.71, respectively.

Experiments to Estimate Degree of Azidation of 5.1

NMR Analysis of Low M_n Azidated Material

A low molecular weight sample (Mn = 6,800 Da) of **5.1** was azidated under the

electrochemical conditions described above (Scheme 5.3; note: a low molecular weight sample was used to facilitate NMR spectral analysis). Following filtration, washing, and drying as described above, the recovered sample of **5.2** was first analyzed by IR spectroscopy, which confirmed azidation had occurred. The material was then analyzed by ^{1}H NMR spectroscopy. A methylene resonance (δ = 1.35 ppm) on the cyclopentane ring of **5.1** was integrated relative to a new broad signal at δ = 3.84 ppm, which we assigned as the newly generated methine signal in the azidated repeat unit. These integrations were consistent with ~30% azidation (Scheme 5.3; Figure 5.72).

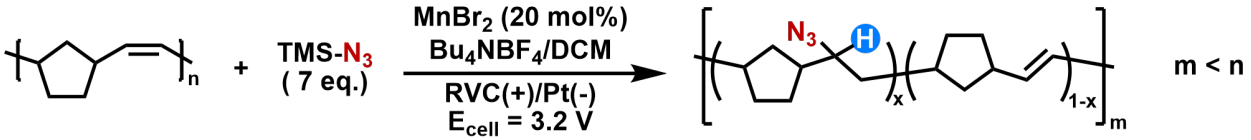
Cu-Mediated Cycloaddition for UV-vis Determination of Azide Content

A Schlenk tube was charged with **5.2** (34.9 mg, 0.37 mmol assuming unfunctionalized **5.1**), CuI (12.1 mg, 0.075 mmol), Me_6TREN (11.1 μL), 1-ethynyl pyrene (26.9 mg, 0.118 mmol), toluene (2.5 mL), and Teflon stir bar (Scheme 5.4). The solution was degassed via 3 cycles of freeze-pump-thaw and allowed to warm under N_2. The reaction was heated to 100 °C for 61 h. The reaction was then cooled to room temperature and transferred to a separatory funnel and washed with sat. NH_4Cl (2 X 3 mL) and the NH_4Cl layer was extracted with DCM (1 X 3 mL). The toluene layer was washed with brine (1 X 3 mL), and the organic layers were combined and concentrated to dryness. The residue was dissolved in minimal DCM and precipitated from acetone. The precipitated material (5.3) was isolated as a yellow solid following two rounds of ultra-centrifugation (9 mg; 26% mass recovery). 5.3 was analyzed by SEC, and visualization of the data using UV-detection at 350 nm (a λ_{max} of pyrene) was consistent with successful labeling (Figure 5.23B). We note that 5.2 showed no absorbance at this wavelength (Figure 5.23A). ^{1}H NMR spectroscopic analysis of 5.3 revealed new resonances (δ = 7.78 - 8.87) that were consistent with the desired pyrene labeling (Figure 5.75). Substituting the integration of these resonances into Equation 5.1 allowed us to estimate the total amount of pyrene per polymer chain (~24%). There is a one-to-one correspondence between pyrene content and the original azide content in **5.2**.

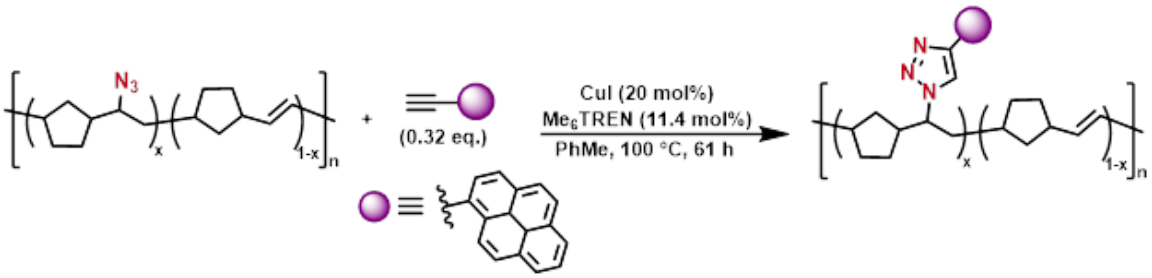
*Determination of % pyrene content in **5.3***

7.2 mg of **5.3** (M_n = 6065 Da) was dissolved in DCM (25 mL; 1.19 μM), and an aliquot (1 mL) of this solution was removed and diluted to 25 mL of DCM (1.9 μM). This solution was analyzed

Scheme 5.3. Azidation of **1** Under Optimized Conditions



Scheme 5.4. Cu-Mediated Cycloaddition Between **2** and Ethynyl Pyrene



by UV-vis spectroscopy (the absorbance was determined to be 0.330). The equation of the line from the pyrene calibration curve was used to determine the concentration of pyrene in solution (9.296 μM; Equation 5.8). The concentration of pyrene in solution was assumed to be the same as the concentration of pyrene repeat units in solution. Equation 5.9 was then used to determine the percentage of pyrene repeat units in **5.3** (29%).

Summary

In conclusion, we have developed a mild electrochemical approach toward backbone editing of olefin-containing polymers. Importantly, this strategy is chemoselective and can be conducted under heterogenous conditions. Furthermore, the reactive intermediates generated upon anodic oxidation can be intercepted using exogenous reagents to afford functionalized macromonomers. We envision that electroediting of a wide range of non-olefin containing substrates (e.g., polyolefins) should be possible when combined with catalytic dehydrogenation. We believe this work represents a new opportunity to explore electrochemistry as a viable strategy for polymer modification.

Appendix

Determination of Faradaic Efficiency

Faradaic efficiency for the reaction was determined according to literature precedent.[75] Current during the reaction was determined by analysis of a solution of NBu_4BF_4 in DCM (0.067 M) with a conductivity probe, and the conductivity was found to be 0.1680 Siemens meters^{-1} (S/m). This measurement was then converted to resistivity using Equation 5.2, and the current was found using Ohm's law (Equation 5.3).

According to our proposed mechanism, the theoretical number of electrons per cleavage = 1 (Z_p), and the theoretical number of moles of product (N_p) was assumed to be the same as the moles of substrate used for the reaction. These values were used to determine the theoretical charge (Q_{theo}) for the reaction (Equation 5.4). The experimental charge (Q_{exp}) for the reaction was determined using Equation 5.5. Both Q_{theo} and Q_{exp} were then used to determine Faradaic efficiency (Equation 5.6).

We determined the Faradaic efficiency for the azidation of polynorbornene to be 9.5%, and the faradaic efficiency for electrochemical degradation of olefin-containing polymers was determined to be 7.5% at 2.5 V or 9.5% at 3.2 V.

Equation 5.2. Relationship between conductivity and resistivity, where σ = conductivity in S/m and ρ = resistivity in ohms.

$$\boldsymbol{\sigma = \frac{1}{\rho}}$$

Equation 5.3. Ohm's law, where I = current in Amps seconds (A s), V = voltage, and ρ = resistivity in ohms.

$$\boldsymbol{I = \frac{V}{\rho}}$$

Equation 5.4. Theoretical charge, where Q_{theo} = theoretical charge passed through the reaction in Coulombs (C), Z_p = number of electrons used per product, N_p = theoretical mol of product, and F = Faraday's constant (96,485 A s mol^{-1})

$$\boldsymbol{Q_{theo} = Z_p \times N_p \times F}$$

Equation 5.5. Experimental charge, where Q_{exp} = experimental charge passed through the reaction, I = current in A s, and t = time in s.

$$\boldsymbol{Q_{exp} = I \times t}$$

Equation 5.6. Faradaic efficiency (n), where Q_{exp} = experimental charge passed through the reaction in C, and Q_{theo} = theoretical charge passed through the reaction in C.

$$\boldsymbol{n = \frac{Q_{exp}}{Q_{theo}} \times 100\%}$$

Equation 5.7. Determination of azide content by ^{1}H NMR spectroscopy for **5.2.** I_A is the integration of the azidated methine proton (δ = 3.73-4.01 ppm), I_X is the integration of a set of unfunctionalized methylene protons on the cyclopentane ring of polynorbornene (δ = 1.30-1.44 ppm), N_A is the theoretical maximum integration for the azidated methine proton (N_A = 1.0), and N_X is the theoretical maximum integration (N_X = 2.0) of a set of unfunctionalized methylene protons on the cyclopentane ring of polynorbornene.

$$\frac{\frac{\boldsymbol{I_A}}{\boldsymbol{I_X}} \cdot \frac{\boldsymbol{N_X}}{\boldsymbol{N_A}}}{\mathbf{1} + (\frac{\boldsymbol{I_A}}{\boldsymbol{I_X}} \cdot \frac{\boldsymbol{N_X}}{\boldsymbol{N_A}})}$$

Equation 5.8. Beer-Lambert's Law, where *c* is the concentration of pyrene in *μM*.

$$0.330 = 35545 \cdot 1 \cdot c \qquad c = 9.296\ \mu M$$

Equation 5.9. Conversion factors for determination of percentage of pyrene repeat units in **5.3**, where RU_{py} is pyrene repeat units.

$$\frac{9.296\ \mu mol\ RU_{py}}{1\ L\ DCM} \cdot \frac{1\ L\ DCM}{1.9\ \mu mol\ \mathbf{5.3}} \cdot \frac{365.2\ g\ RU_{py}}{1\ mol\ RU_{py}} \cdot \frac{1\ mol\ \mathbf{5.3}}{6065\ g\ \mathbf{5.3}} \cdot 100\% = 29\%\ RU_{py}$$

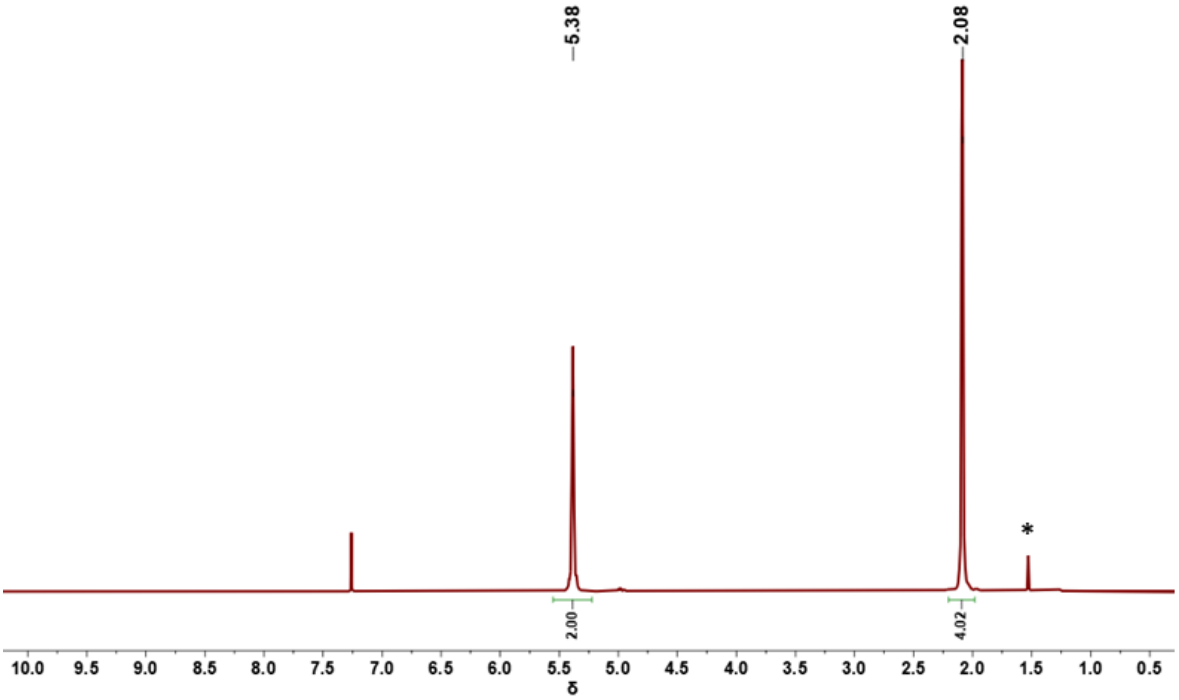


Figure 5.42. ^{1}H NMR spectrum for cis-1,4-polybutadiene in $CDCl_3$. Spectrum taken following filtration and reprecipitation. * denotes water

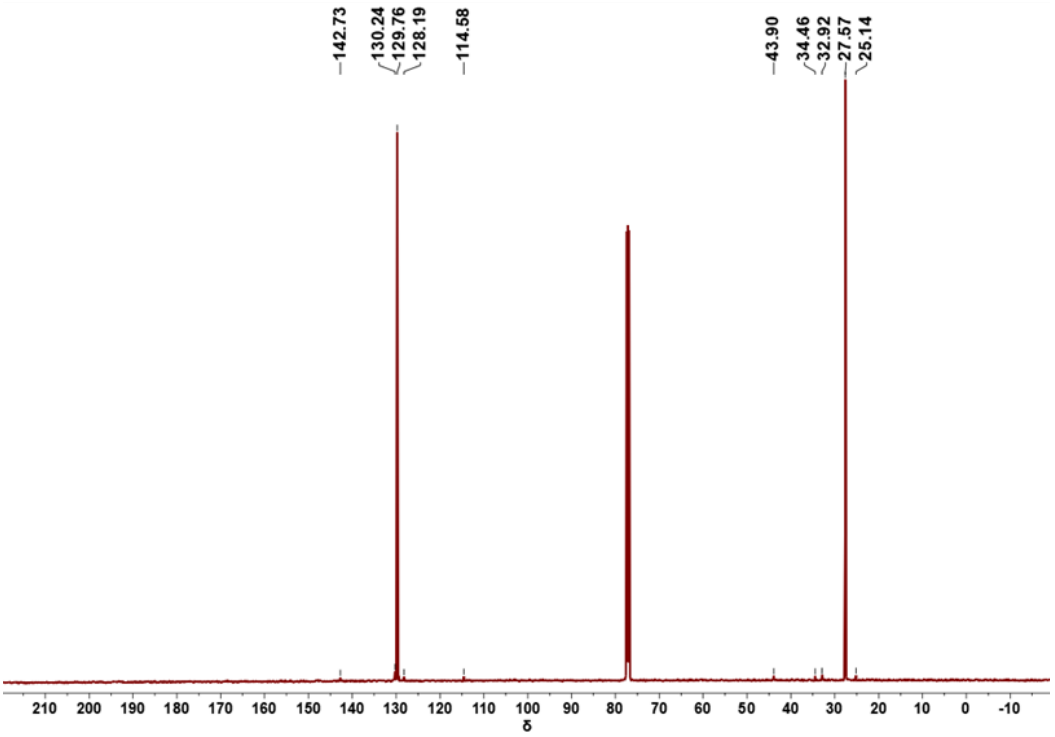


Figure 5.43. ^{13}C NMR spectrum for *cis*-1,4-polybutadiene in $CDCl_3$. Spectrum taken following filtration and reprecipitation

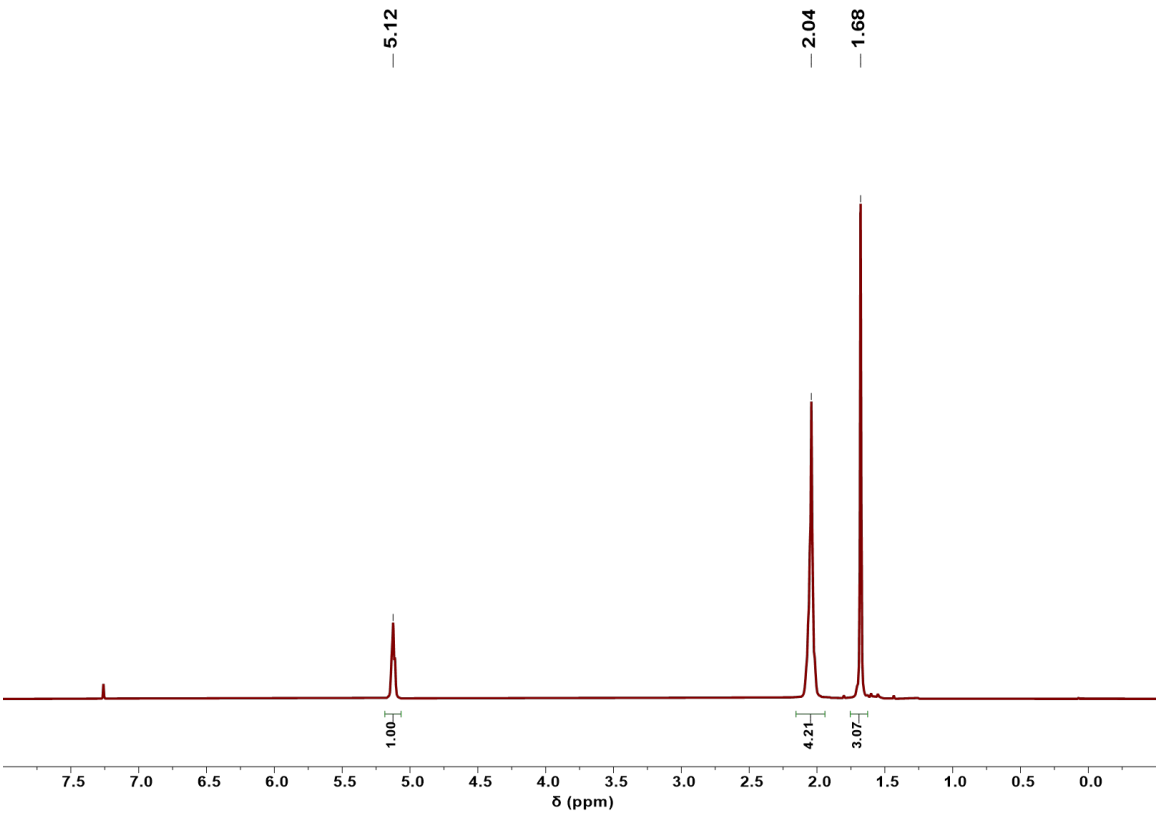


Figure 5.44. ^{1}H NMR spectrum for *cis*-1,4-polyisoprene in $CDCl_3$

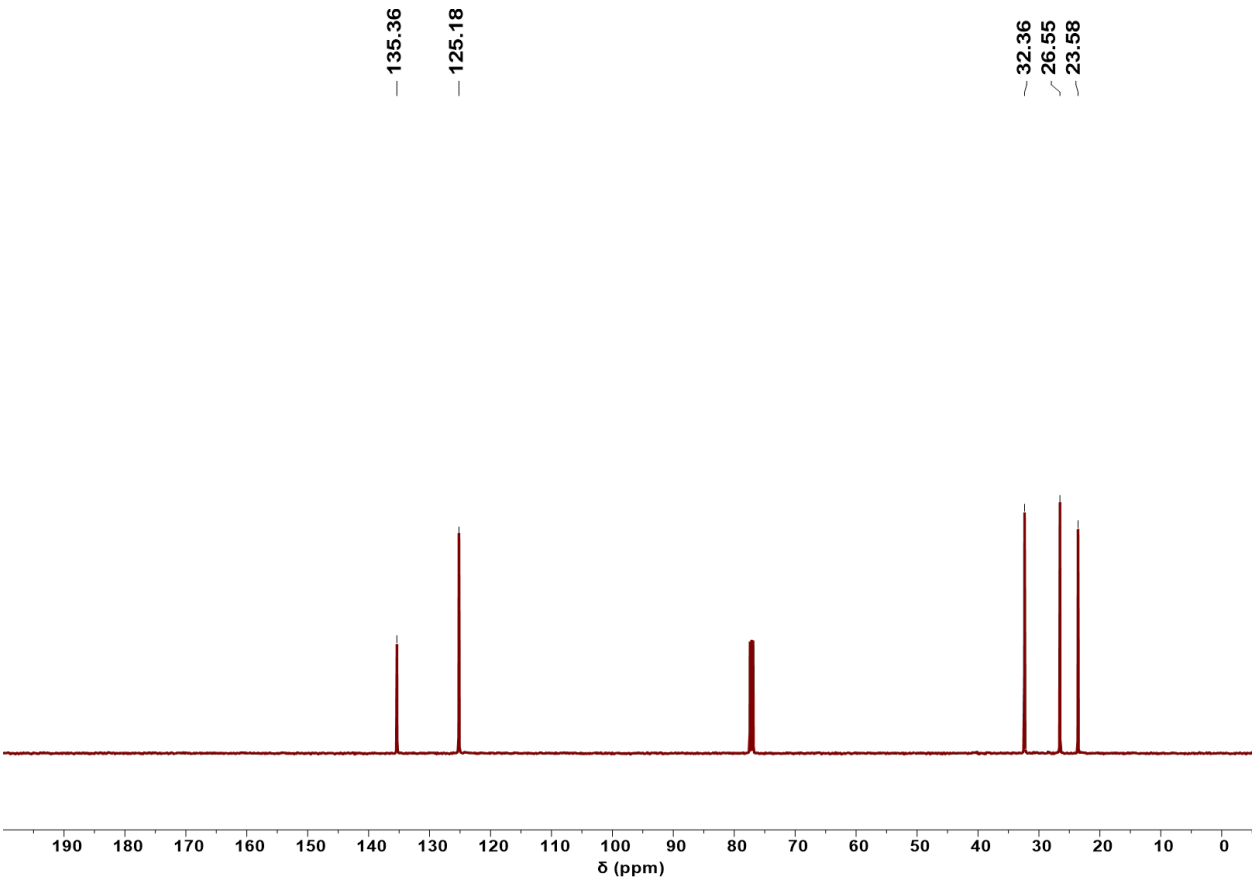


Figure 5.45. ^{13}C NMR spectrum for *cis*-1,4-polyisoprene in $CDCl_3$

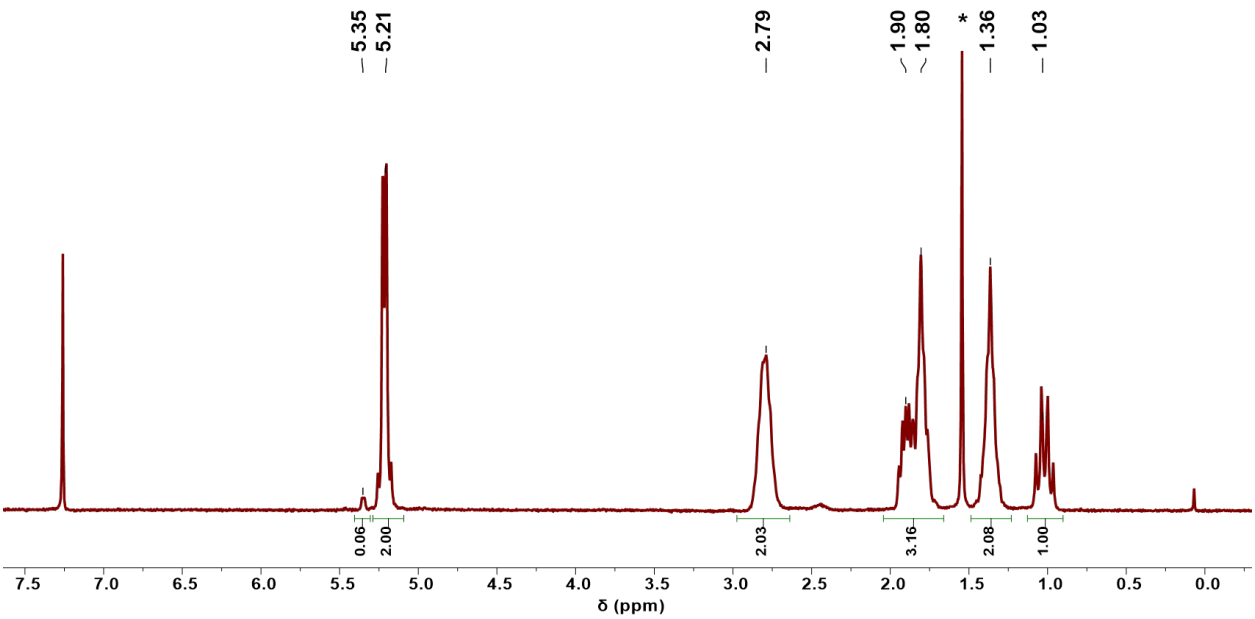


Figure 5.46. ^{1}H NMR spectrum of high-*cis* polynorbornene in $CDCl_3$. * denotes water.

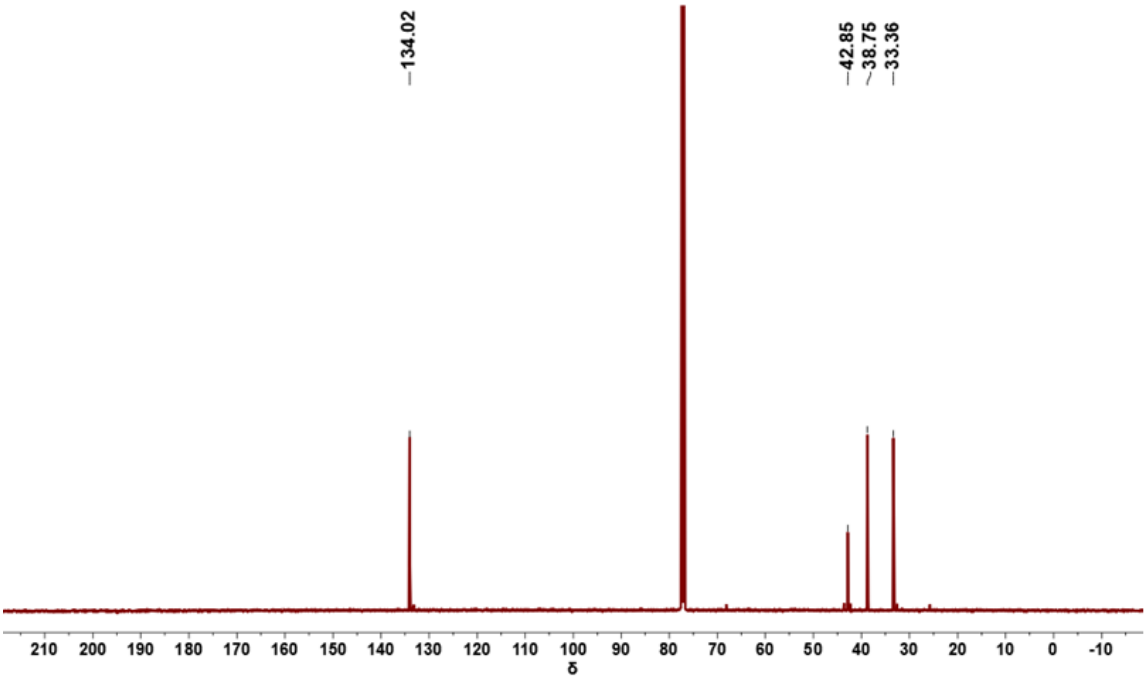


Figure 5.47. ^{13}C NMR spectrum of high-*cis* polynorbornene in $CDCl_3$.

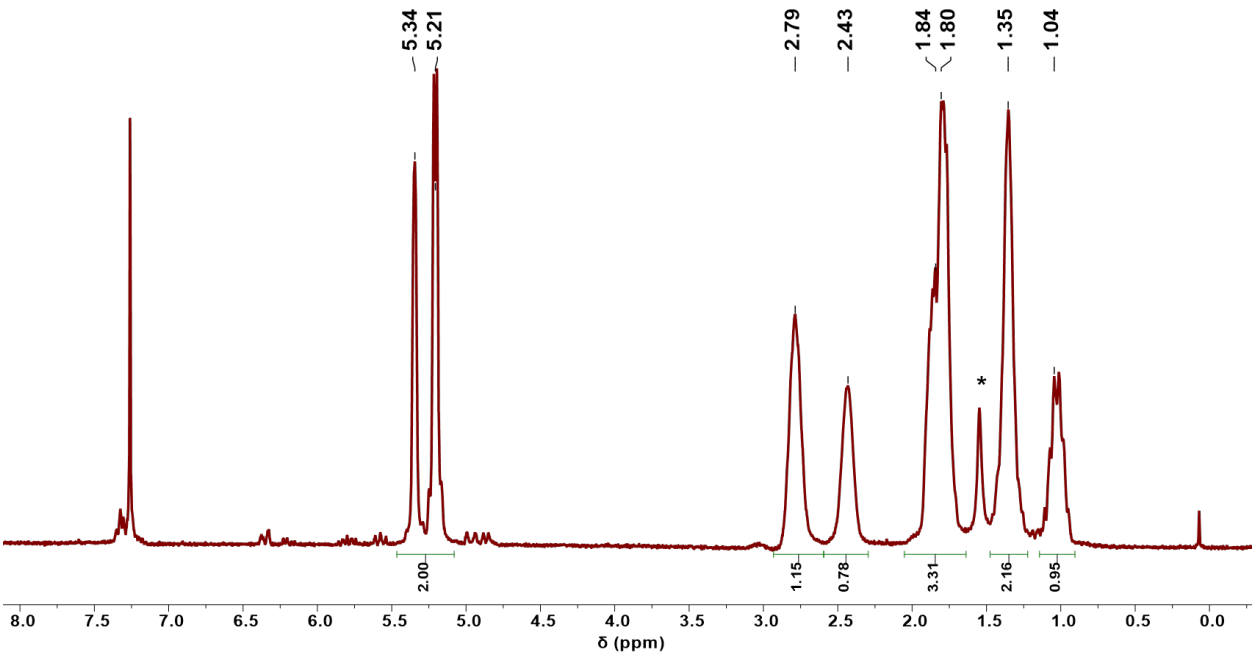


Figure 5.48. ^{1}H NMR spectrum for low M_n polynorbornene in $CDCl_3$. * denotes water.

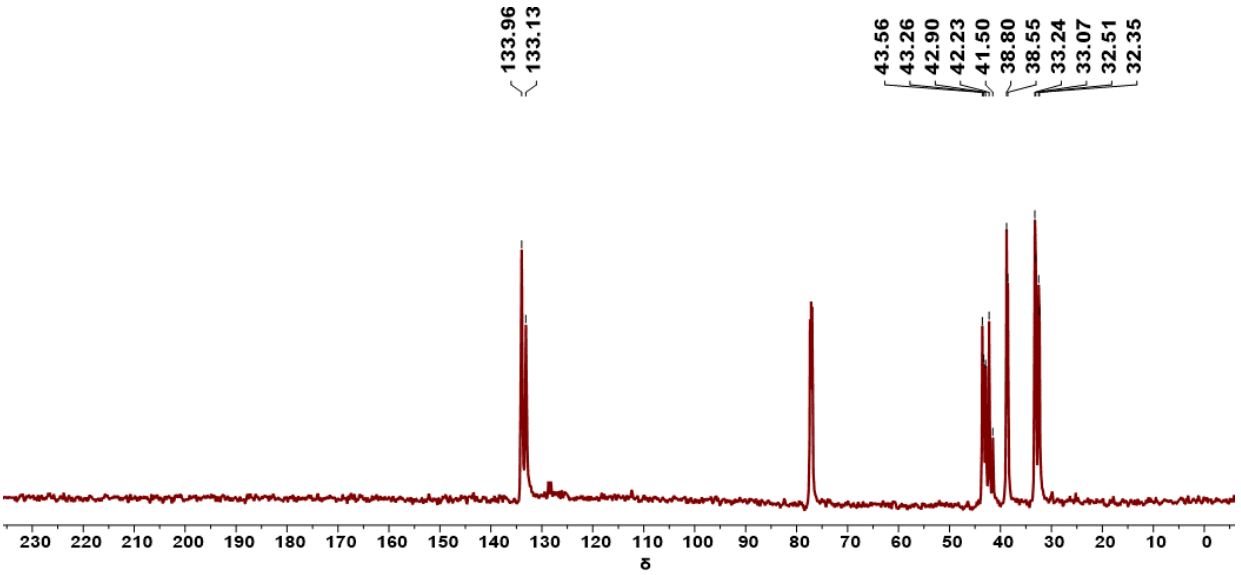


Figure 5.49. ^{13}C NMR spectrum for low M_n polynorbornene in $CDCl_3$.

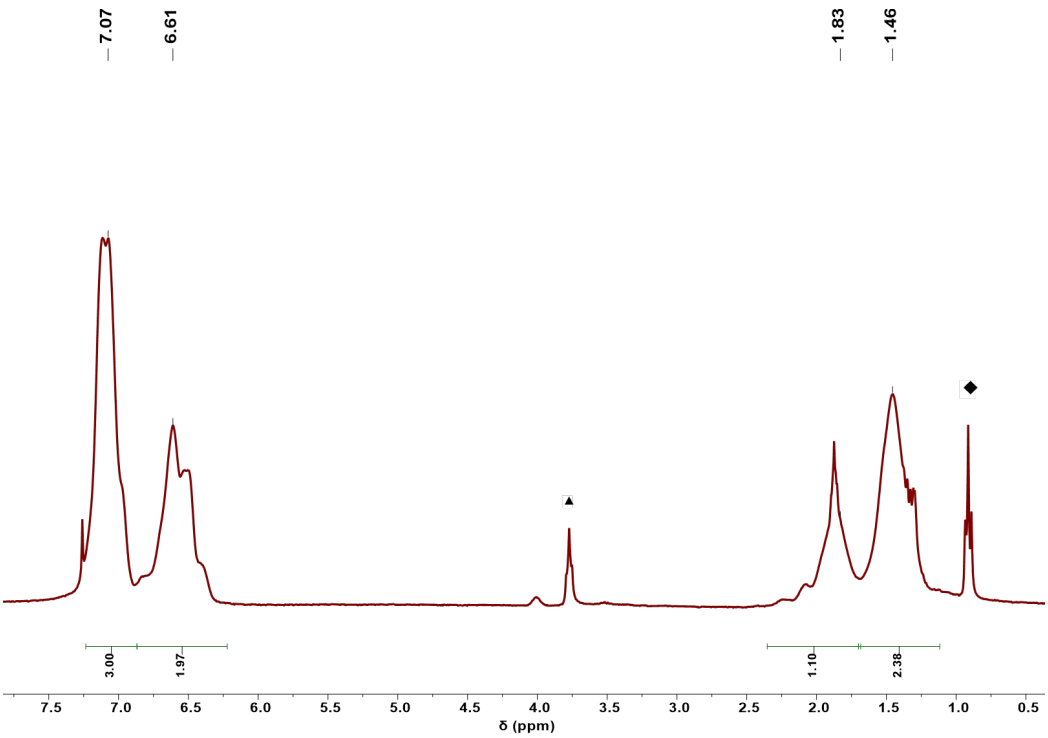


Figure 5.50. ^{1}H NMR spectrum for polystyrene in $CDCl_3$. ▲ denotes tetrahydrofuran and ◆ denotes grease

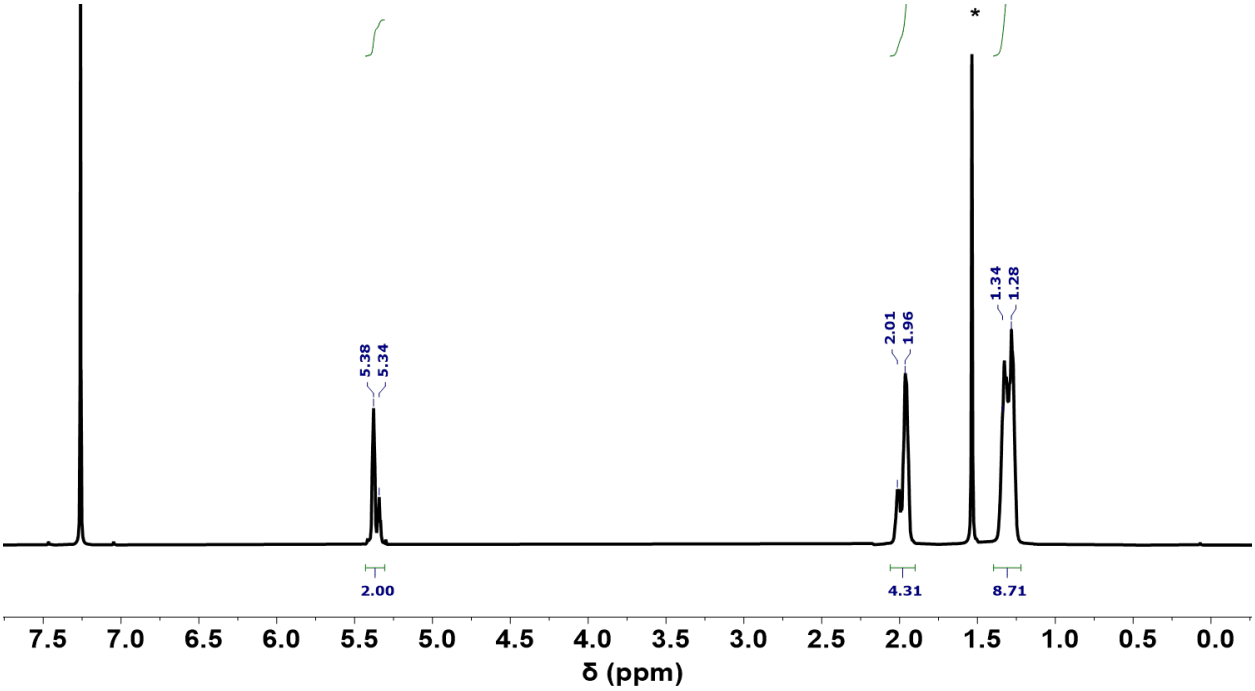


Figure 5.51. ^{1}H NMR spectrum for poly(cyclooctene) in $CDCl_3$. * denotes water

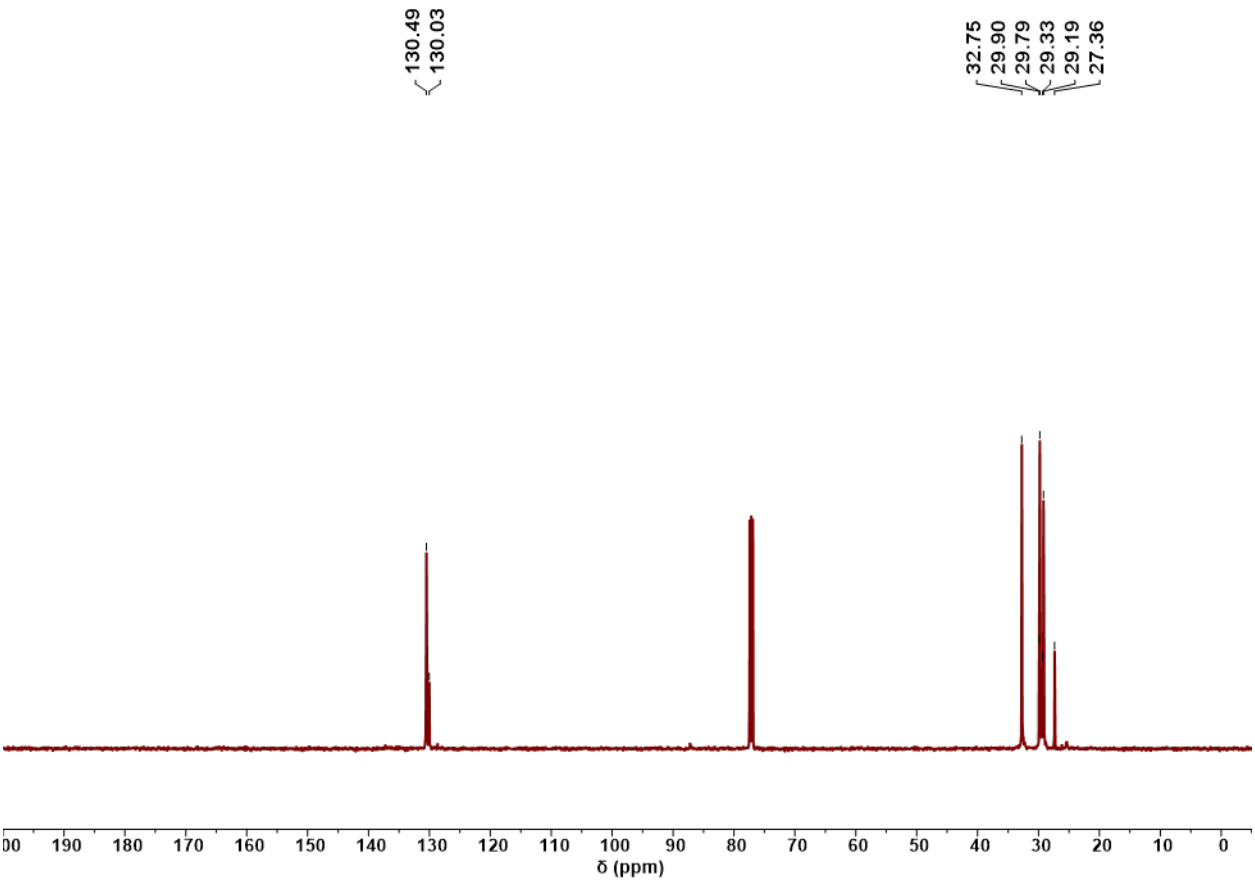


Figure 5.52. ^{13}C NMR spectrum for poly(cyclooctene) in $CDCl_3$.

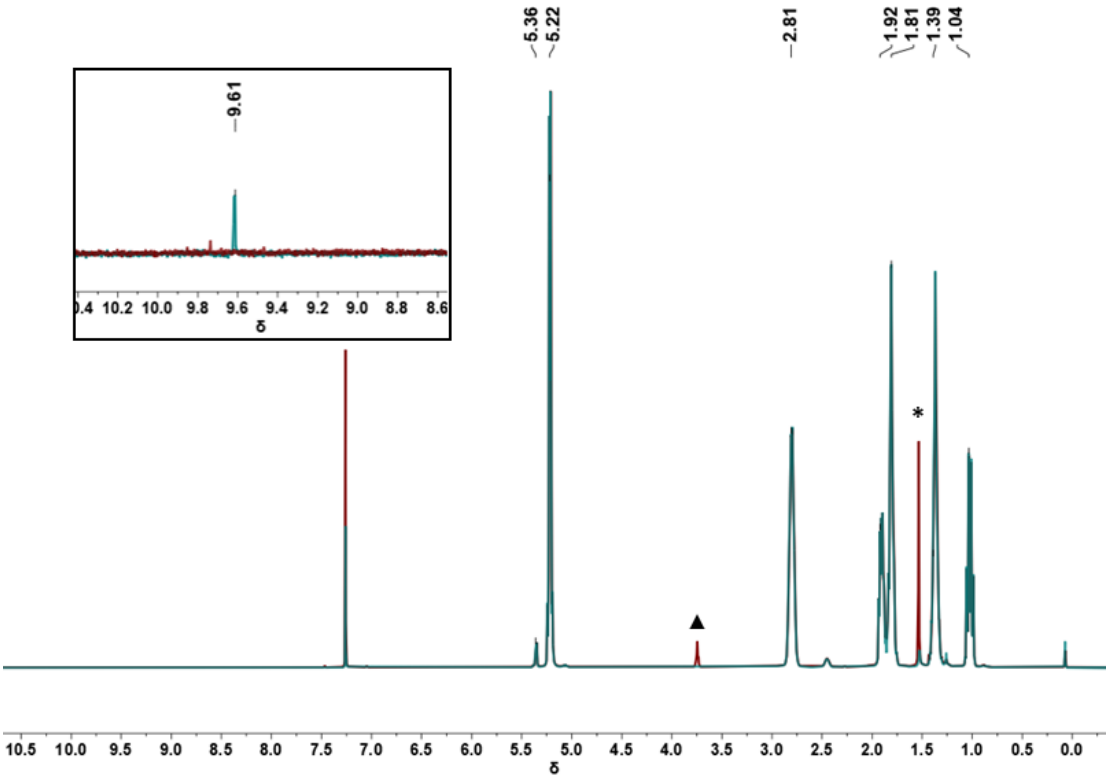


Figure 5.53. ^{1}H NMR overlay for **5.1** in $CDCl_3$ following electrolysis. Red shows material before electrolysis, and blue shows material after electrolysis. Inset contains enhanced baseline to show new aldehydic resonance in post-electrolysis material. * denotes water, and ▲ denotes THF.

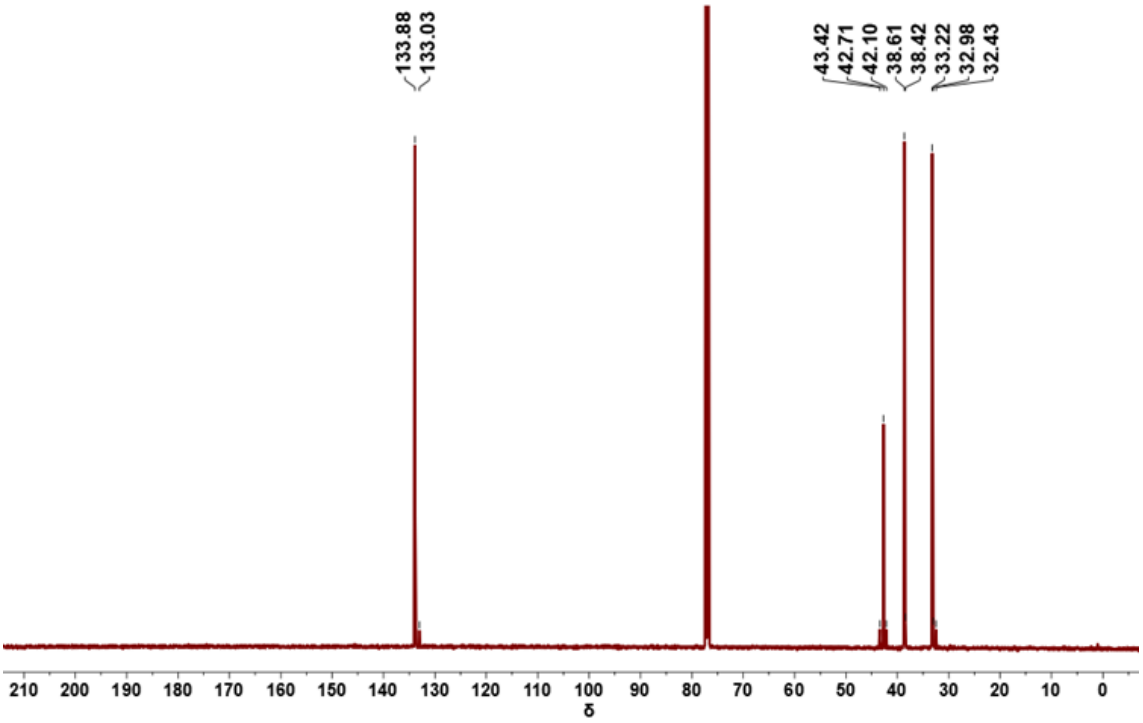


Figure 5.54. ^{13}C NMR spectrum for **5.1** in $CDCl_3$ following electrolysis.

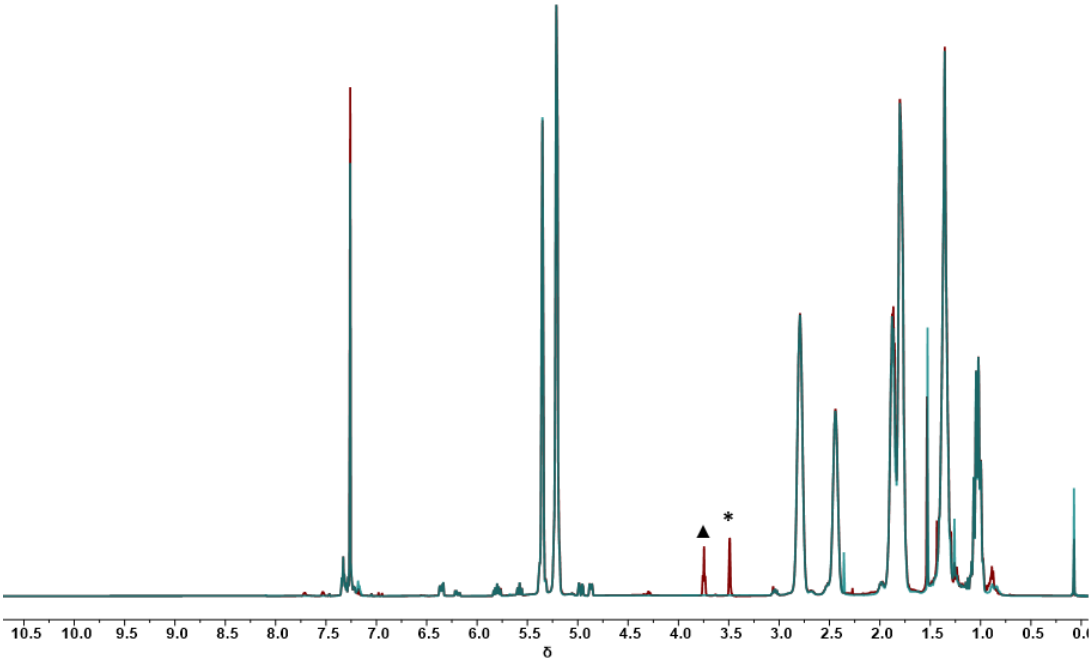


Figure 5.55. ^{1}H NMR overlay for a low M_n sample of **5.1** before (red) and after (blue) electrolysis. ▲ denotes THF and * denotes methanol

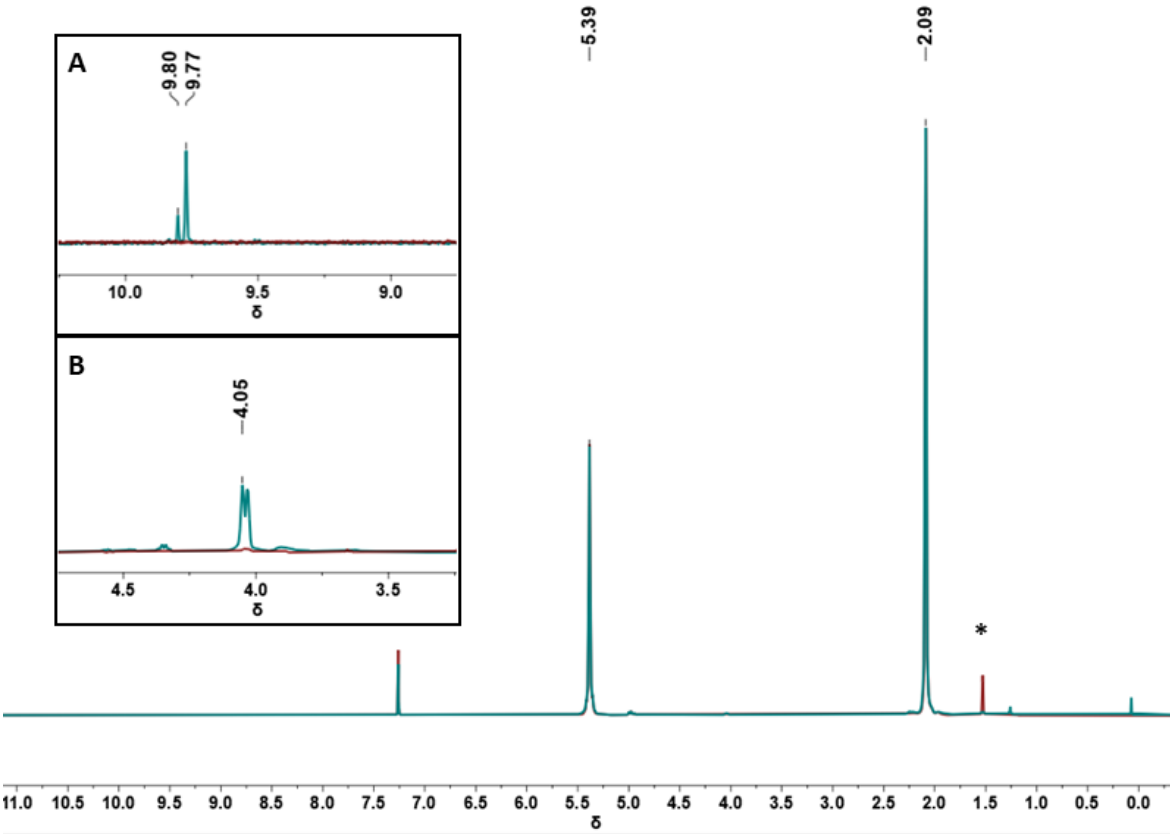


Figure 5.56. ^{1}H NMR overlay for *cis*-1,4-polybutadiene in $CDCl_3$ following electrolysis. Red shows material before electrolysis, and blue shows material after electrolysis. Insets contain enhanced baselines to show new aldehydic (A) and vinyl (B) resonances in post-electrolysis material. * denotes water

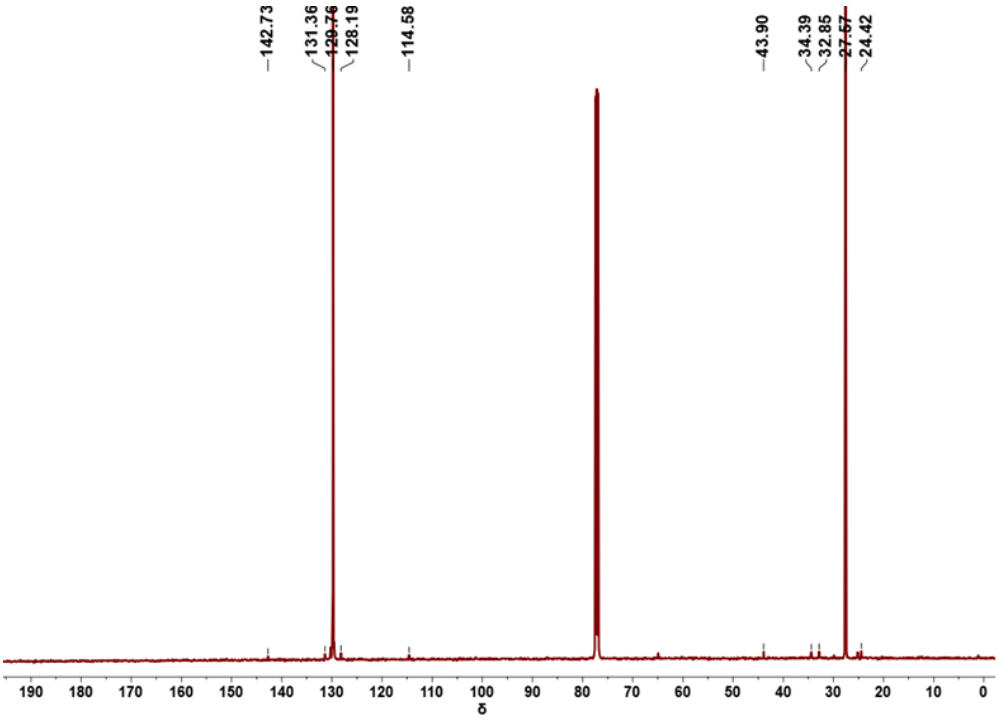


Figure 5.57. ^{13}C NMR spectrum for *cis*-1,4-polybutadiene in $CDCl_3$ following electrolysis.

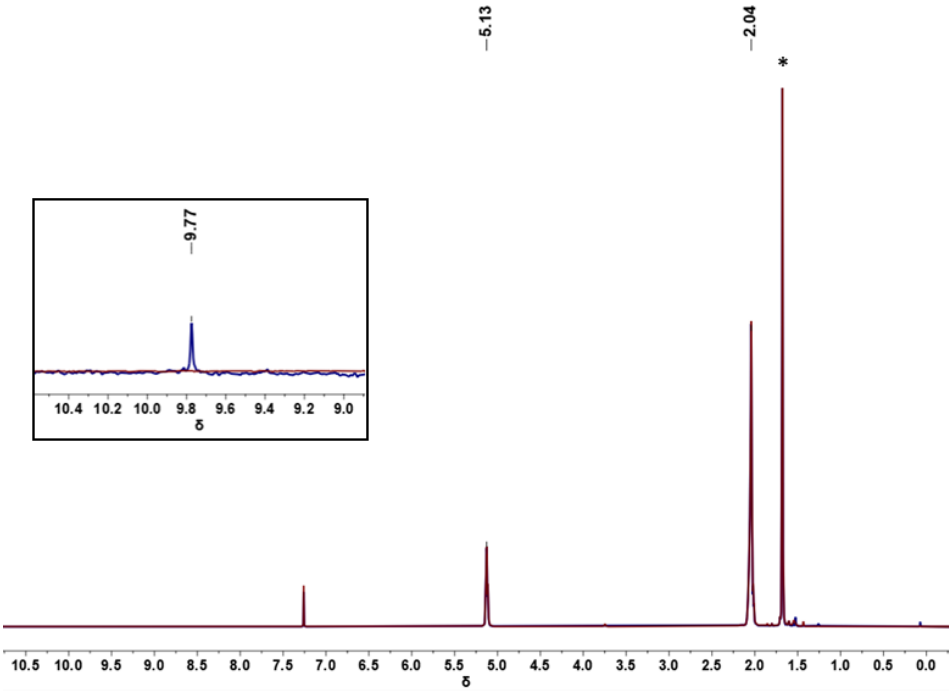


Figure 5.58. ^{1}H NMR overlay for *cis*-1,4-polyisoprene in $CDCl_3$ following electrolysis. Red shows material before electrolysis, and blue shows material after electrolysis. Inset contains enhanced baseline to show new aldehydic resonances in post-electrolysis material. * denotes water.

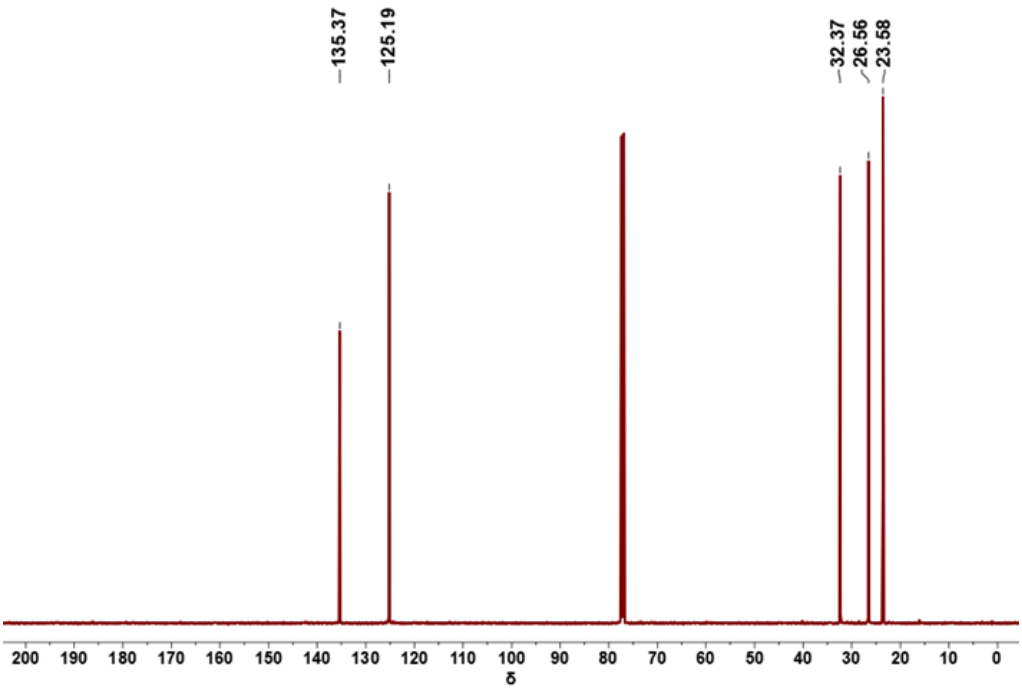


Figure 5.59. ^{13}C NMR spectrum for *cis*-1,4-polyisoprene in $CDCl_3$ following electrolysis.

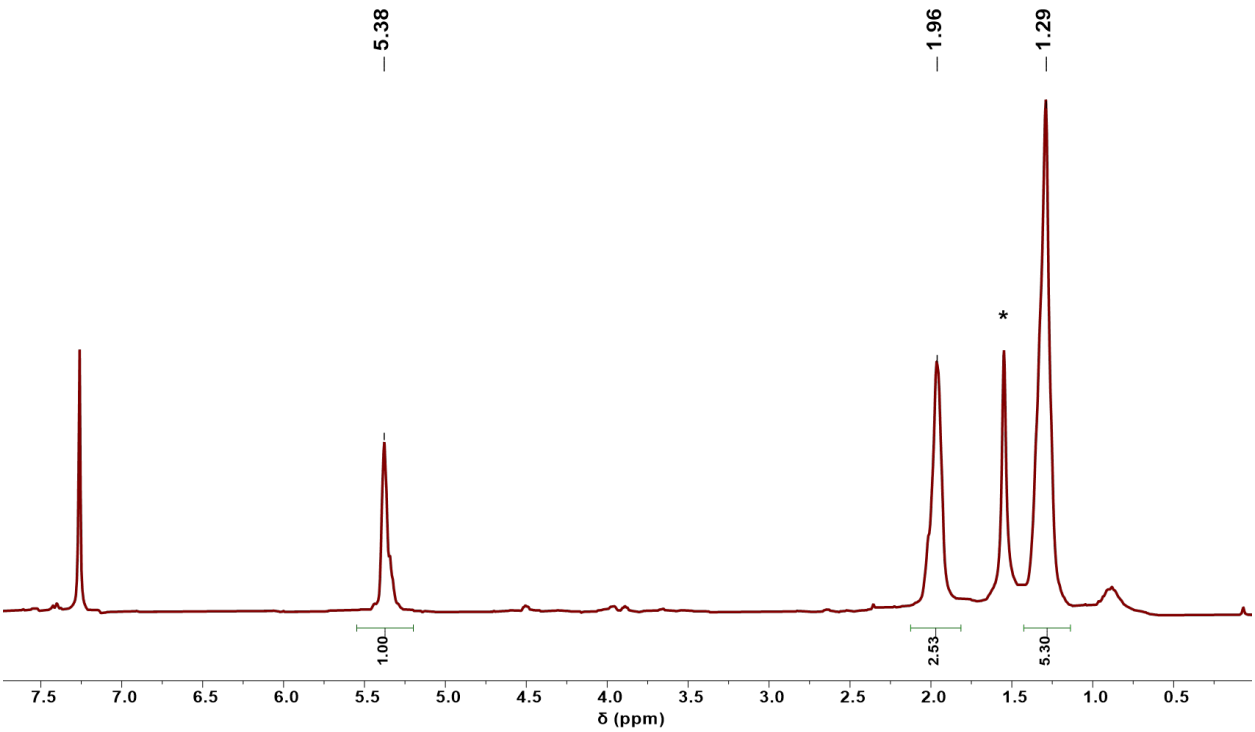


Figure 5.60. ^{1}H NMR spectrum for poly(cyclooctene) in $CDCl_3$ following electrolysis. * denotes water.

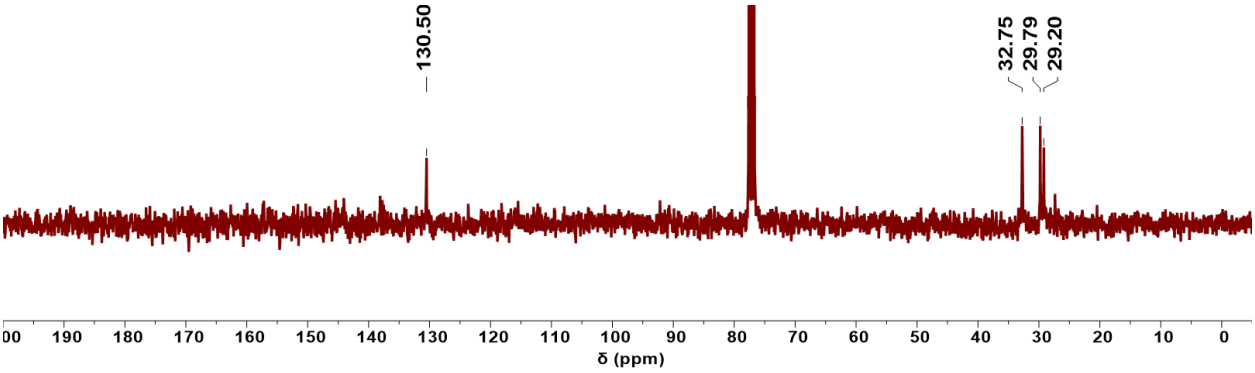


Figure 5.61. ^{13}C NMR spectrum for poly(cyclooctene) in $CDCl_3$ following electrolysis.

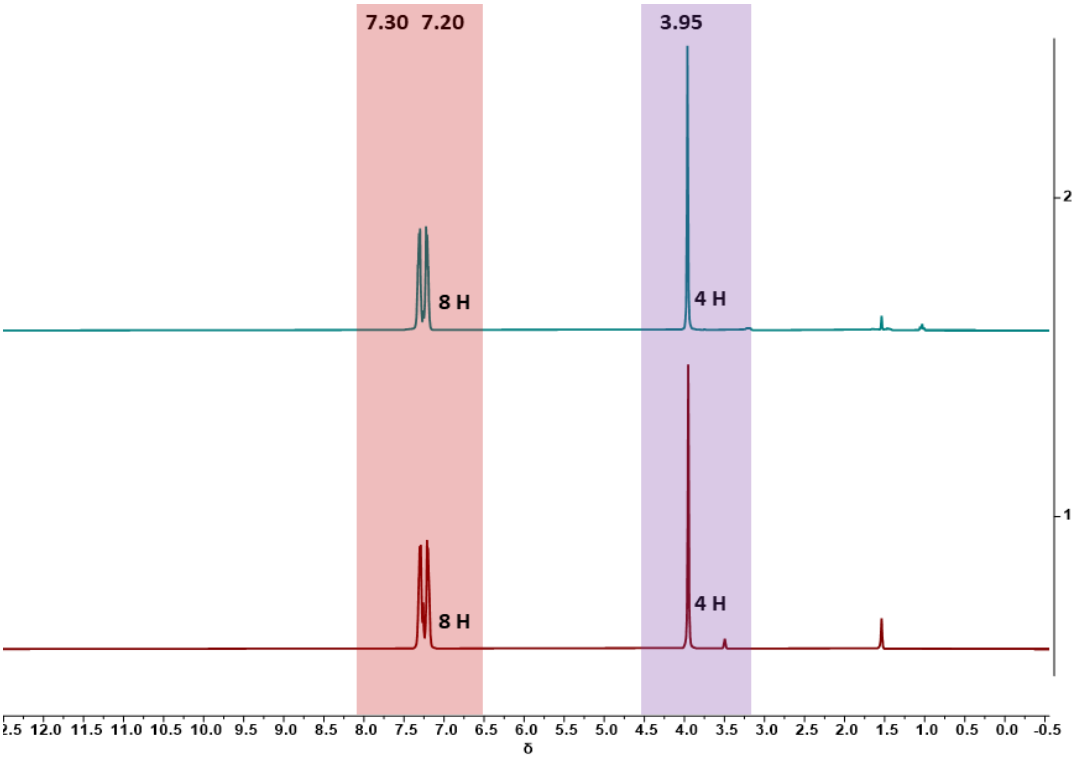


Figure 5.62. ^{1}H NMR spectra for electrolysis of DHA control. 1) DHA prior to electrolysis. 2) DHA following silica plug after electrolysis.

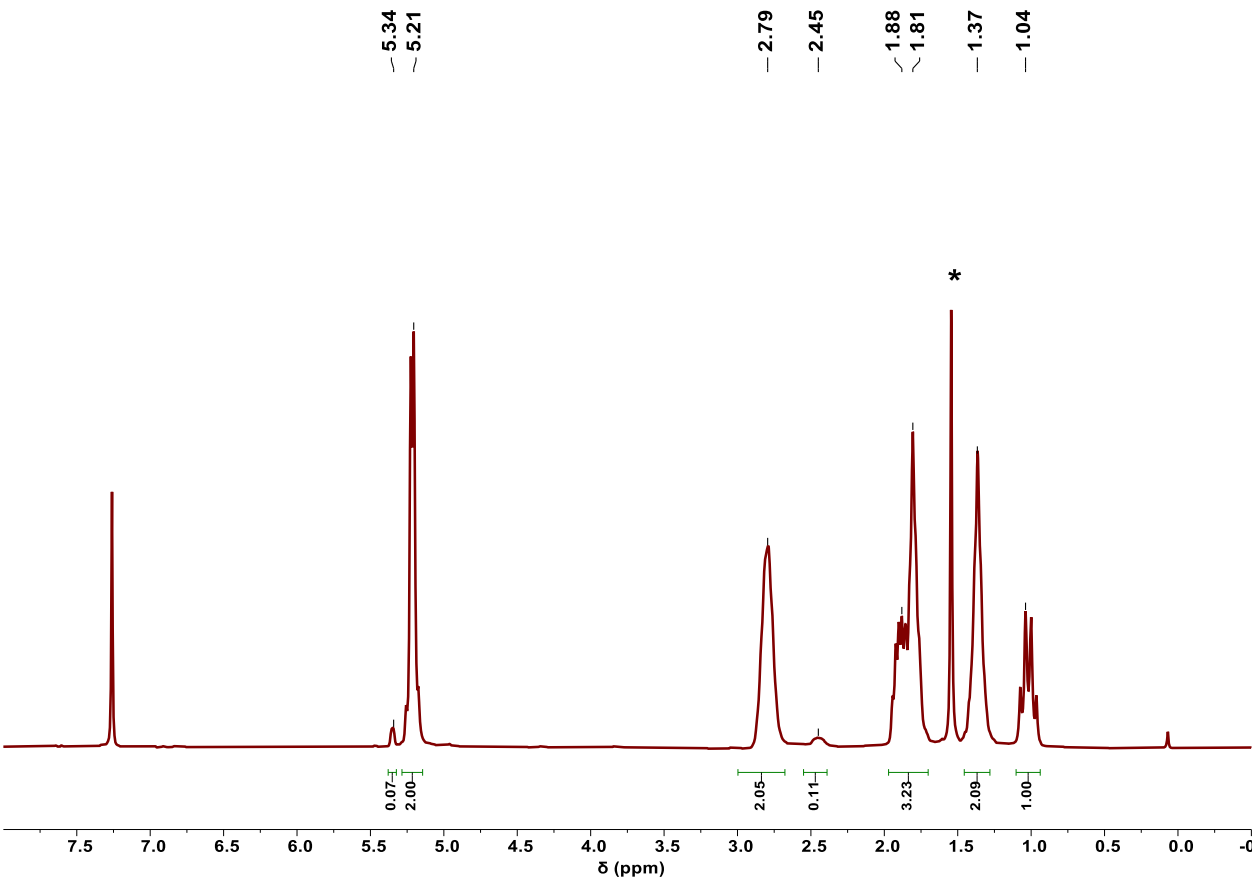


Figure 5.63. ^{1}H NMR spectrum for **5.1** in $CDCl_3$ following photochemical degradation. * denotes water

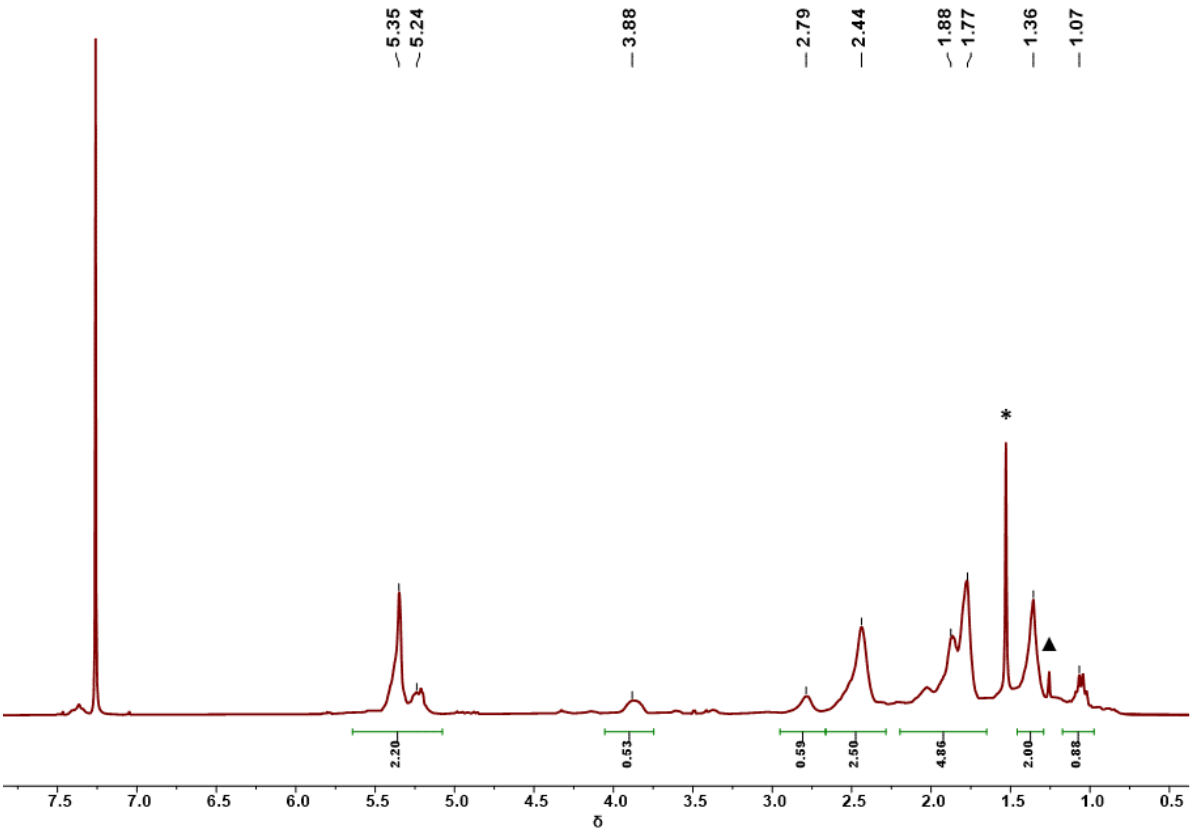


Figure 5.64. ^{1}H NMR spectrum for **5.2** in $CDCl_3$. * denotes water and ▲ denotes grease.

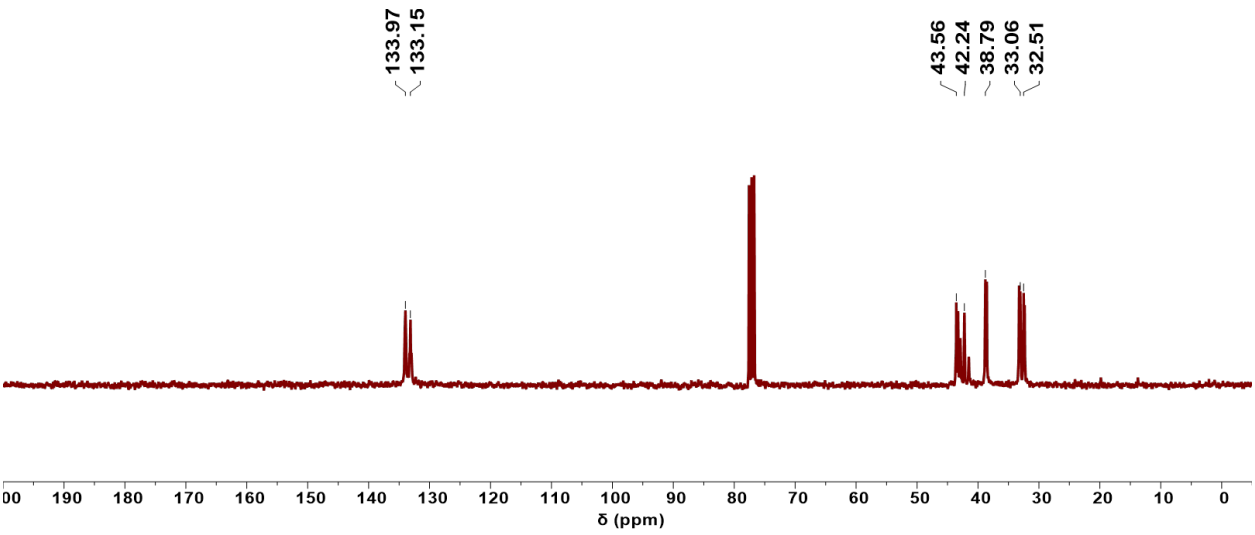


Figure 5.65. ^{13}C NMR spectrum for **5.2** in $CDCl_3$.

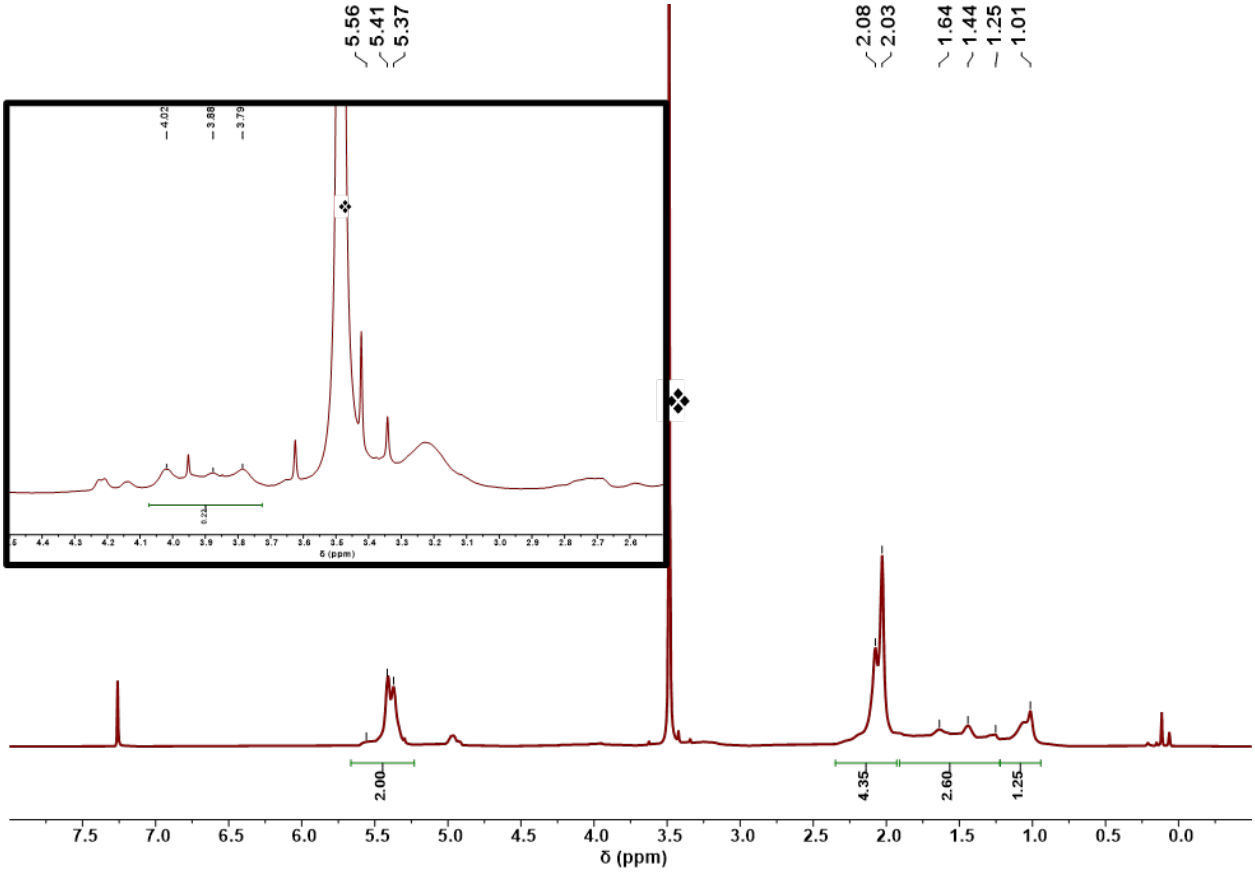


Figure 5.66. ^{1}H NMR spectrum for electrochemically azidated 1,4-polybutadiene in $CDCl_3$ following electrolysis. ❖ denotes MeOH. Inset contains enhanced baseline to show new signals consistent with azidation.

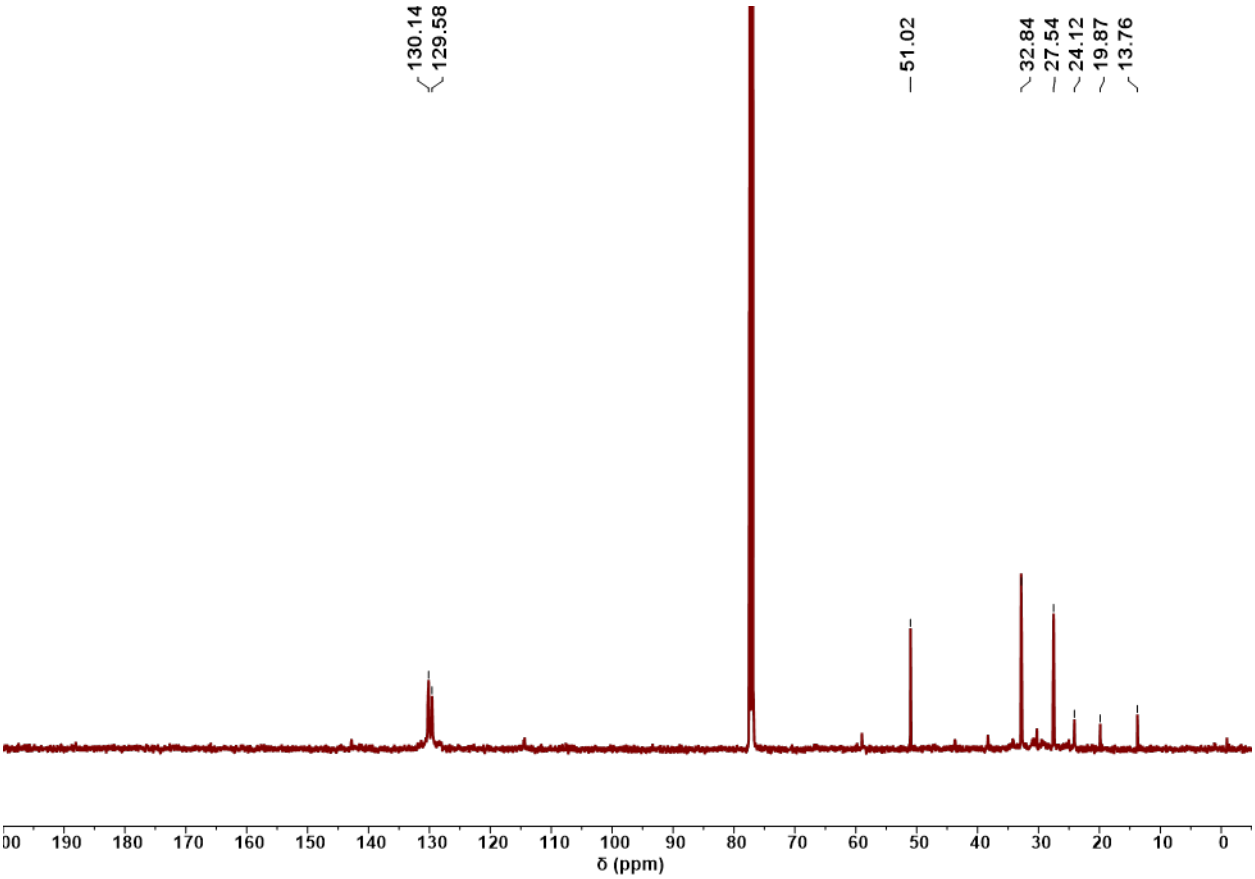


Figure 5.67. ^{13}C NMR spectrum for electrochemically azidated 1,4-polybutadiene in $CDCl_3$ following electrolysis.

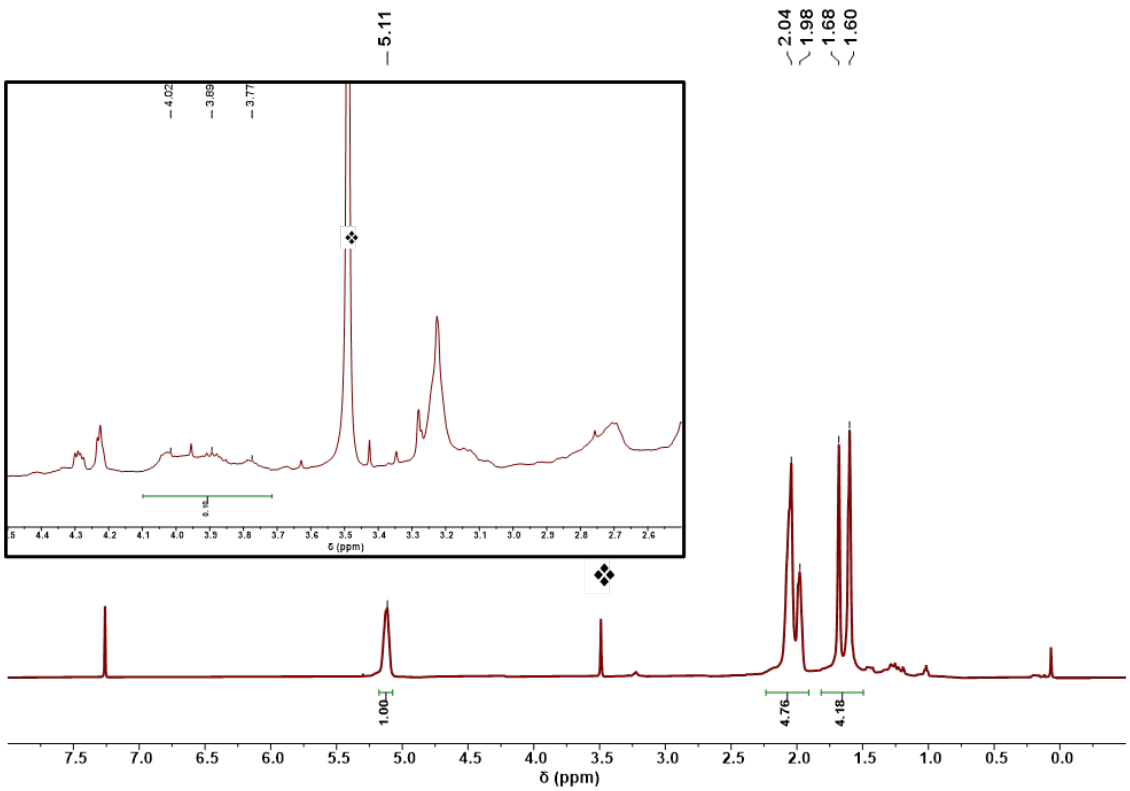


Figure 5.68. ^{1}H NMR spectrum for electrochemically azidated *cis*-1,4-polyisoprene in $CDCl_3$ following electrolysis. ❖ denotes MeOH. Inset contains enhanced baseline to show new signals consistent with azidation.

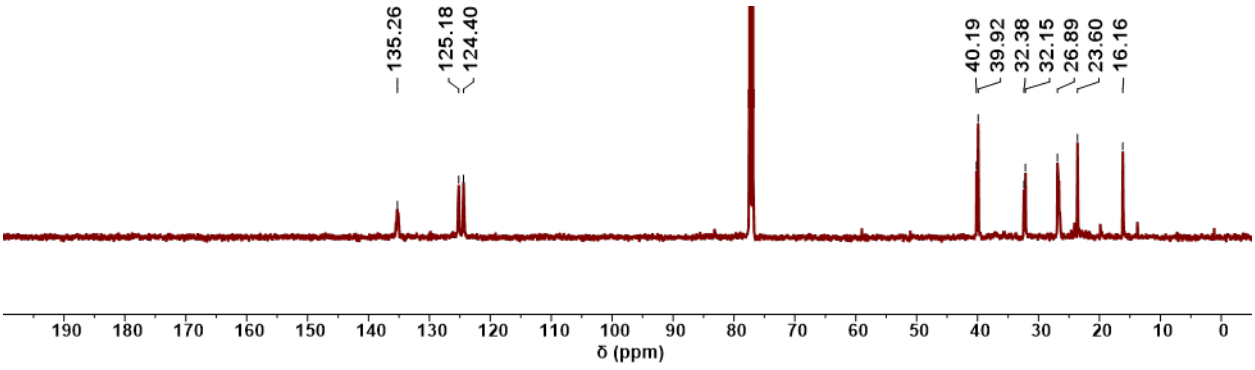


Figure 5.69. ^{13}C NMR spectrum for electrochemically azidated *cis*-1,4-polyisoprene in $CDCl_3$ following electrolysis.

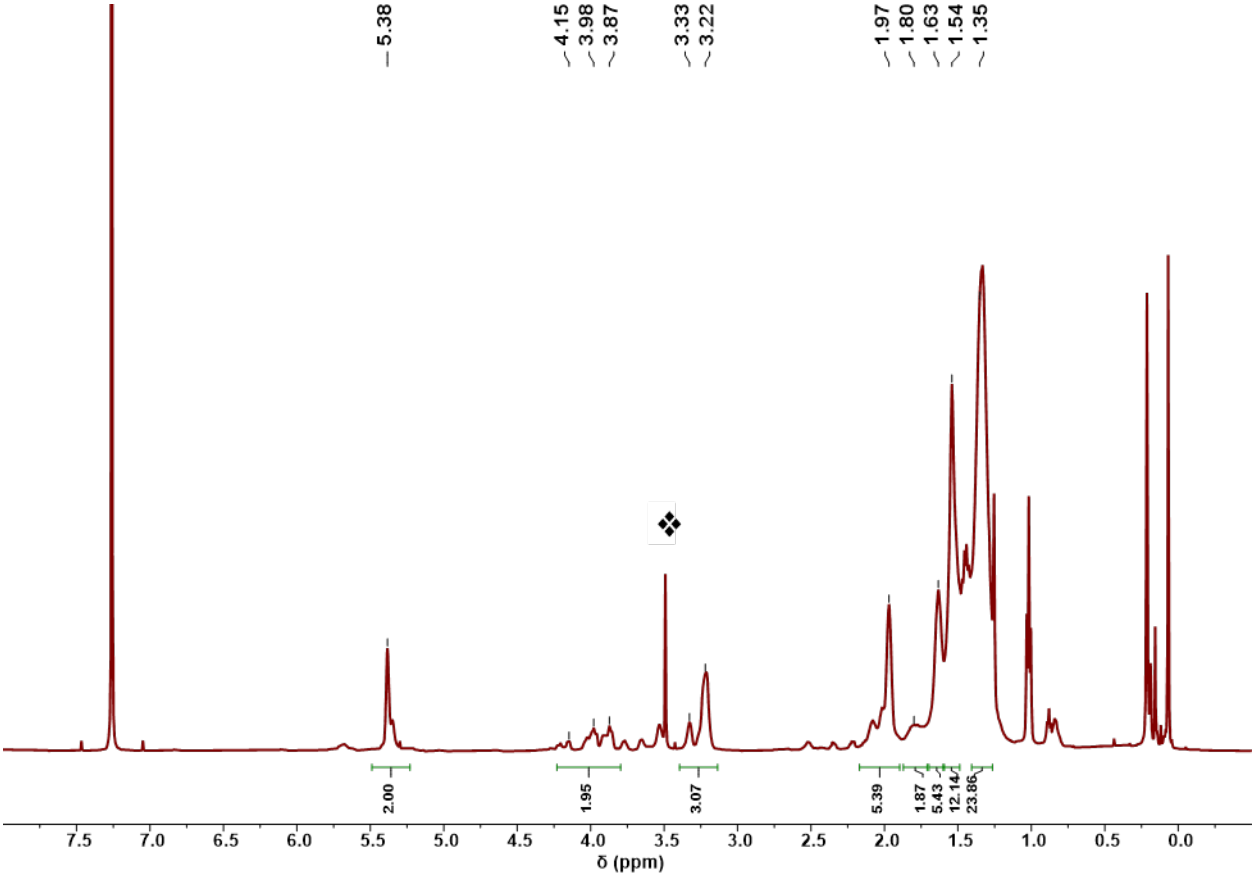


Figure 5.70. ^{1}H NMR spectrum for electrochemically azidated poly(cyclooctene) in $CDCl_3$ following electrolysis. ❖ denotes MeOH.

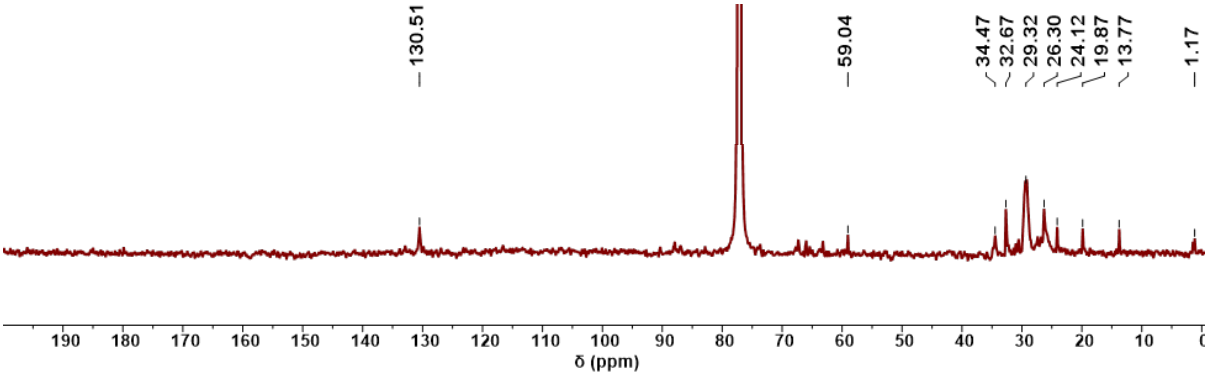


Figure 5.71. ^{13}C NMR spectrum for electrochemically azidated poly(cyclooctene) in $CDCl_3$ following electrolysis.

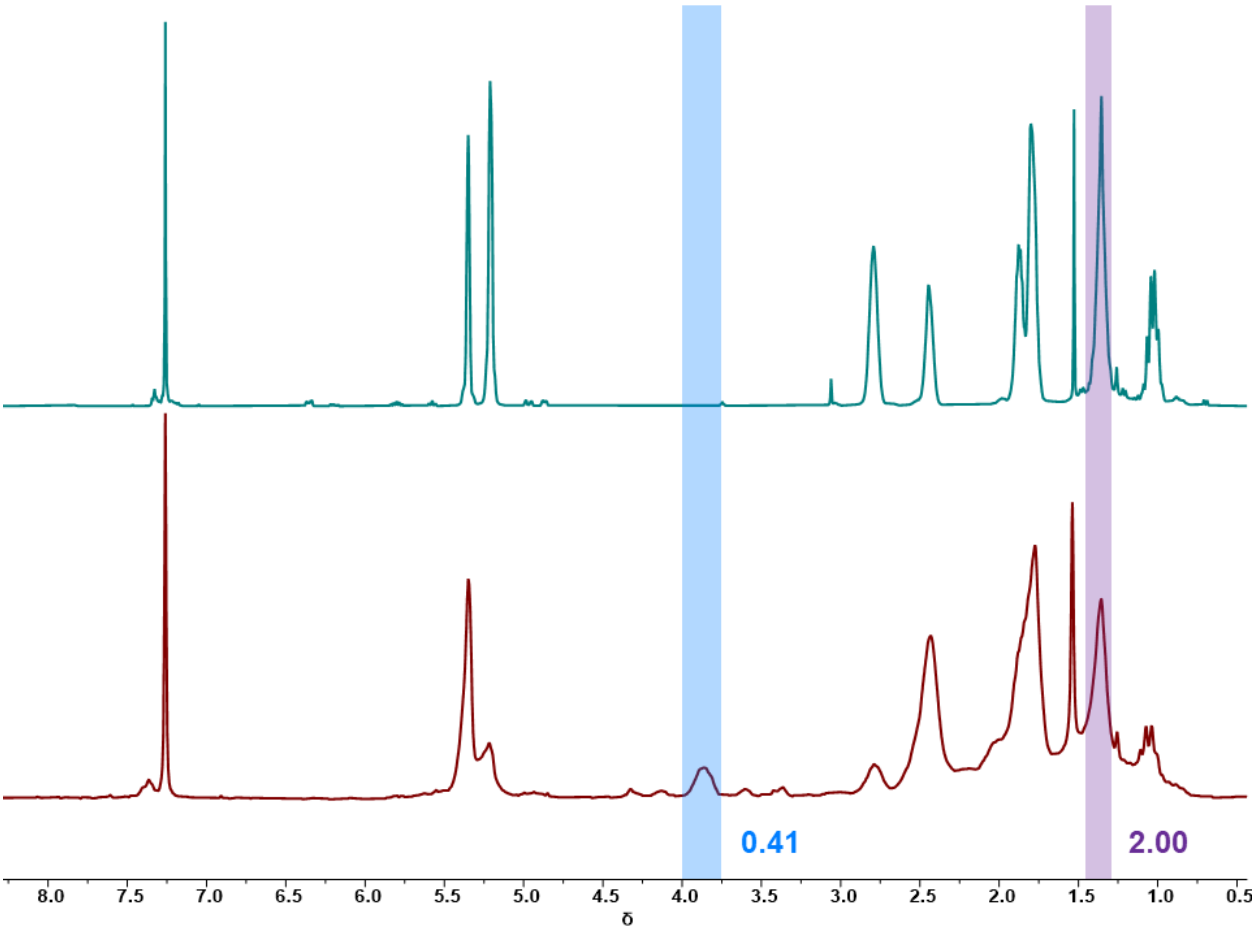


Figure 5.72. ^{1}H NMR spectra for determination of degree of azidation. Top spectrum represents **5.1** and bottom spectrum represents **5.2**. Purple and blue boxes highlight the cyclopentyl methylene and azidated methine resonances, respectively.

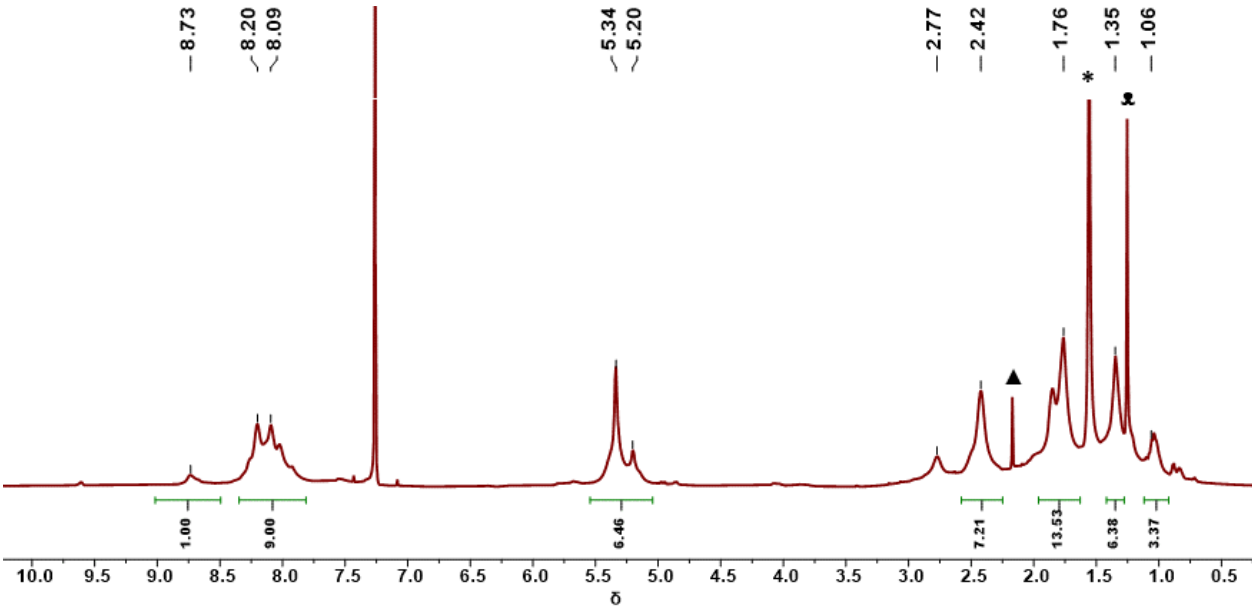


Figure 5.73. ^{1}H NMR spectrum for **5.3** in $CDCl_3$. ▲ denotes acetone, * denotes water, and ᵴ denotes grease.

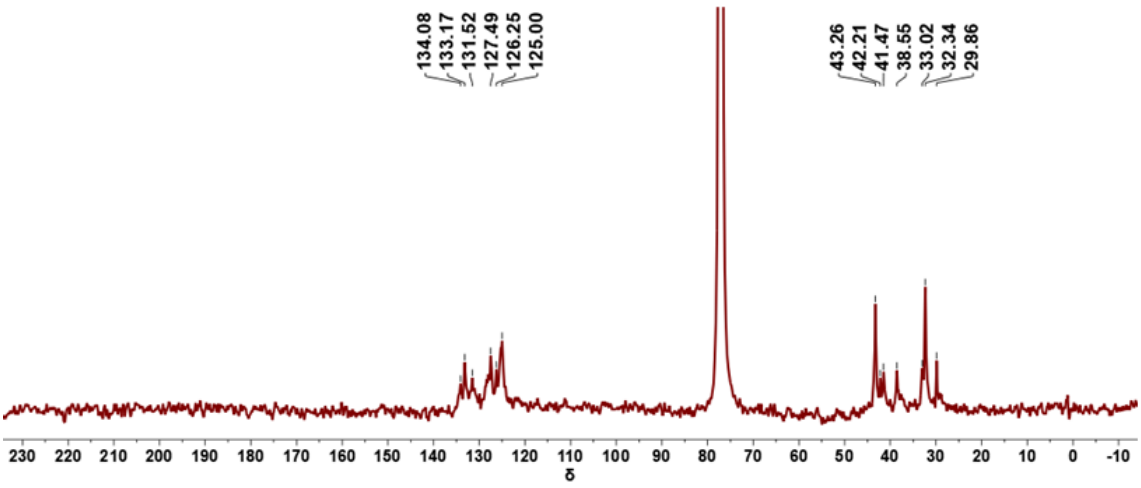


Figure 5.74. ^{13}C NMR spectrum for **5.3** in $CDCl_3$.

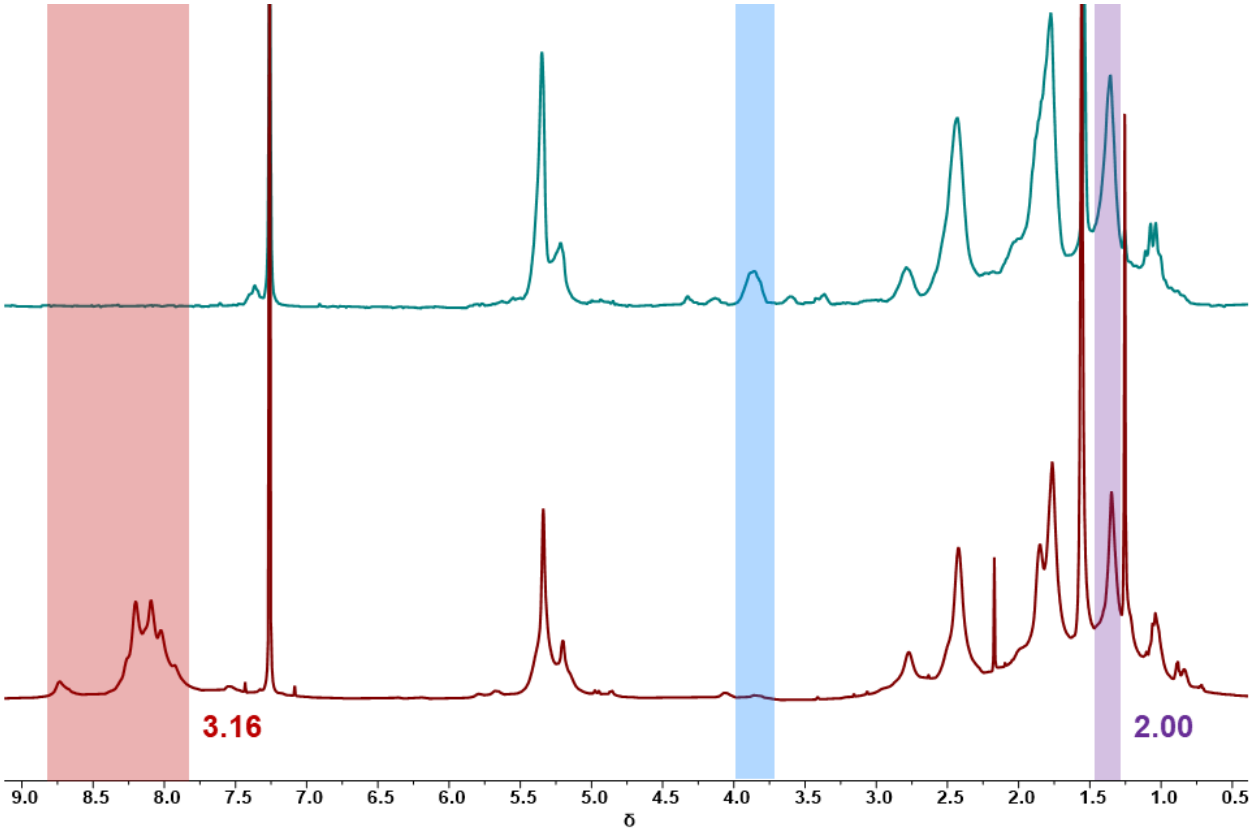


Figure 5.75. ^{1}H NMR spectra of **5.2** (top) and **5.3** (bottom). Shaded regions show signals for coupled pyrene (red), azide methine (blue), and unfunctionalized methylene (purple).

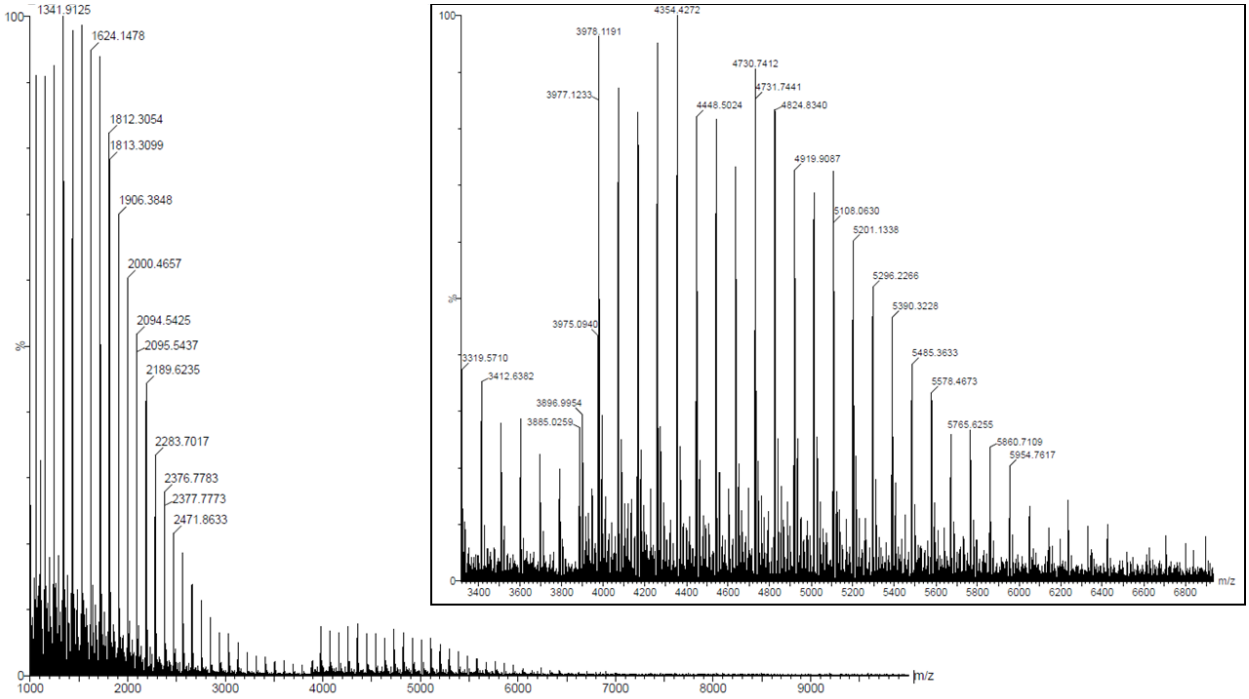


Figure 5.76. MALDI-TOF spectrum following electrolysis of a low M_n **5.1**. Inset shows expansion of region from 4000-7000 m/z.

References

(1) Staudinger, H. Über Polymerisation. *Berichte der deutschen chemischen Gesellschaft (A and B Series)* **1920**, *53* (6), 1073–1085. https://doi.org/10.1002/CBER.19200530627.

(2) Mülhaupt, R. Hermann Staudinger and the Origin of Macromolecular Chemistry. *Angewandte Chemie International Edition* **2004**, *43* (9), 1054–1063. https://doi.org/10.1002/ANIE.200330070.

(3) Frey, H.; Johann, T. Celebrating 100 Years of "Polymer Science": Hermann Staudinger's 1920 Manifesto. *Polymer Chemistry* **2019**, *11* (1), 8–14. https://doi.org/10.1039/C9PY90161B.

(4) Kondo, Y.; García-Cuadrado, D.; Hartwig, J. F.; Boaen, N. K.; Wagner, N. L.; Hillmyer, M. A. Rhodium-Catalyzed, Regiospecific Functionalization of Polyolefins in the Melt. *J Am Chem Soc* **2002**, *124* (7), 1164–1165. https://doi.org/10.1021/JA016763J/SUPPL_FILE/JA016763J_S1.PDF.

(5) Bae, C.; Hartwig, J. F.; Boaen Harris, N. K.; Long, R. O.; Anderson, K. S.; Hillmyer, M. A. Catalytic Hydroxylation of Polypropylenes. *J Am Chem Soc* **2005**, *127* (2), 767–776. https://doi.org/10.1021/JA044440S/SUPPL_FILE/JA044440SSI20041019_094410.PDF.

(6) Ray, A.; Zhu, K.; Kissin, Y. V; Cherian, A. E.; Coates, G. W.; Goldman, A. S. Dehydrogenation of Aliphatic Polyolefins Catalyzed by Pincer-Ligated Iridium Complexes. *Chemical Communications* **2005**, No. 27, 3388–3390. https://doi.org/10.1039/B502120K.

(7) Ray, A.; Kissin, Y. V.; Zhu, K.; Goldman, A. S.; Cherian, A. E.; Coates, G. W. Catalytic Post-Modification of Alkene Polymers: Chemistry and Kinetics of Dehydrogenation of Alkene Polymers and Oligomers with Pincer Ir Complexes. *Journal of Molecular Catalysis A: Chemical* **2006**, *256* (1–2), 200–207. https://doi.org/10.1016/J.MOLCATA.2006.04.017.

(8) Williamson, J. B.; Czaplyski, W. L.; Alexanian, E. J.; Leibfarth, F. A. Regioselective C–H Xanthylation as a Platform for Polyolefin Functionalization. *Angewandte Chemie* **2018**, *130* (21), 6369–6373. https://doi.org/10.1002/ANGE.201803020.

(9) Williamson, J. B.; Na, C. G.; Johnson, R. R.; Daniel, W. F. M.; Alexanian, E. J.; Leibfarth, F. A. Chemo- and Regioselective Functionalization of Isotactic Polypropylene: A Mechanistic and Structure–Property Study. *J Am Chem Soc* **2019**, *141* (32), 12815–12823. https://doi.org/10.1021/jacs.9b05799.

(10) Fazekas, T. J.; Alty, J. W.; Neidhart, E. K.; Miller, A. S.; Leibfarth, F. A.; Alexanian, E. J. Diversification of Aliphatic C-H Bonds in Small Molecules and Polyolefins through Radical Chain Transfer. *Science (1979)* **2022**, *375* (6580), 545–550. https://doi.org/10.1126/SCIENCE.ABH4308/SUPPL_FILE/SCIENCE.ABH4308_SM.PDF.

(11) Hopewell, J.; Dvorak, R.; Kosior, E. Plastics Recycling: Challenges and Opportunities. *Philosophical Transactions of the Royal Society B: Biological Sciences* **2009**, *364* (1526), 2115–2126. https://doi.org/10.1098/RSTB.2008.0311.

(12) Panda, A. K.; Singh, R. K.; Mishra, D. K. Thermolysis of Waste Plastics to Liquid Fuel: A Suitable Method for Plastic Waste Management and Manufacture of Value Added Products—A World Prospective. *Renewable and Sustainable Energy Reviews* **2010**, *14* (1), 233–248. https://doi.org/10.1016/J.RSER.2009.07.005.

(13) Miandad, R.; Barakat, M. A.; Aburiazaiza, A. S.; Rehan, M.; Nizami, A. S. Catalytic Pyrolysis of Plastic Waste: A Review. *Process Safety and Environmental Protection* **2016**, *102*, 822–838. https://doi.org/10.1016/J.PSEP.2016.06.022.

(14) Vollmer, I.; Jenks, M. J. F.; Roelands, M. C. P.; White, R. J.; van Harmelen, T.; de Wild, P.; van der Laan, G. P.; Meirer, F.; Keurentjes, J. T. F.; Weckhuysen, B. M. Beyond Mechanical Recycling: Giving New Life to Plastic Waste. *Angewandte Chemie International Edition* **2020**, *59* (36), 15402–15423. https://doi.org/10.1002/ANIE.201915651.

(15) Ronique Dufaud, V. Â.; Basset, J.-M. Catalytic Hydrogenolysis at Low Temperature and Pressure of Polyethylene and Polypropylene to Diesels or Lower Alkanes by a Zirconium Hydride Supported on Silica-Alumina: A Step Toward Polyolefin Degradation by the Microscopic Reverse of Ziegler ± Natta Polymerization. *Angew. Chem. Int. Ed* **1998**, *37* (6), 806–810. https://doi.org/10.1002/(SICI)1521-3773(19980403)37:6.

(16) Celik, G.; Kennedy, R. M.; Hackler, R. A.; Ferrandon, M.; Tennakoon, A.; Patnaik, S.; Lapointe, A. M.; Ammal, S. C.; Heyden, A.; Perras, F. A.; Pruski, M.; Scott, S. L.; Poeppelmeier, K. R.; Sadow, A. D.; Delferro, M. Upcycling Single-Use Polyethylene into High-Quality Liquid Products. *ACS Central Science* **2019**, *5* (11), 1795–1803. https://doi.org/10.1021/ACSCENTSCI.9B00722/SUPPL_FILE/OC9B00722_SI_003.PDF.

(17) Zhang, F.; Zeng, M.; Yappert, R. D.; Sun, J.; Lee, Y. H.; LaPointe, A. M.; Peters, B.; Abu-Omar, M. M.; Scott, S. L. Polyethylene Upcycling to Long-Chain Alkylaromatics by Tandem Hydrogenolysis/Aromatization. *Science (1979)* **2020**, *370* (6515), 437–441. https://doi.org/10.1126/SCIENCE.ABC5441/SUPPL_FILE/ABC5441_ZHANG_SM.PDF.

(18) Jia, X.; Qin, C.; Friedberger, T.; Guan, Z.; Huang, Z. Efficient and Selective Degradation of Polyethylenes Into Liquid Fuels and Waxes Under Mild Conditions. *Science Advances* **2016**, *2* (6), e1501591. https://doi.org/10.1126/SCIADV.1501591/SUPPL_FILE/1501591_SM.PDF.

(19) Solanky, S. S.; Campistron, I.; Laguerre, A.; Pilard, J. F. Metathetic Selective Degradation of Polyisoprene: Low-Molecular-Weight Telechelic Oligomer Obtained from Both Synthetic and Natural Rubber. *Macromolecular Chemistry and Physics* **2005**, *206* (10), 1057–1063. https://doi.org/10.1002/MACP.200400416.

(20) Smith, R. F.; Boothroyd, S. C.; Thompson, R. L.; Khosravi, E. A Facile Route for Rubber Breakdown via Cross Metathesis Reactions. *Green Chemistry* **2016**, *18* (11), 3448–3455. https://doi.org/10.1039/C5GC03075G.

(21) Yan, M.; Kawamata, Y.; Baran, P. S. Synthetic Organic Electrochemical Methods Since 2000: On the Verge of a Renaissance. *Chemical Reviews* **2017**, *117* (21), 13230–13319. https://doi.org/10.1021/ACS.CHEMREV.7B00397.

(22) Kingston, C.; Palkowitz, M. D.; Takahira, Y.; Vantourout, J. C.; Peters, B. K.; Kawamata, Y.; Baran, P. S. A Survival Guide for the "Electro-Curious." *Accounts of Chemical Research* **2019**, *53* (1), 72–83. https://doi.org/10.1021/ACS.ACCOUNTS.9B00539.

(23) Little, R. D. A Perspective on Organic Electrochemistry. *The Journal of Organic Chemistry* **2020**, *85* (21), 13375–13390. https://doi.org/10.1021/ACS.JOC.0C01408.

(24) Pollok, D.; Waldvogel, S. R. Electro-Organic Synthesis – A 21st Century Technique. *Chemical Science* **2020**. https://doi.org/10.1039/D0SC01848A.

(25) Magenau, A. J. D.; Strandwitz, N. C.; Gennaro, A.; Matyjaszewski, K. Electrochemically Mediated Atom Transfer Radical Polymerization. *Science (1979)* **2011**, *332* (6025), 81–84. https://doi.org/10.1126/SCIENCE.1202357/SUPPL_FILE/MAGENAU_SOM.PDF.

(26) Chmielarz, P.; Fantin, M.; Park, S.; Isse, A. A.; Gennaro, A.; Magenau, A. J. D.; Sobkowiak, A.; Matyjaszewski, K. Electrochemically Mediated Atom Transfer Radical Polymerization (EATRP). *Progress in Polymer Science* **2017**, *69*, 47–78. https://doi.org/10.1016/J.PROGPOLYMSCI.2017.02.005.

(27) Fabre, B.; Simonet, J. Post-Polymerization Electrochemical Functionalization of a Conducting Polymer: Anodic Cyanation of Poly(p-Dimethoxybenzene). *Journal of Electroanalytical Chemistry* **1996**, *416* (1–2), 187–189. https://doi.org/10.1016/S0022-0728(96)01014-5.

(28) Qi, Z.; Rees, N. G.; Pickup, P. G. Electrochemically Induced Substitution of Polythiophenes and Polypyrrole. *Chemistry of Materials* **1996**, *8* (3), 701–707. https://doi.org/10.1021/CM950416P.

(29) Soudan, P.; Lucas, P.; Breau, L.; Bélanger, D. Electrochemical Modification of Poly(3-(4-Fluorophenyl)Thiophene). *Langmuir* **2000**, *16* (9), 4362–4366. https://doi.org/10.1021/LA991676E.

(30) Hayashi, S.; Inagi, S.; Hosaka, K.; Fuchigami, T. Post-Functionalization of Poly(3-Hexylthiophene) via Anodic Chlorination. *Synthetic Metals* **2009**, *159* (17–18), 1792–1795. https://doi.org/10.1016/J.SYNTHMET.2009.05.028.

(31) Inagi, S.; Hayashi, S.; Hosaka, K.; Fuchigami, T. Facile Functionalization of a Thiophene–Fluorene Alternating Copolymer via Electrochemical Polymer Reaction. *Macromolecules* **2009**, *42* (12), 3881–3883. https://doi.org/10.1021/ma900561f.

(32) Hayashi, S.; Inagi, S.; Fuchigami, T. Efficient Electrochemical Polymer Halogenation Using a Thin-Layered Cell. *Polymer Chemistry* **2011**, *2* (8), 1632–1637. https://doi.org/10.1039/C1PY00150G.

(33) Shida, N.; Okazaki, D.; Kurioka, T.; Nishiyama, H.; Seferos, D. S.; Tomita, I.; Inagi, S. Anodic Chlorination of Selenophene-Containing Polymers: Reaction Efficiency and Selective Reaction of Single Segment in Rod–Rod Diblockcopolymer. *ChemElectroChem* **2017**, *4* (8), 1824–1827. https://doi.org/10.1002/CELC.201700205.

(34) Inagi, S.; Fuchigami, T. Electrochemical Post-Functionalization of Conducting Polymers. *Macromolecular Rapid Communications* **2014**, *35* (9), 854–867. https://doi.org/https://doi.org/10.1002/marc.201400023.

(35) Kurioka, T.; Nishiyama, H.; Tomita, I.; Inagi, S. Improvement of Current Efficiency in Anodic Chlorination of Poly(3-Hexylthiophene) by Using a Boron Trifluoride-Diethyl Ether Complex. *ChemElectroChem* **2018**, *5* (5), 753–755. https://doi.org/https://doi.org/10.1002/celc.201701282.

(36) Kurioka, T.; Shida, N.; Tomita, I.; Inagi, S. Post-Functionalization of Aromatic C-H Bonds at the Main Chains of Ï-Conjugated Polymers via Anodic Chlorination Facilitated by Lewis Acids. *Macromolecules* **2021**, *54* (3), 1539–1547. https://doi.org/10.1021/ACS.MACROMOL.0C02556/SUPPL_FILE/MA0C02556_SI_001.PDF.

(37) Wang, P.; Gao, X.; Huang, P.; Lei, A. Recent Advances in Electrochemical Oxidative Cross-Coupling of Alkenes with H2 Evolution. *ChemCatChem* **2020**, *12* (1), 27–40. https://doi.org/10.1002/CCTC.201901773.

(38) Chen, N.; Xu, H. C. Electrochemically Driven Radical Reactions: From Direct Electrolysis to Molecular Catalysis. *The Chemical Record* **2021**, *21* (9), 2306–2319. https://doi.org/10.1002/TCR.202100048.

(39) Moeller, K. D. Intramolecular Anodic Olefin Coupling Reactions: Using Radical Cation Intermediates to Trigger New Umpolung Reactions. *Synlett* **2009**, *2009* (8), 1208–1218. https://doi.org/10.1055/S-0028-1088126/ID/11B.

(40) Feng, R.; Smith, J. A.; Moeller, K. D. Anodic Cyclization Reactions and the Mechanistic Strategies That Enable Optimization. *Accounts of Chemical Research* **2017**, *50* (9), 2346–2352.

https://doi.org/10.1021/ACS.ACCOUNTS.7B00287/SUPPL_FILE/AR7B00287_SI_001.PDF.

(41) Schmittel, M.; Burghart, A. Understanding Reactivity Patterns of Radical Cations. *Angewandte Chemie International Edition in English* **1997**, *36* (23), 2550–2589. https://doi.org/10.1002/ANIE.199725501.

(42) Baciocchi, E.; Bietti, M.; Lanzalunga, O. Mechanistic Aspects of β-Bond-Cleavage Reactions of Aromatic Radical Cations. *Accounts of Chemical Research* **2000**, *33* (4), 243–251. https://doi.org/10.1021/AR980014Y.

(43) Baciocchi, E.; Bietti, M.; Lanzalunga, O. Fragmentation Reactions of Radical Cations. *Journal of Physical Organic Chemistry* **2006**, *19* (8–9), 467–478. https://doi.org/10.1002/POC.1096.

(44) Yoshida, J.; Shimizu, A.; Hayashi, R. Electrogenerated Cationic Reactive Intermediates: The Pool Method and Further Advances. *Chemical Reviews* **2018**, *118* (9), 4702–4730. https://doi.org/10.1021/acs.chemrev.7b00475.

(45) Srivastava, V. K.; Basak, G. C.; Maiti, M.; Jasra, R. V. Synthesis and Utilization of Epoxidized Polybutadiene Rubber as an Alternate Compatibilizer in Green-Tire Composites. *International Journal of Industrial Chemistry* **2017**, *8* (4), 411–424. https://doi.org/10.1007/S40090-017-0130-3.

(46) Wang, J.; Kouznetsova, T. B.; Kean, Z. S.; Fan, L.; Mar, B. D.; Martínez, T. J.; Craig, S. L. A Remote Stereochemical Lever Arm Effect in Polymer Mechanochemistry. *J. Am. Chem. Soc* **2014**, *136*, 15162–15165. https://doi.org/10.1021/ja509585g.

(47) Galan, N. J.; Brantley, J. N. General Access to Allene-Containing Polymers Using the Skattebøl Rearrangement. *ACS Macro Letters* **2020**, *13*, 1662–1666. https://doi.org/10.1021/ACSMACROLETT.0C00745/SUPPL_FILE/MZ0C00745_SI_001.PDF.

(48) Justynska, J.; Schlaad, H. Modular Synthesis of Functional Block Copolymers. *Macromolecular Rapid Communications* **2004**, *25*, 1478–1481. https://doi.org/10.1002/marc.200400228.

(49) Nor, H. M.; Ebdon, J. R. Ozonolysis of Natural Rubber in Chloroform Solution Part 1. A Study by GPC and FTIR Spectroscopy. *Polymer (Guildf)* **2000**, *41* (7), 2359–2365. https://doi.org/10.1016/S0032-3861(99)00417-6.

(50) Leitgeb, A.; Wappel, J.; Slugovc, C. The ROMP Toolbox Upgraded. *Polymer (Guildf)* **2010**, *51* (14), 2927–2946. https://doi.org/10.1016/J.POLYMER.2010.05.002.

(51) Ogba, O. M.; Warner, N. C.; O'Leary, D. J.; Grubbs, R. H. Recent Advances in Ruthenium-Based Olefin Metathesis. *Chemical Society Reviews* **2018**, *47* (12), 4510–4544. https://doi.org/10.1039/C8CS00027A.

(52) Keitz, B. K.; Fedorov, A.; Grubbs, R. H. Cis-Selective Ring-Opening Metathesis Polymerization with Ruthenium Catalysts. *J Am Chem Soc* **2012**, *134* (4), 2040–2043. https://doi.org/10.1021/JA211676Y/SUPPL_FILE/JA211676Y_SI_001.PDF.

(53) Fuchigami, T.; Atobe, M.; Inagi, S. *Fundamentals and Applications of Organic Electrochemistry*, 1st ed.; John Wiley & Sons, Ltd, 2015.

(54) RVC/Pt (anode/cathode) electrodes gave high degrees of degradation, but resulted in biomodal sample populations. We ultimately elected to use graphite/Zn electrodes because (i) they are low cost, abundant materials; (ii) these electrodes are easily cleaned for multiple uses; and (iii) these electrodes provided good control over degradation. Degradation was also observed when 1 was stirred at 2.18 V in a referenced cell for 1 h (Figure 5.31).

(55) Malhotra, S. L. Ultrasonic Modification of Polymers. II. Degradation of Polystyrene, Substituted Polystyrene, and Poly(n-Vinyl Carbazole) in the Presence of Flexible Chain Polymers. *Journal of Macromolecular Science: Part A - Chemistry* **2006**, *18* (7–8), 1055–1085. https://doi.org/10.1080/00222338208066479.

(56) Malhotra, S. L. Ultrasonic Solution Degradations of Poly(Alkyl Methacrylates). *Journal of Macromolecular Science: Part A - Chemistry* **1985**, *23* (6), 729–748. https://doi.org/10.1080/00222338608063419.

(57) Warren, J. J.; Tronic, T. A.; Mayer, J. M. Thermochemistry of Proton-Coupled Electron Transfer Reagents and Its Implications. *Chemical Reviews* **2010**, *110* (12), 6961–7001. https://doi.org/10.1021/CR100085K.

(58) Control experiments suggested minimal oxidation of 9,10-dihydroanthracene occurred under our conditions (Figure 5.62).

(59) Romero, N. A.; Nicewicz, D. A. Mechanistic Insight into the Photoredox Catalysis of Anti-Markovnikov Alkene Hydrofunctionalization Reactions. *J Am Chem Soc* **2014**, *136* (49), 17024–17035. https://doi.org/10.1021/JA506228U/SUPPL_FILE/JA506228U_SI_001.PDF.

(60) RVC/Pt (anode/cathode) electrodes gave high degrees of degradation, but resulted in biomodal sample populations. We ultimately elected to use graphite/Zn electrodes because (i) they are low cost, abundant materials; (ii) these electrodes are easily cleaned for multiple uses; and (iii) these electrodes provided good control over degradation. Degradation was also observed when 1 was stirred at 2.18 V in a referenced cell for 1 h (Figure 5.31).

(61) Fu, N.; Sauer, G. S.; Saha, A.; Loo, A.; Lin, S. Metal-Catalyzed Electrochemical Diazidation of Alkenes. *Science (1979)* **2017**, *357* (6351), 575–579. https://doi.org/10.1126/SCIENCE.AAN6206/SUPPL_FILE/AAN6206_FU_SM.PDF.

(62) Kolb, H. C.; Finn, M. G.; Sharpless, K. B. Click Chemistry: Diverse Chemical Function from a Few Good Reactions. *Angewandte Chemie International Edition* **2001**, *40*, 2004–2021.

(63) Meldal, M.; Tomøe, C. W. Cu-Catalyzed Azide−Alkyne Cycloaddition. *Chemical Reviews* **2008**, *108* (8), 2952–3015. https://doi.org/10.1021/CR0783479.

(64) Schilling, C. I.; Jung, N.; Biskup, M.; Schepers, U.; Bräse, S. Bioconjugation via Azide–Staudinger Ligation : An Overview. *Chemical Society Reviews* **2011**, *40* (9), 4840–4871. https://doi.org/10.1039/C0CS00123F.

(65) Palacios, F.; Alonso, C.; Aparicio, D.; Rubiales, G.; de los Santos, J. M. The Aza-Wittig Reaction: An Efficient Tool for the Construction of Carbon-Nitrogen Double Bonds. *Tetrahedron* **2007**, *63* (3), 523–575. https://doi.org/10.1016/J.TET.2006.09.048.

(66) Huang, D.; Yan, G. Recent Advances in Reactions of Azides. *Advanced Synthesis & Catalysis* **2017**, *359* (10), 1600–1619. https://doi.org/10.1002/ADSC.201700103.

(67) $TMSN_3$ was selected as the azide source due to its superior solubility in DCM when compared to NaN_3 and $N(Bu_4)N_3$. Reactions conducted at E_{cell} = 3.2 V resulted in a

stronger apparent azide stretch than reactions conducted at E_{cell} = 2.5 V (as determined by IR spectroscopy; Figure 5.14). Although graphite/Zn promoted azidation, RVC/Pt resulted in the highest azide yield (as determined by ^{1}H NMR spectroscopy; Table 5.4). To facilitate additional characterization of the azidated materials, we elected to use the electrode combination that gave us the highest yield. A low M_n material was used for this study to facilitate NMR spectral analysis; however, lower rates of degradation were observed for low M_n polymers.

(68) Sanford, M. S.; Love, J. A.; Grubbs, R. H. A Versatile Precursor for the Synthesis of New Ruthenium Olefin Metathesis Catalysts. *Organometallics* **2001**, *20* (25), 5314–5318. https://doi.org/10.1021/OM010599R/SUPPL_FILE/OM010599R_S.PDF.

(69) Love, J. A.; Morgan, J. P.; Trnka, T. M.; Grubbs, R. H.; Bissell, A.; Boden, N.; Bushby, R. J.; G Fishwick, C. W.; Holland, E.; Movaghar, B. A Practical and Highly Active Ruthenium-Based Catalyst That Effects the Cross Metathesis of Acrylonitrile. *Angewandte Chemie International Edition* **2002**, *41*, 4035–4037. https://doi.org/10.1002/1521-3757.

(70) Wu, S. Y.; Guo, X. Q.; Zhou, L. P.; Sun, Q. F. Fine-Tuned Visible and Near-Infrared Luminescence on Self-Assembled Lanthanide-Organic Tetrahedral Cages with Triazole-Based Chelates. *Inorganic Chemistry* **2019**, *58* (10), 7091–7098. https://doi.org/10.1021/ACS.INORGCHEM.9B00756/SUPPL_FILE/IC9B00756_SI_001.PDF.

(71) Armarego, W. L. F.; Chai, C. L. L. *Purification of Laboratory Chemicals*, 6th ed.; Elsevier, 2013. https://doi.org/10.1016/C2009-0-64000-9.

(72) Mathers, R. T.; Damodaran, K.; Rendos, M. G.; Lavrich, M. S. Functional Hyperbranched Polymers Using Ring-Opening Metathesis Polymerization of Dicyclopentadiene with Monoterpenes. *Macromolecules* **2009**, *42* (5), 1512–1518. https://doi.org/10.1021/MA802441T/SUPPL_FILE/MA802441T_SI_001.PDF.

(73) Schotten, C.; Nicholls, T. P.; Bourne, R. A.; Kapur, N.; Nguyen, B. N.; Willans, C. E. Making Electrochemistry Easily Accessible to the Synthetic Chemist. *Green Chemistry* **2020**, *22* (11), 3358–3375. https://doi.org/10.1039/D0GC01247E.

(74) Fu, N.; Sauer, G. S.; Lin, S. A General, Electrocatalytic Approach to the Synthesis of Vicinal Diamines. *Nature Protocols 2018 13:8* **2018**, *13* (8), 1725–1743. https://doi.org/10.1038/s41596-018-0010-0.

(75) *General Guidelines for Cleaning Electrodes*; 2021.

CHAPTER 6: SUMMARY AND OUTLOOK

Functional Materials

The synthesis of tunable materials continues to be an ongoing area of intense research among polymer chemists. These materials hold promise for a wide array of applications due to the nature of polymeric materials (e.g., lightweight, controllable molar mass, elasticity, hardness). Utilization of new synthetic methodologies and the polymerization of metal-containing fragments has allowed for the expansion of polymer chemical space. The research described in this document has expanded polymer chemical space through the polymerization of new monomers as well as the development of new methodologies for modification of polymers.

Polymerization of Fischer Carbenes

In summary, we have reported the first example of well-defined Fischer carbene containing polymers from ROMP. These materials exhibited increased thermal and ambient stability when compared to previous examples by Macomber and Masuda. These polymers were found to be stimuli-responsive and release CO upon exposure to light. Future experiments with this system could include further CO-release studies to determine whether the additional stimuli is oxygen or water. Specifically, CO-release experiments utilizing **2.5** could be carried out in which the **2.1** is held in the dark under N_2 with the addition of water to the solution as well as when **2.1** is held in the dark in anhydrous solvent under an atmosphere of $O_{2(g)}$.

These metallocarbene polymers could be incorporated into more complex architectures (e.g., block copolymers), and the metallocarbene motifs retained their intrinsic chemical reactivity. During this study, we found that the tungsten carbenes did not polymerize using Grubbs-type ruthenium catalysts, and in further studies we observed polymerization of the analogous chromium carbenes with ruthenium catalysts. Therefore, we sought to understand the fundamental origin of this divergent reactivity. Deeper understanding of the phenomenon studied in chapter 3 could be further investigated through the synthesis of carbenes without a methylene linker. Recent reports show that conversion of boronic ester groups to amines is quite simple through the synthesis of a DABCO salt, and this process proceeds with inversion of stereochemistry. Additionally, further stoichiometric experiments

to determine the effect of the alkoxy substituted carbene **3.1$_W$** and the amino substituted carbene **3.5$_W$**. Utilizing **3.4$_W$** eliminates propagation pathways and should allow for investigation of the deleterious side-reactions noted in Chapter 3. An additional metathesis inactive amino-carbene (analogous to **3.4**) will need to be synthesized.

Future work concerning metallocarbene containing polymers could investigate the material properties of these polymers. For example, the refractive indices of the norbornene substituted tungsten and chromium carbenes have been observed to be variable dependent upon molecular weight, an observation that is not typical of standard polymers. Therefore, investigation into the range of refractive indices that can be observed from variation of molecular weights could occur.

Additionally, the polymerization of Fischer carbenes should investigate the synthesis of more complex polymers. We reported an example utilizing **2.1** and norbornene to make hybrid organic-inorganic materials, but further investigations are possible. For example, heterometallic statistical, block, and gradient copolymers could be synthesized. Synthesis of an array of block copolymers with varying mol fractions of tungsten and chromium carbenes should be easily accomplished through utilization of the Schrock catalyst (**2.4**). These materials could possess interesting properties such as phase separation, modified thermal and mechanical data, and variable optical properties. Finally, additional work to expand the polymerization methods utilized can be conducted. Anionic, ring opening, radical, and vinyl addition polymerizations can be studied to further determine how Fischer carbenes behave in polymeric architectures, as well as the impact of these species on material properties.

Further studies should include the investigation of the reactivity of these carbenes. There is vast synthetic utility imparted by Fischer carbenes; therefore, utilizing these reactive handles to perform transformations on and with polymers could lead to valuable new materials. Additionally, the metal species involved could impart divergent reactivity, as tungsten and chromium carbenes have differing stabilities. This difference could allow for chemoselective modification of Fischer carbene containing polymers.

Post-polymerization Modifications

Brown Allylation Chemistry

Interest in Boron-containing polymers has seen rapid growth in recent years. These materials have found a variety of applications. Our approach utilized brown allylation chemistry to transform boronate esters into homoallylic alcohols. We were able to show that our methodology was applicable to a wide range of aromatic and heteroaromatic aldehydes. These materials could be isolated in good yield. The properties of the resultant materials have yet to be investigated. Further studies to expand the work discussed in Chapter 4 could include investigation of asymmetric allylations. For example, the transformation of **4.1** into the tartrate ester could provide a chiral environment for asymmetric synthesis of these materials. If synthesis of the tartrate proves difficult, other examples have shown chiral phosphoric acids can be used to impart stereoselectivity; therefore, the utilization of these compounds could aid in providing an asymmetric allyation.

Future work involving the utilization of allylation chemistry in polymers could seek to transform boronate esters to homoallylic amines using imines. We should also seek methodologies to expand the substrate scope from aromatic and heteroaromatic substrates to include aliphatic substrates as well to study the impact of incorporation of alkyl chains on polymer properties. Furthermore, these boron containing materials could undergo additional reaction types, such as Petasis chemistry, to further diversify the toolbox of synthetic methodologies for altering existing polymer frameworks. The ability to alter polymer backbones has led to significant changes in polymer properties, and therefore, is breaking new ground in terms of material applications.

Electrochemistry

Synthetic electrochemistry has blossomed as a field in recent years, but this powerful methodological tool has found limited applications in materials science. Through the utilization of polymer electrochemistry, we were able to both degrade and functionalize olefin-containing polymers to high degrees. These reports hold promise for future endeavors, as a step towards addressing the global plastic waste problem. Additionally, the utilization of electrochemistry as a new methodology for polymer functionalization could provide facile

access to a variety of polymeric materials previously inaccessible. These new materials could find applications in a number of areas.

Future work involving the application of synthetic electrochemistry on polymers could seek to functionalize polyolefins through catalytic dehydrogenation followed by electrochemical modification. Alternatively, preliminary studies from our group have shown that functionalization of polyolefins is achievable under our conditions, without background degradation. Additionally, other types of transformations could be investigated in olefin-containing polymers, as well as in polyesters and polyurethanes. These transformations could include oxidation or reduction at the benzylic position of polystyrenes, in carbonyl containing polymers, or as a method to add new functionalities to existing polymer architectures.

The development of this methodology for polymer degradation and functionalization is a new approach mechanistically. Radical cations are well known species in photoredox catalysis. We envision utilization of photoredox catalysis as an improvement to this system, and preliminary studies have shown that polymer degradation and functionalization is significantly improved under those conditions.

VITA

Breana Jade Kyker grew up in Oliver Springs, TN, where she participated in marching band and was Valedictorian of the Oliver Springs High School Class of 2014. She attended Coastal Carolina University, where she graduated in three years with a B.S. in biochemistry. During her time at Coastal Carolina University, she was in the Honor's Program and was an active member of the quiz bowl team and Biochemistry and Chemistry Club. Breana was also named Outstanding Biochemistry Student of the Year in 2017. She then attended the University of Tennessee Knoxville for graduate school. At UTK, she volunteered at several events that promoted STEM education at the middle and high school levels. Additionally, she published peer-reviewed research and presented her research both within the department and externally.